Cell-Free Massive MIMO: Challenges and Promising Solutions

Salah Elhoushy

A Thesis
in
The Department
of
Electrical and Computer Engineering

Presented in Partial Fulfillment of the Requirements
For the Degree of
Doctor of Philosophy (Electrical and Computer Engineering) at
Concordia University
Montréal, Québec, Canada

April 2022

©Salah Elhoushy, 2022

CONCORDIA UNIVERSITY
SCHOOL OF GRADUATE STUDIES

This is to certify that the thesis prepared

By: **Salah Elhoushy**

Entitled: **Cell-Free Massive MIMO: Challenges and Promising Solutions**

and submitted in partial fulfillment of the requirements for the degree of

Doctor of Philosophy (Electrical and Computer Engineering)

complies with the regulations of the University and meets the accepted standards with respect to originality and quality.

Signed by the final examining committee:

	Chair
Dr. Ramin Sedaghati	
	External Examiner
Dr. Xianbin Wang	
	Thesis Supervisor
Dr. Walaa Hamouda	
	Examiner
Dr. Alina Stancu	
	Examiner
Dr. Yousef Shayan	
	Examiner
Dr. Reza Soleymani	

Approved by

Dr. Wei-Ping Zhu, Graduate Program Director

4/28/2022

Dr. Mourad Debbabi, Dean
Gina Cody School of Engineering and Computer Science

Abstract

Cell-Free Massive MIMO: Challenges and Promising Solutions

Salah Elhoushy, Ph.D.

Concordia University, 2022

Along with its primary mission in fulfilling the communication needs of humans as well as intelligent machines, fifth generation (5G) and beyond networks will be a virtual fundamental component for all parts of life, society, and industries. These networks will pave the way towards realizing the individuals' technological aspirations including holographic telepresence, e-Health, pervasive connectivity in smart environments, massive robotics, three-dimensional unmanned mobility, augmented reality, virtual reality, and internet of everything. This new era of applications brings unprecedented challenging demands to wireless network, such as high spectral efficiency, low-latency, high-reliable communication, and high energy efficiency. One of the major technological breakthroughs that has recently drawn the attention of researchers from academia and industry to cope with these unprecedented demands of wireless networks is the cell-free (CF) massive multiple-input multiple-output (mMIMO) systems. In CF mMIMO, a large number of spatially distributed access points are connected to a central processing unit (CPU). The CPU operates all APs as a single mMIMO network with no cell boundaries to serve a smaller number of users coherently on the same time-frequency resources. The system has shown substantial gains in improving the network performance from different perspectives, especially for cell-edge users, compared it other candidate technologies for 5G networks, i.e., co-located mMIMO and small-cell (SC) systems. Nevertheless, the full picture of a practical scalable deployment of the system is not clear yet. In this thesis, we provide more in-depth investigations on the CF mMIMO performance under various practical system considerations. Also, we provide promising solutions to fully realize the potential of CF mMIMO in practical scenarios. In this regard, we focus on three vital practical challenges, namely hardware and channel impairments, malicious attacks, and limited-capacity fronthaul network.

Regarding the hardware and channel impairments, we analyze the CF mMIMO performance under such practical considerations and compare its performance with SC systems.

In doing so, we consider that both APs and user equipment (UE)s are equipped with non-ideal hardware components. Also, we consider the Doppler shift effect as a source of channel impairments in dynamic environments with moving users. Then, we derive novel closed-form expressions for the downlink (DL) spectral efficiency of both systems under hardware distortions and Doppler shift effect. We reveal that the effect of non-ideal UEs is more prominent than the non-ideal APs. Also, while increasing the number of deployed non-ideal APs can limit the hardware distortion effect in CF mMIMO systems, this leads to an extra performance loss in SC systems. Besides, we show that the Doppler shift effect is more harsh in SC systems. In addition, the SC system operation is more suitable for low-velocity users, however, it is more beneficial to adopt CF mMIMO system for network operation under high-mobility conditions. Capitalizing on the latter, we propose a hybrid CF mMIMO/SC system that can significantly outperforms both CF mMIMO and SC systems by providing different mobility conditions with high data rates simultaneously.

Towards a further improvement in the CF mMIMO performance under high mobility scenarios, we propose a novel framework to limit the performance degradation due to the Doppler shift effect. To this end, we derive novel expressions for tight lower bound of the average DL and uplink (UL) data rates. Capitalizing on the derived analytical results, we provide an analytical framework that optimizes the frame length to minimize the Doppler shift effect on DL and UL data rates according to some criterion. Our results reveal that the optimal frame lengths for maximizing the DL and UL data rates are different and depend mainly on the users' velocities. Besides, adapting the frame length according to the velocity conditions significantly limits the Doppler shift effect, compared to applying a fixed frame length.

To empower the CF mMIMO systems with secure transmission against malicious attacks, we propose two different approaches that significantly increases the achievable secrecy rates. In the first approach, we introduce a novel secure DL transmission technique that efficiently limits the eavesdropper (Eve) capability in decoding the transmitted signals to legitimate users. Differently, in the second approach, we adopt the distinctive features of Reconfigurable intelligent surfaces (RIS)s to limit the information leakage towards the Eve.

Regarding the impact of limited capacity of wired-based fronthaul links, we drive the achievable DL data rates assuming two different CF mMIMO system operations,

namely, distributed and centralized system operations. APs and CPU are the responsible entities for carrying out the signal processing functionalities in the distributed and centralized system operations, respectively. We show that the impact of limited capacity fronthaul links is more prominent on the centralized system operation. In addition, while the distributed system operation is more preferable under low capacities of fronthaul links, the centralized counterpart attains superior performance at high capacities of fronthaul links. Furthermore, considering the distributed and centralized system operations, and towards a practical and scalable operation of CF mMIMO systems, we propose a wireless-based fronthaul network for CF mMIMO systems under three different operations, namely, microwave-based, mmWave-based, and hybrid mmWave/microwave. Our results show that the integration between the centralized operation and the hybrid-based fronthaul network provides the highest DL data rates when APs are empowered with signal decoding capabilities. However, integrating the distributed operation with the microwave-based fronthaul network achieves ultimate performance when APs are not supported with decoding capabilities.

Acknowledgement

First and foremost, all praise and thanks are due to Allah (God), the Almighty, the Most Gracious, and the Most Merciful, for his countless blessings and for giving me the strength to pursue my dreams. I could have never finished this thesis without the faith I have in Him.

I would to express my great gratitude to my supervisor Prof. Walaa Hamouda for being such a great advisor who supported me technically and personally. His support and insightful advice were crucial to my academic achievement and development as an independent researcher. Honestly, I consider Prof. Hamouda an elder brother, not only a supervisor or a teacher. Prof. Hamouda, thank you for all the technical and ethical values I have learned from you. Without your valuable support, encouragement, and mentoring, I could not have achieved this.

I would also like to thank my committee members, Prof. Yousef Shayan, Prof. Reza Soleymani, Prof. Alina Stancu, and Prof. Xianbin Wang, for serving as my committee members and providing me with valuable comments and suggestions.

I am sincerely thankful to Concordia Graduate Student Support Program (GSSP) for funding my Ph.D. studies.

My gratitude also goes to my friends Mohamed Ibrahim and Mohammed Elbayoumi. Thank you for your unwavering support, for cheering me up in the most stressful moments, and for the pleasant times and fruitful discussions we had over the past four years. Wishing you the best of luck in your future endeavors.

I would like to express my sincere gratitude to my beloved parents, Abdelsalam Elhoushy and Nahla Elbestawy. Without your endless support, sound advice, and prayers, I would not have become the person I am today. I am also extremely grateful to my sisters, Aya and Gehad, for their unconditional love and continuous support throughout my life. Last but not least, I would like to give special thanks to my future wife, Lamees El-Nagar. You have been a great support to me during the past year. I am so lucky to have you in my life. Thanks so much Lamees!

To my parents, Abdelsalam Elhoushy and Nahla Elbestawy,
To my future wife, Lamees El-Nagar,
To my sisters, Aya and Gehad,
To my nephews, Abdelhamed, Abdullah, and Adam.

Contents

List of Figures

List of Common Symbols

M	number of APs
K	number of users
N_{ap}	number of antennas per AP
$\boldsymbol{g}_{mk}$	channel vector between the m^{th} AP and the k^{th} user
$\boldsymbol{h}_{mk}$	small-scale fading channel vector between the m^{th} AP and the k^{th} user
β_{mk}	large-scale fading coefficient between the m^{th} AP and the k^{th} user
$\hat{\boldsymbol{g}}_{mk}$	estimated channel vector between the m^{th} AP and the k^{th} user
$\tau_{u,p}$	length of UL pilot sequences
τ_c	coherence time
$\boldsymbol{\psi}_k$	UL transmitted pilot sequence from user k
$\tau_{d,p}$	length of DL pilot sequences
$\boldsymbol{\phi}_k$	DL transmitted pilot sequence for user k
P_d	DL data transmit power
$P_{u,p}$	UL pilot transmit power
P_u	UL data transmit power
η_{mk}	DL power control coefficient for the transmitted data from AP m to user k
λ_A	density of APs
λ_U	density of users
σ_w^2	noise variance

List of Acronyms

AF	amplify-and-forward.
AP	access point.
CB	conjugate beamforming.
CDF	cumulative distribution function.
CF	Cell-free.
CFE	compress-forward-estimate.
COMP	Coordinated Multi-Point.
CPU	central processing unit.
CSI	channel-state information.
DAS	Distributed Antenna System.
DF	decode-and-forward.
DL	downlink.
ECF	estimate-compress-forward.
ECP	edge-cloud processor.
EDCF	estimate-detect-compress-forward.
eMBB	enhanced mobile broadband.
Eve	eavesdropper.
FDD	frequency-division duplexing.
FHPPP	Finite Homogeneous Poisson Point Process.
FSO	free space optics.
HPPP	Homogeneous Poisson Point Process.
HTC	human-type communication.
i.i.d.	independent and identically distributed.
IoT	internet of things.
LoS	line-of-sight.
LS	least-square.
LSF	large-scale fading.
LSFD	large-scale fading decoding.

LTE	Long Term Evolution.
mMIMO	massive multiple-input multiple-output.
MMSE	minimum mean-square error.
mMTC	massive machine-type communication.
mmWave	millimeter wave.
MRC	maximum-ratio-combining.
NLoS	non line-of-sight.
NOMA	non-orthogonal multiple-access.
OMA	orthogonal multiple-access.
PLS	physical layer security.
RIS	Reconfigurable intelligent surfaces.
RSMA	Rate-Splitting Multiple Access.
SC	small-cell.
SDMA	spatial division multiple-access.
SDP	semi-definite programming.
SIC	successive interference cancellation.
SINR	signal-to-interference-plus-noise-ratio.
TDD	Time-division duplexing.
UC	user-centric.
UDN	ultra-dense network.
UEs	user equipments.
UL	uplink.
URLLC	ultra-reliable low-latency communication.
w.r.t	with respect to.
ZF	zero-forcing.

Chapter 1
Introduction

Along with each generation of cellular networks, there is a corresponding development towards fulfilling the mission of providing excellent communication service to anyone, anywhere, any anytime. Indeed, the evolution of cellular networks from the first generation (1G) to the fifth generation (5G) had a profound impact on different aspects of our life. One can notice that through the tactile impact of smartphones on our daily social interactions that became virtual than real as well as our cultural beliefs that can be easily affected by accessing real-time information from all over the world. Indeed, the needs of mobile users have been continuously changing over the past few decades. At first, mobile networks were analog and designated to exclusively handle voice traffic. Differently, the majority of mobile users traffic has recently switched to digital traffic such as video/audio streaming, web browsing, file sharing, etc. rather than voice traffic. Furthermore, along with its primary mission in fulfilling the communication needs of humans, future cellular networks will be a virtual fundamental component for all parts of life, society, and industries.

5G and beyond networks will pave the way towards realizing the individuals technological aspirations including holographic telepresence, e-Health, pervasive connectivity in smart environments, massive robotics, three dimensional massive unmanned mobility, augmented reality, virtual reality, and internet of everything [1,2]. Towards fulfilling such emerging applications, 5G and beyond networks are conceived to offer much higher data rates than its predecessors to cope with the seemingly ever increasing demand of enhanced mobile broadband (eMBB) along with providing ultra-reliable low-latency communication (URLLC) and massive machine-type communication (mMTC) [3]. In that, eMBB, URLLC, and mMTC are considered as the three cornerstones of the magic triangle for 5G and beyond networks. Particularly, eMBB enables the data hungry applications such as virtual reality and holographic telepresence [4] while URLLC enables real-time applications, characterized by time-critical communications, such as autonomous vehicles [5,6],

e-Health [7], industrial automation control [8, 9]. Besides, mMTC enables connectivity between a vast number of miscellaneous devices and sensors [10, 11] which is an enabler for internet of everything applications in which heterogeneous devices can exchange data without human intervention. By the end of 2025, 2.8 billion mobile subscriptions are anticipated to be 5G-based, and out of which 88 percent will be targeting eMBB [12]. The eMBB is the use case that networking and telecommunication companies are mainly focusing at since day one of the 5G development journey [13]. Consequently, investigating the provided data rates to users in 5G and beyond networks is the leitmotif in this thesis.

Various emerging technologies have been recently proposed to flourish 5G and beyond networks with exceptional increase in the data rates, such as millimeter wave (mmWave) [14,15], ultra-dense network (UDN) [16], and massive multiple-input multiple-output (mMIMO) [17–19]. mmWave bands, namely the range $30 - 300$ GHz where the wavelength is in the order of the millimeter, are currently considered as a key enabling technology to meet the high data rate requirements in future wireless networks. This is thanks to the immense amount of available bandwidth in such frequency bands compared to the available ones in the microwave band, i.e., sub-6 GHz frequency band. Nevertheless, the large signal attenuation as well as the high sensitivity to blockages in such high frequencies [15] renders mmWave appealing only for short-range line-of-sight (LoS) communications. Aside from that, shrinking the cell size through deploying more small base stations (also known as small-cell (SC)s) is another promising approach to boost the achievable data rates. Further densification of small base stations brings the serving base station closer to the user which in turn improves the quality of received signals at the user side. Also, one can dedicate each small base station to serve only one user which does not have to share any resource with other users. This is what so called UDN. Despite the significant data rate improvements of UDN, it entails high deployment and maintenance costs [13]. Note that, the network densification can be performed in a centralized way rather than the distributed way in UDN. This is known as mMIMO technology in which in base stations are equipped with a number of antennas much larger than the number of active users per time-frequency resource through beamforming techniques [19]. The excess number of base station antennas compared to the users leads to the favorable propagation phenomenon according to which the users' channels become approximately mutually orthogonal as the number of antennas grows [20]. This in turn makes the inter-

user interference vanishes and enables spatial multiplexing of the users. The favorable propagation also makes linear signal processing schemes, such as conjugate beamforming (CB) and zero-forcing (ZF), effective and nearly optimal, hence considerably simplifying the circuitry complexity [18]. In addition, the system can provide extraordinary amounts of beamforming gain that is linearly increasing with the number of deployed antennas at the base station. Despite the reported significant gains of mMIMO technology, it suffers from performance degradation at cell-edge users [13].

A new practical embodiment of mMIMO systems has been recently emerged under the name of Cell-free (CF) mMIMO [21]. CF mMIMO systems can efficiently combine the blessings of mmWave, UDN, and mMIMO technology to provide future wirless networks with unprecedented levels of data rates. In CF mMIMO, many antennas are geographically distributed within the coverage area rather than co-located in a base station. We refer to the distributed antennas as access point (AP)s. These APs are connected to a central processing unit (CPU) which operates all APs as a single mMIMO network with no cell boundaries to serve all users coherently in the same time-frequency resources [22]. Unlike conventional mMIMO systems, CF mMIMO can provide all users within the coverage area with a uniformly good service [21].

1.1 Motivations

The key objectives of this thesis are to:

1. Analyzing the CF mMIMO system performance under various practical system considerations.

2. Empowering CF mMIMO systems with innovative solutions to realize its full potential in boosting the network performance from different perspectives.

3. Providing a practical and scalable implementation for CF mMIMO systems.

4. Develop analytical and simulation frameworks for the developed techniques.

The proposed work is important in various ways. It certainly addresses a timely topic (CF mMIMO system), which has recently received considerable attention in both academic research and industry. Indeed, preliminary studies in the literature have revealed the significant potential of CF mMIMO systems in providing future wireless communication

networks with superior performance to that of other candidates for 5G network operations such as UDN and conventional mMIMO. Nevertheless, the full picture of a practical and scalable CF mMIMO system is not clear yet. Motivated by this, and since the reported theoretical results may not hold in practice as a consequence of the negative impacts of practical limitations on the system performance, we introduce profound insights on the CF mMIMO performance under various practical system considerations. Besides, we provide promising solutions to tackle the performance degradation in practical scenarios. In this regard, we focus on three vital practical system consideration, namely hardware and channel impairments, malicious attacks, and limited-capacity fronthaul network.

It is noteworthy that a prerequisite to achieve the anticipated gains of mMIMO systems is the availability of accurate and up-to-date channel-state information (CSI) during data transmission phases [18, 23]. However, the low quality of hardware components may affect the accuracy of the estimated channels badly. Besides, in dynamic scenarios, the relative movement between users and APs as well as the introduced processing delay at APs lead to temporal variations in the propagation environment. This in turns affects the channel coefficients to continuously evolve with time and change from one symbol to another [24]. This renders the estimated channel coefficients out-of-date when applied for data transmission which in turn leads to an inevitable degradation in the system performance. Such effect is known as the Doppler shift effect and it is considered as one of the main channel impairment sources in dynamic environments [24]. Consequently, we analyze the potential of CF mMIMO in supporting dynamic environments in the presence of non-ideal hardware components. Also, we provide solutions to alleviate the Doppler shift effect on the system performance.

Recently, wireless communication networks play a crucial rule in many military and civilian applications [25]. In particular, it is widely used in the transmission of important/private information, such as energy pricing, credit card information, e-health data, and control messages. As such, security is one of the critical concerns of the future wireless networks. In this regard, we rely on physical layer security (PLS) metrics to assess the secrecy capabilities of CF mMIMO systems. Furthermore, due to the negative impact of malicious attacks on the secrecy performance of the system, we provide innovative solutions to empower CF mMIMO systems with secure data transmission against malicious attacks.

Due to its pivotal role in handling the data exchange between the CPU and APs, the capacity of fronthaul links significantly affects the performance of CF mMIMO systems. Consequently, we investigate the impact fronthaul links capacities on the performance of CF mMIMO systems with emphasis on its impact on the preferred system operation (where to perform the signal processing functionalities, i.e., APs or CPU). Besides, aiming at maintaining a practical and feasible implementation of CF mMIMO as the network gets larger and the number of APs increases, we propose a scalable and practical wireless-based fronthaul network design that can accommodate for all APs and provide them with reliable fronthaul links that can efficiently handle the data exchange between APs and CPU.

1.2 Thesis Contributions

Given the preceding motivating points in the last section, the contributions of this thesis can be summarized as follows.

CF mMIMO and SC Performance Under Hardware and Channel Impairments. In Chapter 3, we analyze the achievable downlink (DL) data rates of CF mMIMO systems and compare it with the achievable ones of SC systems (i.e., UDN) under non-ideal hardware distortions and channel impairments, i.e., Doppler shift effect. To this end, we provide novel closed-form expressions for the achievable DL data rates for both systems under such practical system considerations. Also, we come up with new findings regarding the impact of these system practical considerations on both systems operations. Firstly, we reveal that the effect of non-ideal user equipments (UEs) is more prominent than the non-ideal APs. Besides, the effect of non-ideal APs distortion is more prominent in the SC system. Regarding the channel impairments effect, we reveal that the Doppler shift effect is more prominent in SC systems. In addition, SC systems are preferred to support network operation under low-mobility conditions. However, it is more beneficial to adopt CF mMIMO for network operation under high-mobility conditions. Inspired by these findings, we propose a hybrid CF mMIMO/SC system that supports high-velocity and low-velocity users with high DL data rates simultaneously. We show that the proposed system outperforms SC and CF mMIMO systems by providing users of different mobility conditions with superior data rates simultaneously.

Limiting Doppler Shift Effect on CF mMIMO Systems. In Chapter 4, we propose a novel framework to limit the Doppler shift effect on the achievable DL and

uplink (UL) data rates of CF mMIMO systems. Particularly, we adapt the length of the data transmission frame according to the users' velocities to reduce the impact of outdated CSI on the transmitted data in later symbols in the data transmission frame. We conduct this under different transmission protocols where the first transmission protocol considers performing the channel estimation task before the DL and UL transmission phases, while the second one considers carrying out the channel estimation task between the UL and DL transmission phases. In doing so, we derive novel expressions for tight lower bound of the average DL and UL data rates. Then, capitalizing on the derived analytical results, we provide an analytical framework to determine the optimal frame length that limits the Doppler shift effect on DL and UL rates according to some criterion. Our results show that the optimal frame lengths for maximizing the DL and UL rates are different and depend mainly on the transmission criterion and the users' velocities. Also, selecting the frame length that minimizes a weighted sum of the DL and UL losses can significantly limit the Doppler shift effect on both DL and UL data rates simultaneously. Finally, we demonstrate the high potential of adapting the frame length according to the velocity conditions in limiting the Doppler shift effect, compared to applying a fixed frame length.

Physical Layer Security in CF mMIMO Systems. In Chapter 5, we analyze the secrecy capacities of CF mMIMO systems in the presence of malicious attacks, i.e., active eavesdropper (Eve). Also, we propose two promising approaches to improve the secrecy performance of CF mMIMO systems. The first approach focuses on the case where APs cannot detect the presence of the active Eve. Also, the Eve strives to estimate its DL channel coefficients with APs capitalizing on the DL transmission strategy. To improve the secrecy capacities of the system under this scenario, we propose a novel DL transmission technique to limit the information leakage to the active Eve. The performance of the proposed DL transmission technique is compared with other DL transmission techniques in the literature. We reveal that the proposed DL technique improves the secrecy performance of CF mMIMO systems compared to other transmission techniques in the literature. In the second proposed approach, we focus on the case where the system can detect the presence of active Eve. In that, we exploit the distinctive features of Reconfigurable intelligent surfaces (RIS)s to improve the secrecy performance of CF mMIMO systems. To this end, we propose a novel RIS-assisted CF mMIMO system operation in which RIS phase shifts and DL power control coefficients are jointly optimized to minimize

the information leakage to the active Eve while maintaining the legitimate users' performance above certain thresholds. Our results reveal that RISs can significantly enhance the secrecy capacities of CF mMIMO systems.

Limited-Fronthaul Capacity Effect on CF mMIMO Performance. In Chapter 6, we investigate the DL performance of CF mMIMO systems under limited capacity of wired-based fronthaul links. In particular, we analyze the achievable DL rates assuming two different CF mMIMO system operations, namely, distributed and centralized system operations, assuming limited capacity of fronthaul links. In the distributed system operation, APs are responsible for performing channel estimation and data precoding tasks where a simple precoding technique is applied for DL data transmission due to their low processing capabilities. On the other hand, the CPU carries out both channel estimation and data precoding tasks where more sophisticated DL precoding technique is applied for DL data transmission thanks to the high available processing capabilities at the CPU. Our results reveal that the impact of limited capacity fronthaul links is more prominent on the centralized system operation. In addition, while the distributed system operation is more preferable under low capacities of fronthaul links, the centralized counterpart attains superior performance at high capacities of fronthaul links.

CF mMIMO Performance Under A Wireless-Based Fronthaul Network. In Chapter 7, we propose a practical and scalable wireless mMIMO-based fronthaul network that can efficiently serve APs with reliable and high-capacity fronthaul links. Particularly, we consider multiple edge-cloud processor (ECP)s serving APs using one of three possible fronthaul network operations, namely, microwave, mmWave, and hybrid microwave/mmWave. Under each fronthaul network operation, we analyze the achievable DL data rates for two different microwave-based operations of the access link (AP-users), namely, distributed and centralized operations, while assuming DL with/without decoding capabilities. Our results show that the integration between the centralized access link operation and the hybrid-based fronthaul network provides the highest DL data rates when AP are empowered with decoding capabilities. However, integrating the distributed access link operation with the microwave-based fronthaul network achieves ultimate performance when AP are not supported with decoding capabilities.

1.3 Thesis Organization

The rest of the thesis is organized as follows. In chapter 2, we provide a comprehensive introduction to mMIMO systems with emphasis on the CF mMIMO and the practical challenges that may affect the its performance badly. Considering hardware and channel impairments, we conduct a comparison between the DL performance of CF mMIMO systems and SC systems and propose a hybrid CF mMIMO/SC system for high data rates in dynamic environments in chapter 3. In chapter 4, we propose a framework to limit the negative impact of channel impairments on the performance of CF mMIMO systems. Promising solutions to empower CF mMIMO systems with secure data transmission are introduced in chapter 5. The DL performance of limited-fronthaul CF mMIMO systems is investigated in chapter 6. In chapter 7, we investigate the DL performance of CF mMIMO systems under a practical and scalable wireless mMIMO-based fronthaul network. Finally, the conclusions of this thesis are drawn and the future trends are discussed in Chapter 8.

Chapter 2
Background and Literature Review

2.1 Blessings of Multi-Antenna Systems

Using multiple transmitting/receiving antennas can remarkably boost the quality of the signal at the receiver, and enhances the robustness and reliability of the link. This is a consequence of the possibly independent propagation channels through which the signal is transferred from transmitter to receiver. This in turn reduces the probability that the signal between the transmitter and receiver experiences poor channel conditions. This is known as spatial diversity gain [26]. However, a prerequisite to attain such beamforming gains is to have a sufficient space of half-wavelength between the deployed antennas [27]. Along with that, one can exploit the multiple antennas at the receiver side to send different signals to the same user by means of space-time coding techniques which is defined as the spatial multiplexing gain [28]. Spatial diversity and spatial multiplexing gains were the motive of the initial MIMO system known as point-to-point MIMO [27–30].

Along with the aforementioned benefits of multi-antenna systems, equipping base stations with multiple antennas can efficiently improve the transmission directivity by appropriately synchronize the signal transmissions from the different antennas to direct the signal energy towards a specific direction. The main idea is to adjust the transmitted signal components from each antenna so that they add up constructively at the intended receiver, thus, the receiver observes a much stronger signal than the transmitted one from each antenna. Such technique is widely known as beamforming [31]. Also, the improvement of the signal strength at the receiver side is called the beamforming gain which is equal to the number of the transmitting antennas. Interestingly, along with the remarkable beamforming gains at the desired receiver side, there will be a destructive interference in any undesired direction. Thus, receivers in undesired locations will experience slight interference. Such ability of focusing the signals towards a specific direction leads to an efficient use of the available resources of wireless networks through enabling them to serve

multiple users on the same time-frequency resources by separating them in the spatial domain. This is known as spatial division multiple-access (SDMA) [32] which leads to high multiplexing gains and high data rates accordingly. This is the adopted technique for mMIMO systems.

2.2 Evolution of mMIMO Systems

2.2.1 Multi-User MIMO

mMIMO systems have been firstly considered in Long Term Evolution (LTE) in a small-scale under the name of Multi-user MIMO [33–36]. In multi-user MIMO, a base station with multiple antennas simultaneously serves a multiplicity of single antenna users whose number is equal to the number of antennas in the base station over the same time-frequency resources. The system has shown a significant improvement in the achievable data rates but at the expense of complicated signal processing and the need of substantial channel estimation resources which constitute the inherent bottleneck of multi-user MIMO technology.

2.2.2 Co-located mMIMO

An emerging idea from multi-user MIMO towards fulfilling the eMBB requirements of future wireless networks is mMIMO [19, 37–39]. In mMIMO, base station, equipped with an array of hundreds antenna elements, communicates with tens of single-antenna users over the same time-frequency resources. Along with the high beamforming gains, the excess number of base station antennas leads to approximately mutually orthogonal as the number of antennas grows which is known as the favorable propagation phenomenon [20]. This in turn nulls the inter-user interference and enables spatial multiplexing of the users. The favorable propagation also makes linear signal processing schemes, such as CB and ZF, effective and nearly optimal, hence considerably simplifying the circuitry complexity [18]. Furthermore, the high number of antennas renders the communication channels nearly deterministic as the effect of the small-scale fading is averaged out over the many channel observations according to the law of large numbers. This is known as the channel hardening property [40, 41]. Such property facilitates the derivation of closed-form expressions of the achievable spectral efficiency [18, 42, 43]. This enables

the optimization of spectral and energy efficiencies and simplifies the resource allocation (i.e., power control) since it needs to be carried out according to the slow-varying large-scale fading coefficients rather than the fast-varying small-scale fading [18,43–49]. Indeed, the aforementioned advantages of co-located mMIMO system induced telecommunication companies to consider it as a key enabler of 5G. Recently, co-located mMIMO base stations has been deployed all over the world.

2.2.3 Distributed mMIMO

mMIMO can be deployed in a distributed manner as well in a form of a distributed mMIMO system in which a spatially distributed antenna array in each cell is used to serve the users within the cell in a cooperative way. This system setup is similar to Distributed Antenna System (DAS) setup [50] and Coordinated Multi-Point (COMP) with static disjoint cooperation clusters [51]. The performance of distributed and co-located mMIMO systems is compared in [52–55]. Results reveal that distributed mMIMO provides higher data rates than the co-located mMIMO counterpart.

2.2.4 CF mMIMO

Recently, a new practical embodiment of the distributed mMIMO systems has been emerged under the name of CF mMIMO [21, 56, 57]. Different from distributed mMIMO systems, in CF mMIMO, all the spatially distributed antennas are connected to a CPU which operates all antennas as a single mMIMO network with no cell boundaries to serve all users coherently in the same time-frequency resources [22]. We refer to the spatially distributed antennas as APs. Also, each AP can be equipped with single or multiple antennas for the communication with users. The signal co-processing by the distributed APs yields further benefits to CF mMIMO systems along with the inherited beamforming and spatial multiplexing gains from its mMIMO nature such as

- Macro-diversity gain: Serving each user by a number of distributed well-separated APs enriches the provided spatial diversity to users since the probability of different APs experiences poor channel conditions is low. Along with that, adopting the network densification approach in CF mMIMO brings APs to the proximity of users leads to a remarkable reduction in the path-loss and shadowing effects. Such benefits

improves the reliability of links between users and their serving APs which in turn leads to higher levels of beamforming gains.

- Inter-cell interference mitigation: Conventionally, UDN networks are operated as a i.e., SC system in which each AP serves only one user or the the users in its proximity, and each user is served by one AP. Consequently, the system suffers from high levels of inter-cell interference. Differently, operating all APs in a cooperative manner in CF mMIMO erases the cell-boundaries and turn the resulted inter-cell interference in SC systems into a useful signal. It has been shown in the literature that CF mMIMO significantly outperforms the SC counterpart for cell-edge users [21].

- Uniform QoS: As illustrated, in CF mMIMO, there are no cell-edge users where all users are experiencing good channel conditions. This in turn leads to a fairness in the provided service to all users within the coverage area.

2.3 CF mMIMO Operation

Time-division duplexing (TDD) has been widely adopted by the majority of current works as the candidate transmission protocol for CF mMIMO systems. On the other hand, the works in [58–62] adopted the frequency-division duplexing (FDD) mode for the system operation. For the system operation under TDD mode, the DL and UL data transmission occur over the same frequency band. Thus, the DL and UL channels are reciprocal [37, 63, 64]. This in turn enables APs to estimate the DL channel conditions with users without feedback. As a consequence, the TDD protocol renders CF mMIMO scalable as the number of APs and antennas at APs increase [65, 66]. Under TDD operation, the system frame is divided into three phases, namely, UL training, DL transmission, and UL transmission. During the UL training phase, users send pilot sequences to APs so that APs can estimate the users' UL channel conditions. Capitalizing on the channel reciprocity property, the estimated channels are exploited to determine the vectors used to perform data precoding and detection in DL and UL transmission phases, respectively.

On the other hand, in FDD systems, the DL and UL data transmissions occur simultaneously, but over two different frequency bands. As such, UL and DL channel coefficients are not reciprocal. This in turn obliges the APs to acquire the DL channel coefficients to perform the DL precoding process. In particular, APs can acquire the channel coefficients

through a DL channel estimation phase, followed by a CSI feedback. However, since the amount of CSI acquisition and feedback scales linearly with the number of APs [61], the latter approach is not practical for CF mMIMO systems. As such, different CSI acquisition techniques are proposed to circumvent such issue by exploiting the angle reciprocity in FDD systems as in [58, 59, 61].

We adopt the TDD-based operation for the presented works in this thesis. In what follows, we briefly discuss the three transmission phases of TDD-based CF mMIMO frame structure, namely channel estimation, DL transmission, and UL transmission. Note that, there are two different approaches of CF mMIMO operation to perform the signal processing functionalities. The first one is a distributed approach in which the APs perform the channel estimation as well as the DL precoding and UL detection. Differently, the second one is a centralized approach in which the CPU is the responsible entity for carrying out these tasks. A comparison between the distributed and centralized approaches are conducted in chapter 6 and 7.

2.3.1 Channel Estimation

Channel estimation process plays a crucial role in mMIMO systems performance in-terms of spectral and energy efficiencies [67] since it directly affects the calculations of precoding/detection vectors applied for DL/UL data transmission. In the literature, different techniques are applied to perform the channel estimation process in CF mMIMO systems where the majority of these techniques are pilot-based. In that, users send pilot sequences of length to APs for the sake of channel estimation. The assigned pilot sequences to users can be orthogonal or non-orthogonal depending on the channel coherence time and the number of users. For instance, under low mobility scenarios with large coherence time and small number of users, orthogonal pilot sequences with can be assigned to users. However, in high mobility scenarios with small coherence time, it is preferred to use non-orthogonal pilot sequences to limit the amount of consumed resources to perform the channel estimation task.

A common assumption that is made to perform the channel estimation process is the availability of the large-scale fading (LSF) coefficients of users at the APs/CPU. This is due to their slow changes relative to the channel coherence time [21]. Thus, the minimum mean-square error (MMSE)-based channel estimation technique is the commonly adopted

technique by the majority of works in the literature [68]. Differently, few works analyzed the performance of CF mMIMO systems using the least-square (LS) estimator in the absence of LSF coefficients of users at the APs/CPU [69–72]. The authors in [71, 72] compared the performance of CF mMIMO systems under LS and MMSE channel estimation techniques. Results revealed that applying the LS estimator attains lower DL and UL data rates compared to the MMSE estimator.

2.3.2 DL Transmission

After estimating the users-APs channel conditions, the estimated channel coefficients are exploited to compute the precoding vector for DL transmission. Different distributed and centralized DL precoding techniques are applied for DL transmission in CF mMIMO systems. The most common distributed precoding technique in the literature is the local CB precoding. This is due to its low complexity and the ability to provide closed-form expressions for the DL data rates [21]. On the other hand, more sophisticated centralized techniques such as ZF [73] and MMSE [74] precoding are applied to improve the system performance in terms of the achievable data rates. Since users do not have instantaneous information about is channel conditions with APs, they receive the transmitted data symbols using the channel statistics based on the channel hardening property [75].

2.3.3 UL Transmission

During the UL data transmission phase, all users simultaneously transmit their UL data symbols to APs over the same time-frequency resources. capitalizing on the users' estimated channels at APs, users' data are detected locally at each AP using maximum-ratio-combining (MRC) [21]. Then, the locally detected signals at APs are forwarded to the CPU which detects the users' signals by averaging the locally detected signals. Differently, the authors in [76, 77] introduced more sophisticated MMSE centralized detection techniques to improve the achievable UL data rates. Also, these works proposed a two-stage detection approach which applies a local detection at APs using MRC or local MMSE, followed by a large-scale fading decoding (LSFD) at the CPU.

2.4 Practical Challenges of CF mMIMO

Despite the significant theoretical gains of CF mMIMO in improving the systems performance in-terms of spectral and energy efficiencies, the systems performance is prone to inevitable performance degradation under various practical system considerations. In the following, we shed light on various practical challenges that may confront the realization of the full potential of CF mMIMO in meeting the unprecedented requirements of future wireless networks.

2.4.1 Hardware Distortions

Densifying wireless networks with single or multi-antenna APs as in CF mMIMO systems may lead to a significant energy consumption and hardware cost in case of equipping APs and UEs with ideal hardware components. On the other hand, equipping APs and UEs with non-ideal hardware components will distort the transmitted and received signal by introducing a distortion noise at the transmitter and receiver sides. The distortion effect depends mainly on the efficiency of the utilized hardware components. As a consequence, deploying non-ideal hardware components will significantly harm the system performance.

The effect of non-ideal hardware distortion caused by i.e., multiplicative phase-drifts, additive distortion noise, noise amplification, and inter-carrier interference has been addressed for co-located mMIMO [43, 78–80]. It has been pointed out that the impact of hardware distortion at the UEs side is more prominent than its effect on the AP side. Besides, a hardware scaling law is introduced to show that the detrimental impact of hardware impairments at the APs asymptotically vanishes. Thus, in mMIMO systems, it is tolerable to have a large number of low-quality APs antennas, but it is preferable to have high-quality antennas at the UEs side.

2.4.2 Channel Impairments

A prerequisite to reap all the advantages of mMIMO systems in-terms of high spectral and energy efficiency is to have accurate and up-to-date CSI [18, 23]. As such, the presence of inaccurate channel estimation may deteriorate the systems performance significantly. The inaccuracy in the channel estimation process is caused by the thermal noise as well as the usage of non-orthogonal training sequences during the channel estimation phase which

is known as pilot contamination effect [67]. Besides, in dynamic scenarios, the relative movement between users and APs as well as the introduced processing delay at APs lead to temporal variations in the propagation environment. This in turns affects the channel coefficients to continuously evolve with time and change from one symbol to another. Such a phenomenon is called channel aging or Doppler shift effect [24, 81–83]. This renders the estimated channel coefficients out-of-date when applied for data reception/transmission. This in turn leads to a significant degradation in the systems achievable rates.

The Doppler shift effect on the performance of co-located mMIMO systems in-terms of the achievable DL and UL rates has been studied in the literature assuming system operation under TDD in [81–84] and FDD in [85]. Results show that such effect deteriorates the achievable DL and UL rates of co-located mMIMO systems. In addition, the achievable rates become negligible under severe channel aging conditions, i.e., high velocity conditions. Moreover, the UL performance of distributed mMIMO systems under TDD system operation is analyzed in [86] considering different sources of channel impairments including pilot contamination, phase noise, and Doppler shift effect. It has been revealed that the Doppler shift effect is more detrimental on the achievable rate.

2.4.3 Malicious Attacks

Along with its primary goal in supporting users with high data rates, CF mMIMO systems should protect users' data with high security levels. Indeed, serving each user with a large number of geographically distributed APs attains high spatial diversity gains and high data rates accordingly. However, this makes the user's data symbols more prone to attacks by eavesdroppers. It is noteworthy that the quality of the users' estimated channels has a pivotal role in attaining the anticipated gains of CF mMIMO systems. However, since the transmission protocol and pilot sequences are standardized and public, a smart Eve can exploit this feature to deteriorate the quality of estimated channels by actively sending spoofing pilot sequences to cause a pilot contamination attack. This in turn poses a crucial threat to the system performance. Such attack is known as the pilot spoofing attack [87]. It has been revealed that the pilot spoofing attacks cause a severe performance degradation in the performance of co-located mMIMO systems by degrading the achievable rates of the legitimate users and increasing the information leakage towards the Eve [88].

2.4.4 Capacity of Fronthaul Links

It is noteworthy that the capacity of the fronthaul network dramatically affects the CF mMIMO performance. This is due to its vital role in handling the data exchange between the CPU and APs. More specifically, the higher amount of data to be transferred in the fronthaul network, the higher capacity requirement for fronthaul links. In fact, the fronthaul network can be deployed in different manners, namely, wired and wireless. Deploying a wired fronthaul network can provide lossless data transmission. However, this may lead to a high implementation cost and unscalable system operation. This is a consequence of the large number of links to be established between APs and the CPU. On the other hand, deploying a wireless-based fronthaul network seems to be a more feasible solution for the fronthaul network in-terms of implementation cost and scalable system operation. Nevertheless, the main concern with the wireless-based deployment of fronthaul network is to provide high reliable wireless fronthaul links with high capacity. In particular, the limited available bandwidth in microwave bands may lead to a corresponding degradation in the system performance. Motivated by the high available bandwidth at higher frequency bands such as mmWave and free space optics (FSO), these bands may play an important role in handling the data exchange between the CPU and APs [89]. Nevertheless, one of the main issues of signal transmission over such high bands is the presence of obstacles between transmitter and receiver. Hence, a prerequisite to apply such bands for the fronthaul operation is to have reliable LoS between APs and the CPU.

To the best of our knowledge, no works have studied the CF mMIMO performance under a wireless-based fronthaul network. However, the performance of the wired-based limited-fronthaul CF mMIMO systems has been extensively analyzed in [90–95] and references therein. The works in [90, 91] investigated the limited-fronthaul capacity effect on the DL performance, whereas the authors in [90, 92, 94, 95] analyzed the limited-fronthaul capacity effect on the UL performance. Results showed that the limited capacity of wired fronthaul links degrades the achievable UL and DL data rates.

2.5 Summary

In this chapter, we firstly introduced the main benefits of multi-antenna systems which in turn renders it a promising technology to meet the exceptional requirements of future

wireless networks. This was followed by a comprehensive discussion about the evolution of mMIMO systems and how it was developed from the multi-user MIMO regime to CF mMIMO. Then, we discussed the substantial theoretical gains of CF mMIMO that makes it a leading candidate for 5G and beyond network operation. Also, we discussed the CF mMIMO operation by providing a brief discussion about the communication protocol, channel estimation, DL, and UL data transmissions. Finally, we shed light on various practical challenges that may confront the realization of the full potential of CF mMIMO in practical scenarios.

Chapter 3
CF mMIMO and SC Performance Under Hardware and Channel Impairments

3.1 Introduction

Deploying a large number of distributed APs, connected to a CPU via a fronthaul network, to serve a smaller number of users is one of the promising network architectures for 5G and beyond networks. Such network architecture can be operated as a CF mMIMO system or a SC system. Both CF mMIMO and SC systems have shown a great potential to satisfy the anticipated high rate requirements for future wireless communication systems. However, an early comparison between both systems reveal that the performance of the CF mMIMO systems is superior to that of SC systems in-terms of the 95%-likely per-user throughput. Besides, applying max-min power control in CF mMIMO systems provides a uniformly good service throughout the area of coverage.

The aforementioned comparison is performed assuming ideal hardware components and up-to-date channel estimates for both systems operations. In fact, equipping a large number of APs as well as UEs with perfect hardware components will significantly increase the cost. On the other hand, equipping both APs and UEs with low-quality hardware components may affect the performance of both CF mMIMO and SC systems badly. Besides, under dynamic environments with high-mobility conditions, the Doppler shift effect may deteriorate the achievable data rates of both systems.

In this chapter, we introduce a comprehensive comparison between CF mMIMO and SC systems in-terms of the achievable DL rates under different mobility conditions assuming non-ideal hardware components. Then, considering the channel impairments effect in the presence of users with different mobility conditions in the network, a new system

operation is proposed to achieve high DL rates for all users in the network.

3.2 System Model

We consider a wireless network with M randomly-distributed APs and K randomly-distributed users, where $M \gg K$. Besides, all APs are equipped with N_{ap} antennas, where $N_{ap} \geq 1$, and UEs are considered as single-antenna terminals. All APs are connected to a CPU via a fronthaul network. We consider the network operation under two different systems, mainly, SC and CF mMIMO systems. Under the SC system operation, each user is served by the available AP that provides the best large-scale fading coefficient. In addition, each AP serves only one user at a time. On the other hand, we consider two different approaches for the CF mMIMO operation, namely conventional CF and user-centric (UC) mMIMO. In CF mMIMO, all users are served by all APs over the same time-frequency resources, but in the UC counterpart, each AP communicates with a predetermined subset of nearest $\mathcal{T}$ users (i.e., users with best channel conditions).

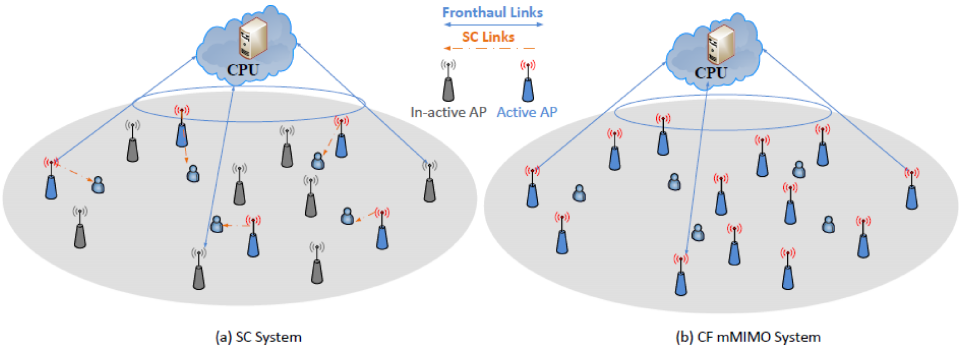

Figure 3.1: CF mMIMO and SC systems.

3.2.1 Transmission Protocol

TDD mode is adopted for the network operation under both systems operations. As shown in 3.2, for the TDD-based CF mMIMO operation, the coherence time interval is divided into three phases. In the first phase, UL training sequences are transmitted from users for the sake of channel estimation, followed by DL and UL data transmission in the second and third phases, respectively. Note that, no DL training sequences are transmitted and users decode their own data relying on the channel hardening property [21, 75]. On the other hand, in SC systems, both UL and DL training sequences are transmitted for the

sake of UL and DL channel estimation. Thus, the coherence time interval in SC systems is divided into four phases. DL training sequences and DL data symbols are transmitted in the first two phases, followed by the transmission of UL training sequences and UL data symbols in the third and fourth phases, respectively.

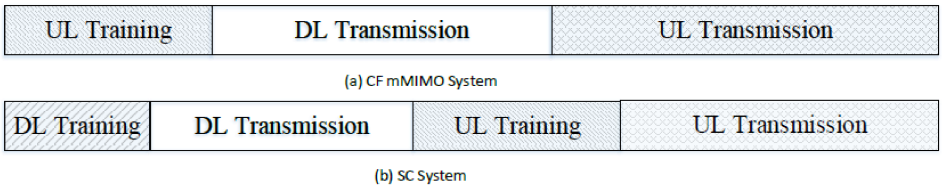

Figure 3.2: TDD-based CF mMIMO and SC transmission frames.

3.2.2 Channel Model

The channel vector $\boldsymbol{g}_{mk}[n] \in \mathbb{C}^{N_{ap}\times 1}$ between the m^{th} AP and the k^{th} user at time instant n is modeled as a Rayleigh fading channel vector that can be expressed by

$$\boldsymbol{g}_{mk}[n] = \sqrt{\beta_{mk}}\boldsymbol{h}_{mk}[n], \tag{3.1}$$

where $\boldsymbol{h}_{mk}[n] \in \mathbb{C}^{N_{ap}\times 1}$ represents the small-scale fading coefficients whose entires are independent and identically distributed (i.i.d.) $\mathcal{CN}(0,1)$. Besides, β_{mk} is the large-scale fading coefficient which accounts for path loss and shadowing effects, and it is assumed to be available at the CPU as it changes slowly over time [21]. The large-scale fading coefficient can be expressed by

$$\beta_{mk} = 10^{\frac{PL_{mk}}{10}} 10^{\sigma_{sh}x_{mk}}, \tag{3.2}$$

where the term $10^{\sigma_{sh}x_{mk}}$ denotes the shadow fading with standard deviation σ_{sh}, and $x_{mk} \sim \mathcal{N}(0,1)$. Besides, PL_{mk} represents the path loss in dB between the m^{th} AP and the k^{th} user which is determined using the three-slope path loss model [21] as follows:

$$PL_{mk} = \begin{cases} -L - 35\log_{10}(d_{mk}), & \text{if} \quad d_{mk} > d_1 \\ -L - 10\log_{10}\left(d_1^{1.5} d_{mk}^2\right), & \text{if} \quad d_0 \le d_{mk} \le d_1 \\ -L - 10\log_{10}\left(d_1^{1.5} d_0^2\right), & \text{if} \quad d_{mk} < d_0 \end{cases} \tag{3.3}$$

where d_0 and d_1 are two constants whose values are set to 10m and 50m, respectively. In addition, d_{mk} is the distance between the m^{th} AP and the k^{th} user in kilometers, and L is expressed by

$$\begin{aligned} L \triangleq\ & 46.3{+}33.9\log -10(f) - 13.82\log_{10}(\hbar_{ap}) \\ & - (1.1\log_{10}(f) - 0.7)\hbar_{ue} + (1.56\log_{10}(f) - 0.8), \end{aligned} \tag{3.4}$$

where f is the carrier frequency in MHz. In addition, $\hbar_{ap}$ and $\hbar_{ue}$ denote the APs and the UEs height in meters, respectively.

3.2.3 Hardware Distortion Model

In practical scenarios, APs and UEs may be equipped with low-quality hardware components to limit the implementation cost. This in turn leads to inevitable signal distortion that may deteriorate the system performance. The combined effect of hardware distortions (i.e., multiplicative phase-drifts, additive distortion noise, noise amplification, and inter-carrier interference) can be modeled as if the transmitted/received signal is distorted by an additive Gaussian noise [43]. In that, the distorted signal can be modeled by

$$x_i = \sqrt{\epsilon_i} x + \nu_i, \tag{3.5}$$

where x denotes the input signal to the non-ideal hardware device. Besides, the term $\epsilon_i \in [0,1], i \in \{ap, ue\}$, denotes the hardware quality coefficient. The term $\nu_i \sim \mathcal{CN}(0, (1-\epsilon_i)\mathbb{E}[|x|^2])$ represents the distortion noise that is independent of the input signal x. The quality of the hardware is determined through $\epsilon_i \in [0,1]$, where $\epsilon_i = 0$ and $\epsilon_i = 1$ represents useless and perfect hardware components, respectively.

3.2.4 Channel Impairments Model

In dynamic environments, another factor that may deteriorate the system performance is the Doppler shift effect which results from the relative movement between users and APs. In the literature, this effect is also known as the channel aging effect [24]. The corresponding degradation in the system performance arises from the fact that the acquired CSI during the training phase becomes outdated during the data transmission and reception phases. In this regard, we adopt the widely used auto-regressive model of first-order [24, 84] to model the Doppler shift effect as follows:

$$\boldsymbol{g}_{mk}[n] = \rho_k \boldsymbol{g}_{mk}[n-1] + \sqrt{1-\rho_k^2}\boldsymbol{z}_{mk}[n], \tag{3.6}$$

where $\boldsymbol{z}_{mk}[n] \sim \mathcal{CN}(0, \beta_{mk})$, represents the innovation component vector at time instant n. In addition, ρ_k represents the temporal correlation coefficient of user k, and it can be calculated using Jakes fading model $\rho_k = J_0(2\pi f_{D,k} T_s)$, where $J_0(.)$ is the zeroth-order Bessel function of the first kind, T_s is the sampling time, and $f_{D,k} = (v_k f_c)/c$, is the corresponding Doppler frequency shift for a user k with velocity v_k, where f_c and c represent the carrier frequency and the speed of light, respectively.

3.3 Channel Estimation Under Hardware and Channel Impairments

During the channel coherence time, in CF mMIMO systems, UL training sequences are transmitted by users in the first phase for the sake of channel estimation. On the other hand, in SC systems, both users and APs need to estimate their effective channel gains to decode their data symbols, hence, both UL and DL training sequences are required for the system operation. In this section, we discuss the UL training phase for UL channel estimation by taking into account the hardware distortions and the Doppler shift effect as a two sources of hardware and channel impairments, respectively. Note that, the DL channel estimation process in SC systems follows the same procedure.

During UL training phase, all users send pilot sequences of length $\tau_{u,p} \ll \tau_c$, where τ_c denotes the channel coherence time. Let $\boldsymbol{\psi}_k \in \mathbb{C}^{\tau_{u,p}\times 1}$ denotes the UL transmitted training sequence from user k where $\|\boldsymbol{\psi}_k\|^2 = 1$, the received pilot sequence matrix $\boldsymbol{Y}_{p,m}[n] \in \mathbb{C}^{N_{ap}\times\tau_{u,p}}$, at the m^{th} AP at time instant n will be

$$\boldsymbol{Y}_{p,m}[n] = \sqrt{\epsilon_{ap}} \sum_{k'=1}^{K} \boldsymbol{g}_{mk'}[n]\big(\sqrt{P_p \tau_{u,p} \epsilon_{ue}}\boldsymbol{\psi}_{k'}^T + \nu_{ue,k'}^p\big) + \boldsymbol{\nu}_{ap}^p + \boldsymbol{W}_{p,m}[n], \tag{3.7}$$

where P_p is the transmission power of each pilot symbol, and $\boldsymbol{W}_{p,m}[n] \in \mathbb{C}^{N_{ap}\times\tau_{u,p}}$, is the additive noise matrix at the m^{th} AP whose elements are i.i.d. $\mathcal{CN}(0,\sigma_w^2)$ random variables. Besides, we consider the pilot sequences, assigned to users are chosen from the identity matrix $\boldsymbol{I}_{\tau_{u,p}}$. Consequently, the distortion signal associated with the transmitted pilot symbol at the user side is $\nu_{ue,k}^p \sim \big(0, P_p\tau_{u,p}(1-\epsilon_{ue})\big)$. Due to the deployment of non-ideal antennas at the AP side, the received signal vector at AP m is distorted. The conditional distribution of the distortion component at the m^{th} AP given the channel vectors $\boldsymbol{g}_{mk}, \forall k$, is modeled by

$$\boldsymbol{\nu}_{ap}^p(n)|(\boldsymbol{g}_{mk}, \forall k) \sim \left(\boldsymbol{0}, P_p\tau_{u,p}(1-\epsilon_{ap}) \sum_{k'=1}^{K} \big|\boldsymbol{g}_{mk'}[n]\big|^2 \boldsymbol{\psi}_{k'}(n)\boldsymbol{I}_{N_{ap}}\right), \tag{3.8}$$

where the channel gain for each user k' at time instant n is multiplied by the transmitted pilot signal at this time instant to consider its effect only when the pilot symbol is transmitted. Taking into account the Doppler shift effect on the channel estimation, we consider performing the channel estimation process at time instant $\tau_{u,p}+1$ as the estimated channels at later instants will be worse. Thus, we are aiming at estimating the channel coefficients $g_{mk,l}[\tau_{u,p}+1], \forall m,k,l$, where l denotes the index of the antenna element at

the AP. Using the channel aging model in (3.6), the channel coefficient $g_{mk,l}[n]$ for user k at time instant n can be expressed in-terms of the corresponding channel condition at time instant $\tau_{u,p}+1$ as

$$g_{mk,l}[n] = \alpha_{k,n} g_{mk,l}[\tau_{u,p}+1] + \sqrt{1-\alpha_{k,n}^2} z_{mk,l}[n], \tag{3.9}$$

where $\alpha_{k,n} = \rho_k^{|\tau_{u,p}+1-n|}$. Consequently, by substituting (3.9) in (3.7), the received pilot sequences vector at antenna l at the m^{th} AP will be

$$\begin{aligned} \boldsymbol{y}_{p,m,l}[n] &= \sqrt{\epsilon_{ap}} \sum_{k'=1}^{K} \alpha_{k',n} g_{mk',l}[\tau_{u,p}+1] \big(\sqrt{P_p \tau_{u,p} \epsilon_{ue}} \boldsymbol{\psi}_{k'}^T + \nu_{ue,k'}^p \big) \\ &+ \sqrt{\epsilon_{ap}} \sum_{k'=1}^{K} \sqrt{1-\alpha_{k',n}^2} z_{mk',l}[n] \big(\sqrt{P_p \tau_{u,p} \epsilon_{ue}} \boldsymbol{\psi}_{k'}^T + \nu_{ue,k'}^p \big) + \nu_{ap,l}^p + \boldsymbol{w}_{p,m,l}[n]. \end{aligned} \tag{3.10}$$

Then, to estimate the channel coefficient for user k at each antenna element l, the received signal $\boldsymbol{y}_{p,m,l}[n]$ is firstly projected on $\boldsymbol{\psi}_k^*$ as follows:

$$\tilde{y}_{p,m,l,k}[n] = \boldsymbol{y}_{p,m,l}[n] \boldsymbol{\psi}_k^*. \tag{3.11}$$

Then, applying MMSE estimation, the estimated channel coefficient for user k will be

$$\hat{g}_{mk,l}[\tau_{u,p}+1] = \mathcal{C}_{m,k,l} \tilde{y}_{p,m,l,k}[n], \tag{3.12}$$

where,

$$\mathcal{C}_{m,k,l} = \frac{\mathbb{E}\big\{ g_{mk,l}^*[\tau_{u,p}+1] \tilde{y}_{p,m,l,k}[n] \big\}}{\mathbb{E}\big\{ \big| \tilde{y}_{p,m,l,k}[n] \big|^2 \big\}}. \tag{3.13}$$

Theorem 3.1. *To find the MMSE channel estimate $\hat{g}_{mk,l}[\tau_{u,p}+1]$ of the channel between user k and antenna l at the m^{th} AP under the hardware distortion and the Doppler shift effects, the term $\mathcal{C}_{m,k,l}$ will be*

$$\mathcal{C}_{m,k,l} = \frac{\sqrt{P_p \tau_{u,p} \epsilon_{ue} \epsilon_{ap}} \alpha_{k,i_k} \beta_{mk}}{\sum_{k'=1}^{K} P_p \tau_{u,p} \beta_{mk'} \big| \boldsymbol{\psi}_{k'}^T \boldsymbol{\psi}_k^* \big|^2 + \sigma_w^2}, \tag{3.14}$$

where i_k represents the symbol index at which user k sends its pilot symbol, where this is a consequence of choosing the pilot sequences from the identity matrix. As the large-scale fading coefficients are identical for different antennas at the same AP, the power of the estimated channel $\hat{g}_{mk,l}[\tau_{u,p}+1]$ will be the same for all antennas belonging to the same AP and can be calculated by

$$\zeta_{mk} = \sqrt{P_p \tau_{u,p} \epsilon_{ue} \epsilon_{ap}} \alpha_{k,i_k} \beta_{mk} \mathcal{C}_{m,k,l}. \tag{3.15}$$

Proof. Firstly, the numerator in (3.13) can be calculated as follows:

$$\mathbb{E}\{g^*_{mk,l}[\tau_{u,p}+1]\tilde{y}_{p,m,l,k}[n]\} = \mathbb{E}\Bigg\{g^*_{mk,l}[\tau_{u,p}+1]\Bigg(\sqrt{\epsilon_{ap}}\sum_{k'=1}^{K}\alpha_{k',i_{k'}}g_{mk',l}[\tau_{u,p}+1] \times \big(\sqrt{P_p\tau_{u,p}\epsilon_{ue}}\boldsymbol{\psi}^T_{k'}+\nu^p_{ue,k'}\big)+\sqrt{\epsilon_{ap}}\sum_{k'=1}^{K}\sqrt{1-\alpha^2_{k',i_{k'}}}z_{mk',l}[n]\big(\sqrt{P_p\tau_{u,p}\epsilon_{ue}}\boldsymbol{\psi}^T_{k'} + \nu^p_{ue,k'}\big)+\nu^p_{ap,l}+\boldsymbol{w}_{p,m,l}[n]\Bigg)\boldsymbol{\psi}^*_k\Bigg\}. \tag{3.16}$$

The distortion component $\nu^p_{ap,l}$ of the antenna element l at the AP can be represented by

$$\nu^p_{ap,l} = \left(P_p\tau_{u,p}(1-\epsilon_{ap})\sum_{k'=1}^{K}\left|g_{mk',l}[n]\right|^2\boldsymbol{\psi}_{k'}(n)\right)^{0.5}\bar{\nu}^p_{ap,l}, \tag{3.17}$$

where $\bar{\nu}^p_{ap,l} \sim \mathcal{CN}(0,1)$. The expression in (3.16) can be decomposed to a summation of different expectations. Since the channels of different users are independent. Besides, the UEs distortion parameter $\nu_{ue,k'}$ and the channel innovation component $z_{mk',l}[n]$ are independent of the channel $g_{mk,l}$. The expression in (3.16) can be rewritten as

$$\mathbb{E}\{g^*_{mk,l}[\tau_{u,p}+1]\tilde{y}_{p,m,l,k}[n]\} = \sqrt{P_p\tau_{u,p}\epsilon_{ap}\epsilon_{ue}}\alpha_{k,i_k}\mathbb{E}\left\{\left|g_{mk,l}[\tau_{u,p}+1]\right|^2\right\}+\mathbb{E}\left\{g^*_{mk,l}\nu^p_{ap,l}\right\}, \tag{3.18}$$

where the second integration in (3.18) can be calculated by

$$\mathbb{E}\{g^*_{mk,l}\nu^p_{ap,l}\} = \mathbb{E}\left\{\mathbb{E}\left\{g^*_{mk,l}\left(P_p\tau_{u,p}(1-\epsilon_{ap})\sum_{k'=1}^{K}\left|g_{mk',l}[n]\right|^2\boldsymbol{\psi}_{k'}(n)\right)^{0.5}\bar{\nu}^p_{ap,l}\middle|g_{mk,l}\right\}\right\}, \tag{3.19}$$

which can be shown to be zero. Hence, (3.16) can be calculated by

$$\mathbb{E}\{g^*_{mk,l}[\tau_{u,p}+1]\tilde{y}_{p,m,l,k}[n]\} = \sqrt{P_p\tau_{u,p}\epsilon_{ue}\epsilon_{ap}}\alpha_{k,i_k}\beta_{mk}. \tag{3.20}$$

Now, it is required to calculate the term $\mathbb{E}\{\left|\tilde{y}_{p,m,l,k}[n]\right|^2\}$ to find the value of $\mathcal{C}_{m,k,l}$. According to the previous discussion, it is noted that all terms in (3.10) are independent. Thus the denominator of (3.13) will be the sum of variances of its terms, which can be easily calculated by

$$\mathbb{E}\{\left|\tilde{y}_{p,m,l,k}[n]\right|^2\} = \sum_{k'=1}^{K}P_p\tau_{u,p}\beta_{mk'}\left|\boldsymbol{\psi}^T_{k'}\boldsymbol{\psi}^*_k\right|^2+\sigma^2_w. \tag{3.21}$$

■

It can be noticed that the channel estimation variance is affected by the quality of the transceivers, the Doppler shift, and non-orthogonal pilot sequences.

3.4 Performance Analysis

In this section, we investigate the DL performance of CF mMIMO and SC systems in-terms of the DL achievable rate under the effect of hardware and channel impairments. CB precoding is adopted for the DL transmission in both systems. Novel expressions to

calculate the spectral efficiency of both systems are introduced, taking into consideration the transceiver hardware distortions and the Doppler shift effect. In addition, we apply two different power control techniques for both systems operation, namely, equal and max-min power allocation.

3.4.1 CF mMIMO System

We analyze the DL performance for the UC approach of CF mMIMO. Then, expressions can be readily adapted for the conventional CF mMIMO system operation. After all APs estimate the corresponding channel coefficients of all users, they treat the estimated channel coefficients at time instant $\tau_{u,p}+1$ as the true channels to perform beamforming for downlink transmission. In UC mMIMO, each AP transmits data only to a subset of users with the best channel conditions [96]. Let us denote $\mathcal{K}(m)$ as the set of users served by the m^{th} AP. Thus, applying CB precoding, the DL precoding vector for user k at the m^{th} AP will be $\hat{\boldsymbol{g}}_{mk}^{*}$ if $k \in \mathcal{K}(m)$ and $\mathbf{0}$ otherwise. Consequently, the transmitted signal from the m^{th} AP at time instant $n > \tau_{u,p}+1$, is given by

$$\boldsymbol{x}_m[n] = \sqrt{P_d \epsilon_{ap}} \sum_{k \in \mathcal{K}(m)} \sqrt{\eta_{mk}} \boldsymbol{g}_{mk}^{*}[\tau_{u,p}+1] s_k[n] + \boldsymbol{\nu}_{ap}^{d}, \tag{3.22}$$

where P_d is the DL power limit of antenna element at the AP, $s_k[n]$ is the transmitted symbol to user k which satisfies $\mathbb{E}\{|s_k[n]|^2\} = 1$. Applying the hardware distortion model in (3.5), the conditional distribution of the transmission distortion at the l^{th} antenna element at AP m, $\nu_{ap,l}^{d}$, will be

$$\nu_{ap,l}^{d} | (\boldsymbol{g}_{mk}, \forall k) \sim \left(0, P_d(1-\epsilon_{ap}) \sum_{k' \in \mathcal{K}(m)} \eta_{mk' } \left| \hat{g}_{mk',l}[\tau_{u,p}+1] \right|^2 \right), \tag{3.23}$$

where η_{mk} denotes the power control coefficient for the transmitted data from AP m to user k, and it is identical for all antenna elements, belonging to the same AP. Besides, the power control coefficients are determined to satisfy the power constraint at each antenna element $\mathbb{E}\{|x_{m,l}[n]|^2\} \leq P_d$. Assuming equal power allocation, the value of η_{mk} that satisfies the power constraint will be

$$\eta_{mk} = \frac{1}{\sum\limits_{k' \in \mathcal{K}(m)} \mathbb{E}\{|\hat{g}_{mk',l}[\tau_{u,p}+1]|^2\}}, \quad \forall k. \tag{3.24}$$

The combined received signal at user k will be

$$r_k[n] = \sqrt{\epsilon_{ue}} \sum_{m=1}^{M} \boldsymbol{g}_{mk}^{T}[n] x_m[n] + \nu_{ue}^{d} + w_k[n], \tag{3.25}$$

where the receiver distortion ν_{ue}^{d} can be modeled by using the hardware distortion model in (3.5) as

$$\nu_{ue}^{d}|(\boldsymbol{g}_{mk}, \forall k) \sim \left(0, (1-\epsilon_{ue})\Big|\sum_{m=1}^{M} \boldsymbol{g}_{mk}^{T}[n]\boldsymbol{x}_{m}[n]\Big|^{2}\right). \tag{3.26}$$

As previously mentioned, in CF mMIMO systems, no DL pilots are transmitted. In addition, the estimated channels are not reported back to the users due to the vast amount of data to be reported. As such, users detect their own signal using their knowledge about the statistics of the estimated channel coefficients $\mathbb{E}\{|\boldsymbol{g}_{mk}^{T}\hat{\boldsymbol{g}}_{mk}^{*}[\tau_{u,p}+1]|\}$. Thus, taking into account the lack of the channel estimation at the user side, and substituting (3.22) in (3.25), the received DL signal at the k^{th} user can be represented by

$$\begin{aligned} r_k[n] = \sqrt{P_d\epsilon_{ap}\epsilon_{ue}}\Bigg[& \underbrace{\alpha_{k,n}\sum_{m\in\mathcal{M}(k)}\sqrt{\eta_{mk}}\mathbb{E}\Big\{\Big|\boldsymbol{g}_{mk}^{T}\hat{\boldsymbol{g}}_{mk}^{*}[\tau_{u,p}+1]\Big|\Big\}s_k[n]}_{\text{desired signal for user } k\ (D_{s_k}^{cf})} \\ & \underbrace{+\alpha_{k,n}\sum_{m\in\mathcal{M}(k)}\sqrt{\eta_{mk}}\Big(\Big|\boldsymbol{g}_{mk}^{T}\hat{\boldsymbol{g}}_{mk}^{*}[\tau_{u,p}+1]\Big| - \mathbb{E}\Big\{\Big|\boldsymbol{g}_{mk}^{T}\hat{\boldsymbol{g}}_{mk}^{*}[\tau_{u,p}+1]\Big|\Big\}\Big)s_k[n]}_{\text{beamforming uncertainty } (BU_k^{cf})} \\ & \underbrace{+\sqrt{1-\alpha_{k,n}^{2}}\sum_{m\in\mathcal{M}(k)}\sqrt{\eta_{mk}}\boldsymbol{z}_{mk}^{T}[n]\hat{\boldsymbol{g}}_{mk}^{*}[\tau_{u,p}+1]s_k[n]}_{\text{Doppler shift effect } (DS_k^{cf})} \\ & + \sum_{k'\neq K}\underbrace{\sum_{m\in\mathcal{M}(k')}\sqrt{\eta_{mk'}}\boldsymbol{g}_{mk}^{T}[n]\hat{\boldsymbol{g}}_{mk'}^{*}[\tau_{u,p}+1]s_{k'}[n]}_{\text{interference from user k' data } (UI_{kk'}^{cf})}\Bigg] + \underbrace{\underbrace{\sqrt{\epsilon_{ue}}\sum_{m=1}^{M}\boldsymbol{g}_{mk}^{T}[n]\boldsymbol{\nu}_{ap}^{d}}_{(HI_{ap}^{d,cf})} + \underbrace{\nu_{ue}^{d}}_{(HI_{ue}^{d,cf})}}_{\text{transceiver hardware distortions}} + \underbrace{w_k[n]}_{\text{noise}}, \end{aligned} \tag{3.27}$$

where $\mathcal{M}(k)$ denotes the set of serving APs for user k. We consider the fact that uncorrelated Gaussian noise represents the worst-case interference [19,21]. Thus, the interference will be the summation of power of different interference components. Applying the use-and-then-forget technique as the channel estimation is not available at the UEs side, the achievable DL rate at user k in CF mMIMO systems under the UC approach can be calculated using (3.28).

$$R_k^{cf}[n] = \log_2\left(1+\frac{|D_{s_k}^{cf}|^2}{\mathbb{E}\{|BU_k^{cf}|^2\}+\mathbb{E}\{|DS_k^{cf}|^2\}+\sum\limits_{k'\neq k}\mathbb{E}\{|UI_{kk'}^{cf}|^2\}+\mathbb{E}\{|HI_{ap}^{d,cf}|^2\}+\mathbb{E}\{|HI_{ue}^{d,cf}|^2\}+\sigma_w^2}\right), \tag{3.28}$$

Theorem 3.2. *The achievable DL data rate for user k at time instant n in CF mMIMO*

systems under the effect of transceiver hardware distortions and Doppler shift effect is given by

$$R_k^{cf}[n] = \log_2\left(1 + \frac{A_{d,k}^{cf}}{B_{d,k}^{cf} + C_{d,k}^{cf} + D_{d,k}^{cf} + E_{d,k}^{cf} + \sigma_w^2}\right), \tag{3.29}$$

where

$$\begin{aligned}
A_{d,k}^{cf} =& \alpha_{k,n}^2 P_d \epsilon_{ap}\epsilon_{ue}\Big(\sum_{m\in\mathcal{M}(k)} \sqrt{\eta_{mk}} N_{ap}\zeta_{mk}\Big)^2, \quad B_{d,k}^{cf} = P_d \sum_{k'=1}^{K}\sum_{m\in\mathcal{M}(k')} N_{ap}\eta_{mk'}\zeta_{mk'}\beta_{mk},\\
C_{d,k}^{cf} =& \alpha_{k,n}^2 P_d \frac{(1-\epsilon_{ap}^2\epsilon_{ue})}{\epsilon_{ap}\epsilon_{ue}} \sum_{k'=1}^{K}\sum_{m\in\mathcal{M}(k')} N_{ap}\eta_{mk'}\beta_{mk'}\zeta_{mk'}^2\left(\frac{\beta_{mk}}{\beta_{mk'}}\right)^2 |\boldsymbol{\psi}_k\boldsymbol{\psi}_{k'}^{\mathsf{H}}|^2,\\
D_{d,k}^{cf} =& \alpha_{k,n}^2 P_d \frac{\epsilon_{ap}}{\epsilon_{ue}} \sum_{k'\neq K}\Big(\sum_{m\in\mathcal{M}(k')} \sqrt{\eta_{mk'}} N_{ap}\zeta_{mk'}\frac{\beta_{mk}}{\beta_{mk'}}\Big)^2 |\boldsymbol{\psi}_k\boldsymbol{\psi}_{k'}^{\mathsf{H}}|^2,\\
E_{d,k}^{cf} =& \alpha_{k,n}^2 P_d\Big(\frac{\epsilon_{ap}}{\epsilon_{ue}} - \epsilon_{ap}\epsilon_{ue}\Big)\Big(\sum_{m\in\mathcal{M}(k)} \sqrt{\eta_{mk}} N_{ap}\zeta_{mk}\Big)^2.
\end{aligned}$$

Proof. The power of different signal components in (3.27) can be calculated as follows. Firstly, the desired signal power can be calculated by

$$\begin{aligned}
|D_{s_k}^{cf}|^2 =& \alpha_{k,n}^2 P_d \epsilon_{ap}\epsilon_{ue}\Big(\sum_{m\in\mathcal{M}(k)} \sqrt{\eta_{mk}}\mathbb{E}\Big\{\Big|\boldsymbol{g}_{mk}^T[n]\hat{\boldsymbol{g}}_{mk}^*[\tau_{u,p}+1]\Big|\Big\}\Big)^2,\\
=& \alpha_{k,n}^2 P_d \epsilon_{ap}\epsilon_{ue}\Big(\sqrt{\eta_{mk}}\mathbb{E}\Big\{\Big|\big(\hat{\boldsymbol{g}}_{mk}^T[\tau_{u,p}+1] + \tilde{\boldsymbol{g}}_{mk}^T[\tau_{u,p}+1] + \boldsymbol{z}_{mk}^T[n]\big)\hat{\boldsymbol{g}}_{mk}^*[\tau_{u,p}+1]\Big|\Big\}\Big)^2,\\
=& \alpha_{k,n}^2 P_d \epsilon_{ap}\epsilon_{ue}\Big(\sqrt{\eta_{mk}}\mathbb{E}\Big\{\Big|\hat{\boldsymbol{g}}_{mk}^T\hat{\boldsymbol{g}}_{mk}^*[\tau_{u,p}+1]\Big|\Big\}\Big)^2,\\
=& \alpha_{k,n}^2 P_d \epsilon_{ap}\epsilon_{ue}\Big(\sum_{m\in\mathcal{M}(k)} \sqrt{\eta_{mk}} N_{ap}\zeta_{mk}\Big)^2,
\end{aligned} \tag{3.30}$$

Then, the interference power due to beamforming uncertainly power can be calculated as follows:

$$\begin{aligned}
\mathbb{E}\{|BU_k^{cf}|^2\} =& \alpha_{k,n}^2 P_d \epsilon_{ap}\epsilon_{ue}\sum_{m\in\mathcal{M}(k)} N_{ap}\eta_{mk}\zeta_{mk}\beta_{mk} + \alpha_{k,n}^2 P_d(1-\epsilon_{ap})\\
&\times \sum_{m\in\mathcal{M}(k)} N_{ap}\eta_{mk}\zeta_{mk}^2 + \alpha_{k,n}^2 P_d\epsilon_{ap}(1-\epsilon_{ue})\Big(\sum_{m\in\mathcal{M}(k)} \sqrt{\eta_{mk}} N_{ap}\zeta_{mk}\Big)^2.
\end{aligned} \tag{3.31}$$

The power of the interference component due to the Doppler shift effect is given by

$$\mathbb{E}\{|DS_k^{cf}|^2\} = P_d\epsilon_{ap}\epsilon_{ue}(1-\alpha_n^2)\sum_{m\in\mathcal{M}(k)} N_{ap}\eta_{mk}\zeta_{mk}\beta_{mk}, \tag{3.32}$$

The interference power due to the transmitted signals to other users is given by

$$\begin{aligned}
\mathbb{E}\{|UI_{kk'}^{cf}|^2\} =& P_d\epsilon_{ap}\epsilon_{ue}\sum_{m\in\mathcal{M}(k')} N_{ap}\eta_{mk'}\zeta_{mk'}\beta_{mk} + \alpha_{k,n}^2 P_d\epsilon_{ap}\Big(\sum_{m\in\mathcal{M}(k')} \sqrt{\eta_{mk'}} N_{ap}\zeta_{mk'}\\
&\times \frac{\beta_{mk}}{\beta_{mk'}}\Big)^2 |\Psi_k\Psi_{k'}^{\mathsf{H}}|^2 + \alpha_{k,n}^2 P_d(1-\epsilon_{ap})\sum_{m\in\mathcal{M}(k')} N_{ap}\eta_{mk'}\zeta_{mk'}^2\left(\frac{\beta_{mk}}{\beta_{mk'}}\right)^2 |\boldsymbol{\psi}_k\boldsymbol{\psi}_{k'}^{\mathsf{H}}|^2,
\end{aligned} \tag{3.33}$$

The interference power due to the APs hardware impairments is given by

$$\mathbb{E}\{|HI_{ap}^{d,cf}|^2\} = \mathbb{E}\Big\{\Big|\sum_{m=1}^{M} \boldsymbol{g}_{mk}^T[n]\boldsymbol{\nu}_{ap}^d\Big|^2\Big\}. \tag{3.34}$$

hen, using the conditional model of $\boldsymbol{\nu}_{ap}^d$ on the channel conditions, (3.34) can be rewritten as

$$\mathbb{E}\{|HI_{ap}^{d,cf}|^2\} = \mathbb{E}\Bigg\{\Bigg|\sum_{m=1}^{M} \boldsymbol{g}_{mk}^T[n]\Bigg(P_d(1-\epsilon_{ap})\sum_{k'\in\mathcal{K}(m)}\eta_{mk'}\big|\hat{\boldsymbol{g}}_{mk'}[\tau_{u,p}+1]\big|^2\Bigg)^{0.5}\bar{\boldsymbol{\nu}}_{ap}^d\Bigg|^2\Bigg\}, \tag{3.35}$$

where $\bar{\boldsymbol{\nu}}_{ap}^d \sim \mathcal{CN}(\mathbf{0}, \boldsymbol{I}_{N_{ap}})$, and this random variable is independent from the channel conditions and the transmitted signal. Hence, the expectation in (3.35) is given by

$$\mathbb{E}\{|HI_{ap}^{d,cf}|^2\} = \mathbb{E}\Bigg\{\mathbb{E}\Bigg\{\Bigg|\sum_{m=1}^{M} \boldsymbol{g}_{mk}^T[n]\Bigg(P_d(1-\epsilon_{ap})\sum_{k'\in\mathcal{K}(m)}\eta_{mk'}\big|\hat{\boldsymbol{g}}_{mk'}[\tau_{u,p}+1]\big|^2\Bigg)^{0.5}\bar{\boldsymbol{\nu}}_{ap}^d\Bigg|^2\Bigg|\boldsymbol{g}_{mk}\Bigg\}\Bigg\}, \tag{3.36}$$

which can be calculated by

$$\begin{aligned}\mathbb{E}\{|HI_{ap}^{d,cf}|^2\} &= \mathbb{E}\Bigg\{\sum_{m=1}^{M} P_d(1-\epsilon_{ap})\big|\boldsymbol{g}_{mk}^T[n]\big|^2\sum_{k'\in\mathcal{K}(m)}\eta_{mk'}\big|\hat{\boldsymbol{g}}_{mk'}[\tau_{u,p}+1]\big|^2\Bigg\}\\ &= \sum_{k'=1}^{K}\sum_{m\in\mathcal{M}(k')} P_d\epsilon_{ue}(1-\epsilon_{ap})N_{ap}\eta_{mk'}\zeta_{mk'}\beta_{mk}\\ &+ \sum_{k'=1}^{K}\sum_{m\in\mathcal{M}(k')}\alpha_n^2 P_d\frac{(1-\epsilon_{ap})}{\epsilon_{ap}}N_{ap}\eta_{mk'}\zeta_{mk'}\left(\frac{\beta_{mk}}{\beta_{mk'}}\right)^2|\boldsymbol{\psi}_k\boldsymbol{\psi}_{k'}^{\mathsf{H}}|^2.\end{aligned} \tag{3.37}$$

For the power of the receiver distortion at the UEs side, it can be calculated by

$$\mathbb{E}\{|HI_{ue}^{d,cf}|^2\} = \mathbb{E}\Bigg\{\mathbb{E}\Bigg\{\Bigg|\Big((1-\epsilon_{ue})\Big|\sum_{m=1}^{M}\boldsymbol{g}_{mk}^T[n]\boldsymbol{x}_m[n]\Big|^2\Big)^{0.5}\bar{\nu}_{ue}^d\Bigg|^2\Bigg|\boldsymbol{g}_{mk}\Bigg\}\Bigg\}, \tag{3.38}$$

where $\bar{\nu}_{ue}^d \sim \mathcal{CN}(0,1)$. Hence, the expectation in (3.38) can be rewritten as

$$\begin{aligned}\mathbb{E}\{|HI_{ue}^{d,cf}|^2\} &= \mathbb{E}\Bigg\{(1-\epsilon_{ue})\Big|\sum_{m=1}^{M}\boldsymbol{g}_{mk}^T[n]\boldsymbol{x}_m[n]\Big|^2\Bigg\},\\ &= \mathbb{E}\Bigg\{(1-\epsilon_{ue})\Bigg|\sum_{m=1}^{M}\boldsymbol{g}_{mk}^T[n]\Bigg(\sqrt{P_d\epsilon_{ap}}\sum_{k'\in\mathcal{K}(m)}\sqrt{\eta_{mk'}}\hat{\boldsymbol{g}}_{mk'}^*[\tau_{u,p}+1]s_{k'}[n]\\ &+ \Bigg(P_d(1-\epsilon_{ap})\sum_{k'\in\mathcal{K}(m)}\eta_{mk'}\big|\hat{\boldsymbol{g}}_{mk'}[\tau_{u,p}+1]\big|^2\Bigg)^{0.5}\bar{\boldsymbol{\nu}}_{ap}^d\Bigg)\Bigg|^2\Bigg)\Bigg\}.\end{aligned} \tag{3.39}$$

Since the transmitted signal $s_k[n]$ and the AP distortion are independent, the power of the UEs distortion is expressed by

$$\begin{aligned}\mathbb{E}\{|HI_{ue}^{d,cf}|^2\} = (1-\epsilon_{ue})\Bigg(&\mathbb{E}\Bigg\{P_d\epsilon_{ap}\sum_{k'=1}^{K}\Bigg|\sum_{m\in\mathcal{M}(k')}\sqrt{\eta_{mk'}}\boldsymbol{g}_{mk}^T[n]\hat{\boldsymbol{g}}_{mk'}^*[\tau_{u,p}+1]\Bigg|^2\\ &+ P_d(1-\epsilon_{ap})\sum_{k'=1}^{K}\sum_{m\in\mathcal{M}(k')}\eta_{mk'}\big|\boldsymbol{g}_{mk}^T[n]\big|^2\big|\hat{\boldsymbol{g}}_{mk'}[\tau_{u,p}+1]\big|^2\Bigg\}\Bigg),\end{aligned} \tag{3.40}$$

which can be calculated as follows:

$$\mathbb{E}\{|HI_{ue}^{cf,d}|^2\} = P_d(1-\epsilon_{ue})\sum_{k'=1}^{K}\sum_{m\in\mathcal{M}(k')} N_{ap}\eta_{mk'}\zeta_{mk'}\beta_{mk}$$
$$+ \alpha_{k,n}^2 P_d \frac{\epsilon_{ap}(1-\epsilon_{ue})}{\epsilon_{ue}}\sum_{k'=1}^{K}\Big(\sum_{m\in\mathcal{M}(k')}\sqrt{\eta_{mk'}}N_{ap}\zeta_{mk'}\frac{\beta_{mk}}{\beta_{mk'}}\Big)^2|\boldsymbol{\psi}_k\boldsymbol{\psi}_{k'}^{\mathsf{H}}|^2 \quad (3.41)$$
$$+ \alpha_{k,n}^2 P_d \frac{(1-\epsilon_{ue})}{(\epsilon_{ap}\epsilon_{ue})}\sum_{k'=1}^{K}\sum_{m\in\mathcal{M}(k')} N_{ap}\eta_{mk'}\zeta_{mk'}^2\left(\frac{\beta_{mk}}{\beta_{mk'}}\right)^2|\boldsymbol{\psi}_k\boldsymbol{\psi}_{k'}^{\mathsf{H}}|^2.$$

Note that the derived expressions for different interference sources have common terms which can be combined to simplify the expression for the DL achievable rate. After combining the common terms in (3.31)-(3.33), (3.37), and (3.41) by applying some mathematical manipulations, the proof can be readily completed. ■

After calculating the achievable DL rate at each time symbol n, the average achievable DL rate over a coherence time interval τ_c will be

$$\bar{R}_k^{cf} = \frac{1}{\tau_c}\sum_{n=\tau_{u,p}+1}^{\tau_c} R_k^{cf}[n]. \quad (3.42)$$

Max-Min Power Allocation: To improve the DL performance of CF mMIMO systems, max-min power allocation is adopted for the system operation. Different from equal power control, under max-min power allocation, the transmitted power for different users from each AP are adjusted in a way that attains fairness in the achievable DL rates of different users. The fairness here denotes preserving the achievable DL rate of all users above a certain threshold that is required to be maximized. Note that, the total transmitted power from each AP should be less than or equal to the maximum transmit power to satisfy the power constraints. We consider that power control coefficients are the same during the whole coherence block since it depends on the large scale fading coefficients. Thus, we do not account for the aging effect in determining the power control coefficients as it changes from one symbol to another and this will significantly increase the backhaul overhead of the system. As such, the max-min optimization problem for CF mMIMO systems can be formulated as

$$\max_{\eta_{mk}} \min_{k=1,\ ...,\ K} \quad R_k^{cf}$$
$$\text{s.t.} \sum_{k\in\mathcal{K}(m)} \eta_{mk}\zeta_{mk} \le 1, \quad m = 1,\ \ldots,\ M. \quad (3.43)$$
$$\eta_{mk} \ge 0, \quad m = 1,\ \ldots,\ M, \quad k \in \mathcal{K}(m).$$

By introducing slack variables λ_m, $\delta_{kk'}, \phi_{kk'}$, and θ_k, and define $w_{mk} \triangleq \eta_{mk}^{\frac{1}{2}}$, the problem

can be rewritten as

$$\max_{\{\lambda_m,\delta_{kk'},\phi_{kk'},\theta_k\}} \min_{k=1,\ ...,\ K} \quad \gamma_k^{cf} \tag{3.44a}$$

$$\begin{aligned}
\text{s.t.} \sum_{m\in\mathcal{M}(k')} & \sqrt{N_{ap}} w_{mk'}\zeta_{mk'}\frac{\beta_{mk}}{\beta_{mk'}} \leq \delta_{kk'}, \quad \forall k' \neq k \\
& \sum_{k'\in\mathcal{K}(m)} w_{mk'}^2\zeta_{mk'} \leq \lambda_m^2, \quad \forall m = 1,\ \ldots,\ M \\
& \sum_{m\in\mathcal{M}(k')} w_{mk'}^2\zeta_{mk'}^2\left(\frac{\beta_{mk}}{\beta_{mk'}}\right)^2 \leq \phi_{kk'}, \quad k' = 1,\ \ldots,\ K \\
& \sum_{m\in\mathcal{M}(k)} \sqrt{N_{ap}} w_{mk}\zeta_{mk} \leq \theta_k, \quad \theta_k \geq 0, \quad k = 1,\ \ldots,\ K \\
& \delta_{kk'} \geq 0, \quad \forall k' \neq k, \quad 0 \leq \lambda_m \leq 1, \quad \forall m = 1,\ \ldots,\ M, \\
& \phi_{kk'} \geq 0, k, \quad \phi_{kk'} \geq 0, k, k' = 1, \ldots, K,
\end{aligned} \tag{3.44b}$$

where γ_k^{cf} denotes the corresponding signal-to-interference-plus-noise-ratio (SINR) for user k. The problem in (3.44) is quasi-concave which can be solved efficiently by a bisection search, in each step solving a sequence of convex feasibility problems [97] as illustrated in Algorithm 3.1. It is noteworthy that all the obtained expressions for the UC approach can be adapted to the conventional CF mMIMO system by setting the number of served users by each AP to K, i.e., $\mathcal{K}(m) = 1, \cdots, K, \forall m$.

3.4.2 SC System

We consider a SC system where each user is served by one AP that serves only one user at a time. In that, each user k is served by the available AP with the maximum large scale fading coefficient $\beta_{m_k k}$, where the AP selection process is carried out in random sequential order.

$$m_k \triangleq arg \max_{m\in AvailableAPs} \beta_{mk}. \tag{3.46}$$

After the AP selection process is performed, the non-selected APs are turned off to limit the interference in the network. We refer to the set of active APs selected for serving the users during the AP selection process by $\dot{\mathcal{A}}$. Besides, we consider a short enough time scale so that handovers between APs do not occur. Furthermore, since APs are equipped with multiple-antennas. Thus, different from previous works such as [21], CB precoding is applied for DL data transmission. Then, each user decodes the transmitted DL data symbols using the knowledge of the instantaneous channel conditions with its serving AP.

Algorithm 3.1: Bisection Algorithm for solving (3.44)

1. Initialization: choose the initial values of $t_{min} = 0$ and $t_{max} = \max(SINR_1, \cdots, SINR_K)$ define a range of relevant values of the objective function in (3.44). Choose a small positive-valued tolerance ς.

2. Set $t := \frac{t_{min}+t_{max}}{2}$, and solve a convex feasibility program including (3.44b) and (3.45) to find the values of $w_{mk}, \quad \forall m = 1, \ \ldots, \ M, \ k \in \mathcal{K}(m)$.

$$\|\mathbf{v}_k\| \leq \frac{1}{\sqrt{t}} \sqrt{\epsilon_{ap}\epsilon_{ue}} \sum_{m \in \mathcal{M}(k)} w_{mk}\zeta_{mk}, k = 1, \ldots, K, \tag{3.45}$$

   where, $\mathbf{v} \triangleq \left[\mathbf{v}_{k1}^T \boldsymbol{I}_{-\boldsymbol{k}} \ \ \mathbf{v}_{k2}^T \ \mathbf{v}_{k3}^T \ \ v_{k4} \ \ \frac{\sigma_w^2}{p_d^l N_{ap}}\right]$, $\mathbf{v}_{k1} \triangleq \sqrt{\frac{\epsilon_{ap}}{\epsilon_{ue}}} \times \left[\boldsymbol{\psi}_k \boldsymbol{\psi}_1^{\mathsf{H}} \delta_{k1} \ldots \boldsymbol{\psi}_k \boldsymbol{\psi}_K^{\mathsf{H}} \delta_{kK}\right]^T$, $\boldsymbol{I}_{-\boldsymbol{k}}$ is a $K \times (K-1)$ matrix obtained from the $K \times K$ identity matrix with the k^{th} column removed, $\mathbf{v}_{k2}^T \triangleq \left[\sqrt{\beta_{1k}}\lambda_1 \ldots \sqrt{\beta_{Mk}}\lambda_M\right]^T$, $\mathbf{v}_{k3}^T \triangleq \sqrt{\frac{1-\epsilon_{ap}^2\epsilon_{ue}}{\epsilon_{ap}\epsilon_{ue}}} \times \left[\boldsymbol{\psi}_k \boldsymbol{\psi}_1^{\mathsf{H}} \phi_{k1} \ldots \boldsymbol{\psi}_k \boldsymbol{\psi}_K^{\mathsf{H}} \phi_{kK}\right]^T$, and the scalar parameter $v_{k4} \triangleq \sum_{m \in \mathcal{M}(k)} \sqrt{N_{ap}} w_{mk}\zeta_{mk}$.

3. If problem (3.45) is feasible, then set $t_{min} = t$, else set $t_{max} = t$.

4. Stop if $t_{max} - t_{min} < \varsigma$. Otherwise, go to Step 2,

Note that, the channel conditions at the user side can be identified either by sending DL training sequences or through feedback of the estimated channel conditions from the serving APs. Hence, the received DL signal at user k will be
$r_k[n] =$

$$\sqrt{P_d\epsilon_{ap}\epsilon_{ue}}\Bigg[\underbrace{\alpha_{k,n}\sqrt{\eta_{m_k}}\boldsymbol{g}_{m_kk}^T[n]\hat{\boldsymbol{g}}_{m_kk}^*[\tau_{u,p}+1]s_k[n]}_{\text{desired signal for user } k \ (D_{s_k}^{sc})} + \sum_{k' \neq K} \underbrace{\sqrt{\eta_{m_{k'}}}\boldsymbol{g}_{m_{k'}k}^T[n]\hat{\boldsymbol{g}}_{m_{k'}k'}^*[\tau_{u,p}+1]s_{k'}[n]}_{\text{interference from user k' data}(UI_{kk'}^{sc})}$$

$$+ \underbrace{\sqrt{\eta_{m_k}(1-\alpha_{k,n}^2)}\boldsymbol{z}_{m_kk}^T[n]\hat{\boldsymbol{g}}_{m_kk}^*[\tau_{u,p}+1]s_k[n]}_{\text{Doppler shift effect}(DS_k^{sc})}\Bigg] + \underbrace{\underbrace{\sqrt{\epsilon_{ue}}\sum_{m \in \dot{\mathcal{A}}} \boldsymbol{g}_{mk}^T[n]\boldsymbol{\nu}_{ap}^d s_k[n]}_{HI_{ap}^{d,sc}} + \underbrace{\nu_{ue}^d}_{HI_{ue}^{d,sc}}}_{\text{transceiver hardware distortions}} + \underbrace{w_k[n]}_{\text{noise}}, \tag{3.47}$$

where η_{m_k} denotes the power control coefficient at the serving AP of user k. This coefficient will be set to satisfy the power constraint at the AP $\eta_{m_k}\zeta_{m_kk} \leq 1$. Besides, we assume that each active AP transmits data with its full power where the power control coefficient for the serving AP of user k is set to $\eta_{m_k} = \frac{1}{\zeta_{m_kk}}$. In what follows, we refer to

this power control technique as equal power control since each AP serves the associated user with full power.

To find the DL achievable rate for SC systems, we apply the same approach used in [21] where all sources of interference are assumed to be uncorrelated since this assumption represents the worst-case interference. As such, the DL achievable rate for user k in SC systems can be obtained as follows:

$$R_k^{sc}[n] = \mathbb{E}\left\{ \log_2 \left(1 + \frac{|D_{s_k}^{sc}|^2}{\mathbb{E}\{|DS_k^{sc}|^2\} + \sum\limits_{k' \neq k} \mathbb{E}\{|UI_{kk'}^{sc}|^2\} + \mathbb{E}\{|HI_{ap}^{sc,d}|^2\} + \mathbb{E}\{|HI_{ue}^{sc,d}|^2\} + \sigma_w^2} \right) \right\}, \tag{3.48}$$

Then, using Jensen's inequality, an upper bound of the DL achievable rate can be obtained by

$$\breve{R}_k^{sc}[n] = \log_2 \left(1 + \frac{\mathbb{E}\{|D_{s_k}^{sc}|^2\}}{\mathbb{E}\{|DS_k^{sc}|^2\} + \sum\limits_{k' \neq k} \mathbb{E}\{|UI_{kk'}^{sc}|^2\} + \mathbb{E}\{|HI_{ap}^{sc,d}|^2\} + \mathbb{E}\{|HI_{ue}^{sc,d}|^2\} + \sigma_w^2} \right), \tag{3.49}$$

Fig. 3.3 compares the upper bound of the achievable DL rates in (3.49) with the exact one in (3.48). Two different number of users $K = 20,\ 40$ are considered and non-orthogonal pilot sequences of length $\tau_{u,p} = 10$ are adopted for the sake of channel estimation. It is noted that the proposed bound is a tight bound of the achievable DL rates in SC systems. As such, in the sequel, we focus on the proposed upper bound and a closed-form expression to find this upper bound is given in the next theorem.

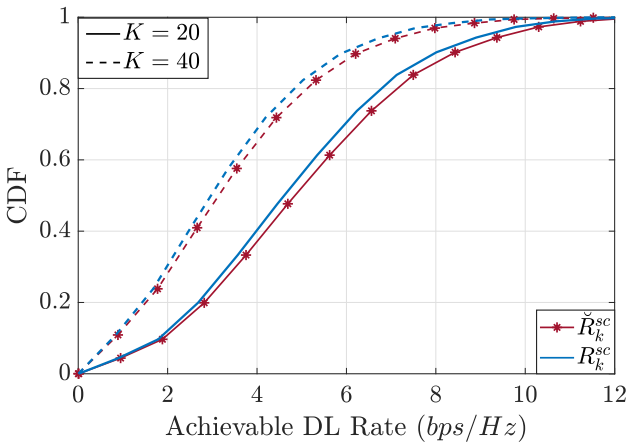

Figure 3.3: Exact DL rate and upper bound of the achievable DL rate in SC systems ($M = 100$ *and* $N_{ap} = 4$).

Theorem 3.3. *A tight upper bound of the achievable DL data rate for user k at time*

instant n in SC systems is expressed by

$$R_k^{sc}[n] = \log_2\left(1 + \frac{A_{d,k}^{sc}}{B_{d,k}^{sc} + C_{d,k}^{sc} + D_{d,k}^{sc} + \sigma_w^2}\right), \tag{3.50}$$

where

$$\begin{aligned}
A_{d,k}^{sc} =&\ \alpha_{k,n}^2 P_d \epsilon_{ap}\epsilon_{ue} N_{ap}\eta_{m_k}\beta_{m_k k}\zeta_{m_k k} + \alpha_{k,n}^2 P_d \eta_{m_k}\zeta_{m_k k}^2\big(\epsilon_{ap}N_{ap}^2 + (1-\epsilon_{ap})N_{ap}\big),\\
B_{d,k}^{sc} =&\ P_d \sum_{k'=1}^{K} N_{ap}\eta_{m_{k'}}\zeta_{m_{k'}k'}\beta_{m_{k'}k},\\
C_{d,k}^{sc} =&\ \alpha_{k,n}^2 P_d\big(N_{ap}^2\epsilon_{ap}^2 + N_{ap}(1-\epsilon_{ap}^2)\big)\sum_{k'\neq k}\eta_{m_{k'}}\zeta_{m_{k'}k'}^2\left(\frac{\beta_{m_{k'}k}}{\beta_{m_{k'}k'}}\right)^2|\boldsymbol{\psi}_k\boldsymbol{\psi}_{k'}^{\mathsf{H}}|^2,\\
D_{d,k}^{sc} =&\ P_d(1-\alpha_{k,n}^2\epsilon_{ap}\epsilon_{ue})N_{ap}\eta_{m_k}\beta_{m_k k}\zeta_{m_k k} + \alpha_{k,n}^2 P_d N_{ap}\zeta_{m_k k}^2\left(\frac{\beta_{m_{k'}k}}{\beta_{m_{k'}k'}}\right)^2|\boldsymbol{\psi}_k\boldsymbol{\psi}_{k'}^{\mathsf{H}}|^2\\
&\times\left(\frac{N_{ap}^2(\epsilon_{ap}^2 - \epsilon_{ap}^2\epsilon_{ue}) + N_{ap}\big(1-\epsilon_{ue}\epsilon_{ap}-\epsilon_{ap}^2+\epsilon_{ue}\epsilon_{ap}^2\big)}{\epsilon_{ue}\epsilon_{ap}}\right).
\end{aligned}$$

Proof. The power of different signal components in (3.47) can be calculated as follows. Firstly, the desired signal power can be calculated by

$$\mathbb{E}\{|D_{s_k}^{sc}|^2\} = \alpha_{k,n}^2\Big(P_d\epsilon_{ap}\epsilon_{ue}N_{ap}\eta_{m_k}\zeta_{m_k k}\beta_{m_k k} + P_d\big(\epsilon_{ap}N_{ap}^2 + N_{ap}(1-\epsilon_{ap})\big)\eta_{m_k}\zeta_{m_k k}^2\Big), \tag{3.51}$$

The power of the interference component due to the Doppler shift effect is given by

$$\mathbb{E}\{|DS_k^{sc}|^2\} = P_d\epsilon_{ap}\epsilon_{ue}(1-\alpha_{k,n}^2)N_{ap}\eta_{m_k}\zeta_{m_k k}\beta_{m_k k}, \tag{3.52}$$

The interference power due to the transmitted signals to other users is given by

$$\begin{aligned}
\mathbb{E}\{|UI_{kk'}^{sc}|^2\} =&\ P_d\epsilon_{ap}\epsilon_{ue}N_{ap}\eta_{m_{k'}}\zeta_{m_{k'}k'}\beta_{m_{k'}k} + \alpha_n^2 P_d\Big(\epsilon_{ap}N_{ap}^2 + N_{ap}(1-\epsilon_{ap})\Big)\\
&\times\eta_{m_{k'}}\zeta_{m_{k'}k'}^2\left(\frac{\beta_{m_{k'}k}}{\beta_{m_{k'}k'}}\right)^2|\boldsymbol{\psi}_k\boldsymbol{\psi}_{k'}^{\mathsf{H}}|^2.
\end{aligned} \tag{3.53}$$

Following the same steps as in CF mMIMO systems, the transceiver hardware impairments of APs and UEs in SC systems can be obtained as follows:

$$\begin{aligned}
\mathbb{E}\{|HI_{ap}^{sc,d}|^2\} =&\sum_{k'=1}^{K} P_d\epsilon_{ue}(1-\epsilon_{ap})N_{ap}\eta_{m_{k'}}\zeta_{m_{k'}k'}\beta_{m_{k'}k}\\
&+\sum_{k'=1}^{K}\alpha_n^2 P_d\frac{(1-\epsilon_{ap})}{\epsilon_{ap}}N_{ap}\eta_{m_{k'}}\zeta_{m_{k'}k'}\left(\frac{\beta_{m_{k'}k}}{\beta_{m_{k'}k'}}\right)^2|\boldsymbol{\psi}_k\boldsymbol{\psi}_{k'}^{\mathsf{H}}|^2.
\end{aligned} \tag{3.54}$$

$$\begin{aligned}
\mathbb{E}\{|HI_{ue}^{sc,d}|^2\} =&\ P_d(1-\epsilon_{ue})\sum_{k'=1}^{K}N_{ap}\eta_{mk'}\zeta_{mk'}\beta_{mk} + \alpha_n^2 P_d\frac{1}{\epsilon_{ap}\epsilon_{ue}}\Big(N_{ap}^2\epsilon_{ap}^2(1-\epsilon_{ue})\\
&+N_{ap}\big((1-\epsilon_{ue})(1-\epsilon_{ap}^2)\big)\Big)\sum_{k'=1}^{K}\eta_{m_{k'}}\zeta_{m_{k'}k'}^2\left(\frac{\beta_{m_{k'}k}}{\beta_{m_{k'}k'}}\right)^2|\boldsymbol{\psi}_k\boldsymbol{\psi}_{k'}^{\mathsf{H}}|^2.
\end{aligned} \tag{3.55}$$

Then, by combining the common terms in (3.52)-(3.55) to simplify the expression of the achievable DL rate, the proof can be readily completed by some mathematical manipulations. ■

After calculating the achievable DL rate at each time symbol n, the average achievable

DL rate over a coherence time interval τ_c will be

$$\bar{R}_k^{sc} = \frac{1}{\tau_c} \sum_{n=\tau_{u,p}+1}^{\tau_c} R_k^{sc}[n]. \tag{3.56}$$

Max-Min Power Allocation: Aiming at attaining fairness in the achievable DL rates by maximizing the achievable DL rate of the user in the worst channel conditions, we consider applying max-min power allocation for the SC system operation where the problem can be formulated by

$$\begin{aligned} &\max_{\eta_{m_k}} \min_{k=1,\ ...,\ K} \quad R_k^{sc} \\ &s.t.\ \ \eta_{m_k}\zeta_{m_k k} \leq 1, \quad m = 1,\ \ldots,\ M. \\ &\eta_{m_k} \geq 0, \quad k = 1,\ \ldots,\ K. \end{aligned} \tag{3.57}$$

It can be noted that the problem is a special case of the CF mMIMO problem where each user will receive its DL data symbols from only one AP. Besides, the max-min problem in (3.57) is a quasi-linear problem which can be solved using a bisection algorithm.

3.5 Discussions and Numerical Results

3.5.1 Simulation Setup

We consider a network with M APs and K users where both APs and users are uniformly distributed in a square area of size 0.5×0.5 km^2. The carrier frequency $f_c = 2$ GHz. The pilot transmission power P_p and DL data transmission power P_d are 100, 200 mW, respectively. The APs and UEs heights are set to $\hbar_{ap} = 15$m and $\hbar_{ue} = 1.65$m, respectively. The noise variance is denoted by $\sigma_w^2 = 290 \times \kappa \times B \times NF$ where κ is the Boltzman constant, $B =$ 20 MHz, denoting the system bandwidth, and $NF =$ 9 dB is the noise figure. We consider a long coherence time interval $\tau_c = 1000$ samples, corresponding to low-velocity scenarios, and the effect of the presence of high-velocity users on the system performance will be revealed.

3.5.2 Ideal Scenario

Fig. 3.4 compares the cumulative distribution function (CDF) of the achievable DL rates of SC systems and CF mMIMO systems in the absence of hardware and channel impairments. The comparison is carried out under equal and max-min power allocation techniques. Moreover, it is assumed that 100 APs are uniformly distributed in the cell, where each AP is equipped with 4 antennas. Besides, two different users configurations

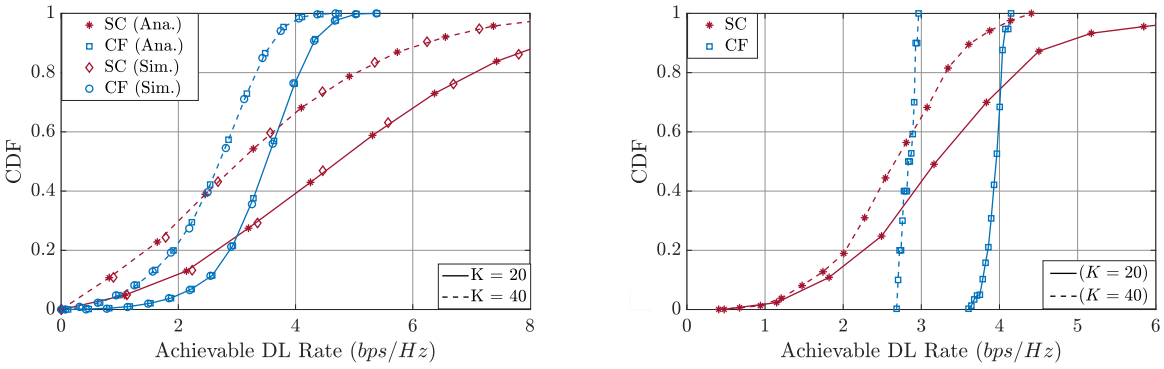

(a) Equal power allocation

(b) Max-min power allocation

Figure 3.4: CDF comparison between conventional CF mMIMO and SC systems under ideal hardware components and channel conditions.

are considered with 20 users and 40 users. As noted from the results, both simulations and analytical results are in excellent agreement at different scenarios. Besides, It is noted that the achievable DL rates in SC systems are superior for the majority of users under equal power allocation. In addition, as the number of users decreases, the performance of both systems improves, and the SC system becomes preferable to a higher portion of users. On the other hand, when applying max-min power allocation, the CF mMIMO system exploits the advantage of serving all users by all APs to adjust the power control coefficients to achieve a uniformly good service for all users over the coverage area. However, when applying max-min power allocation technique in SC system, the system strives to improve the achievable rates of users in poor channel conditions at the cost of decreasing the achievable rates of users in good channel conditions. As a consequence, under max-min power allocation, the CF mMIMO system becomes the preferred system for the vast majority of the users.

Fig. 3.5 compares the CDF of the achievable DL rates of conventional CF and UC mMIMO systems, assuming 100 multiple-antennas APs ($N_{ap} = 4$), and 20 users are uniformly distributed through the cell. For the UC mMIMO approach, APs are assumed to communicate with different numbers of users, namely, $\mathcal{T} = 2,\ 4$, and 6 users. Notably, assuming that each AP serves a small number of users i.e., $\mathcal{T} = 2$, under equal power allocation degrades the UC mMIMO performance. However, increasing the number of served users by each AP to $\mathcal{T} = 4,\ 6$, improves the achievable DL rates significantly, and it becomes identical to the achievable DL rates in CF mMIMO systems. On the other hand, assuming system operation under max-min power allocation, Fig. 3.5b reveals

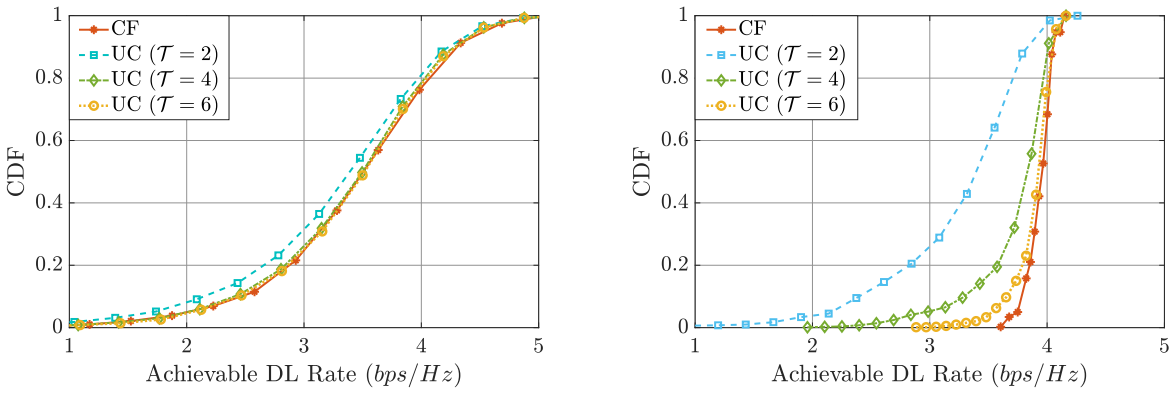

(a) Equal power allocation

(b) Max-min power allocation

Figure 3.5: CDF comparison between conventional CF and UC mMIMO in the absence of system impairments.

that limiting the number of served users by each AP to $\mathcal{T} = 2,\ 4$, harms the system performance significantly. Besides, the system loses its leverage in achieving uniformly good data rates for all users. Nevertheless, increasing the number of served users per AP to $\mathcal{T} = 6$, alleviates such degradation in the system performance, and the performance UC mMIMO approaches the performance of conventional CF mMIMO in achieving a uniformly good service for all users.

Fig. 3.6 compares the average per-user DL rate of SC and CF mMIMO systems under equal and max-min power allocation techniques. The average per-user DL rate of UC mMIMO is calculated at different number of served users per AP ($\mathcal{T}$). Notably, the average per-user DL rate in SC systems under equal power allocation outperforms the performance of CF mMIMO systems even under max-min power allocation. However, applying max-min power allocation technique worsen the performance of SC systems, and the average per-user DL achievable rate becomes very low compared to CF mMIMO systems. Furthermore, as previously mentioned, while UC mMIMO suffers from a low performance at small values of $\mathcal{T}$, especially under max-min power allocation, its performance improves significantly and approaches the CF mMIMO one as $\mathcal{T}$ increases.

3.5.3 Hardware Distortion Effect

Fig. 3.7 depicts the effect of transceiver hardware distortion on the DL performance of SC systems and CF mMIMO systems under equal and max-min power allocation. As shown in the figure, the analytical curves are consistent with the simulation results under

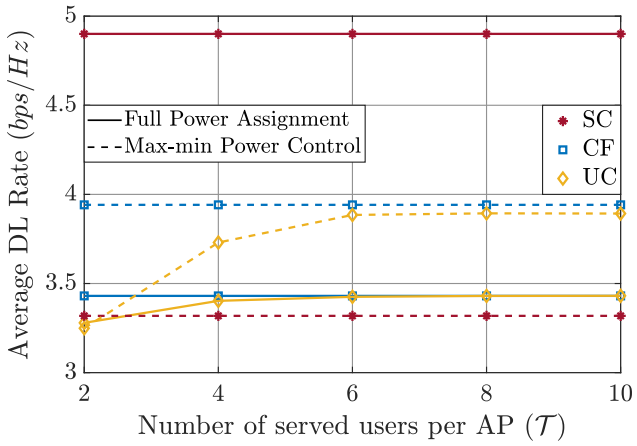

Figure 3.6: Average per-user DL rate in CF mMIMO and SC systems systems in the absence of practical system impairments ($M = 100,\ N_{ap} = 4,\ and\ K = 20$).

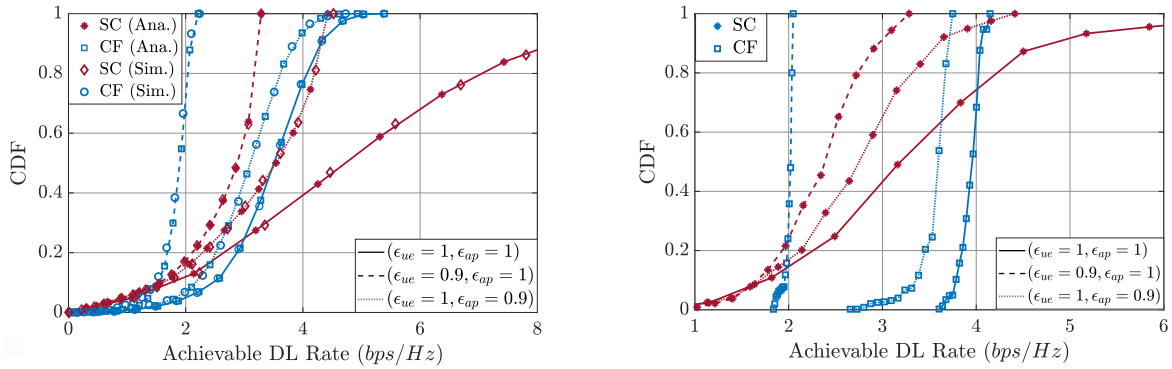

(a) Equal power allocation

(b) Max-min power allocation

Figure 3.7: CDF comparison between CF mMIMO and SC systems under transceiver hardware impairments ($M = 100,\ N_{ap} = 4,\ and\ K = 20$).

different hardware distortion effects. It is clear that the effect of hardware distortion at the UEs side in both systems is more prominent than the effect of hardware distortion at the APs side. This result coincides with the hardware scaling law, previously discussed in the literature. Considering the impact of UEs distortion, it is clear that SC systems outperform CF mMIMO systems under equal and max-min power allocation techniques, respectively. On the other hand, under the effect of APs distortion, each system achieves a slight improvement in the achievable DL rate over the other system for a certain portion of users when applying equal power allocation. Nevertheless, when applying max-min power allocation, the CF mMIMO systems performance becomes superior to SC systems performance.

Considering equal power allocation, Fig. 3.8 studies the average achievable DL rates of SC and CF mMIMO systems in the presence of APs hardware distortion at different

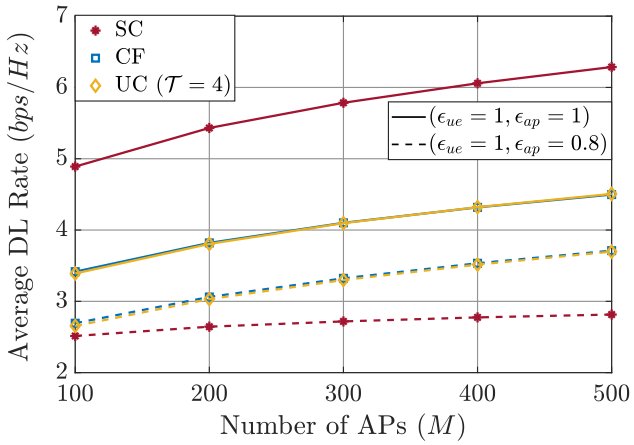

Figure 3.8: Average per-user DL rate of SC and CF mMIMO systems in the presence of APs hardware distortion ($N_{ap} = 4$ *and* $K = 20$).

numbers of APs. It is noted that increasing the number of APs not only improves the CF mMIMO performance, but also alleviates the effect of hardware distortion at the AP side. In contrary, while increasing the number of ideal APs significantly improves the performance of SC system, the average DL rates slightly improve with increasing the number of non-ideal APs. Thus, the introduced loss in the SC system performance due to the deployment of non-ideal APs becomes more prominent at higher number of APs. This is a consequence that in SC systems, each user is served by only one AP, and hence, increasing the number of APs is not beneficial in alleviating the APs distortion effect. Finally, it is noted that, both UC and conventional CF mMIMO systems achieve identical DL rates under the deployment of ideal and non-ideal APs.

3.5.4 Channel Impairments Effect

This section analyses the Doppler shift effect on both SC and CF mMIMO systems. In doing so, firstly, we neglect all other effects. Thus, the achievable DL rates of CF mMIMO systems can be rewritten by

$$R_k^{cf}[n] = \log_2\left(1 + \frac{|D_{s_k}^{cf}|^2}{\mathbb{E}\{|BU_k^{cf}|^2\} + \mathbb{E}\{|DS_k^{cf}|^2\} + \sum\limits_{k' \neq k} \mathbb{E}\{|UI_{kk'}^{cf}|^2\} + \sigma_w^2}\right), \tag{3.58}$$

and the achievable DL rates of SC systems will be

$$R_k^{sc}[n] = \log_2\left(1 + \frac{\mathbb{E}\{|D_{s_k}^{sc}|^2\}}{\mathbb{E}\{|DS_k^{sc}|^2\} + \sum\limits_{k' \neq k} \mathbb{E}\{|UI_{kk'}^{sc}|^2\} + \sigma_w^2}\right). \tag{3.59}$$

Regarding the desired signal power in both systems, taking into account the Doppler shift effect as the only impairment in the system, the desired signal power of CF mMIMO

systems in (3.30) will be

$$P_{D,k}^{cf} = |D_{s_k}^{cf}|^2 = \alpha_{k,n}^2 P_d \Big(\sum_{m \in \mathcal{M}(k)} \sqrt{\eta_{mk}} N_{ap} \zeta_{mk} \Big)^2, \tag{3.60}$$

and the desired signal power of CF mMIMO systems in (3.51) will be

$$P_{D,k}^{sc} = \mathbb{E}\{|D_{s_k}^{sc}|^2\} = \alpha_{k,n}^2 P_d N_{ap} \eta_{m_k} \zeta_{m_k k} \Big(\beta_{m_k k} + N_{ap} \zeta_{m_k k} \Big), \tag{3.61}$$

where it is noted that the desired power in both systems is affected by the same factor α_n^2 under channel aging effect. Focusing on the power of different interference sources. It can be noticed that the composite interference power due to the beamforming uncertainty and the Doppler shift effect will be

$$\begin{aligned} \mathbb{E}\{|BU_k^{cf}|^2\} + \mathbb{E}\{|DS_k^{cf}|^2\} &= \big(\alpha_{k,n}^2 P_d + P_d (1 - \alpha_{k,n}^2) \big) \sum_{m \in \mathcal{M}(k)} N_{ap} \eta_{mk} \zeta_{mk} \beta_{mk}, \\ &= P_d \sum_{m \in \mathcal{M}(k)} N_{ap} \eta_{mk} \zeta_{mk} \beta_{mk}, \end{aligned} \tag{3.62}$$

which equals to the beamforming uncertainty power under no Doppler shift effect. The reason is that the users detect the transmitted symbols by the knowledge of the channel statistics. Hence, the variations of the small-scale fading coefficients due to the Doppler shift effect do not have further impact on the interference. Besides the interference due to other users' data symbols (3.33) can be rewritten by

$$\mathbb{E}\{|UI_{kk'}^{cf}|^2\} = P_d \sum_{m \in \mathcal{M}(k')} N_{ap} \eta_{mk'} \zeta_{mk'} \beta_{mk}. \tag{3.63}$$

Hence, the total interference in CF mMIMO systems when considering the Doppler shift effect as the only source of system impairments will be

$$I_{k,tot}^{cf} = P_d \sum_{k'=1}^{K} \sum_{m \in \mathcal{M}(k')} N_{ap} \eta_{mk'} \zeta_{mk'} \beta_{mk}. \tag{3.64}$$

Note that, the total interference in CF mMIMO systems is independent of the temporal correlation coefficient. On the other hand, focusing on the interference terms in SC systems, the total interference can be expressed as follows:

$$\begin{aligned} I_{k,tot}^{sc} &= |DS_k^{sc}|^2\} + \sum_{k' \neq k} \mathbb{E}\{|UI_{kk'}^{sc}|^2\} \\ &= P_d N_{ap} \Big(\sum_{k'=1}^{K} \eta_{m_{k'}} \zeta_{m_{k'} k'} \beta_{m_{k'} k} + (1 - \alpha_{k,n}^2) \eta_{m_k} \zeta_{m_k k} \beta_{m_k k} \Big), \end{aligned} \tag{3.65}$$

where it is clear that the total interference is affected by the Doppler shift effect and it increases as the Doppler shift effect gets more severe. The reason is that the users in SC systems detect the transmitted symbols by the knowledge of the instantaneous channel, and hence the Doppler shift effect will increase the introduced interference in the system.

Fig. 3.9 illustrates the Doppler shift effect on the average desired power, interference powers and SINR values as time progresses assuming 20 users existing in the system with

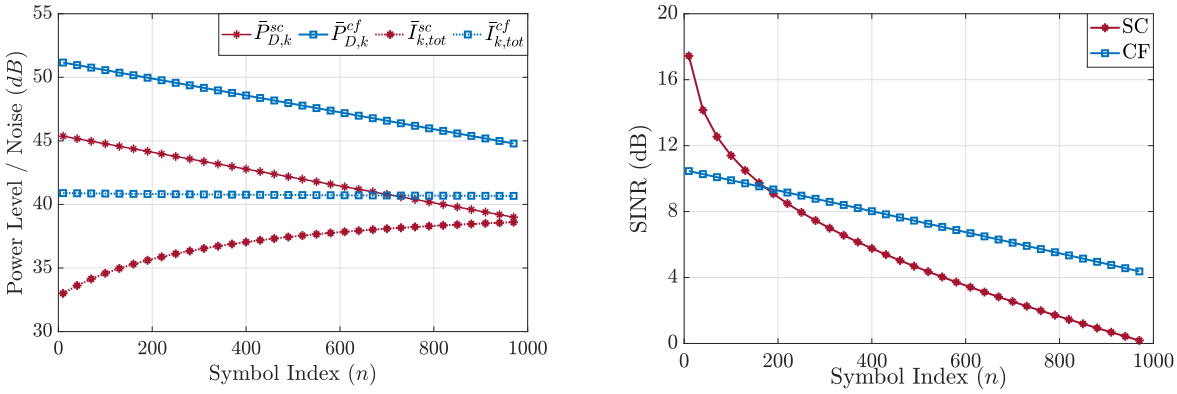

(a) (b)

Figure 3.9: The Doppler shift effect on (a) the average power of different signal components and (b) SINR of CF mMIMO and SC systems as time progresses.

a velocity 50 km/hr. It is clear that as time progresses, the average desired power in both systems decreases. In addition, the interference power in CF mMIMO systems is not affected by the Doppler shift effect as time progresses. However, the interference power in SC systems increases as time progresses since the Doppler shift effect becomes more severe. As such, while the average SINR is superior at SC systems under slight Doppler shift effect in the early time symbols, the performance of CF mMIMO systems becomes better at later time symbols.

Fig. 3.10 compares the performance of SC and CF mMIMO systems under the Doppler shift effect. It is assumed that 20 users exist in the system and use non-orthogonal pilot sequences of length $\tau_{u,p} = 10$ for the sake of UL channel estimation. It is clear that increasing the users' velocities deteriorates the achievable DL rates of both systems. In addition, the degradation in the achievable DL rates is more significant in SC systems. Under equal power allocation, while SC systems performance is superior at low-velocities, i.e., $v = 5$ km/hr, for the majority of users, the performance of CF mMIMO outperforms the SC counterpart for all users under high velocities, i.e., $v = 50$ km/hr. Notably, in Fig. 3.10b, despite the power control coefficients are not adjusted according to the Doppler shift effect in max-min power allocation as mentioned in Section 3.4, the CF mMIMO system can still attain uniform DL rates for all users. In addition, the performance of the system outperforms the performance of SC systems under high and low-mobility conditions.

Fig. 3.11 compares the average per-user DL rate of SC and CF mMIMO systems at different users' velocities under equal power allocation. It is noted that the Doppler shift effect is identical on both conventional CF and UC mMIMO systems since they

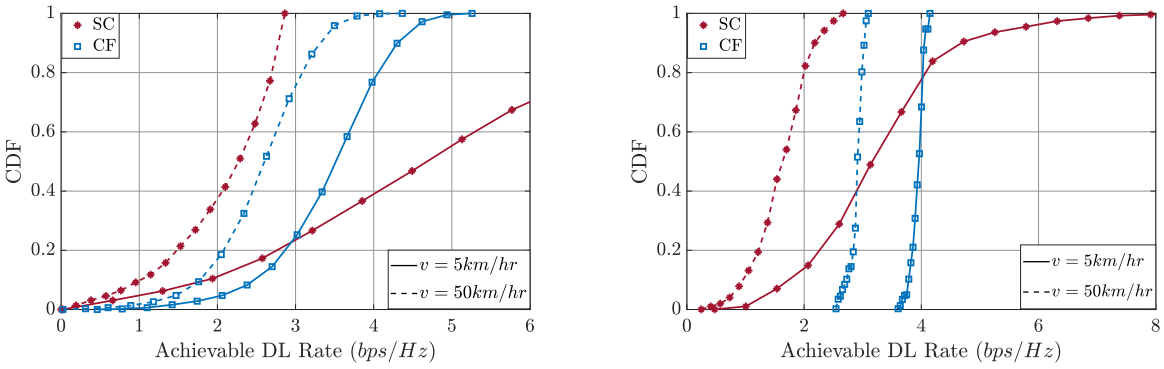

(a) Equal power allocation

(b) Max-min Power allocation

Figure 3.10: CDF comparison between CF mMIMO and SC systems under Doppler shift effect ($M = 100,\ N_{ap} = 4,\ and\ K = 20$).

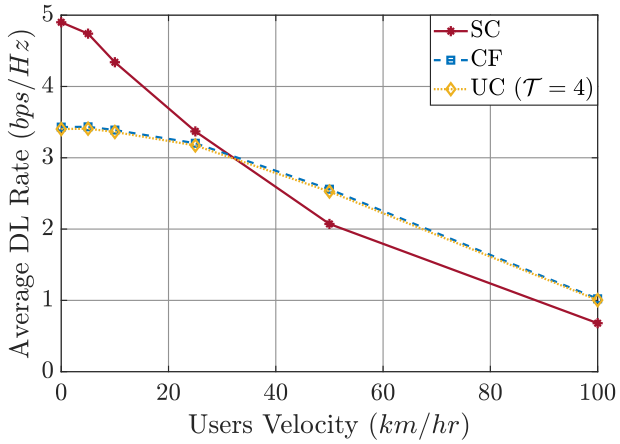

Figure 3.11: Average per-user DL rate of SC and CF mMIMO systems under the Doppler shift effect ($M = 100,\ N_{ap} = 4,\ and\ K = 20$).

achieve the same average per-user DL rate at different users' velocities. Besides, while the average per-user achievable rate is superior in SC systems under low-mobility conditions, it becomes larger in the CFmMIMO systems under high velocities. Hence, to achieve high average per-user rate in low-mobility scenarios, it is recommended to operate the network as a SC system. On the other hand, it is preferred to operate networks with high-velocity users as CF mMIMO systems.

3.6 Hybrid CF mMIMO/SC System in Dynamic Environments

As noted from the reported results in previous Section, the performance of SC systems under equal power allocation outperforms that of CF mMIMO systems under equal and

max-min power allocation techniques when the network serves users with low velocities, i.e., pedestrians. Nevertheless, as the users' velocities get higher, SC systems suffer from a more prominent performance loss compared to CF mMIMO systems. Thus, CF mMIMO systems provide users with high velocities, i.e., vehicles, with higher rates. In practice, the network includes users with different velocities whose preferences of network operation are different. In addition, providing high data rates to users under different mobility conditions is one of the main challenges in future wireless communication networks [98]. As such, in this section, we propose a hybrid CF mMIMO/SC system to provide different users in the network with high data rates simultaneously.

3.6.1 Proposed Operation

We consider that the network includes both high-velocity and low-velocity users that are randomly distributed in the coverage area. Also, we assume that both APs and UEs are equipped with ideal hardware components ($\epsilon_{ap} = \epsilon_{ue} = 1$). Motivated by the reported results in Section 3.5, we divide the network into two tiers where the CPU selects the APs assigned to each tier. The first-tier consists of APs, operating in a standalone mode to serve low-velocity users under the SC system operation. On the other hand, the second-tier accommodates APs, selected to operate in a cooperative manner to serve high-velocity users as a CF mMIMO system. Furthermore, the available bandwidth is assumed to be utilized in both tiers with a reuse factor of one. Nevertheless, if the SC system provides high-velocity users with higher data rates than CF mMIMO, i.e., at low mobility scenarios, the network will operate as a SC system. Otherwise, the network operation will be as follows. Firstly, all low-velocity users select their serving APs from the entire available APs in a random sequential order. In that, for a low-velocity user $i \in \mathcal{I}$ where $\mathcal{I}$ denotes the set of low-velocity users, the serving AP m_i is the available AP with the maximum large-scale fading coefficient ($\beta_{m_i i}$). After all low-velocity users select their serving APs, the selected APs are assigned to the SC-tier. Then, based on some criterion, the CPU determines the set of APs for the CF mMIMO-tier operation. Thus, there will be three categories of APs as shown in Fig. 3.12, namely SC-APs, CF-APs, and inactive-APs. Inactive-APs represent the APs that are not selected either for the SC-tier nor the CF mMIMO-tier. In the sequel, $\mathcal{A}_{sc}$ and $\mathcal{A}_{cf}$ denote the set of APs serving low-velocity users and the available APs for CF mMIMO-tier operation, respectively. Also, the set of

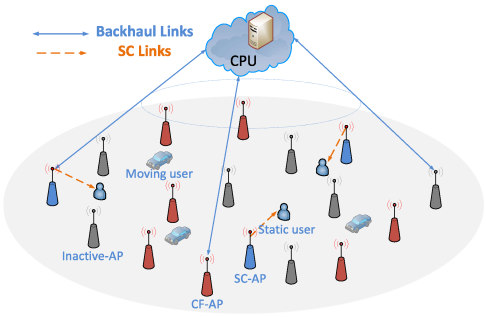

Figure 3.12: Hybrid CF mMIMO/SC system model.

high-velocity users is denoted by $\mathcal{V}$.

3.6.2 Achievable DL Rates

3.6.2.1 High-Velocity Users

Let us denote $\boldsymbol{g}_{m_c v}$ as the channel vector between the AP m_c that belongs to the CF-tier and the high-velocity user v. Regarding the DL transmission, the CF-APs exploit the estimated channels of all users $\in \mathcal{V}$ during the UL training phase to perform the precoding process for DL transmission. Applying CB precoding, the transmitted signal from AP m_c is given by

$$\boldsymbol{x}_{m_c}[n] = \sqrt{P_d} \sum_{v \in \mathcal{V}} \sqrt{\eta_{m_c v}} \hat{\boldsymbol{g}}^*_{m_c v} s_v[n], \tag{3.66}$$

Assuming equal power allocation, the value of $\eta_{m_c v}$ that satisfies the power constraint will be $\eta_{m_c v} = \left(1/\sum_{v \in \mathcal{V}} \mathbb{E}\{|\hat{\boldsymbol{g}}_{m_c v}|^2\}\right)$. With the assumption of ideal hardware components

of APs and UEs, the received DL signal at user v can be expressed by

$$r_v[n] = \sqrt{P_d}\Bigg[\underbrace{\alpha_{v,n}\sum_{m_c\in\mathcal{A}_{cf}}\delta_{m_c}\sqrt{\eta_{m_cv}}\mathbb{E}\Big\{\Big|\boldsymbol{g}_{m_cv}^T\hat{\boldsymbol{g}}_{m_cv}^*[\tau_{u,p}+1]\Big|\Big\}s_v[n]}_{\text{desired signal for user } v\ (D_{s_v}^{hy})}$$
$$+\underbrace{\alpha_{v,n}\sum_{m_c\in\mathcal{A}_{cf}}\delta_{m_c}\sqrt{\eta_{m_cv}}\Big(\Big|\boldsymbol{g}_{m_cv}^T\hat{\boldsymbol{g}}_{m_cv}^*[\tau_{u,p}+1]\Big|-\mathbb{E}\Big\{\Big|\boldsymbol{g}_{m_cv}^T\hat{\boldsymbol{g}}_{m_cv}^*[\tau_{u,p}+1]\Big|\Big\}\Big)s_v[n]}_{\text{beamforming uncertainty } (BU_v^{hy})}$$
$$+\underbrace{\sqrt{1-\alpha_{v,n}^2}\sum_{m_c\in\mathcal{A}_{cf}}\delta_{m_c}\sqrt{\eta_{m_cv}}\boldsymbol{z}_{m_cv}^T[n]\hat{\boldsymbol{g}}_{m_cv}^*[\tau_{u,p}+1]s_v[n]}_{\text{Doppler shift effect } (DS_v^{hy})}$$
$$+\sum_{v'\neq v}\underbrace{\sum_{m_c\in\mathcal{A}_{cf}}\delta_{m_c}\sqrt{\eta_{m_cv'}}\boldsymbol{g}_{m_cv}^T[n]\hat{\boldsymbol{g}}_{m_cv'}^*[\tau_{u,p}+1]s_{v'}[n]}_{\text{intra-tier interference } (UI_{vv'}^{hy,1})}+\sum_{i\in\mathcal{I}}\underbrace{\sqrt{\eta_{m_ii}}\boldsymbol{g}_{m_iv}^T[n]\hat{\boldsymbol{g}}_{m_ii}^*s_i[n]}_{\text{inter-tier interference } (UI_{vi}^{hy,2})}\Bigg]+\underbrace{w_v[n]}_{\text{noise}},\tag{3.67}$$

where δ_{m_c} denotes the CF-AP indicator which is set to 1 if the AP is selected for the CF-tier operation and 0 otherwise. Note that, $UI_v^{hy,1}$ represents the intra-tier interference resulting from the transmitted data to other high-velocity users. Also, $UI_v^{hy,2}$ reflects the inter-tier interference arising from the SC-tier operation. Consequently, the achievable DL rate for a high-velocity user v at time instant n is given by

$$R_v^{hy}[n] = \log_2\left(1+\frac{|D_{s_v}^{hy}|^2}{\mathbb{E}\{|BU_v^{hy}|^2\}+\mathbb{E}\{|DS_v^{hy}|^2\}+\sum\limits_{v'\neq v}\mathbb{E}\{|UI_{vv'}^{hy,1}|^2\}+\sum\limits_{i\in\mathcal{I}}\mathbb{E}\{|UI_{vi}^{hy,2}|^2\}+\sigma_w^2}\right),\tag{3.68}$$

where the desired signal power is given by

$$|D_{s_v}^{hy}|^2 = \alpha_{v,n}^2P_d\Big(\sum_{m_c\in\mathcal{A}_{cf}}\delta_{m_c}\sqrt{\eta_{m_cv}}N_{ap}\zeta_{m_cv}\Big)^2.\tag{3.69}$$

Besides, as shown in (3.62), the composite power of beamforming uncertainty and Doppler shift effect for the high-velocity user v is given by

$$\mathbb{E}\{|BU_v^{hy}|^2\}+\mathbb{E}\{|DS_v^{hy}|^2\} = P_d\sum_{m_c\in\mathcal{A}_{cf}}\delta_{m_c}N_{ap}\eta_{m_cv}\zeta_{m_cv}\beta_{m_cv},\tag{3.70}$$

The intra-tier interference power due to the transmitted data to other high-velocity users can be calculated as in (3.33) as follows:

$$\begin{aligned}\mathbb{E}\{|UI_{vv'}^{hy,1}|^2\} &= P_d\sum_{m_c\in\mathcal{A}_{cf}}N_{ap}\delta_{m_c}\eta_{m_cv'}\zeta_{m_cv'}\beta_{m_cv}\\&\quad+P_d\alpha_{v,n}^2\Big(\sum_{m_c\in\mathcal{A}_{cf}}\sqrt{\eta_{m_cv'}}\delta_{m_c}N_{ap}\zeta_{m_cv'}\frac{\beta_{m_cv}}{\beta_{m_cv'}}\Big)^2|\boldsymbol{\psi}_v\boldsymbol{\psi}_{v'}^{\mathsf{H}}|^2.\end{aligned}\tag{3.71}$$

Also, the inter-tier interference due to the transmitted data from active APs in the small-cell tier can be determined as in (3.53) as follows:

$$\mathbb{E}\{|UI_{vi}^{hy,2}|^2\} = P_d\eta_{m_i}\Big(N_{ap}\zeta_{m_ii}\beta_{m_iv} + \alpha_{v,n}^2 N_{ap}^2\zeta_{m_ii}^2\left(\frac{\beta_{m_iv}}{\beta_{m_ii}}\right)^2|\boldsymbol{\psi}_v\boldsymbol{\psi}_i^{\mathsf{H}}|^2\Big). \tag{3.72}$$

3.6.2.2 Low-Velocity Users

In the SC-tier, each low-velocity user is served by one AP which serves only one user at a time. We consider low-velocity users have a temporal correlation coefficient $\rho_i = 1, \forall i \in \mathcal{I}$, and CB precoding is adopted for the DL data transmission. For user i, served by AP $m_i \in \mathcal{A}_{sc}$, the received DL signal will be

$$\begin{aligned} r_i[n] = &\underbrace{\sqrt{P_d}\sqrt{\eta_{m_i}}\boldsymbol{g}_{m_ii}^T\hat{\boldsymbol{g}}_{m_ii}^* s_i[n]}_{\text{desired signal for user } i\ (D_{s_i}^{hy})} + \underbrace{\sqrt{P_d}\sum_{i'\neq i}\sqrt{\eta_{m_{i'}}}\boldsymbol{g}_{m_{i'}i}^T\hat{\boldsymbol{g}}_{m_{i'}i'}^* s_{i'}[n]}_{\text{intra-tier interference } (UI_{ii'}^{hy,1})} \\ &+ \underbrace{\sqrt{P_d}\sum_{v\in\mathcal{V}}\sum_{m_c\in\mathcal{A}_{cf}}\delta_{m_c}\sqrt{\eta_{m_cv}}\boldsymbol{g}_{m_ci}^T[n]\hat{\boldsymbol{g}}_{m_cv}^* s_v[n]}_{\text{intra-tier interference } (UI_{iv}^{hy,2})} + \underbrace{w_i[n]}_{\text{noise}}. \end{aligned} \tag{3.73}$$

Then, a tight upper bound for the achievable DL rate of the low-velocity user i at time instant n is given by

$$\breve{R}_i^{hy}[n] = \log_2\left(1 + \frac{\mathbb{E}\{|D_{s_i}^{hy}|^2\}}{\sum_{i'\neq i}\mathbb{E}\{|UI_{ii'}^{hy,1}|^2\} + \sum_{v\in\mathcal{V}}\mathbb{E}\{|UI_{iv}^{hy,2}|^2\} + \sigma_w^2}\right), \tag{3.74}$$

where the desired signal power is given by

$$\mathbb{E}\{|D_{s_i}^{hy}|^2\} = P_d\eta_{m_i}\big(N_{ap} + N_{ap}^2\big)\zeta_{m_ii}^2. \tag{3.75}$$

The intra-tier interference power due to the transmitted data to other low-velocity users can be calculated as in (3.53) as follows:

$$\mathbb{E}\{|UI_{ii'}^{hy,1}|^2\} = P_d\Big(N_{ap}\eta_{m_{i'}}\zeta_{m_{i'}i'}\beta_{m_{i'}i} - N_{ap}\eta_{m_i}\zeta_{m_ii}^2 + N_{ap}^2\eta_{m_{i'}}\zeta_{m_{i'}i'}^2\left(\frac{\beta_{m_{i'}i}}{\beta_{m_{i'}i'}}\right)^2|\boldsymbol{\psi}_i\boldsymbol{\psi}_{i'}^{\mathsf{H}}|^2\Big). \tag{3.76}$$

Also, the inter-tier interference power due to the transmitted in the CF-mMIMO tier can be calculated as in (3.33) as follows:

$$\mathbb{E}\{|UI_{iv}^{hy,2}|^2\} = P_d\Big(\sum_{m_c\in\mathcal{A}_{cf}}N_{ap}\delta_{m_c}\eta_{m_cv}\zeta_{m_cv}\beta_{m_ci} + \Big(\sum_{m_c\in\mathcal{A}_{cf}}\sqrt{\eta_{m_cv'}}\delta_{m_c}N_{ap}\zeta_{m_cv}\frac{\beta_{m_ci}}{\beta_{m_cv}}\Big)^2|\boldsymbol{\psi}_i\boldsymbol{\psi}_v^{\mathsf{H}}|^2\Big). \tag{3.77}$$

3.6.3 CF-APs Selection

The performance of the proposed system mainly depends on the selected APs for the CF-tier operation. Undoubtedly, increasing the number of active CF-APs improves the

performance of high-velocity users, but degrades the performance of low-velocity users, and vice versa. Thus, the CF-APs should be selected in a way that improves the achievable rates of high-velocity users while not harming the achievable rates of low-velocity users. As such, we assume that the CPU selects the CF-APs according to the following problem:

$$\begin{aligned} &\max_{\delta_{m_c}} \bar{R}_v, \\ &\text{s.t.} \;\; \delta_{m_c} \in \{0,1\}, \forall \; m_c \in \mathcal{A}_{cf}, \\ &\qquad \bar{R}_i \geq R_{i,th}, \end{aligned} \tag{3.78}$$

where the problem strives to maximize the average DL rates for high-velocity users while preserving the average DL rate of low-velocity users above a certain threshold $R_{i,th}$. Note that, finding the optimal set of APs for the CF-tier operation is an NP-hard problem. To solve (3.78), we firstly adopt penalty methods to relax it to unconstrained problem as follows [99]:

$$\begin{aligned} &\max_{\delta_{m_c}} \bar{R}_v + B_{\breve{j}} \min(0, \bar{R}_i - R_{i,th}), \\ &\text{s.t.} \;\; \delta_{m_c} \in \{0,1\}, \forall \; m_c \in \mathcal{A}_{cf}, \end{aligned} \tag{3.79}$$

where $B_{\breve{j}}$ is a positive penalty parameter at the $\breve{j}^{\text{th}}$ iteration. The added penalty in (3.79) will introduce a large negative value if the constraint does not hold. On the other hand, it will add 0 if the constraint holds. Then, we propose a low-complexity scheme to solve (3.79) as shown in Algorithm 3.2.

The proposed Algorithm for CF-APs selection can be summarized as follows. Firstly, we start with a small penalty that increases with the iteration order. The algorithm stops if the difference between the performance of two consecutive iterations is less than a certain tolerance ϵ. In each iteration, we start with a solution that violates the constraint [99]. Also, we initially consider a solution that provides both low-velocity and high-velocity users with acceptable performance. Then, aiming at maximizing the DL rates for high-velocity users, the algorithm iteratively activates and deactivates the APs that improves the performance in a greedy manner. Finally, it stops adding or dropping APs if no further improvement can be attained.

3.6.4 Numerical Results

We consider a dynamic environment of size 1×1 km^2 that includes V high-velocity users and I low-velocity users. Besides, the CF-APs are selected to provide low-velocity users

Algorithm 3.2: CF-APs Selection Algorithm for solving (3.79)

1. *Initialization*:

   i. Initialize $B_{\breve{j}}$ with a small positive value.

   ii. Activate all APs $\in \mathcal{A}_{cf}$ except the first and second nearest ones to low-velocity users.

   iii. Check the constraint ($\bar{R}_i \geq R_{i,th}$), if it violates, continue. Otherwise, activate more APs until it violates.

   iv. If all APs are activated while the constraint is satisfied, stop the algorithm and report the solution for the CF-APs selection. Otherwise, go to next step.

   v. Evaluate the performance G at current AP selection δ_{m_c}, where G represents the value of the objective function in (3.79).

2. *Activate APs*:

   i. Find the set of inactive APs ($\mathcal{L}$).

   ii. Activate APs $\in \mathcal{L}$ separately, then evaluate $G^l,\ \forall l = 1, \cdots, L$, where L denotes the total number of APs in $\mathcal{L}$.

   iii. Find $G^b \geq G^l,\ \forall l = 1, \cdots, L$.

   iv. *if* $G^b > G$, update the AP selection $\delta_{m_c} = \delta^b_{m_c}$, $G = G^b$, and set $Add = 1$. Otherwise, set $Add = 0$.

3. *Deactivate APs*:

   i. Find the set of activated APs ($\mathcal{U}$).

   ii. Deactivate APs $\in \mathcal{U}$ individually, then evaluate $G^u,\ \forall u = 1, \cdots, U$, where U is the number of activated APs.

   iii. Find $G^b \geq G^u,\ \forall u = 1, \cdots, U$.

   iv. *if* $G^b > G$, update the AP selection $\delta_{m_c} = \delta^b_{m_c}$, $G = G^b$, and set $Drop = 1$. Otherwise, set $Drop = 0$.

4. *Stop if* $Add = 0$ *and* $Drop = 0$. *Otherwise, repeat Step* 2 *and* 3.

5. *Stop if* $G_{\breve{j}} - G_{\breve{j}-1} \leq \epsilon$. *Otherwise, update* $B_{\breve{j}} = \mu B_{\breve{j}-1}$ *with a positive* μ, *i.e.,* $\mu = 2$, *and repeat Step 1:5.*

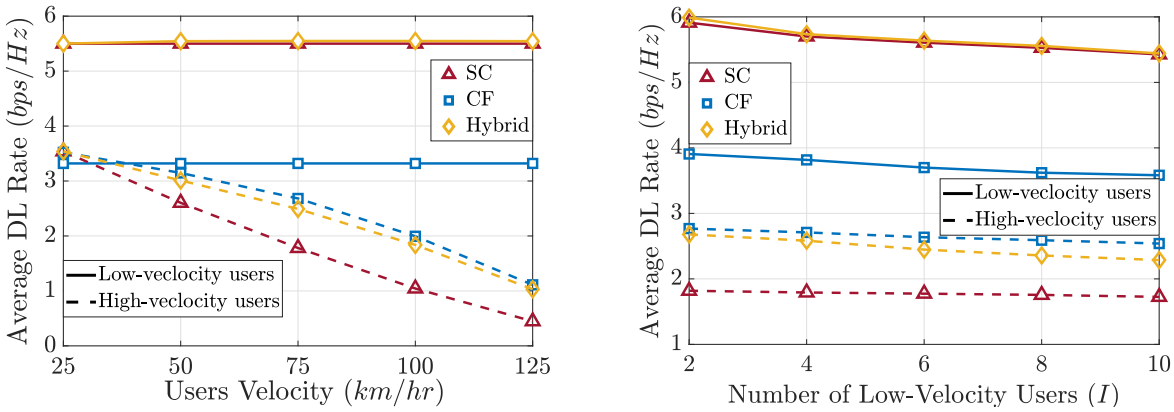

(a) Different velocities

(b) Different number of low-velocity users

Figure 3.13: Average DL rates of low-velocity and high-velocity users.

with their average DL rate in SC systems, i.e., $R_{i,th} = \bar{R}_{i,sc}$, where $\bar{R}_{i,sc}$ is the average DL rate of low-velocity users in SC systems.

Fig. 3.13a depicts the average DL rates of low-velocity and high-velocity users in SC, CF mMIMO, and the proposed system under different mobility velocities of the high-velocity users. It is assumed that $M = 200$ APs, $V = 25$ users, and $I = 5$ users. Intuitively, increasing the velocity of high-velocity users degrades the average DL rates of high-velocity users as a consequence of the more harsh Doppler shift effect. However, this does not affect the performance of low-velocity users. Interestingly, the average DL rate of high-velocity users in the proposed system approaches their achievable rates in CF mMIMO systems while attaining the maximum rate of low-velocity users as $\bar{R}_i \geq \bar{R}_{i,sc}$. In addition, as the velocity of high-velocity users increases, the potential of the proposed system in providing both low-velocity and high-velocity users with high data rates becomes more prominent.

Fig. 3.13b depicts the performance of low-velocity and high-velocity users under different number of low-velocity users. We consider $M = 200$ APs and $V = 25$ high-velocity users with with an average velocity 75 km/hr. It is clear that increasing the number of low-velocity users decreases the average DL rates of low-velocity and high-velocity users. This is due to the more interference resulting from the increased number of users. Besides, the proposed system achieves comparable DL rates to those of CF mMIMO. However, the gap between the performance of the proposed system and CF mMIMO increases with the number of low-velocity users. This is a consequence of the smaller degree-of-freedom in the CF-APs selection at higher numbers of low-velocity users.

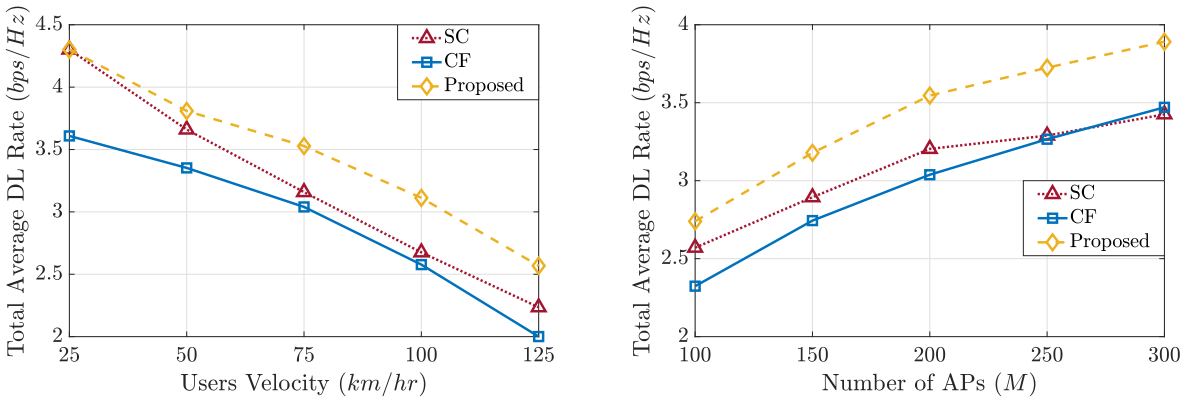

(a) Different velocities

(b) Different number of APs

Figure 3.14: Total average DL rates.

Fig. 3.14 depicts the average DL rates for all users (low-velocity and high-velocity users) versus different mobility conditions of high-velocity users (Fig. 3.14a) and different number of deployed APs (Fig. 3.14b). It is assumed that $V = 20$ moving users and $I = 10$ static users. In addition, Fig. 3.14a considers $M = 200$ APs while Fig. 3.14b assumes high-velocity users have an average velocity 75 km/hr. Fig. 3.14a reveals that the proposed system outperforms SC and CF mMIMO systems in-terms of the average DL rates of all users under different velocities of high-velocity users. Furthermore, Fig. 3.14b shows that the average DL rates improves with the number of APs. Notably, the average DL rates of the proposed system are superior to the rates of SC and CF mMIMO systems under different number of APs.

Fig. 3.15 depicts the complexity of the proposed CF-APs selection algorithm in-terms of the total number of iterations. Notably, the proposed Algorithm has a low complexity which is linear in the number of APs. Also, the required number of iterations increases with the number of high-velocity users (V) since it becomes more challenging to maximize the average DL rates of a higher number of high-velocity users while preserving the average rates for low-velocity users at high values.

3.7 Summary

We investigated the achievable DL data rates of CF mMIMO systems and compared it with the achievable ones of SC systems under different practical system considerations including non-ideal hardware distortions and channel impairments, i.e., Doppler shift effect. Firstly, we provided analytical expressions for MMSE estimated channels taking into

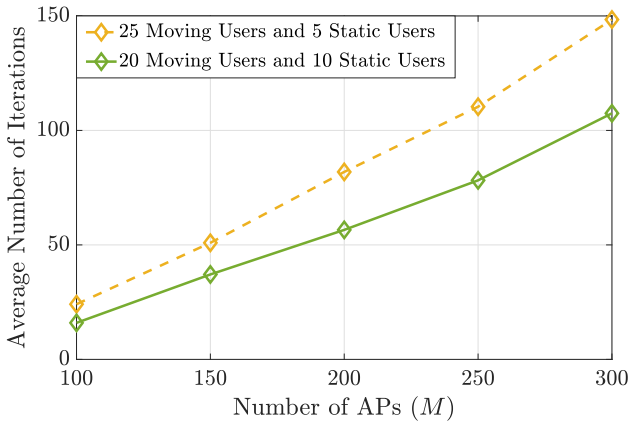

Figure 3.15: Average number of iterations for the proposed CF-APs selection algorithm at different number of APs.

account the non-ideal hardware distortions and the Doppler shift effect. Then, we have developed novel closed-form expressions for the DL achievable rates for both systems under such practical system considerations. We revealed that when applying CB precoding and equal power allocation for both systems operations, SC systems can achieve superior DL rates to the CF mMIMO. However, the SC system performance significantly degrades under max-min power allocation. In contrary, the CF mMIMO system attains uniformly good performance for all users under max-min power allocation. Nevertheless, decreasing the number of served users per APs in CF mMIMO system by applying the UC mMIMO approach remarkably degrades the system performance.

Regarding the non-ideal hardware effects, we have shown that the effect of non-ideal UEs is more prominent than the non-ideal APs. Besides, the effect of non-ideal APs distortion is more prominent in the SC system. Also, we revealed that the Doppler shift effect is more prominent in SC systems. In addition, SC systems are preferred to support network operation under low-mobility conditions. However, it is more beneficial to adopt CF mMIMO system for network operation under high-mobility conditions.

Based on the aforementioned findings, we proposed a hybrid CF mMIMO/SC system to provide high-velocity and low-velocity users with high DL rates. The proposed system considers the network as a two-tier network where users with high-velocity and low-velocity are associated to the CF mMIMO-tier and the SC-tier, respectively. Results showed that the proposed system outperforms SC and CF mMIMO systems by providing users of different mobility conditions with high rates simultaneously.

Chapter 4
Limiting Doppler Shift Effect on CF mMIMO Systems

4.1 Introduction

As previously illustrated, the Doppler shift effect can significantly degrades the CF mMIMO system performance, especially under high mobility conditions. This is a consequence of the relative movement between users and APs leading to temporal variations in the propagation environment that affects the channel coefficients to continuously evolve with time and change from one symbol to another. Such channel variations renders the estimated channel coefficients out-of-date when applied for data reception/transmission and results in a corresponding degradation in the achievable data rates. Despite the harsh effect of Doppler shift on the system performance, we showed in chapter 3 that the CF mMIMO is more robust against such effect than SC systems. However, solutions to alleviate the Doppler shift effect on CF mMIMO are essential to further improve its performance in dynamic environments.

The traditional way to limit the Doppler shift effect on mMIMO systems is through applying channel prediction techniques. In particular, causal linear finite impulse response Wiener predictors are adopted for channel prediction in co-located mMIMO systems in [24, 81]. Furthermore, the potential of applying Kalman filter-based estimator to predict the channel conditions is analyzed in [100]. Results reveal that using channel predictors can alleviate the Doppler shift effect on the achievable data rates. Also, the prediction accuracy of the adopted auto-regressive (AR) prediction models improves with increasing the AR model order [84]. According to the Levinson-Durbin recursion, used for determining the model parameters, the model order is limited by the data amount of previous CSI samples. In addition, the computational complexity is proportional to the square of the model order. Note that, in CF mMIMO systems, the channel estimation

and channel prediction are preferred to be carried out in the distributed APs to limit the burden on the fronthaul network. However, since the channel prediction task requires extremely higher processing capabilities than the channel estimation, it is impractical to perform such a task in the APs due to their low processing capabilities.

An alternative and simpler way to limit the Doppler shift effect is to adapt the system frame length according to the mobility conditions [85]. The authors in [85] studied the Doppler shift effect on the performance of FDD co-located mMIMO systems. In that, the DL and UL frame lengths are optimized to tackle the DL and UL rate degradation problem due to the Doppler shift effect. The goal is to adapt the system to severe aging conditions by reducing the frame length. The optimal frame length for each transmission link is determined separately using line search, and the results show that adjusting the frame length of each transmission link according to the aging conditions can limit the Doppler shift effect in FDD mMIMO systems. However, such approach cannot be applied to TDD systems. In fact, the authors in [85] exploit the FDD system properties, where DL and UL data transmission occurs simultaneously over two different frequency bands to optimize the DL and UL frame lengths separately. Nevertheless, in TDD systems, DL and UL data transmissions occur over the same bandwidth at different time instants. In addition, optimizing the frame length to maximize the achievable DL rate may affect the achievable UL rate badly and vice versa. As a consequence, the TDD frame length optimization problem for DL and UL rate maximization cannot be studied separately.

In this chapter, we introduce our proposed solution to limit the the Doppler shift effect on the performance of CF mMIMO systems. Firstly, using tools of stochastic geometry, we provide novel analytical expressions for tight lower bound of the average DL and UL rates of CF mMIMO systems. Then, capitalizing on the derived analytical results for the average DL and UL rates, we provide an analytical framework to determine the optimal frame length that maximizes the DL and UL rates separately. In that, we consider the system operation under TDD mode where different transmission protocols are adopted for the system operation. Next, aiming at limiting the Doppler shift effect on both DL and UL rates simultaneously, we derive new analytical expressions to minimize the Doppler shift effect on a total weighted sum of losses in system's rates under different transmission protocols.

4.2 System Model

We consider a CF mMIMO system in which multi-antenna APs and single-antenna users are distributed in a finite area $A \subset \mathbb{R}^2$, with radius $\mathcal{D}$. In this chapter, we consider that both APs and users are distributed in the coverage area according to a Finite Homogeneous Poisson Point Process (FHPPP) with densities λ_A and λ_U, respectively, as shown in Fig. 4.1. In particular, the FHPPP is defined as $\Phi = \mathcal{P} \cap A$, where $\mathcal{P}$ represents a Homogeneous Poisson Point Process (HPPP) [101, 102].

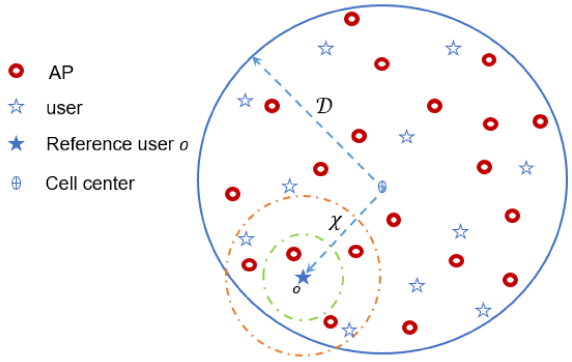

Figure 4.1: CF mMIMO system model.

4.2.1 Channel Model

Similar to Chapter 3, we consider Rayleigh fading channels between users and APs. However, for ease of analysis and tractability, we do not account for the shadowing effect in this Chapter. Consequently, the large-scale fading coefficient between the m^{th} AP and the k^{th} user in (3.2) will be a function only on the distance-based path-loss and can be rewritten as follows:

$$\beta_{mk} = d_{mk}^{-3.5}\, \mathbf{1}(d_{mk} > d_1) + d_1^{-1.5} d_{mk}^{-2}\, \mathbf{1}(d_0 \leq d_{mk} \leq d_1) + d_1^{-1.5} d_0^{-2}\, \mathbf{1}(d_{mk} < d_0), \quad (4.1)$$

where $\mathbf{1}(\cdot)$ denotes the indicator function and d_{mk} represents the distance between the m^{th} AP and the k^{th} user. Besides, we consider that the channel $\boldsymbol{g}_{mk}$ between the m^{th} AP and the k^{th} user evolves with time according to the AR model of first-order [24] as in (3.6) in which the user's channel evolves from time symbol to another according to its velocity. In this regard, we assume that users are categorized into groups where the users belong to the same group have the same average velocity.

4.2.2 Transmission Protocols

We consider two different TDD-based transmission protocols as shown in Fig. 4.2. Fig. 4.2a depicts the most common transmission protocol in literature for TDD-based mMIMO systems, presented in [39]. This transmission protocol considers the transmission of UL training sequences in the first phase, followed by DL and UL data transmission in the second and third phases, respectively. Hence, in dynamic environments with high mobility conditions, the Doppler shift will be more significant in the UL transmission phase. The reason is that the estimated channel coefficients in the UL training phase will be more outdated during the UL data transmission than the DL data transmission. On the other hand, aiming at alleviating the Doppler shift effect on the UL data transmission phase, the second transmission protocol in Fig. 4.2b [78] places the UL training sequences between the UL transmission phase and the DL transmission phase. As such, the received UL data symbols should be buffered while waiting for the UL training sequences to enable the UL data detection. Thus, the second transmission protocol reduces the Doppler effect on the UL phase with no regard to the implementation complexity. It is noteworthy that both transmission protocols have the same Doppler shift impact on the DL transmission phase. Besides, despite the first transmission protocol has more impact on the UL transmission phase, it is better from the implementation complexity perspective since there is no need to buffer the incoming UL data symbols.

(a) First transmission protocol

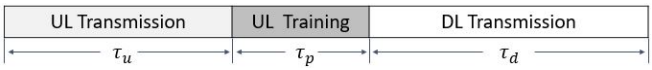

(b) Second transmission protocol

Figure 4.2: Different transmission protocols under TDD system operation.

4.3 Channel Estimation

This section discusses the UL training phase for UL channel estimation, taking into account the Doppler shift effect. In this regard, we consider the same pilot-based channel estimation approach in Section 3.3 to estimate users' channels. However, we herein do not account for the hardware distortion effect by assuming that both APs and users are

equipped with ideal hardware components. Thus, the MMSE estimated channel coefficient for user k with the l^{th} antenna element in the m^{th} AP at time instant $\tau_{u,p}+1$ is given by

$$\hat{g}_{mk,l}[\tau_{u,p}+1] = \mathcal{C}_{m,k,l}\tilde{y}_{p,m,l,k}[n], \tag{4.2}$$

where the term $\tilde{y}_{p,m,l,k}[n]$ in the absence of hardware impairment effect is given by

$$\begin{aligned}\tilde{y}_{p,m,l,k}[n] = \sqrt{P_p\tau_{u,p}}\sum_{k'=1}^{K}\alpha_{k',n}g_{mk',l}[\tau_{u,p}+1]\boldsymbol{\psi}_{k'}^{T}\boldsymbol{\psi}_{k}^{*} \\ + \sqrt{P_p\tau_{u,p}}\sum_{k'=1}^{K}\sqrt{1-\alpha_{k',n}^{2}}z_{mk',l}[n]\boldsymbol{\psi}_{k'}^{T}\boldsymbol{\psi}_{k}^{*} + \boldsymbol{w}_{p,m,l}[n]\boldsymbol{\psi}_{k}^{*}.\end{aligned} \tag{4.3}$$

Also, the term $\mathcal{C}_{m,k,l}$ under the presence of ideal hardware components is given by

$$\mathcal{C}_{m,k,l} = \frac{\sqrt{P_p\tau_{u,p}}\alpha_{k,i_k}\beta_{mk}}{\sum\limits_{k'=1}^{K}P_p\tau_{u,p}\beta_{mk'}\left|\boldsymbol{\psi}_{k'}^{T}\boldsymbol{\psi}_{k}^{*}\right|^{2}+\sigma_{w}^{2}}. \tag{4.4}$$

Consequently, the power of the estimated channel $\hat{g}_{mk,l}[\tau_{u,p}+1]$ under the Doppler shift effect can be calculated by

$$\zeta_{mk} = \sqrt{P_p\tau_{u,p}}\alpha_{k,i_k}\mathcal{C}_{m,k,l}\beta_{mk}. \tag{4.5}$$

It can be noticed that the channel estimation variance is affected by the Doppler shift and pilot contamination effects. Moreover, the Doppler shift effect varies from one user to another depending on the users' velocities and the assigned pilot sequence to each user. In that, users with pilot signals, carried on early symbols experience worse Doppler shift effect than users whose pilot signals are carried on the latter symbols. This is expected as the channels of users with pilot signals carried on early symbols become more outdated when performing the channel estimation process.

4.4 Performance Analysis

In this section, using tools of stochastic geometry, we derive a tight lower bound of the average achievable DL and UL rates for CF mMIMO systems under the Doppler shift effect. In doing so, local CB precoding and MRC detection are locally applied at APs for DL transmission and UL detection, respectively. Besides, equal power allocation is considered for both DL and UL data transmission phases.

4.4.1 Achievable DL Data Rate

In CF mMIMO, each AP transmits the DL data symbols of different users over the same time-frequency resources by means of beamforming. Applying CB precoding, and since all users are served by all APs in CF mMIMO, the transmitted signal from the m$^{\text{th}}$ AP at time instant $n > \tau_{u,p} + 1$, will be

$$\boldsymbol{x}_m[n] = \sqrt{P_d \eta_m} \sum_{k=1}^{K} \hat{\boldsymbol{g}}_{mk}^{*}[\tau_{u,p} + 1] s_k[n], \tag{4.6}$$

where $\eta_m = \eta_{mk}, \forall k = 1, \cdots, K$, denotes the power normalization factor for the transmitted data from AP m, and it is identical for all antenna elements, belonging to the same AP. Taking into consideration that each AP serves all users in the system, the power normalization factor at the m^{th} AP is given by

$$\eta_m = \frac{1}{\sum\limits_{k'=1}^{K} \mathbb{E}\{|\hat{g}_{mk',l}[\tau_{u,p} + 1]|^2\}}. \tag{4.7}$$

Note that, users can be located everywhere within the coverage area. With no loss of generality, we conduct the analysis for a reference user o, located at a distance χ from the cell center as shown in Fig. 4.1. The received signal from all APs at the reference user o will be

$$r_{d,o}[n] = \sum_{m=1}^{M} \boldsymbol{g}_{mo}^{T}[n] x_m[n] + w_{d,o}[n]. \tag{4.8}$$

Consequently, taking into account the lack of channel estimation at the user side, and substituting (4.6) in (4.8), the received DL signal at user o will be

$$\begin{aligned} r_{d,o}[n] = \sqrt{P_d} \Bigg[& \underbrace{\alpha_{o,n} \sum_{m=1}^{M} \sqrt{\eta_m} \mathbb{E}\Big\{ \Big| \boldsymbol{g}_{mo}^{T}[n] \hat{\boldsymbol{g}}_{mo}^{*}[\tau_{u,p} + 1] \Big| \Big\} s_o[n]}_{\text{desired signal for user } o \ (D_{s_o}^{d})} \\ & + \underbrace{\alpha_{o,n} \sum_{m=1}^{M} \sqrt{\eta_m} \Big(\Big| \boldsymbol{g}_{mo}^{T}[n] \hat{\boldsymbol{g}}_{mo}^{*}[\tau_{u,p} + 1] \Big| - \mathbb{E}\Big\{ \Big| \boldsymbol{g}_{mo}^{T}[n] \hat{\boldsymbol{g}}_{mo}^{*}[\tau_{u,p} + 1] \Big| \Big\} \Big) s_o[n]}_{\text{beamforming uncertainty } (BU_o^d)} \\ & + \underbrace{\sqrt{1 - \alpha_{o,n}^2} \sum_{m=1}^{M} \sqrt{\eta_m} \boldsymbol{z}_{mo}^{T}[n] \hat{\boldsymbol{g}}_{mo}^{*}[\tau_{u,p} + 1] s_o[n]}_{\text{Doppler shift effect } (DS_o^d)} \\ & + \sum_{k \neq o} \underbrace{\sum_{m=1}^{M} \sqrt{\eta_m} \boldsymbol{g}_{mo}^{T}[n] \hat{\boldsymbol{g}}_{mk}^{*}[\tau_{u,p} + 1] s_k[n]}_{\text{interference from user k data } (UI_{ok}^{d})} \Bigg] + \underbrace{w_{d,o}[n]}_{\text{noise}}. \end{aligned} \tag{4.9}$$

Capitalizing on the obtained results in Theorem 3.2, the achievable DL data rate for user o at time instant n will be

$$R_{d,o}[n] = \log_2\left(1 + \frac{A_d}{B_d + C_d + \sigma_w^2}\right), \tag{4.10}$$

where

$$A_d = \alpha_{o,n}^2 P_d \Big(\sum_{m=1}^{M} \sqrt{\eta_m} N_{ap} \zeta_{mo}\Big)^2, \qquad B_d = P_d \sum_{k=1}^{K} \sum_{m=1}^{M} N_{ap} \eta_m \zeta_{mk} \beta_{mo},$$

$$C_d = \alpha_{o,n}^2 P_d \sum_{k \neq o} \Big(\sum_{m=1}^{M} \sqrt{\eta_m} N_{ap} \zeta_{mk} \frac{\beta_{mo}}{\beta_{mk}}\Big)^2 |\boldsymbol{\psi}_o \boldsymbol{\psi}_k^{\mathsf{H}}|^2.$$

Note that, the effect of non-orthogonal pilot sequences depends mainly on the number and locations of users, assigned the same pilot sequence. Also, the Doppler shift effect on the channel estimation of a certain user depends on its assigned pilot sequence. Accounting for these effects renders the analysis more complicated. As such and for ease of analysis and tractability, we assume that all users have the worst-case Doppler shift effect in the estimated channel conditions. Also, we do not consider the pilot contamination effect. However, the effect of the presence of non-orthogonal pilot sequences will be discussed later in Section 4.6. As such, the achievable DL rate can be rewritten as

$$R_{d,o}[n] = \log_2\left(1 + \alpha_{o,n}^2 \gamma_{d,o}\right), \tag{4.11}$$

with

$$\gamma_{d,o} = \frac{P_d \Big(\sum\limits_{m=1}^{M} \sqrt{\eta_m} N_{ap} \zeta_{mo}\Big)^2}{P_d N_{ap} \sum\limits_{m=1}^{M} \eta_m \beta_{mo} \sum\limits_{k=1}^{K} \zeta_{mk} + \sigma_w^2}. \tag{4.12}$$

Due to the finite cell size, the point process is not statistically similar at different locations within the cell [101, 102]. For instance, cell-edge users see lower APs densities than users located close to the cell center. Thus, the system performance depends on the receiver location. As such, to calculate the average data rates over different locations of users, one firstly needs to determine the APs density as a function of the user location. In this regard, we introduce the APs density as a function of the reference user location in the following Lemma.

Lemma 4.1. *Assume a cell $A = \boldsymbol{b}(x_o, \mathcal{D})$, where $\boldsymbol{b}(x_o, \mathcal{D})$ represents a disk centered at x_o with radius $\mathcal{D}$, and a reference user at a distance χ from the cell center as shown in Fig. 4.1. The APs density in the region $\boldsymbol{b}(o, r)$ around the reference user o is given by*

$$\Lambda_A(r) = \pi r^2 \lambda_A \ \mathbf{1}(0 \leq r < \mathcal{D} - \chi) + \mathcal{A} \lambda_A \ \mathbf{1}(\mathcal{D} - \chi \leq r < \mathcal{D} + \chi), \tag{4.13}$$

where

$$\mathcal{A} = \mathcal{D}^2 \cos^{-1}\left(\frac{d_1}{\mathcal{D}}\right) - d_1 \sqrt{\mathcal{D}^2 - d_1^2} + r^2 \cos^{-1}\left(\frac{d_2}{r}\right) - d_2 \sqrt{r^2 - d_2^2}, \tag{4.14}$$

with

$$d_1 = \chi - d_2, \qquad d_2 = \frac{r^2 + \chi^2 - \mathcal{D}^2}{2\chi}. \tag{4.15}$$

Proof. The APs density in $\boldsymbol{b}(o,r)$ within a finite area cell $\boldsymbol{b}(x_o,\mathcal{D})$ can be calculated according to two different cases as illustrated in [101]

Case 1 : If $\boldsymbol{b}(x_o,\mathcal{D}) \cap \boldsymbol{b}(o,r) = \boldsymbol{b}(o,r)$, i.e., $0 \leq r < \mathcal{D} - \chi$, then

$$\Lambda_A(r) = \lambda_A \times \int_0^{2\pi} \int_0^{r} y \; dyd\theta = \pi r^2 \lambda_A. \tag{4.16}$$

Case 2 : If $\boldsymbol{b}(x_o,\mathcal{D}) \cap \boldsymbol{b}(o,r) \neq \boldsymbol{b}(o,r)$, i.e., $\mathcal{D} - \chi \leq r < \mathcal{D} + \chi$, then

$$\Lambda_A(r) = \lambda_A \times \mathcal{A}, \tag{4.17}$$

where $\mathcal{A}$ denotes the intersection area between the two circles $\boldsymbol{b}(x_o,\mathcal{D})$ and $\boldsymbol{b}(o,r)$ which can be calculated using (4.14). ■

Theorem 4.1. *A lower bound of the average DL rates for CF mMIMO systems under a specific mobility condition using CB and equal power control can be approximated by*

$$\breve{R}_{d,o}[n] \approx \log_2\left(1 + \alpha_{o,n}^2 \breve{\gamma}_{d,o}^{-1}\right), \tag{4.18}$$

where $\breve{\gamma}_{d,o}$ *is given by*

$$\breve{\gamma}_{d,o} = \int_0^{\mathcal{D}} \int_0^{\mathcal{D}+\chi} \frac{\beta(r_1) + I_{4,d}}{N_{ap}\Big(\frac{\zeta(r_1)}{\sqrt{\zeta(r_1)+I_{1,d}}} + \frac{I_{2,d}}{\sqrt{I_{3,d}}}\Big)^2} \frac{\partial \Lambda_A(r_1)}{\partial r_1} e^{-\Lambda_A(r_1)} \frac{2\chi}{\mathcal{D}^2} dr_1 \; d\chi, \tag{4.19}$$

where

$$I_{1,d} = \int_{r_1}^{\mathcal{D}} \zeta(r) \; \frac{\partial \Lambda_u(r)}{\partial r} \; dr, \quad I_{2,d} = \int_{r_1}^{\mathcal{D}+\chi} \zeta(r) \; \frac{\partial \Lambda_A(r)}{\partial r} \; dr,$$

$$I_{3,d} = \int_{0}^{\mathcal{D}} \zeta(r) \; \frac{\partial \Lambda_u(r)}{\partial r} \; dr, \quad I_{4,d} = \int_{r_1}^{\mathcal{D}+\chi} \beta(r) \; \frac{\partial \Lambda_A(r)}{\partial r} \; dr.$$

Proof. Firstly, the average DL achievable rate is given by

$$\bar{R}_{d,o}[n] = \mathbb{E}\Big\{ \log_2\left(1 + \alpha_{o,n}^2 \gamma_{d,o}\right)\Big\}. \tag{4.20}$$

Then, applying Jensen's inequality, a lower bound of the average DL achievable rate in (4.20) can be expressed by

$$\breve{R}_{d,o}[n] = \log_2\Big(1 + \alpha_{o,n}^2 \breve{\gamma}_{d,o}^{-1}\Big), \tag{4.21}$$

with

$$\breve{\gamma}_{d,o} = \mathbb{E}\big\{1/\gamma_{d,o}\big\} = \mathbb{E}\Big\{\mathbb{E}\big\{(1/\gamma_{d,o})\big|\chi\big\}\Big\}. \tag{4.22}$$

Note that the exact analytical evaluation of $\breve{\gamma}_{d,o}$ is challenging since it requires averaging over all APs and users locations. However, considering the SINR in (4.12), it can be noticed that ζ_{mo}, β_{mo}, and ζ_{mk} decrease with the distance. Also, in such network deployment, at each user, the contribution of nearby APs is dominated, and the received signals at APs will be dominated by the signals from nearby users. As such, we apply the mean plus nearest approximation [91] to simplify the SINR in (4.12).

Regarding the numerator in (4.12), we assume that applying the power normalization factor η_m will not affect the relative contributions of different APs to the reference user o. Thus, the numerator can be approximated by

$$\sum_{m=1}^{M} \sqrt{\eta_m}\zeta_{mo} = \sqrt{\eta_1}\zeta(r_1) + \mathbb{E}\Big[\sum_{m'=2}^{M} \sqrt{\eta_{m'}}\zeta_{m'o}\Big|r_1\Big], \tag{4.23}$$

where m' denotes the order of the APs with respect to (w.r.t) the reference user o. Note that, the first term denotes the contribution of the nearest AP to the reference user as a function of the distance r_1 between user o and its nearest AP. In addition, the second term denotes the average contribution of all other APs from the second nearest AP to the M$^{\text{th}}$ nearest AP conditioned on the distance with the first nearest AP r_1. Different from the work in [91], we consider that conditioning on the first nearest distance r_1, the distance distribution of all other APs is not identical, however, it depends on the order of the AP.

Regarding the first term in (4.23), one can simplify the power normalization coefficient η_1 in (4.7) at the first nearest AP by using the mean plus nearest approximation as follows:

$$\begin{aligned} \eta_1^{-1} &\approx \zeta(r_1) + \mathbb{E}\Big[\sum_{k'=2}^{K} \zeta_{1k'}\Big|r_1\Big], \\ &\approx \zeta(r_1) + \sum_{k'=2}^{K} \int_{r_1}^{\mathcal{D}} \zeta(r) f_{R_{1k'}}\big(r\big|r_1\big)dr, \end{aligned} \tag{4.24}$$

where k' represents the order of users with the first nearest AP to the reference user o. Capitalizing on the joint distance distribution $f_{R_{k'},R_1}\big(r, r_1\big)$ between the first nearest and k'^{th} nearest distances [103], the distance distribution of the k'^{th} nearest distance given the first nearest distance r_1 can be expressed by

$$f_{R_{k'}}\big(r\big|r_1\big) = \frac{\partial \Lambda_u(r)}{\partial r} \frac{\big[\Lambda_u(r) - \Lambda_u(r_1)\big]^{k'-2}}{(k'-2)!} e^{\Lambda_u(r_1)-\Lambda_u(r)}, \tag{4.25}$$

where $\Lambda_u(r)$ denotes the density of users at a distance r from the first nearest AP to the reference user o. In fact, the first nearest AP to user o can be located anywhere around its location. Despite $\Lambda_u(r)$ should account for the AP location w.r.t user o, doing so will complicate the analysis. Hence, we assume that the density of users is independent of the AP location and can be calculated by $\Lambda_u(r) = \pi\lambda_U r^2$. Using (4.25), (4.24) can be calculated as follows:

$$\begin{aligned} \eta_1^{-1} &= \zeta(r_1) + \sum_{k'=2}^{K} \int_{r_1}^{\mathcal{D}} \zeta(r) \frac{\partial \Lambda_u(r)}{\partial r} \frac{\big[\Lambda_u(r) - \Lambda_u(r_1)\big]^{k'-2}}{(k'-2)!} e^{\Lambda_u(r_1)-\Lambda_u(r)} dr, \\ &= \zeta(r_1) + \int_{r_1}^{\mathcal{D}} \zeta(r) \frac{\partial \Lambda_u(r)}{\partial r} e^{\Lambda_u(r_1)-\Lambda_u(r)} \sum_{k'=2}^{K} \frac{\big[\Lambda_u(r) - \Lambda_u(r_1)\big]^{k'-2}}{(k'-2)!} dr, \end{aligned} \tag{4.26}$$

where

$$\begin{aligned}\sum_{k'=2}^{K}\frac{\big[\Lambda_u(r)-\Lambda_u(r_1)\big]^{k'-2}}{(k'-2)!} &= \sum_{k'=0}^{K-2}\frac{\big[\Lambda_u(r)-\Lambda_u(r_1\big]^{k'}}{k'!},\\ &= e^{\Lambda_u(r)-\Lambda_u(r_1)}\frac{\Gamma(K-1,\Lambda_u(r)-\Lambda_u(r_1))}{\Gamma(K-1)},\\ &\overset{(a)}{\approx} e^{\Lambda_u(r)-\Lambda_u(r_1)}.\end{aligned} \tag{4.27}$$

where $\Gamma(\cdot,\cdot)$ is the lower incomplete gamma function. Also, we consider an asymptotic approach assuming $K\to\infty$ to simplify the summation as shown in $\overset{(a)}{\approx}$. Thus, η_1 can be approximated by

$$\eta_1^{-1} \approx \ \zeta(r_1)+\int_{r_1}^{\mathcal{D}}\zeta(r)\frac{\partial\Lambda_u(r)}{\partial r}dr. \tag{4.28}$$

Regarding the second term in (4.23) which includes two random variables, namely, $\eta_{m'}$ and $\zeta_{m'o}$. Also, $\eta_{m'}$ depends on the distribution of users w.r.t the AP m' which differs from one AP to another. This in turn renders the calculation of this term intractable. As such, we approximate this term by

$$\begin{aligned}\mathbb{E}\Big[\sum_{m'=2}^{M}\sqrt{\eta_{m'}}\zeta_{m'o}\big|r_1\Big] &\approx \sqrt{\bar{\eta}}\mathbb{E}\Big[\sum_{m'=2}^{M}\zeta_{m'o}\big|r_1\Big]\\ &\approx \sqrt{\bar{\eta}}\sum_{m'=2}^{M}\int_{r_1}^{\mathcal{D}+\chi}\zeta(r)f_{R_{m'o}}\big(r\big|r_1\big)dr,\end{aligned} \tag{4.29}$$

where we assume that $\eta_{m'}\approx\bar{\eta}$ will be independent of the AP index. In that, $\bar{\eta}$ denotes the inverse of the average summation of channel estimation variances of all users at AP $m',\forall m'=2,\cdots,M$, which can be calculated by

$$\bar{\eta} = \ \bigg(\int_{0}^{\mathcal{D}}\zeta(r)\ \frac{\partial\Lambda_u(r)}{\partial r}\ dr\bigg)^{-1}. \tag{4.30}$$

Then, applying the same procedure as in (4.26) and (4.27), and letting $M\to\infty$, (4.29) can be asymptotically calculated by

$$\begin{aligned}\mathbb{E}\Big[\sum_{m'=2}^{M}\sqrt{\eta_{m'}}\zeta_{m'o}\big|r_0\Big] =& \bigg(\int_{0}^{\mathcal{D}}\zeta(r)\frac{\partial\Lambda_u(r)}{\partial r}\ dr\bigg)^{-\frac{1}{2}}\sum_{m'=2}^{M}\int_{r_1}^{\mathcal{D}+\chi}\zeta(r)\frac{\big[\Lambda_A(r)-\Lambda_A(r_1)\big]^{m'-2}}{(m'-2)!}\\ &\times\frac{\partial\Lambda_A(r)}{\partial r}e^{\Lambda_A(r_1)-\Lambda_A(r)}\ dr,\\ \approx& \bigg(\int_{0}^{\mathcal{D}}\zeta(r)\ \frac{\partial\Lambda_u(r)}{\partial r}\ dr\bigg)^{-\frac{1}{2}}\int_{r_1}^{\mathcal{D}+\chi}\zeta(r)\ \frac{\partial\Lambda_A(r)}{\partial r}\ dr.\end{aligned} \tag{4.31}$$

Accordingly, (4.23) can be approximated by (4.32).

$$\sum_{m=1}^{M}\sqrt{\eta_m}\zeta_{mo} = \frac{\zeta(r_1)}{\sqrt{\zeta(r_1)+\int_{r1}^{\mathcal{D}}\zeta(r)\ \frac{\partial\Lambda_u(r)}{\partial r}\ dr}} + \left(\int_{0}^{\mathcal{D}}\zeta(r)\ \frac{\partial\Lambda_u(r)}{\partial r}\ dr\right)^{-\frac{1}{2}}\int_{r_1}^{\mathcal{D}+\chi}\zeta(r)\ \frac{\partial\Lambda_A(r)}{\partial r}\ dr. \tag{4.32}$$

Regarding the denominator in (4.12), neglecting the noise impact, the term $\sum_{m=1}^{M}\eta_m\beta_{mo}\sum_{k=1}^{K}\zeta_{mk}$ can be approximated by

$$\begin{aligned}\sum_{m=1}^{M}\eta_m\beta_{mo}\sum_{k=1}^{K}\zeta_{mk} &\overset{(a)}{=} \sum_{m=1}^{M}\beta_{mo},\\ &\overset{(b)}{\approx} \beta(r_1)+\int_{r_1}^{\mathcal{D}+\chi}\beta(r)\ \frac{\partial\Lambda_A(r)}{\partial r}\ dr,\end{aligned} \tag{4.33}$$

where $\overset{(a)}{=}$ stems from the fact that the power normalization coefficient $\eta_m = 1/\sum_{k=1}^{K}\zeta_{mk}$. Also, $\overset{(b)}{\approx}$ stems from applying the mean plus nearest approximation. Finally, by substituting (4.32) and (4.33) in (4.12), $\breve{\gamma}_{d,o}$ can be calculated as shown in (4.19). Then, the proof is completed by substituting (4.19) in (4.21). ■

Note that $\breve{R}_{d,o}[n]$ represents the lower bound of the average DL rate under a certain mobility condition. Since we consider the presence of multiple users groups whose mobility conditions are different, the lower bound of the average composite DL rate is given by

$$\breve{R}_d[n] = \sum_{s=1}^{\mathcal{S}}\log_2\left(1+\alpha_{s,n}^2\breve{\gamma}_{d,o}^{-1}\right)\mathbb{P}(o\in\mathcal{G}_s), \tag{4.34}$$

where $\mathcal{S}$ denotes the total number of groups and $\alpha_{s,n}^2$ reflects the Doppler shift effect at time instant n on users belonging to group $\mathcal{G}_s$. Let us consider $\varphi \triangleq \frac{\tau_d}{T-\tau_{u,p}}$ as the ratio of the data symbols, assigned for DL transmission. Also, let $\xi \triangleq \frac{\tau_{u,p}}{T}$ represents the pilot sequence ratio to the whole frame length. For a given frame length T symbols, the average DL rate in bps/Hz considering the aforementioned transmission protocols will be

$$\breve{R}_d = \frac{\xi}{\tau_{u,p}}\sum_{n=\tau_{u,p}+1}^{\tau_{u,p}+\varphi(\frac{\tau_{u,p}}{\xi}-\tau_{u,p})}\breve{R}_d[n]. \tag{4.35}$$

4.4.2 Achievable UL Data Rate

During the UL data transmission phase, all users simultaneously transmit their UL data symbols to APs over the same time-frequency resources. Then, each AP exploits the estimated channel conditions to detect the UL transmitted symbols. Assuming equal power allocation, and applying MRC detection, the local detected UL signal of user o at

the m$^{\text{th}}$ AP at time instant n will be

$$r_{u,o}[n] = \sqrt{P_u}\sum_{k=1}^{K}\hat{\boldsymbol{g}}_{mo}^{H}[\tau_{u,p}+1]\boldsymbol{g}_{mk}[n]s_k[n] + \hat{\boldsymbol{g}}_{mo}^{H}[\tau_{u,p}+1]\boldsymbol{w}_u[n]. \tag{4.36}$$

Then, the detected signal at each AP will be forwarded to the CPU where the detection of each user's data is carried out. Since the estimated channel vectors at each AP are not available at the CPU, the detected signal of user o at the CPU at time instant n from all APs can be expressed by

$$\begin{aligned} r_{u,o}[n] = \sqrt{P_u}\Bigg[& \underbrace{\alpha_{o,n}\sum_{m=1}^{M}\mathbb{E}\Big\{\Big|\hat{\boldsymbol{g}}_{mo}^{H}[\tau_{u,p}+1]\boldsymbol{g}_{mo}[n]\Big|\Big\}s_o[n]}_{\text{desired signal for user } o\ (D_{s_o}^{u})} \\ & + \underbrace{\alpha_{o,n}\sum_{m=1}^{M}\Big(\Big|\hat{\boldsymbol{g}}_{mo}^{H}[\tau_{u,p}+1]\boldsymbol{g}_{mo}[n]\Big| - \mathbb{E}\Big\{\Big|\hat{\boldsymbol{g}}_{mo}^{H}[\tau_{u,p}+1]\boldsymbol{g}_{mo}[n]\Big|\Big\}\Big)s_o[n]}_{\text{beamforming uncertainty } (BU_o^u)} \\ & + \underbrace{\sqrt{1-\alpha_{o,n}^2}\sum_{m=1}^{M}\hat{\boldsymbol{g}}_{mo}^{H}[\tau_{u,p}+1]\boldsymbol{z}_{mo}[n]s_o[n]}_{\text{Doppler shift effect } (DS_o^u)} + \underbrace{\sum_{k\neq o}\sum_{m=1}^{M}\hat{\boldsymbol{g}}_{mo}^{H}[\tau_{u,p}+1]\boldsymbol{g}_{mk}[n]s_k[n]}_{\text{interference from other users } (UI_{ok}^u)}\Bigg] \\ & + \underbrace{\hat{\boldsymbol{g}}_{mo}^{H}[\tau_{u,p}+1]\boldsymbol{w}_{u,o}[n]}_{\text{noise}}. \end{aligned} \tag{4.37}$$

The achievable UL data rate for user o at time instant n is given by

$$R_{u,o}[n] = \log_2\left(1+\frac{A_u}{B_u+C_u+D_u}\right), \tag{4.38}$$

where

$$A_u = \alpha_{o,n}^2 p_u\Big(\sum_{m=1}^{M}N_{ap}\zeta_{mo}\Big)^2, \qquad B_u = p_u\sum_{k=1}^{K}\sum_{m=1}^{M}N_{ap}\zeta_{mo}\beta_{mk},$$

$$C_u = \alpha_{o,n}^2 p_u\sum_{k\neq o}\Big(\sum_{m=1}^{M}N_{ap}\zeta_{mo}\frac{\beta_{mk}}{\beta_{mo}}\Big)^2|\boldsymbol{\psi}_o\boldsymbol{\psi}_k^{\mathsf{H}}|^2, \qquad D_u = \sigma_w^2\sum_{m=1}^{M}N_{ap}\zeta_{mo}\beta_{mo}.$$

Similar to DL, we do not count for the effect of non-orthogonal pilot sequences as this renders the analysis more complicated. Thus, for a typical user o, the achievable UL rate at a certain network realization can be rewritten as

$$R_{u,o}[n] = \log_2\left(1+\alpha_{o,n}^2\gamma_{u,o}\right), \tag{4.39}$$

where

$$\gamma_{u,o} = \frac{p_u\Big(\sum\limits_{m=1}^{M}N_{ap}\zeta_{mo}\Big)^2}{p_u N_{ap}\sum\limits_{m=1}^{M}\zeta_{mo}\sum\limits_{k=1}^{K}\beta_{mk} + \sigma_w^2 N_{ap}\sum\limits_{m=1}^{M}\zeta_{mo}\beta_{mo}}. \tag{4.40}$$

Theorem 4.2. *A lower bound of the average UL rates for CF mMIMO systems under a specific mobility condition using MRC and equal power control can be approximated by*

$$\breve{R}_{u,o} = \log_2\left(1+\alpha_{o,n}^2\breve{\gamma}_{u,o}^{-1}\right). \tag{4.41}$$

where $\breve{\gamma}_{u,o}$ *is given by*

$$\breve{\gamma}_{u,o} = \int_0^{\mathcal{D}} \int_0^{\mathcal{D}+\chi} \frac{\zeta(r_1)\beta(r_1) + I_{2,u} + I_{3,u}(\zeta(r_1) + I_{1,u})}{N_{ap}(\zeta(r_1) + I_{1,u})^2} \frac{\partial \Lambda_A(r_1)}{\partial r_1} \; e^{-\Lambda_A(r_1)} \frac{2\chi}{D^2} dr_1 \; d\chi. \tag{4.42}$$

where

$$I_{1,u} = \int_{r_1}^{\mathcal{D}+\chi} \zeta(r) \frac{\partial \Lambda_A(r_1)}{\partial r_1} \; dr, \; I_{2,u} = \int_{r_1}^{\mathcal{D}+\chi} \zeta(r)\beta(r) \frac{\partial \Lambda_A(r_1)}{\partial r_1} \; dr, \; I_{3,u} = \int_0^{\mathcal{D}} \beta(r) \frac{\partial \Lambda_U(r_1)}{\partial r_1} \; dr.$$

Proof. Firstly, the average UL achievable rate is given by

$$\bar{R}_{u,o}[n] = \mathbb{E}\Big[\log_2 \left(1 + \alpha_{o,n}^2 \gamma_{u,o}\right)\Big]. \tag{4.43}$$

Then, following the same procedure in DL by applying Jensen's inequality, a lower bound of the average UL achievable rate in (4.43) can be expressed by

$$\breve{R}_{u,o} = \; \log_2 \Big(1 + \alpha_{o,n}^2 \breve{\gamma}_{u,o}^{-1}\Big), \tag{4.44}$$

with

$$\breve{\gamma}_{u,o} = \mathbb{E}\big[1/\gamma_{u,o}\big] = \mathbb{E}\Big[\mathbb{E}\big[(1/\gamma_{u,o})\big|\chi\big]\Big]. \tag{4.45}$$

To find $\breve{R}_{u,o}$, we firstly need to simplify the expression of $\gamma_{u,o}$ in (4.40). Regarding the numerator, applying the mean plus nearest approximation, the term $\sum_{m=1}^{M} \zeta_{mo}$ can be approximated by

$$\begin{aligned} \sum_{m=1}^{M} \zeta_{mo} &\approx \zeta(r_1) + \mathbb{E}\Big[\sum_{m'=2}^{M} \zeta_{m'o} \big| r_1 \Big], \\ &\approx \zeta(r_1) + \int_{r_1}^{\mathcal{D}+\chi} \zeta(r) \; \frac{\partial \Lambda_A(r)}{\partial r} \; dr. \end{aligned} \tag{4.46}$$

For the denominator, firstly, we neglect the noise effect. Then, applying some mathematical manipulations, the term $\sum_{m=1}^{M} \zeta_{mo} \sum_{k=1}^{K} \beta_{mk}$ in the denominator can be expressed by

$$\begin{aligned} \sum_{m=1}^{M} \zeta_{mo} \sum_{k=1}^{K} \beta_{mk} &= \sum_{m=1}^{M} \zeta_{mo} \big(\beta_{mo} + \sum_{k \neq o}^{K} \beta_{mk}\big), \\ &= \sum_{m=1}^{M} \zeta_{mo}\beta_{mo} + \sum_{m=1}^{M} \zeta_{mo} \sum_{k \neq o}^{K} \beta_{mk}, \\ &\approx \zeta(r_1)\beta(r_1) + \mathbb{E}\Big[\sum_{m'=2}^{M} \zeta_{m'o}\beta_{m'o} \big| r_1 \Big] + \sum_{m=1}^{M} \zeta_{mo} \sum_{k \neq o}^{K} \beta_{mk}. \end{aligned} \tag{4.47}$$

Following the same procedure as in Theorem 4.1, the second term can be calculated by

$$\begin{aligned} \mathbb{E}\Big[\sum_{m'=2}^{M} \zeta_{m'o}\beta_{m'o} \big| r_1 \Big] &= \sum_{m'=2}^{M} \int_{r_1}^{\mathcal{D}+\chi} \zeta(r)\beta(r) f_{R_{om'}}\big(r \big| r_1\big) \; dr, \\ &= \int_{r_1}^{\mathcal{D}+\chi} \zeta(r)\beta(r) \; \frac{\partial \Lambda_A(r)}{\partial r} \; dr. \end{aligned} \tag{4.48}$$

In addition, the third term in (4.47) can be approximated by

$$\sum_{m=1}^{M}\zeta_{mo}\sum_{k\neq o}^{K}\beta_{mk} \overset{(a)}{\approx} \mathbb{E}\Big[\sum_{k\neq o}^{K}\beta_{mk}\Big]\sum_{m=1}^{M}\zeta_{mo},$$
$$\approx \Big(\int_{0}^{\mathcal{D}}\beta(r)\ \frac{\partial\Lambda_U(r)}{\partial r}\ dr\Big)\Big(\zeta(r_1)+\mathbb{E}\Big[\sum_{m'=2}^{M}\zeta_{m'o}\big|r_1\Big]\Big). \tag{4.49}$$
$$\approx \Big(\int_{0}^{\mathcal{D}}\beta(r)\ \frac{\partial\Lambda_U(r)}{\partial r}\ dr\Big)\Big(\zeta(r_1)+\int_{r_1}^{\mathcal{D}+\chi}\zeta(r)\ \frac{\partial\Lambda_A(r)}{\partial r}\ dr\Big),$$

where $\overset{(a)}{\approx}$ stems from applying the same approximation as (4.29), but on the large-scale fading coefficient rather than the channel estimation variances. Thus, the inner summation will be independent of the AP index and will be equal to its expected value. Then, we apply the mean plus nearest approximation on the summation over the channel estimation variances for the reference user. Using (4.46)-(4.49) in (4.40), $\breve{\gamma}_{u,o}$ can be calculated as shown in (4.42). Then, the proof can be completed by substituting (4.42) into (4.44). ■

Similar to DL, the lower bound of the average composite UL rate over different groups of users is given by

$$\breve{R}_u[n]=\sum_{s=1}^{\mathcal{S}}\log_2\left(1+\alpha_{s,n}^2\breve{\gamma}_{u,o}^{-1}\right)\mathbb{P}(o\in\mathcal{G}_s). \tag{4.50}$$

For a given frame length T symbols, the average UL rate in bps/Hz using the first transmission protocol will be

$$\breve{R}_u=\frac{\xi}{\tau_{u,p}}\sum_{n=\varphi(\frac{\tau_{u,p}}{\xi}-\tau_{u,p})+\tau_{u,p}+1}^{\frac{\tau_{u,p}}{\xi}}\breve{R}_u[n]. \tag{4.51}$$

On the other hand, considering the second transmission protocol, the average UL rate is given by

$$\breve{R}_u=\frac{\xi}{\tau_{u,p}}\sum_{n=\tau_{u,p}+1}^{(1-\varphi)(\frac{\tau_{u,p}}{\xi}-\tau_{u,p})+\tau_{u,p}+1}\breve{R}_u[n]. \tag{4.52}$$

Note that, the difference between the achievable UL rates in (4.51) and (4.52) is the symbols over which the UL data are transmitted for the first transmission protocol (Fig. 4.2a) and the second transmission protocol (Fig. 4.2b), respectively.

4.5 Frame Length Optimization

Here, we investigate the effect of frame length optimization on the DL and UL data rates of CF mMIMO systems under TDD system operation. In addition, we derive novel analytical expressions to determine the appropriate frame length under different environments with

different users' velocities. In doing so, we optimize the frame length to limit the Doppler shift effect on the average achievable DL and UL rates.

We consider the two different transmission protocols for the system operation, discussed in Section 4.2.2. For the first transmission protocol (Fig. 4.2a), the Doppler shift effect will be more prominent on the UL system performance since it experiences worse Doppler shift conditions. Hence, the required frame length for DL and UL rate maximization will be different. Regarding the second transmission protocol (Fig. 4.2b), since the buffered UL data symbols will be processed right after the UL training phase, the UL transmission experiences similar Doppler shift conditions as the DL transmission. However, in fact, the DL transmission phase lasts for longer duration than the UL as higher rates are required in DL transmission. As such, the overall Doppler shift effect on the DL and UL transmission phases will be different. Hence, different frame lengths are required to maximize the DL and UL achievable rates.

In accordance with the previous discussion, maximizing the DL and UL rates simultaneously based on frame length selection is not doable under TDD system operation. In addition, choosing the frame length to maximize the DL achievable rates will result in a degradation in the maximum achievable UL rates, and vice versa. Hence, aiming at achieving near maximum DL and UL rates simultaneously, one can determine the system frame length by solving the following problem:

$$\begin{aligned} &\min_{\xi} \ \varepsilon \varrho_1 + (1-\varepsilon)\varrho_2 \\ &\text{s.t.} \ \ 0 \ < \xi < 1, \end{aligned} \tag{4.53}$$

where

$$\varrho_1 = \ 1 - \frac{\breve{R}_d(\xi)}{\breve{R}_d(\xi_d)}, \qquad \varrho_2 = \ 1 - \frac{\breve{R}_u(\xi)}{\breve{R}_u(\xi_u)}.$$

Besides, $0 \leq \varepsilon \leq 1$ denotes a weight factor and we consider it as a system parameter. Also, ξ_d and ξ_u denote the values of the pilot sequence ratio that achieve maximum DL and UL rates, respectively. The problem in (4.53) strives to minimize a weighted loss of the achievable DL and UL rates relative to their maximum values. Thus, one firstly needs to find the values of ξ_d and ξ_u to solve the problem in (4.53).

Theorem 4.3. *The value of $\xi^* = \xi_d$ that maximizes the DL rates in CF mMIMO systems under the Doppler shift effect can be determined by solving the following*

$$\sum_{s=1}^{\mathcal{S}} \Big((\xi^{*^{-1}} + 1) \ln \left(1 + \breve{\gamma}_{d,o}^{-1} \rho_s^{2\varphi \tau_{u,p} (\xi^{*^{-1}} - 1)}\right) + (1 - \xi^{*^{-1}}) \ln(1 + \breve{\gamma}_{d,o}^{-1}) \Big) \mathbb{P}(o \in \mathcal{G}_s) = 0, \tag{4.54}$$

where ρ_s denotes the temporal correlation coefficient of the channels of users in group $\mathcal{G}_s$.

Proof. The required pilot sequence ratio ξ_d that maximizes the average DL rate can be found by solving the following problem:

$$\begin{aligned} &\max_{\xi} \breve{R}_d \\ &\text{s.t. } 0 < \xi < 1. \end{aligned} \tag{4.55}$$

Note that, the average DL rate can be rewritten as

$$\breve{R}_d = \sum_{s=1}^{\mathcal{S}} \breve{R}_{d,s} \mathbb{P}(o \in \mathcal{G}_s), \tag{4.56}$$

with

$$\breve{R}_{d,s} = \frac{\xi}{\tau_{u,p}} \sum_{n=1}^{\varphi(\frac{\tau_{u,p}}{\xi} - \tau_{u,p})} \log_2\left(1 + \rho_s^{2n} \breve{\gamma}_{d,o}^{-1}\right), \tag{4.57}$$

being the lower bound of average DL rates of users in group $\mathcal{G}_s$. One should note that the objective function in (4.55) is not differentiable w.r.t ξ since ξ is in the upper limit of the summation in (4.57). Hence, we consider replacing the summation operator by the integration operator. In fact, since the achievable data rate at each time symbol n is positive-valued, replacing the summation operator by the integration operator will introduce an upper bound which can be expressed by

$$\breve{R}_d^u = \sum_{s=1}^{\mathcal{S}} \breve{R}_{d,s}^u \mathbb{P}(o \in \mathcal{G}_s), \tag{4.58}$$

with

$$\breve{R}_{d,s}^u = \frac{\xi}{\tau_{u,p}} \int_0^{\varphi(\frac{\tau_{u,p}}{\xi} - \tau_{u,p})} \log_2\left(1 + \rho_s^{2t} \breve{\gamma}_{d,o}^{-1}\right) \, dt. \tag{4.59}$$

Since $\breve{R}_d^u$ and $\breve{R}_d$ have the same behavior as ξ varies, we consider maximizing $\breve{R}_d^u$ instead of $\breve{R}_d$. Note that, the problem now is differentiable w.r.t ξ. Furthermore, the problem can be shown to be concave in ξ as follows. The first and second derivative of $\breve{R}_d^u$ w.r.t ξ will be

$$\begin{aligned} \frac{\partial \breve{R}_d^u}{\partial \xi} &= \sum_{s=1}^{\mathcal{S}} \frac{\partial \breve{R}_{d,s}^u}{\partial \xi} \mathbb{P}(o \in \mathcal{G}_s) \\ &= \sum_{s=1}^{\mathcal{S}} \frac{1}{\tau_{u,p}} \Big(\int_0^{\varphi(\frac{\tau_{u,p}}{\xi} - \tau_{u,p})} \log_2(1 + \breve{\gamma}_{d,o}^{-1} \rho_s^{2t}) \, dt - \varphi \xi^{-1} \log_2\left(1 + \breve{\gamma}_{d,o}^{-1} \rho_s^{2\varphi(\frac{\tau_{u,p}}{\xi} - \tau_{u,p})}\right) \Big) \mathbb{P}(o \in \mathcal{G}_s), \end{aligned} \tag{4.60}$$

$$\begin{aligned} \frac{\partial^2 \breve{R}_d^u}{\partial \xi^2} &= \sum_{s=1}^{\mathcal{S}} \frac{\partial^2 \breve{R}_{d,s}^u}{\partial \xi^2} \mathbb{P}(o \in \mathcal{G}_s) \\ &= \sum_{s=1}^{\mathcal{S}} \frac{2\varphi^2 \breve{\gamma}_{d,o}^{-1} \rho_s^{2\varphi(\frac{\tau_{u,p}}{\xi} - \tau_{u,p})} \ln(\rho_s)}{\xi^3 \ln(2) \left(1 + \breve{\gamma}_{d,o}^{-1} \rho_s^{2\varphi(\frac{\tau_{u,p}}{\xi} - \tau_{u,p})}\right)} \mathbb{P}(o \in \mathcal{G}_s). \end{aligned} \tag{4.61}$$

Since the the value of the channel correlation coefficient $\rho_s < 1, \ \forall s = 1, \cdots, S$, the

second derivative in (4.61) will be always negative-valued. Hence, the problem is concave in ξ and the pilot sequence ratio that maximizes the DL rate ξ^* can be derived by solving

$$\left.\frac{\partial \breve{R}_d^u}{\partial \xi}\right|_{\xi^*} = 0, \tag{4.62}$$

which can be expressed by

$$\sum_{s=1}^{\mathcal{S}} \Bigg(\int_0^{\varphi(\frac{\tau_{u,p}}{\xi}-\tau_{u,p})} \log_2(1+\breve{\gamma}_{d,o}^{-1}\rho_s^{2t})\, dt - \varphi\xi^{-1}\log_2\left(1+\breve{\gamma}_{d,o}^{-1}\rho_s^{2\varphi(\frac{\tau_{u,p}}{\xi}-\tau_{u,p})}\right)\Bigg)\mathbb{P}(o\in\mathcal{G}_s) = 0. \tag{4.63}$$

As it can be seen, (4.63) involves a complex integral whose closed-form expression is not readily available. Therefore, aiming at obtaining the optimal solution ξ^*, we simplify this integral as follows. The term $\breve{\gamma}_{d,o}^{-1}\rho_s^{2t}$ in (4.63) is a monotonically decreasing exponential function in t. Thus, we assume that $\log_2(1+\breve{\gamma}_{d,o}^{-1}\rho_s^{2t})$ can be approximated by a linear decreasing function w.r.t t. Based on this, the first LHS term in (4.63) can be approximated by

$$\begin{aligned}\int_0^{\varphi(\frac{\tau_{u,p}}{\xi}-\tau_{u,p})} \log_2(1+\breve{\gamma}_{d,o}^{-1}\rho_s^{2t})\, dt \approx{}& \frac{\varphi}{2}(\frac{\tau_{u,p}}{\xi}-\tau_{u,p})\log_2(1+\breve{\gamma}_{d,o}^{-1}\rho_s^{2\varphi(\frac{\tau_{u,p}}{\xi}-\tau_{u,p})})\\ &+\frac{\varphi}{2}(\frac{\tau_{u,p}}{\xi}-\tau_{u,p})\log_2(1+\breve{\gamma}_{d,o}^{-1}),\end{aligned} \tag{4.64}$$

and this approximation is tight as will be shown in Section 4.6. After some mathematical manipulations, the proof is completed by substituting (4.64) in (4.63). ■

Regarding the required frame length to maximize the achievable UL data rate, this mainly depends on the adopted transmission protocol. Therefore, we will derive the values of $\xi = \xi_u$ for the two different aforementioned transmission protocols shown in Fig. 4.2.

Theorem 4.4. *The value of $\xi^* = \xi_u^1$ and $\xi^* = \xi_u^2$ that maximizes the UL rates under the Doppler shift effect considering the first and second transmission protocols can be determined by solving* (4.65) *and* (4.66)*, respectively.*

$$\begin{aligned}&\sum_{s=1}^{\mathcal{S}}\Big(\big(0.5(1-\varphi)(\xi^{*^{-1}}-1)-\xi^{*^{-1}}\big)\ln\left(1+\breve{\gamma}_{u,o}^{-1}\rho_s^{2(\tau_{u,p}\xi^{*^{-1}}-\tau_{u,p})}\right)+\\ &\big(0.5(1-\varphi)(\xi^{*^{-1}}-1)+\varphi\xi^{*^{-1}}\big)\ln\left(1+\breve{\gamma}_{u,o}^{-1}\rho_s^{2\varphi(\tau_{u,p}\xi^{*^{-1}}-\tau_{u,p})}\right)\Big)\mathbb{P}(o\in\mathcal{G}_s)=0.\end{aligned} \tag{4.65}$$

$$\begin{aligned}&\sum_{s=1}^{\mathcal{S}}\Big(\big(\xi^{-1}+1\big)\ln\left(1+\breve{\gamma}_{u,o}^{-1}\rho_s^{2(1-\varphi)(\frac{\tau_{u,p}}{\xi}-\tau_{u,p})+2\tau}\right)\\ &\qquad+\big(\big(\xi^{-1}-1\big)\ln\left(1+\breve{\gamma}_{u,o}^{-1}\rho_s^{2\tau_{u,p}}\right)\Big)\mathbb{P}(o\in\mathcal{G}_s)=0.\end{aligned} \tag{4.66}$$

Proof. The expressions can be readily obtained following the same steps to find ξ_d. ■

After calculating ξ_d and ξ_u, $\breve{R}_d(\xi_d)$ can be determined using (4.35) while $\breve{R}_u(\xi_u)$ can

be determined either using (4.51) or (4.52) according to the transmission protocol. Thus, (4.53) can be solved as shown in the following theorem.

Theorem 4.5. *Following the same approach in the proof of Theorem 4.3, the problem in* (4.53) *can be shown to be a convex optimization problem where the optimal pilot sequence ratio* ξ^* *that minimizes the total loss in DL and UL rates is given by*

$$\xi^* = \Upsilon(\xi^*), \tag{4.67}$$

where $\Upsilon(\xi^*)$ *is the solution of* (4.68) *and* (4.69) *for the first and second transmission protocols, respectively.*

$$\begin{aligned}
&\sum_{s=1}^{\mathcal{S}} \Bigg(\frac{\varepsilon\varphi}{2\breve{R}_d(\xi_d)} \Big(-(\xi^{*^{-1}}+1)\ln\left(1+\breve{\gamma}_{d,o}^{-1}\rho_s^{2\varphi\tau_{u,p}(\xi^{*^{-1}}-1)}\right) + (1-\xi^{*^{-1}})\ln(1+\breve{\gamma}_{d,o}^{-1}) \Big) + \frac{1-\varepsilon}{\breve{R}_u(\xi_u)} \\
&\times \Big(\big(0.5(1-\varphi)(\xi^{*^{-1}}-1) - \xi^{*^{-1}}\big)\ln\left(1+\breve{\gamma}_{u,o}^{-1}\rho_s^{2(\tau_{u,p}\xi^{*^{-1}}-\tau_{u,p})}\right) + \big(0.5(1-\varphi)(\xi^{*^{-1}}-1) \\
&+ \varphi\xi^{*^{-1}}\big)\ln\left(1+\breve{\gamma}_{u,o}^{-1}\rho_s^{2\varphi(\tau_{u,p}\xi^{*^{-1}}-\tau_{u,p})}\right) \Big) \Bigg) \mathbb{P}(o\in\mathcal{G}_s) = 0,
\end{aligned} \tag{4.68}$$

$$\begin{aligned}
&\sum_{s=1}^{\mathcal{S}} \Bigg(\frac{\varepsilon\varphi}{\breve{R}_d(\xi_d)} \Big(-(\xi^{*^{-1}}+1)\ln\left(1+\breve{\gamma}_{d,o}^{-1}\rho_s^{2\varphi\tau_{u,p}(\xi^{*^{-1}}-1)}\right) + (1-\xi^{*^{-1}})\ln(1+\breve{\gamma}_{d,o}^{-1}) \Big) \\
&\quad + \frac{(1-\varepsilon)(1-\varphi)}{\breve{R}_u(\xi_u)} \Big(-\big(\xi^{-1}+1\big)\ln\left(1+\breve{\gamma}_{u,o}^{-1}\rho_s^{2(1-\varphi)(\frac{\tau_{u,p}}{\xi}-\tau_{u,p})+2\tau}\right) \\
&\quad + \big(\big(\xi^{-1}-1\big)\ln\left(1+\breve{\gamma}_{u,o}^{-1}\rho_s^{2\tau_{u,p}}\right) \Big) \Bigg) \mathbb{P}(o\in\mathcal{G}_s) = 0.
\end{aligned} \tag{4.69}$$

Note that, (4.68) *and* (4.69) *can be readily solved using any numerical equation solver since both equations are function of one variable* ξ^*.

Proof. The expressions can obtained by following the same steps to find ξ_d and ξ_u. ■

4.6 Numerical Results

We consider APs and users are distributed according to FHPPP in an area with a cell radius $\mathcal{D} = 500\ m$. The pilot transmission power, DL, and UL data transmission power are $P_p = 100$ mW, $P_d = 200$ mW, and $P_p = 100$ mW, respectively. The carrier frequency $f_c = 2$ GHz and the sampling time $T_s = 66.66\ \mu s$. The noise variance $\sigma_w^2 = 290 \times \kappa \times B \times NF$ where κ is the Boltzman constant, $B =$ 10 MHz, denoting the system bandwidth, and $NF =$ 9 dB is the noise figure. Besides, we consider that we have two groups of users in the network. The first group $\mathcal{G}_1$ includes low-velocity users, i.e., pedestrians, whose velocity is 5 km/hr. In addition, the second group $\mathcal{G}_2$ includes high-velocity users with velocity v km/hr. In that, we consider different values of v to study the system

performance under different mobility scenarios. Furthermore, the probability that a user belongs to $\mathcal{G}_1$ is 0.2, unless otherwise specified.

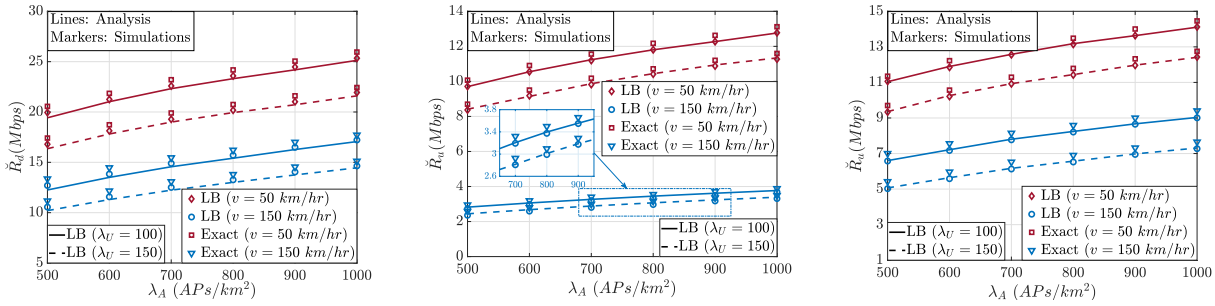

(a) DL (b) UL (Protocol 1) (c) UL (Protocol 2)

Figure 4.3: Average DL and UL rates under the Doppler shift effect.

To assess the accuracy of the derived analytical expressions for the average DL and UL rates, Fig. 4.3 compares the analytical expressions for the lower bound DL and UL data rates with the exact and lower bound achievable ones from numerical results. In that, the average UL rates are calculated for the two transmission protocols in Fig. 4.2. The performance is compared under different mobility conditions of users belonging to $\mathcal{G}_2$, namely, $v = 50,\ 150\ km/hr$. Also, we consider different densities of APs while all APs are equipped with $N_{ap} = 4$ antennas. Besides, two different user densities are considered $\lambda_U = 100,\ 150\ UEs/Km^2$. The frame length $T = 1000$ symbols and the portion of the data symbols assigned for the DL transmission phase is $\varphi = 0.6$. As noted from the results, the proposed lower bound DL and UL rates represent a tight bound of the exact achievable ones. Also, the derived analytical expressions for the lower bound average DL and UL rates are in excellent matching with their counterparts using simulations. Furthermore, it is clear that increasing the velocity of users in $\mathcal{G}_2$ leads to a degradation in the total average DL and UL rates. Also, it is also noted that the Doppler shift effect is more prominent on the achievable UL rates using the first transmission protocol (Fig. 4.2a). This is due to the constant frame length $T = 1000$ symbols for both transmission protocols.

Fig. 4.4 depicts the required pilot sequence ratio that maximizes the average DL and UL rates considering different transmission protocols. We assume that the percentage of data symbols, dedicated for DL transmission is $\varphi = 0.75$. In addition, we assume non-orthogonal pilot sequences are assigned to users for the sake of channel estimation with $\tau_{u,p} = 40$. Fig. 4.4a shows the required pilot sequence ratio for $\lambda_A = 700\ APs/km^2$

assuming different values of λ_U while Fig. 4.4b shows the required pilot sequence ratio for $\lambda_U = 100\ UEs/km^2$ assuming different values of λ_A. Also, Fig. 4.4c depicts the required pilot sequence ratio under different probabilities of a user to be a low-velocity user, i.e., user belongs to $\mathcal{G}_1$, assuming $\lambda_U = 100\ UEs/km^2$ and $\lambda_A = 700\ APs/km^2$. The required pilot sequence ratio to maximize the average DL rates is calculated analytically using (4.54) while the required one to maximize the average UL rates in the first and second transmission protocols is calculated using (4.65) and (4.66), respectively. In addition, the required pilot sequence ratios for DL and UL maximization are calculated by simulations using exhaustive search. As noted, both simulations and analytical results are in perfect matching under different system parameters. Interestingly, since the analysis does not account for the presence of non-orthogonal pilots, this reflects that the optimal frame length for maximizing DL and UL rates is not affected by the pilot contamination effect. Also, it is clear that the required frame length for DL and UL rate maximization decreases with the users' velocity (ξ increases) to limit the Doppler shift effect. Besides, while the required frame length to maximize the average UL rates is the smallest considering the first transmission protocol, it is the largest for the second transmission protocol.

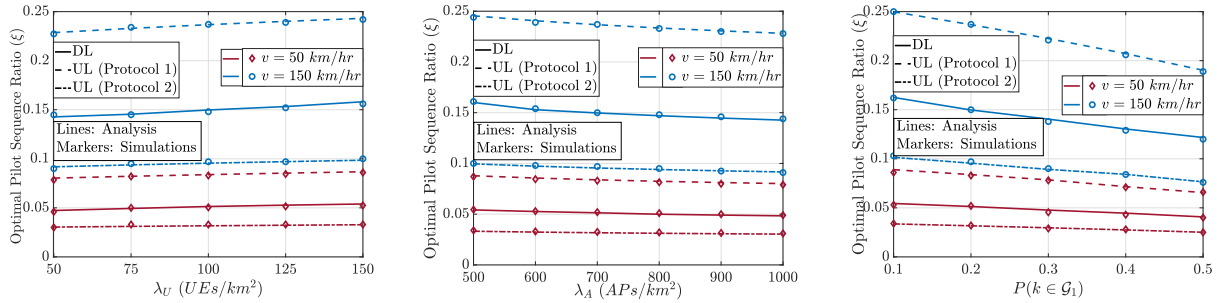

(a) Different λ_U (b) Different λ_A (c) Different $\mathbb{P}(o \in \mathcal{G}_1)$

Figure 4.4: Required pilot sequence ratio to maximize the average DL and UL rates under different system setups.

Notably, increasing the number of users in the system leads to a slight increase in the optimal pilot sequence ratio. Also, this increase becomes more prominent under higher users' velocities. The is a consequence that increasing the number of users degrades the achievable data rates. Thus, the Doppler shift effect will lead to negligible data rates at smaller frame lengths than the required ones for systems with smaller number of users. On the other hand, increasing the number of APs improves the achievable data rates, and hence, increases the required frame lengths to maximize the achievable rates. Further-

more, the optimal pilot sequence ratio decreases as the probability of having low-velocity users increases. This is due to the slight Doppler shift effect on low-velocity users. Hence, increasing the probability of having low-velocity users improves the total average data rates which in turn increases the required frame lengths to maximize the achievable rates. Interestingly, the difference in the required pilot sequence for DL and UL rate maximization becomes more prominent at higher velocities since the experienced Doppler shift effects by both transmission phases become more distinct. This also renders the difference more prominent in the first transmission protocol than in the second transmission protocol.

Fig. 4.5 depicts the average DL and UL data rates considering fixed and optimized frame lengths under different users' velocities. We consider two fixed frame lengths where the first one consider $T = 400$ symbols which is widely used in the literature for CF mMIMO systems, and the second one considers $T = 2000$ symbols. Regarding the optimized frame length, we consider limiting the introduced losses assuming $\varepsilon = 0.5$ in both transmission protocols. Also, the achievable DL and UL rates are compared with the maximum DL and UL rates at $\varepsilon = 1$ and $\varepsilon = 0$, respectively. Fig. 4.5a reveals that adjusting the system frame length according to users' velocities attains superior data rates to the achievable ones using fixed frame length under both transmission protocols. Furthermore, there is a slight improvement that increases with velocity in the optimized achievable rates under the second transmission protocol to those of the first transmission protocol. In addition, while the fixed frame length with $T = 400$ symbols can achieve near optimal DL rates at moderate velocities, i.e., $v = 75,\ 100\ km/hr$, it leads to a degradation in the achievable rates at small and high velocities. Moreover, considering the second fixed frame length $T = 2000$ symbols, it is noted that while it can achieve high DL rates, close to the maximum at low mobility conditions, it results in severe degradation in the achievable rates as the users' velocities increase. Note that, Fig. 4.5c shows a similar behavior of the achievable UL rates in the second transmission protocol to that of DL rates in Fig. 4.5a since both experience comparable Doppler shift effects.

Regarding the achievable UL rates in the first transmission protocol, depicted in Fig. 4.5b, it is noticed that the second fixed frame length with $T = 2000$ symbols always leads to a degradation in the achievable UL rates that becomes severer at higher mobility scenarios. In addition, the first fixed frame length with $T = 400$ symbols is suitable

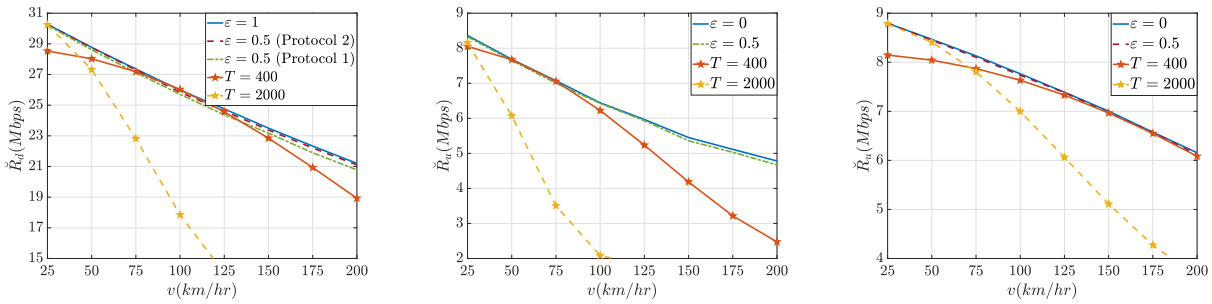

(a) DL (b) UL (Protocol 1) (c) UL (Protocol 2)

Figure 4.5: Average DL and UL rates under fixed and optimized frame length.

for system operation under users' velocities $v = 50,\ 75\ km/hr$. However, as the users' velocities increase, the system performance degrades significantly. In contrary, adjusting the frame length according to the users' velocities can provide near optimal UL rates at different velocities. As such, by adjusting the frame length according to the mobility conditions, one can adopt the first transmission protocol to provide reasonable DL and UL rates with low implementation complexity.

4.7 Summary

We revealed the potential of adapting the system frame length to limit the Doppler shift effect on the DL and UL rates of CF mMIMO systems. This has been studied under different transmission protocols where the first transmission protocol considers placing the UL training before the DL and UL transmission phases, while the second one considers the transmission of UL training between the UL and DL transmission phases. We derived novel analytical expressions for tight lower bounds of the average DL and UL data rates. Then, we exploited the derived analytical results to derive the optimal frame length that maximizes the DL and UL rates under different transmission protocols. Capitalizing on our analytical results, we proposed a frame length selection criterion that minimizes the Doppler shift effect on a total weighted sum of losses in system's rates. We revealed that the optimal frame length for the system operation is significantly affected by the users' velocities. But, it is slightly affected by the APs and UEs densities. Also, selecting the frame length that minimizes a weighted sum of the DL and UL losses can significantly limit the Doppler shift effect on both DL and UL rates simultaneously. Besides, considering equal weights of DL and UL losses, we showed that adapting the frame length according

to the transmission protocol and users' velocities has a great potential in achieving high DL and UL data rates under the Doppler shift effect compared to having a fixed frame length.

Chapter 5
Physical Layer Security in CF mMIMO Systems

5.1 Introduction

Recently, wireless communication networks play a crucial rule in many military and civilian applications. In particular, it is widely used in the transmission of important/private information, such as energy pricing, credit card information, e-health data, and control messages. As such, security is one of the critical concerns of the future wireless networks. The conventional way to improve the security is through bit-level cryptographic techniques and associated protocols at various levels of the data processing stack. However, enhanced ciphering and authentication protocols should be implemented to reinforce the system security. This in turn introduces strong constraints as well as additional costs on UEs. In contrary to conventional cryptographic techniques, a low-cost information theoretic-based security approach that focuses on the secrecy capacity of the propagation channel is through PLS [25]. In fact, PLS can be integrated with the existing security schemes as an additional level of protection as a promising security solution for future wireless communication networks. Interestingly, PLS techniques do not rely on computational complexity and hence, a secure and reliable communication can be attained even if the eavesdroppers have high computational resources for hard mathematical problems.

The secrecy capacity of mMIMO systems has been widely studied assuming passive and active eavesdropper. In that, passive eavesdroppers do not intervene in the communication, but attempt to decode the information sent to one of the legitimate users. On the other hand, since the pilot sequences are public and standardized, active eavesdroppers can actively send spoofing pilot sequence to cause a pilot contamination attack which in turn poses a crucial threat to the system performance. Such attack is known as the pilot spoofing attack [87]. The effect of active eavesdroppers has shown to be more harsh than

passive ones since higher information rate can be leaked to the eavesdropper [88].

Recent works investigate the effect of the pilot spoofing attacks on CF mMIMO systems [104, 105]. The authors in [104] consider the impact of the pilot spoofing attack on the performance of multi-group multi-casting CF mMIMO. In that, the DL beamforming training is adopted to improve the secrecy capacity when the Eve perfectly knows the channel gains. In addition, a simple minimum description length approach is proposed to detect the pilot spoofing attacks by finding the subspace dimension of the received signal correlation matrix. The authors in [105] consider the power allocation problem to maximize the achievable rates of the user under attack considering the case where users are suspected to be an Eve. Nevertheless, these works consider orthogonal pilot sequences are assigned to users (Groups) during the UL channel estimation phase. Different from previous works, we consider non-orthogonal pilot sequences for the UL channel estimation phase. Also, we propose two different approaches to improve the secrecy performance of CF mMIMO systems.

For the first proposed approach, we assume that APs cannot detect the attack of an active Eve. Thus, APs have no statistical or instantaneous information about the Eve. In addition, the Eve does not perfectly know the channel gains with the APs. However, the Eve strives to estimate its channel conditions with the APs to overhear the attacked user's signal by capitalizing on the applied DL transmission technique. In that, we propose a novel DL pilots transmission technique that significantly improves the secrecy rate of CF mMIMO systems. The proposed technique is a distributed technique that aims at limiting the Eve's capability in estimating its channel conditions with the deployed APs, and hence, improving the secrecy capacities of CF mMIMO systems.

In the second approach, we exploit RISs to improve the secrecy capacities of CF mMIMO systems. RIS has been recently proposed as a promising technology to improve the performance of wireless communication networks by re-configuring the wireless propagation channels through software-controlled reflections [106]. In particular, RIS is a planar surface that includes a large number of low-cost passive reflecting elements that can induce phase change to the incident signals to collaboratively achieve fine-grained beams. As such, RISs can smartly modify the channel conditions between the transmitter and the receiver to meet the target requirements of wireless networks. The integration of RIS and CF mMIMO is still in its infancy where only a few works have considered RIS-

aided CF mMIMO [107, 108] to boost the network DL performance in-terms of spectral and energy efficiencies. Aside from that, different works have investigated the potential of RISs in improving the PLS performance of wireless networks as in [109, 110] and references therein. However, these investigations are limited to conventional networks in which legitimate users are communicating with a single base station in the presence of passive Eve. Furthermore, different impractical assumptions have been considered such as the perfect knowledge of legitimate users' channels which does not capture the inevitable pilot contamination effect that strongly degrades the quality of estimated channels in real scenarios. Also, some works assumed perfect knowledge of Eve's channel which represents a strong assumption that cannot be held in practice.

Based on the above, we propose a centralized RIS-based CF mMIMO operation to improve the secrecy capacities of CF mMIMO systems under the assumption that the system can detect the presence of an active Eve while considering imperfect channel state information of both legitimate users and the active Eve. In that, we jointly optimize the phase shifts of RIS elements and the transmit power coefficients at APs to minimize the leakage rate towards the active Eve while maintaining a certain QoS for legitimate users.

5.2 Secure DL Transmission Using Nearest APs-Based DL Pilots

In this section, we introduce a highly-secure distributed DL transmission approach for CF mMIMO systems. In particular, a novel DL pilots transmission technique is proposed to limit the Eve's capability in estimating its channel conditions with the deployed APs while improving the achievable rates for legitimate users. Thus, improving the secrecy capacities of CF mMIMO systems. Also, we compare the performance of the proposed technique with other conventional DL transmission techniques, namely, no DL pilots and DL beamforming training.

5.2.1 System Model

We consider that the CF mMIMO system includes a randomly located active Eve that attempts to overhear the intended signal of the nearest legitimate user as depicted in Fig. 5.1. Also, we assume that all APs, users, and Eve are equipped with single-antenna

terminals. The users-APs channels are modeled as Rayleigh fading channels.

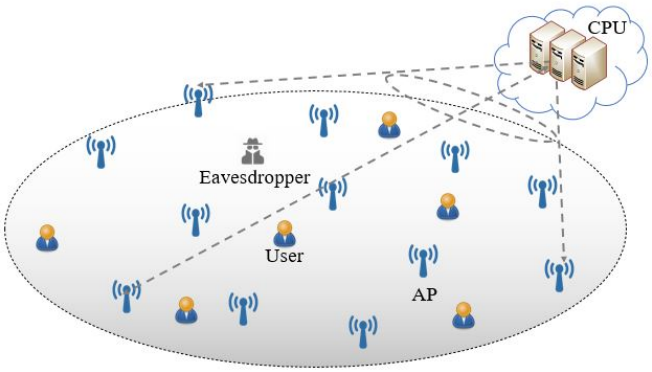

Figure 5.1: CF mMIMO system with an active Eve.

5.2.1.1 Channel Model

Since we consider single-antenna APs, the users-APs channels are represented by scalar variables rather than the vector representation in (3.1). Also, We consider block fading channels. Consequently, the channel between the m^{th} AP and the k^{th} user is given by

$$g_{mk} = \sqrt{\beta_{mk}} h_{mk}, \tag{5.1}$$

where $h_{mk} \sim \mathcal{CN}(0,1)$ denotes the small-scale fading coefficients. Besides, β_{mk} represents the large-scale fading coefficient that accounts for path-loss and shadowing effects as defined in (3.2). Similarly, the channel between the m^{th} AP and the active Eve is modeled by

$$g_{mE} = \sqrt{\beta_{mE}} h_{mE}, \tag{5.2}$$

with $h_{mE} \sim \mathcal{CN}(0,1)$.

5.2.2 Channel Estimation Under Pilot Attack

During the UL training phase, the Eve exploits the advantage that the pilot sequences are public and standardized to obtain the pilot sequences. To account for the worst-case scenario, we assume that the Eve attempts to intercept the data of its nearest legitimate user. Letting $\boldsymbol{\psi}_E \in \mathbb{C}^{\tau_{u,p} \times 1}$ denotes the spoofing pilot sequence, the received pilot sequence vector $\boldsymbol{y}_{p,m} \in \mathbb{C}^{1 \times \tau_{u,p}}$, at the m^{th} AP will be

$$\boldsymbol{y}_{p,m} = \sqrt{P_u \tau_{u,p}} \sum_{k'=1}^{K} g_{mk'} \boldsymbol{\psi}_{k'}^T + \sqrt{P_E \tau_{u,p}} g_{mE} \boldsymbol{\psi}_E^T + \boldsymbol{w}_{p,m}, \tag{5.3}$$

where P_E denotes the power of the transmitted pilot symbols from the active Eve, respectively. In addition, $\boldsymbol{w}_{p,m} \in \mathbb{C}^{1 \times \tau_{u,p}}$, represents the additive noise vector at the m^{th} AP

whose elements are i.i.d. random variables $\mathcal{CN}(0, \sigma_w^2)$. To estimate the channel coefficient of user k at the m^{th} AP, the received pilot signal $\boldsymbol{y}_{p,m}$ is firstly projected on $\boldsymbol{\psi}_k^*$ as follows:

$$\tilde{y}_{p,m,k} = \boldsymbol{y}_{p,m}\boldsymbol{\psi}_k^*. \tag{5.4}$$

Different from previous works where the Eve's channel statistics are assumed to be available at the AP, we assume that the APs have no information about the channel statistics of the Eve. As such, instead of applying the MMSE estimation, we apply a partial-MMSE by exploiting the knowledge of the legitimate users' channels statistics only. Therefore, the estimated channel conditions of user k at the m^{th} AP can be determined by

$$\hat{g}_{mk} = c_{mk}\tilde{y}_{p,m,k}, \tag{5.5}$$

with

$$c_{mk} = \frac{\sqrt{P_p\tau_{u,p}}\beta_{mk}}{\sum\limits_{k'=1}^{K} P_p\tau_{u,p}\beta_{mk'}\left|\boldsymbol{\psi}_{k'}^T\boldsymbol{\psi}_k^*\right|^2+\sigma_w^2}. \tag{5.6}$$

Hence, the power of the estimated channel $\hat{g}_{mk}$ will be

$$\zeta_{mk} = \zeta'_{mk} + P_E\tau_{u,p}c_{mk}^2\beta_{mE}|\boldsymbol{\psi}_E^T\boldsymbol{\psi}_k^*|, \tag{5.7}$$

where

$$\zeta'_{mk} = c_{mk}\sqrt{P_p\tau_{u,p}}\beta_{mk}, \tag{5.8}$$

where the effect of the Eve attack on the channel estimation variance is present when it transmits the same pilot sequence of the k^{th} user.

5.2.3 DL Transmission Techniques for CF mMIMO Systems

In CF mMIMO, each AP transmits the DL data symbols of different users over the same time-frequency resources by means of beamforming. Applying CB precoding, the transmitted signal from the m^{th} AP can be expressed by

$$x_m = \sqrt{P_d}\sum_{k=1}^{K}\sqrt{\eta_{mk}}\hat{g}_{mk}^* s_k, \tag{5.9}$$

where η_{mk} denotes the power control coefficient. Assuming equal power allocation, the power control coefficient can be calculated as in (4.7). The received signal from all APs at the k^{th} user and the Eve will be

$$r_b = \sum_{m=1}^{M} g_{mb}x_m + w_b, \tag{5.10}$$

where $b \in \{k, E\}$. Note that, this notation will be applied across this Chapter to avoid repetition.

In the literature, different techniques are applied to detect the DL transmitted signals. For instance, betting on the channel hardening property, users can detect their own data symbols based on their knowledge of the channel statistics. However, in CF mMIMO systems, the channel hardening property does not hold, especially at small and moderate APs densities [75]. Hence, this approach leads to a degradation in the achievable data rates. On the other hand, the authors in [111] apply the DL beamforming training so that users can estimate their instantaneous channel gains. Results show that applying DL beamforming training improves the DL rates significantly.

Recent works consider applying the DL beamforming training to improve the secrecy rate of CF mMIMO systems under the assumption that the Eve has perfect knowledge of the channel gains [104]. We differently assume that the Eve does not perfectly know their channel gains. Nevertheless, they can exploit the DL transmission protocol to estimate their channel conditions with the APs. In that, we discuss the DL secrecy rate of the system considering three different DL transmission techniques where the secrecy rate is given by

$$R_{sec} = \Big[R_k - R_E\Big]^+, \tag{5.11}$$

with R_k and R_E denote the achievable rate for the legitimate user and the Eve, respectively. Besides, $[x]^+ = \max\{0, \mathrm{x}\}$.

5.2.3.1 No DL Pilots

Considering no DL pilot, the legitimate users detect their intended data symbols by the knowledge of the channel statistics. Note that, in this scenario, it will be harder for the Eve to estimate its instantaneous channel conditions. Thus, we assume that the Eve attempts to detect the signal of the user under attack depending on its channel statistics with the APs which is assumed to be available at the Eve. Hence, assuming that the Eve attempts to overhear the signal of the k^{th} user, the received DL signal at the k^{th} and the Eve can be as expressed by

$$r_b^{NP} = \sqrt{P_d}\mathbb{E}\{a_{bk}\} + \sqrt{P_d}\big(a_{bk} - \mathbb{E}\{a_{bk}\}\big) + \sqrt{P_d}\sum_{k' \neq K} a_{bk'} + w_b, \tag{5.12}$$

where $a_{bk'} \triangleq \sum_{m=1}^{M} \sqrt{\eta_{mk'}} g_{mb} \hat{g}^*_{mk'}$, $\forall k' = 1, \cdots, K$. Considering the fact that uncorrelated Gaussian noise represents the worst-case interference and applying the use-and-then-forget

technique, the achievable DL rate of the k^{th} legitimate user and the Eve will be

$$R_b^{NP} = \log_2\left(1 + \frac{P_d|\mathbb{E}\{a_{bk}\}|^2}{P_d Var\{a_{bk}\} + P_d \sum\limits_{k'\neq k} \mathbb{E}\{|a_{bk'}|^2\} + \sigma_w^2}\right). \tag{5.13}$$

Considering the performance of the k^{th} legitimate user ($b = k$), the different terms in (5.13) can be calculated as follows:

$$\begin{aligned}
\mathbb{E}\{a_{kk}\} &= \sum_{m=1}^{M} \sqrt{\eta_{mk}}\zeta'_{mk}, \\
Var\{a_{kk}\} &= \sum_{m=1}^{M} \eta_{mk}\big(\zeta'_{mk}\beta_{mk} + P_E\tau_{u,p}c_{mk}^2\beta_{mk}\beta_{mE}|\boldsymbol{\psi}_E^T\boldsymbol{\psi}_k^*|^2\big), \\
\mathbb{E}\{|a_{kk'}|^2\} &= \sum_{m=1}^{M} \eta_{mk'}\big(\zeta'_{mk'}\beta_{mk} + P_E\tau_{u,p}c_{mk'}^2\beta_{mk}\beta_{mE}|\boldsymbol{\psi}_E^T\boldsymbol{\psi}_{k'}^*|^2\big) \\
&\quad + \Big(\sum_{m=1}^{M} \sqrt{\eta_{mk'}}\zeta'_{mk'}\frac{\beta_{mk}}{\beta_{mk'}}\Big)^2|\Psi_k\Psi_{k'}^{\mathsf{H}}|^2.
\end{aligned} \tag{5.14}$$

In addition, regarding the performance of the Eve ($b = E$), the different terms in (5.13) can be determined as follows:

$$\begin{aligned}
\mathbb{E}\{a_{Ek}\} &= \sum_{m=1}^{M} \sqrt{P_E\tau_{u,p}\eta_{mk}}c_{mk}^2\beta_{mE}|\boldsymbol{\psi}_E^T\boldsymbol{\psi}_k^*|, \\
Var\{a_{Ek}\} &= \sum_{m=1}^{M} \eta_{mk}\big(\zeta'_{mk}\beta_{mE} + P_E\tau_{u,p}c_{mk}^2\beta_{mE}^2|\boldsymbol{\psi}_E^T\boldsymbol{\psi}_k^*|^2\big), \\
\mathbb{E}\{|a_{Ek'}|^2\} &= \sum_{m=1}^{M} \eta_{mk'}\big(\zeta'_{mk'}\beta_{mE} + 2P_E\tau_{u,p}c_{mk'}^2\beta_{mE}^2|\boldsymbol{\psi}_E^T\boldsymbol{\psi}_{k'}^*|^2\big).
\end{aligned} \tag{5.15}$$

5.2.3.2 DL Beamforming Training

Aiming at providing the users with their effective channel gains to improve the achievable DL rates, DL beamforming training is applied. Using DL beamforming training keeps the system scalable in the number of APs since the DL pilots length is independent of the number of APs, but depends on the number of users. Let $\boldsymbol{\phi}_k \in \mathbb{C}^{\tau_{d,p}^{DT}\times 1}$ denotes the DL training sequence, transmitted from user k where $\|\boldsymbol{\phi}_k\|^2 = 1$. We consider orthogonal DL pilots are allocated to users with $\tau_{d,p}^{DT} \geq K$. In the DL training beamforming, the pilot sequences are beamformed to the users by applying CB precoding technique. As such, the transmitted pilot sequence vector from the m^{th} AP will be

$$\boldsymbol{x}_{p,m}^{DT} = \sqrt{P_{d,p}\tau_{d,p}^{DT}}\sum_{k'=1}^{K} \sqrt{\eta_{mk'}}\hat{g}_{mk'}^*\boldsymbol{\phi}_{k'}^T, \tag{5.16}$$

where $P_{d,p}$ denotes the transmit power per DL pilot symbol. Then, the received pilot sequence vectors at the k^{th} legitimate user and the Eve can be expressed by

$$\boldsymbol{r}_{p,b}^{DT} = \sqrt{P_{d,p}\tau_{d,p}^{DT}} \sum_{k'=1}^{K} a_{bk'} \boldsymbol{\phi}_{k'}^{T} + \boldsymbol{w}_{p,b}. \tag{5.17}$$

Assuming the Eve knows the assigned pilot sequence to the target user k, it exploits this to estimate the channel gain a_{Ek}. Thus, the received DL training signal at user k and the Eve will be firstly projected on $\boldsymbol{\phi}_k$ as follows:

$$\tilde{y}_{p,b}^{DT} = \sqrt{P_{d,p}\tau_{d,p}^{DT}} a_{bk} + \boldsymbol{w}_{p,b}\boldsymbol{\phi}_k^{*}. \tag{5.18}$$

Then, the linear MMSE estimation can be applied to estimate the channel gains as follows:

$$\hat{a}_{bk} = \mathbb{E}\{a_{bk}\} + \frac{\sqrt{P_{d,p}\tau_{d,p}^{DT}} Var\{a_{bk}\}}{P_{d,p}\tau_{d,p}^{DT} Var\{a_{bk}\} + 1} \Big(\tilde{y}_{p,b}^{DT} - \sqrt{P_{d,p}\tau_{d,p}^{DT}} \mathbb{E}\{a_{bk}\} \Big). \tag{5.19}$$

Let $\tilde{a}_{bk} = a_{bk} - \hat{a}_{bk}$ denotes the estimation error of a_{bk}. Hence, the achievable DL rate of the k^{th} legitimate user and the Eve can be calculated by [111]

$$R_b^{DT} = \mathbb{E}\left\{ \log_2 \left(1 + \frac{P_d |\hat{a}_{bk}|^2}{P_d \mathbb{E}\{|\tilde{a}_{bk}|^2\} + P_d \sum\limits_{k' \neq k} \mathbb{E}\{|a_{bk'}|^2\} + \sigma_w^2} \right) \right\}, \tag{5.20}$$

with

$$\mathbb{E}\{|\tilde{a}_{bk}|^2\} = \frac{Var\{a_{bk}\}}{P_{d,p}\tau_{d,p}^{DT} Var\{a_{bk}\} + 1}, \tag{5.21}$$

where the expectation and the variance of different channel gains in (5.20) and (5.21) are given in (5.14) and (5.15) for the legitimate user and the Eve, respectively.

5.2.3.3 Nearest APs DL Pilots

In fact, the DL training beamforming significantly improves the achievable DL rates in CF mMIMO systems. However, since the DL pilots are transmitted from all APs, the Eve can exploit the beamforming training technique to estimate its channel gain with APs. This in turn increases the information rate, leaked to the Eve. As such, we propose a new DL pilots transmission technique that can limit the information leakage to the Eve to attain high secrecy rates in CF mMIMO systems.

In CF mMIMO systems, each user is effectively served by a finite number of APs since APs are distributed over a large area. An important question is how many APs will dominate the contribution to the received signal. To address this, let us consider $\dot{\gamma}_m$ as the channel gain of the m^{th} nearest AP to the composite channel gain from all APs. In other words, $\dot{\gamma}_m$ represents the contribution of the m^{th} nearest AP to the total received signal. Fig. 5.2 depicts the CDFs of the contributions of the different orders of APs over different

network realizations assuming $K = 20$ and $M = 100$. Intuitively, the first nearest AP has the dominant contribution to the total channel gain, however, the contribution decreases significantly for higher orders of APs. Besides, the distinction between the contributions of different APs fades out as the APs orders increase.

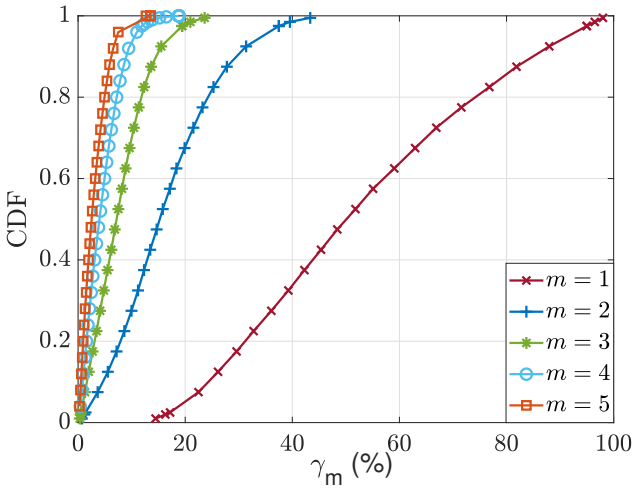

Figure 5.2: CDF of the m^{th} nearest AP channel gain to the total channel gain.

To limit the capabilities of the Eve to estimate its DL channels with the APs while attaining considerable signal strengths at the legitimate users, we consider transmitting DL pilots from the first two nearest APs for each user. As such, the user can estimate the channels, carrying the effective contribution of the received signal. Besides, it detects the received signals from other APs by the knowledge of the channel statistics. Letting $\mathcal{A}_{NA}$ denotes the set of the first two nearest APs for all legitimate users. In addition, $\daleth \in \mathbb{C}^{\tau_{d,p}^{NA} \times \dot{M}}$ is the DL pilot sequence matrix in the proposed technique, where $\tau_{d,p}^{NA}$ is the length of DL pilot sequences and $\dot{M}$ denotes the number of APs in $\mathcal{A}_{NA}$. We consider non-orthogonal pilot sequences where $\tau_{d,p}^{NA} < \dot{M}$. In addition, the pilots are assigned to the APs in a random manner, but under a condition that the assigned pilot sequences to the first two nearest APs for each user k are orthogonal. For instance, $\beth_{m_{k,1}}^T \beth_{m_{k,2}}^* = 0, \forall k = 1, \cdots, K$, where $\beth_{m_{k,1}}, \beth_{m_{k,2}} \in \daleth$, are the assigned pilot sequences to the first and second nearest APs of user k, respectively. Thus, the received pilot sequence at the k^{th} legitimate user and the Eve will be

$$\boldsymbol{r}_{p,b}^{NA} = \sqrt{P_{d,p} \tau_{d,p}^{NA}} \sum_{m'=1}^{\dot{M}} g_{m'b} \beth_{m'}^T + \boldsymbol{w}_{p,b}. \tag{5.22}$$

After user k receives the DL pilot signal, it performs linear MMSE estimation of the

nearest APs channel conditions as follows:

$$\hat{g}^{NA}_{m_{k,j}k} = D_{m_{k,j}k} \boldsymbol{r}^{NA}_{p,k} \boldsymbol{\beth}^{*}_{m_{k,j}}, \tag{5.23}$$

where

$$D_{m_{k,j}k} = \frac{\sqrt{P_{d,p}\tau^{NA}_{d,p}}\beta_{m_{k,j}k}}{\sum\limits_{m'=1}^{N} P_{d,p}\tau^{NA}_{d,p}\beta_{m'k}\left|\boldsymbol{\beth}^{T}_{m'}\boldsymbol{\beth}^{*}_{m_{k,j}}\right|^2+\sigma^2_w}, \tag{5.24}$$

and $j \in \{1,2\}$ represents the order of the AP, i.e., first nearest ($j=1$) or second nearest ($j=2$). Regarding the Eve performance, we consider two different operations. Firstly, it follows the same procedure of the legitimate user by estimating its channel conditions with the first two nearest APs. Secondly, we assume that the Eve may estimate the corresponding channel conditions of all APs in the set $\mathcal{A}_{NA}$. Therefore, it can detect the target user's data arriving from these APs based on instantaneous knowledge of the channel conditions. The MMSE estimate of the Eve's channel conditions with AP $n \in \mathcal{A}_{NA}$ will be

$$\hat{g}^{NA}_{mE} = D_{mE}\ \boldsymbol{r}^{NA}_{p,E}\ \boldsymbol{\beth}^{*}_{m}, \tag{5.25}$$

where D_{mE} can be calculated as $D_{m_{k,j}k}$ in (5.24). Using the proposed DL pilots technique, the received DL signal at the k^{th} legitimate user and the Eve will be

$$r^{NA}_{b} = \sqrt{P_d}a^{NA}_{bk} + \sqrt{P_d}\mathbb{E}\{a'_{bk}\} + \sqrt{P_d}\big(a'_{bk} - \mathbb{E}\{a'_{bk}\}\big) + \sqrt{P_d}\sum_{k'\neq K} a_{bk'} + w_b, \tag{5.26}$$

where $a'_{bk} \triangleq a_{bk} - a^{NA}_{bk}$. Besides, for the k^{th} legitimate user, the term a^{NA}_{bk} can be defined as $a^{NA}_{kk} \triangleq \sum\limits_{j=1}^{2}\sqrt{\eta_{m_{k,j}k}}g_{m_{k,j}k}\hat{g}^{*}_{m_{k,j}k}$. Similarly, considering the Eve, the term a^{NA}_{bk} can be defined by $a^{NA}_{Ek} \triangleq \sum\limits_{m'\in\mathcal{A}_{NA}}\sqrt{\eta_{m'k}}g_{m'E}\hat{g}^{*}_{m'k}$, when the Eve estimates the DL channel conditions with all APs $\in \mathcal{A}_{NA}$. Also, the latter expression can adapt to the case where the Eve estimates the channel conditions with the two nearest APs. Therefore, the achievable DL rates for the k^{th} legitimate user and the Eve can be calculated by

$$R^{NA}_{b} = \mathbb{E}\left\{\log_2\left(1 + \frac{P_d\big(|\hat{a}^{NA}_{bk}|^2+|\mathbb{E}\{a'_{bk}\}|^2\big)}{P_d\mathbb{E}\{|\tilde{a}^{NA}_{bk}|^2\} + P_dVar\{a'_{bk}\} + P_d\sum\limits_{k'\neq k}\mathbb{E}\{|a_{bk'}|^2\} + \sigma^2_w}\right)\right\}, \tag{5.27}$$

Note that, for the legitimate user, the term $\hat{a}^{NA}_{kk} \triangleq \sum\limits_{j=1}^{2}\sqrt{\eta_{m_{k,j}k}}\hat{g}^{NA}_{m_{k,j}k}\hat{g}^{*}_{m_{k,j}k}$ denotes the desired received signal from the first two nearest APs. In addition, the term $\tilde{a}^{NA}_{kk} \triangleq \sum\limits_{j=1}^{2}\sqrt{\eta_{m_{k,j}k}}(g_{m_{k,j}k} - \hat{g}^{NA}_{m_{k,j}k})\hat{g}^{*}_{m_{k,j}k}$ represents the effect of the DL channel estimation error. The terms $\hat{a}^{NA}_{Ek}$ and $\tilde{a}^{NA}_{Ek}$ can be defined in a similar way for the Eve. Besides, $\mathbb{E}\{|\tilde{a}^{NA}_{kk}|^2\}$

and $\mathbb{E}\{|\tilde{a}_{Ek}^{NA}|^2\}$ can be calculated by

$$\begin{aligned}\mathbb{E}\{|\tilde{a}_{kk}^{NA}|^2\} &= \sum_{j=1}^{2} \sqrt{\eta_{m_{k,j}k}}\beta_{m_{k,j}k}\big(1-\sqrt{P_{d,p}\tau_{d,p}^{NA}}D_{m_{k,j}k}\big)\zeta_{m_{k,j}k},\\ \mathbb{E}\{|\tilde{a}_{Ek}^{NA}|^2\} &= \sum_{m'\in\mathcal{A}_{NA}} \sqrt{\eta_{m'k}}\beta_{m'E}\big(1-\sqrt{P_{d,p}\tau_{d,p}^{NA}}D_{m'E}\big)\zeta_{m'k}.\end{aligned} \tag{5.28}$$

5.2.4 Numerical Results and Simulations

In this section, we discuss simulation results to give insights on the impact of pilot spoofing attack on the performance of CF mMIMO systems under different DL transmission strategies. We consider 100 APs and 20 users are uniformly distributed in a square area of size 1×1 km^2. The carrier frequency $f_c = 2$ GHz. In addition, the active Eve is located randomly in the studied area. The UL pilot transmission power of legitimate users $P_p = 0.1$ Watt. Besides, the DL data and pilot transmission powers $P_d = P_{d,p} = 0.2$ Watt. The noise variance is denoted by $\sigma_w^2 = 290 \times \kappa \times B \times NF$ where κ is the Boltzman constant, $B =$ 20 MHz, denoting the system bandwidth, and $NF =$ 9 dB is the noise figure. Also, we consider a coherence time interval $\tau_c = 200$ samples. The length of non-orthogonal pilot sequences in the UL training phase is $\tau_{u,p} = 10$. Regarding the DL training training beamforming, we apply orthogonal pilot sequences during the DL channel estimation phase $\tau_{d,p}^{DT} = 20$. However, in the proposed technique, we assume non-orthogonal pilot sequences with $\tau_{d,p}^{NA} = 10$.

Fig. 5.3 depicts the CDF of the achievable DL rates of legitimate users, the leakage DL rates to Eve, and the secrecy rates in bps/Hz. It is assumed that the transmitting power of pilot symbols from the Eve is $P_E = 0.2$ Watt. Fig. 5.3a shows the CDF of the achievable DL rates of legitimate users. Notably, applying the DL beamforming training increases the achievable rates significantly. In addition, the performance of the proposed technique approaches that of the DL beamforming training technique. Also, the performance gap between the proposed technique and the DL beamforming training is small. The reason behind such gap is that while in the DL beamforming training, each user estimates the actual channel gain, in the proposed technique, each user estimates the channel with the first two nearest APs. Hence, the errors in the detection of the signals, arriving form other APs depending on the channel statistics leads to such gap in the achievable DL rates.

Regarding the leakage DL rates to the Eve depicted in Fig. 5.3b, it is noted that applying no DL pilots technique significantly limits the information leakage to the Eve.

On the other hand, applying the DL beamforming training is in the Eve favor, where the Eve can attain high leakage rates, compared to no DL pilots and the proposed technique. Interestingly, applying the proposed technique can limit the information leakage to the Eve, and the information leakage rates are comparable to those, resulting from applying no DL pilots technique. It is also noted that in the proposed technique, the Eve cannot benefit from estimating the channel conditions with all the selected APs to send DL pilots. This is a consequence that the selected APs for DL pilots transmission are chosen to be in favor of users, and hence, they might not be the best APs from the Eve perspective.

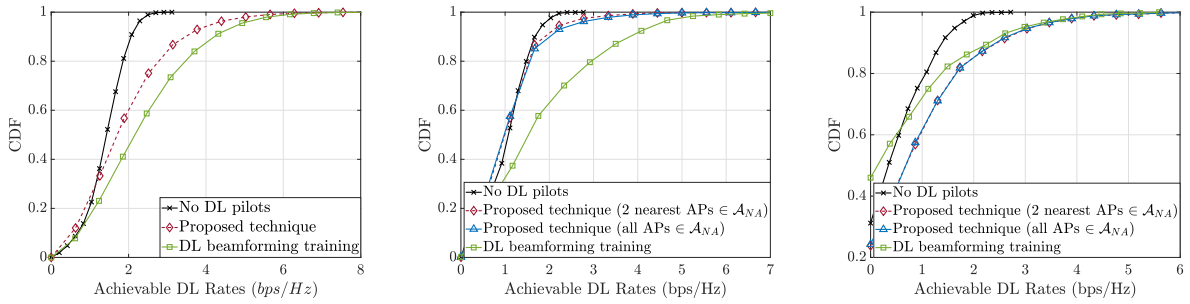

(a) Legitimate users (b) Information leakage (c) Secrecy rates

Figure 5.3: CDF of the DL achievable rates of legitimate users, the information leakage to Eve, and the secrecy rates.

Fig. 5.3c shows the CDF of the achievable secrecy rates using the studied DL transmission strategies. It is clear that the proposed technique outperforms both no DL pilots and the DL beamforming training techniques. Besides, the secrecy outage probability of the DL beamforming training is superior to other techniques. The reason is that the proposed technique can improve the achievable DL rates of the legitimate user, while limiting the information leakage to the Eve. On the other hand, the DL training beamforming increases the information leakage to the Eve while improving the achievable rates of legitimate users.

Fig. 5.4 depicts the average secrecy rates of the aforementioned transmission techniques under different Eve's transmit power of spoofing pilot symbols P_E. The transmit power of pilot symbols from legitimate users is 0.1 Watt. Notably, the proposed technique is more robust as the Eve increases the transmit power of the spoofing pilot symbols. Besides, the achievable gain over the DL beamforming training gets higher as the pilot transmit power from Eve increases. This is due to the fact that in the DL beamforming training, the Eve estimates the composite channel gain from all APs. Thus, as the power

of the spoofing pilot symbols increases, the estimated channel gain at the Eve improves accordingly as it receives favorable gains especially from nearby APs. On the other hand, since the proposed technique allows DL pilot transmission from close APs to legitimate users, the Eve receives non-preferable signal components from these APs. Thus, it needs to increase the spoofing pilot power significantly to overhear the confidential information of the legitimate user.

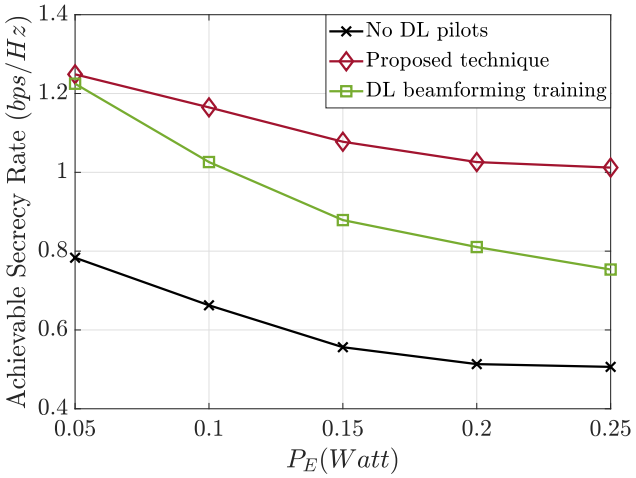

Figure 5.4: Average secrecy rate of different DL transmission strategies at different spoofing pilot power values.

5.3 Exploiting RIS for Limiting Information Leakage to Active Eavesdropper

In this section, we exploit the distinctive features of RISs to propose a novel RIS-based CF mMIMO operation to boost the secrecy rates of CF mMIMO systems. To this end, we jointly optimize the phase shifts of RIS elements and the transmit power coefficients at APs to minimize the leakage rate towards the active Eve while maintaining a certain QoS for legitimate users. Also, we compare the secrecy performance of the proposed system with the traditional CF mMIMO without RISs.

5.3.1 RIS-Assisted CF mMIMO System Model

We consider RIS-supported CF mMIMO network with M multiple-antenna APs, k single antenna users, and T RIS panels. Thanks to the low cost of RISs, we assume that the number of RIS panels is larger than the number of APs ($T > M$). Each AP is equipped

with N_{ap} antennas while each RIS contains $\dot{\mathcal{L}}$ passive elements. Also, the network includes an active Eve who attempts to overhear the intended signal of a target legitimate user. Besides, the CPU is connected to APs and RISs via perfect fronthaul links so that it can control the network operation according to the locations of the legitimate users and the active Eve. In particular, the CPU adjusts the phase shifts of RIS elements and DL precoding vectors to mitigate the information leakage towards the Eve.

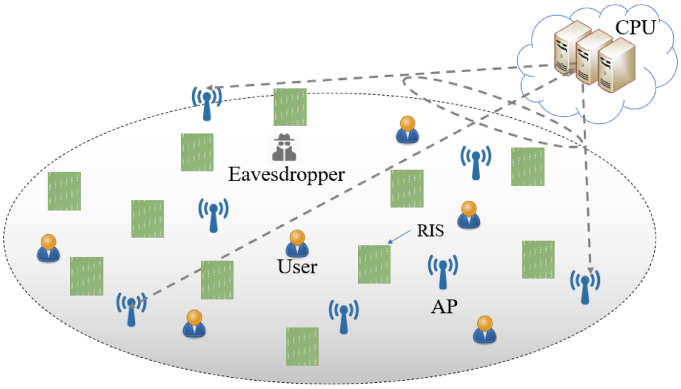

Figure 5.5: RIS-supported CF mMIMO with active Eve.

In fact, only particular RISs will have a remarkable impact on limiting the information leakage to the active Eve depending on their channel conditions with the Eve. For instance, RISs in close proximity to Eve can significantly modify the channel conditions between the APs and the Eve to nullify the received signal at the Eve's side. However, remote RISs from the Eve's location will have a negligible impact on the received signals at the Eve's side. Thus, we consider that only a set of nearest RISs to the Eve's location will be activated to limit the information leakage to the Eve.

5.3.1.1 Channel Model

Let T_A denotes the order of the set of nearest RISs to Eve. Considering block fading channels, the composite channel $\boldsymbol{g}_{mb}$ between the m^{th} AP and a generic user/Eve b can be expressed by

$$\boldsymbol{g}_{mb} = \breve{\boldsymbol{g}}_{mb} + \sum_{t=1}^{T_A} \sum_{\ell=1}^{\dot{\mathcal{L}}} \boldsymbol{g}_{mt\ell b}, \tag{5.29}$$

with

$$\boldsymbol{g}_{mt\ell b} = \boldsymbol{g}_{mt\ell} \times e^{j\theta_{t\ell}} \times g_{t\ell b}, \tag{5.30}$$

representing the cascaded indirect channel through the ℓ^{th} element in the t^{th} nearest RIS to Eve. In that, $\boldsymbol{g}_{mt\ell}$ and $g_{t\ell b}$ denote the channels of the ℓ^{th} element in the t^{th} RIS panel

with the m^{th} AP and b^{th} user/Eve, respectively. Also, $\theta_{t\ell} \in [0, 2\pi]$ is the phase shift of the ℓ^{th} element in the t^{th} RIS. In addition, $\breve{\boldsymbol{g}}_{mb}$ is the direct channel vector between the m^{th} AP and the b^{th} user/Eve whose entries are modeled as Rician fading channel as follows:

$$\breve{\boldsymbol{g}}_{mb} = \sqrt{\beta_{mb}}\Big(\sqrt{\frac{K_{mb}}{K_{mb+1}}}\bar{\boldsymbol{h}}_{mb} + \sqrt{\frac{1}{K_{mb}+1}}\boldsymbol{\Delta}_{\boldsymbol{mb}}^{\frac{1}{2}}\boldsymbol{h}_{mb}\Big), \tag{5.31}$$

where β_{mb} represents the large-scale fading coefficient, K_{mb} is the Rician K-factor, $\bar{\boldsymbol{h}}_{\boldsymbol{mb}} = [1, e^{-j2\pi\bar{r}sin(\Theta_{mb})}, \cdots, e^{-j2\pi\bar{r}(N_{ap}-1)sin(\Theta_{mb})}]$, accounts for the LoS channel components where $\Theta_{mb} \sim \mathbb{U}[-\pi, \pi]$ represents the signal arrival angle and $\bar{r} = 0.5$ is the antenna spacing divided by the carrier wavelength. The vector of small-scale fading channel components $\boldsymbol{h}_{mb}$ follows the circularly symmetric Gaussian noise distribution where $\boldsymbol{h}_{mb} \sim \mathcal{CN}(\boldsymbol{0}, \boldsymbol{I}_N)$. In addition, $\boldsymbol{\Delta}_{mb}$ represents the channel correlation matrix. Accordingly, one can model $\breve{\boldsymbol{g}}_{mb} \sim \mathcal{CN}(\bar{\breve{\boldsymbol{g}}}_{mb}, \boldsymbol{R}_{mb})$, where $\bar{\breve{\boldsymbol{g}}}_{mb} = \sqrt{\frac{\beta_{mb}K_{mb}}{K_{mb+1}}}\bar{\boldsymbol{h}}_{mb}$ and $\boldsymbol{R}_{mb} = \frac{\beta_{mb}}{K_{mb}+1}\boldsymbol{\Delta}_{\boldsymbol{mb}}$ is a positive semi-definite covariance matrix representing the correlation characteristics of the non line-of-sight (NLoS) component. Also, both $\boldsymbol{g}_{mt\ell}$ and $g_{t\ell b}$ are also modeled as Rician fading channels as $\breve{\boldsymbol{g}}_{mb}$ in (5.31).

5.3.2 Channel Estimation of RIS-Assisted CF mMIMO Under Pilot Attacks

A prerequisite to compute the precoding vectors at the APs as well as the phase shifts of RIS elements is to perform the channel estimation task. Note that, previous works which adopted RISs to improve the provided secrecy rates of conventional networks assumed a perfect knowledge of legitimate user's channel. Differently, we take into account the channel estimation errors due to the pilot contamination effect, caused by pilot spoofing attacks as well as pilot reuse among legitimate users. During the channel estimation phase, the active Eve exploits the fact that the pilot sequences are public and standardized to send the same pilot sequence as the target user, aiming at redirecting the DL signal to itself.

The ON-OFF channel estimation approach in [108] is adopted to account for the channel estimation errors in both direct and indirect channels. Both LoS and large-scale fading components of all channels are assumed to be available at the CPU since they change slowly with respect to the channel coherence time. Accordingly, the MMSE-based

estimated channels vector of direct channels between user k and the m^{th} AP is given by

$$\begin{aligned}\hat{\breve{\boldsymbol{g}}}_{mk} = \bar{\breve{\boldsymbol{g}}}_{mk} + \sqrt{P_p \tau_{u,p}} \boldsymbol{R}_{mk} \boldsymbol{\Phi}_{mk} \Big(\breve{\boldsymbol{Y}}_{p,m} \boldsymbol{\psi}_k^* \\ - \sqrt{P_p \tau_{u,p}} \sum_{k'=1}^{K} \bar{\breve{\boldsymbol{g}}}_{mk'} \boldsymbol{\psi}_{k'}^T \boldsymbol{\psi}_k^* - \sqrt{P_E \tau_{u,p}} \bar{\boldsymbol{g}}_{mE} \boldsymbol{\psi}_E^T \boldsymbol{\psi}_k^* \Big),\end{aligned} \tag{5.32}$$

with

$$\breve{\boldsymbol{Y}}_{p,m} = \sqrt{P_p \tau_{u,p}} \sum_{k'=1}^{K} \breve{\boldsymbol{g}}_{mk'} \boldsymbol{\psi}_{k'}^T + \sqrt{P_E \tau_{u,p}} \breve{\boldsymbol{g}}_{mE} \boldsymbol{\psi}_E^T + \breve{\boldsymbol{W}}_{p,m},$$

$$\boldsymbol{\Phi}_{mk} = \left(\sum_{k'=1}^{K} P_p \tau_{u,p} \boldsymbol{R}_{mk'} \boldsymbol{\psi}_{k'}^T \boldsymbol{\psi}_k^* + P_E \tau_{u,p} \boldsymbol{R}_{mE} \boldsymbol{\psi}_E^T \boldsymbol{\psi}_k^* + \sigma_w^2 \boldsymbol{I}_{N_{ap}} \right)^{-1}.$$

where $\breve{\boldsymbol{W}}_{p,m} \in \mathbb{C}^{N_{ap} \times \tau_{u,p}}$, represents the additive noise matrix at the m^{th} AP whose vectors follow $\mathcal{CN}(0, \sigma_w^2 I_{N_{ap}})$. Similarly, the channel estimation of indirect channels follows a similar methodology as the direct counterpart as shown in [108].

5.3.3 Performance of Legitimate Users and Active Eve

This section discusses the DL transmission of RIS-aided CF mMIMO system with emphasis on the achievable DL data rates for legitimate users and the information leakage to the active Eve. We assume that the CPU applies ZF precoding for DL data transmission to manage the inter-user interference. Accordingly, the precoding vector for transmitted data towards user k is given by

$$\boldsymbol{\varpi}_k = \frac{\hat{\boldsymbol{G}}^* \left(\hat{\boldsymbol{G}}^T \hat{\boldsymbol{G}}^* \right)^{-1} \boldsymbol{e}_k}{\sqrt{\left\| \hat{\boldsymbol{G}}^* \left(\hat{\boldsymbol{G}}^T \hat{\boldsymbol{G}}^* \right)^{-1} \boldsymbol{e}_k \right\|^2}}. \tag{5.33}$$

with $\boldsymbol{e}_k$ being the k^{th} column in the identity matrix $\boldsymbol{I}_k$. Also, $\hat{\boldsymbol{G}} \in \mathbb{C}^{MN_{ap} \times K}$ is a matrix of the estimated composite channels between users and APs. Accordingly, the received signal at a generic user/Eve b is given by

$$r_b = \sum_{m=1}^{M} \sum_{k=1}^{K} \sqrt{P_d \eta_k} \boldsymbol{g}_{mb}^T \boldsymbol{\varpi}_{mk} s_k, \tag{5.34}$$

where η_k denotes the DL power control coefficient for transmitted data towards user k, and $\boldsymbol{\varpi}_{mk}$ is a vector that includes the precoding coefficients for user k at the m^{th} AP

antennas. Then, (5.34) can be rewritten as follows:

$$\begin{aligned} r_b &= \sum_{m=1}^{M}\sum_{k=1}^{K}\sqrt{P_d\eta_k}\Big(\breve{\boldsymbol{g}}_{mb}^T + \sum_{t=1}^{T}\sum_{\ell=1}^{\dot{\mathcal{L}}}\boldsymbol{g}_{mt\ell b}^T\Big)\boldsymbol{\varpi}_{mk}s_k, \\ &= \sum_{k=1}^{K}\sqrt{P_d\eta_k}\sum_{m=1}^{M}\Big(a_{mkb} + \boldsymbol{\chi}_{mkb}^T\boldsymbol{\nu}\Big)s_k, \\ &= \sum_{k=1}^{K}\sqrt{P_d\eta_k}\Big(a_{kb} + \boldsymbol{\chi}_{kb}^T\boldsymbol{\nu}\Big)s_k, \end{aligned} \tag{5.35}$$

where

$$\begin{aligned} &a_{mkb} = \breve{\boldsymbol{g}}_{mb}^T\boldsymbol{\varpi}_{mk}, \\ &\boldsymbol{\chi}_{mkb}^T = [\boldsymbol{\chi}_{mkb,1}, \cdots, \boldsymbol{\chi}_{mkb,t}, \cdots, \boldsymbol{\chi}_{mkb,T_A}], \\ &\boldsymbol{\chi}_{mkb,t} = [\boldsymbol{g}_{mt1j}^T\boldsymbol{\varpi}_{mk}, \cdots, \boldsymbol{g}_{mt\ell b}^T\boldsymbol{\varpi}_{mk}, \cdots, \boldsymbol{g}_{mt\ell b}^T\boldsymbol{\varpi}_{mk}], \\ &\boldsymbol{\nu}^T = [\boldsymbol{\nu}_1, \cdots, \boldsymbol{\nu}_t, \cdots, \boldsymbol{\nu}_{T_A}], \\ &\boldsymbol{\nu}_t = [e^{j\theta_{t1}}, \cdots, e^{j\theta_{t\ell}}, \cdots, e^{j\theta_{t\dot{\mathcal{L}}}}], \\ &a_{kb} = \sum_{m=1}^{M} a_{mkb}, \quad \boldsymbol{\chi}_{kb} = \sum_{m=1}^{M}\boldsymbol{\chi}_{mkb}. \end{aligned} \tag{5.36}$$

Accordingly, the achievable DL data rate will be

$$R_b = \log_2(1+\gamma_b), \tag{5.37}$$

with γ_b denoting the achievable SINR which can be calculated for a legitimate user k and the Eve using (5.38) and (5.39), respectively.

$$\gamma_k = \frac{P_d\eta_k\left|a_{kk} + \boldsymbol{\chi}_{kk}^T\boldsymbol{\nu}\right|^2}{P_d\sum\limits_{k'\neq k}\eta_{k'}\left|a_{k'k} + \boldsymbol{\chi}_{k'k}^T\boldsymbol{\nu}\right|^2 + \sigma_w^2}, \tag{5.38}$$

$$\gamma_E = \frac{P_d\eta_k\left|a_{kE} + \boldsymbol{\chi}_{kE}^T\boldsymbol{\nu}\right|^2}{P_d\sum\limits_{k'\neq k}\eta_{k'}\left|a_{k'E} + \boldsymbol{\chi}_{k'E}^T\boldsymbol{\nu}\right|^2 + \sigma_w^2}. \tag{5.39}$$

5.3.4 Secure RIS-Based DL Transmission

In this section, we introduce our proposed scheme to improve the secrecy capabilities of CF mMIMO systems. Particularly, we jointly optimize the DL power control coefficients at APs and the phase shifts of activated RIS panels to minimize the information leakage towards the Eve while maintaining the achievable rates of all legitimate users above certain

thresholds as follows:

$$\begin{aligned} \mathrm{P}_1: \quad & \min_{\boldsymbol{\eta},\boldsymbol{\nu}} \quad \gamma_E \\ & \text{s.t.} \quad \gamma_k \geq \gamma_{th,k}, \quad \forall k, \\ & \qquad 0 \leq \eta_k \leq 1, \quad \forall k, \\ & \qquad \sum_{k=1}^{K} \eta_k \leq 1, \\ & \qquad |\nu_{t\ell}| = 1, \quad \forall t, \ell, \end{aligned} \tag{5.40}$$

where $\gamma_{th,k}$ denotes the required threshold rate for user k. It is noteworthy that by solving P_1, one can maximize the secrecy rates. This is a consequence that P_1 provides legitimate users with their required data rates while minimizing the information leakage to the Eve which in turn maximizes the rate difference between the legitimate and illegitimate links. As one can note, P_1 cannot be jointly solved in-terms of $\boldsymbol{\eta}$ and $\boldsymbol{\nu}$. Thus, existing convex optimization software cannot be applied to solve such problem. To tackle this issue, we decouple P_1 into two sub-problems, namely, phase shift design problem and power allocation problem. Then, the solution of P_1 is obtained by solving these two sub-problems iteratively.

5.3.4.1 Phase Shift Design

Here, we discuss the phase shift design for a given transmit power allocation which can be defined as follows:

$$\begin{aligned} \mathrm{P}_2: \quad & \min_{\boldsymbol{\nu}} \quad \gamma_E \\ & \text{s.t.} \quad \gamma_k \geq \gamma_{th,k}, \quad \forall k, \\ & \qquad |\nu_{t\ell}| = 1, \quad \forall t, \ell. \end{aligned} \tag{5.41}$$

By introducing an auxiliary variable $\digamma$, the achievable SINR for a generic user/Eve b can be rewritten as follows:

$$\gamma_b = \frac{P_d \eta_k \Big(\mathrm{Tr}\big(\boldsymbol{U}_{kb}\boldsymbol{V}\big) + |a_{kb}|^2 \Big)}{P_d \sum\limits_{k' \neq k} \eta_{k'} \Big(\mathrm{Tr}\big(\boldsymbol{U}_{k'b}\boldsymbol{V}\big) + |a_{k'b}|^2 \Big) + \sigma_w^2}, \tag{5.42}$$

where

$$\boldsymbol{U}_{kb} = \begin{bmatrix} \boldsymbol{\chi}_{kb}^{*}\boldsymbol{\chi}_{kb}^{T} & \boldsymbol{\chi}_{kb}^{T}a_{kb}^{H} \\ \boldsymbol{\chi}_{kb}^{*}a_{kb} & 0 \end{bmatrix}, \quad \boldsymbol{V} = \bar{\boldsymbol{\nu}}\bar{\boldsymbol{\nu}}^{H}, \quad \bar{\boldsymbol{\nu}} = \begin{bmatrix} \boldsymbol{\nu} \\ \digamma \end{bmatrix}. \tag{5.43}$$

Since P_2 is a fractional programming problem, we firstly apply the Dinkelbach's transform to reformulate the problem as follows:

$$\begin{aligned}
\mathrm{P}_3: \quad & \min_{\breve{\zeta},\boldsymbol{\nu}} \quad P_d\eta_k\Big(\mathrm{Tr}\big(\boldsymbol{U}_{kE}\boldsymbol{V}\big)+|a_{kE}|^2\Big)-\breve{\zeta}\Big(P_d\sum_{k'\neq k}\eta_{k'}\Big(\mathrm{Tr}\big(\boldsymbol{U}_{k'E}\boldsymbol{V}\big)+|a_{k'E}|^2\Big)+\sigma_w^2\Big),\\
\text{s.t.} \quad & \frac{P_d\eta_k\Big(\mathrm{Tr}\big(\boldsymbol{U}_{kk}\boldsymbol{V}\big)+|a_{kk}|^2\Big)}{P_d\sum\limits_{k'\neq k}\eta_{k'}\Big(\mathrm{Tr}\big(\boldsymbol{U}_{k'k}\boldsymbol{V}\big)+|a_{k'k}|^2\Big)+\sigma_w^2}\geq\gamma_{th,k}, \quad \forall k,\\
& \mathrm{Diag}[\boldsymbol{V}]=1, \quad \mathrm{rank}[\boldsymbol{V}]=1,
\end{aligned} \tag{5.44}$$

where the auxiliary variable $\breve{\zeta}$ is iteratively updated until convergence is reached. In that, the optimal value of $\breve{\zeta}$ at the $\breve{j}^{\mathrm{th}}$ iteration is calculated by

$$\breve{\zeta}^*=\frac{P_d\eta_k\Big(\mathrm{Tr}\big(\boldsymbol{U}_{kE}\boldsymbol{V}^{\breve{j}-1}\big)+|a_{kE}|^2\Big)}{P_d\sum\limits_{k'\neq k}\eta_{k'}\Big(\mathrm{Tr}\big(\boldsymbol{U}_{k'E}\boldsymbol{V}^{\breve{j}-1}\big)+|a_{k'E}|^2\Big)+\sigma_w^2}. \tag{5.45}$$

To solve P_3 over the variable $\boldsymbol{V}$, we apply semi-definite relaxation by removing the $\mathrm{rank}[\boldsymbol{V}]=1$ constraints to handle the non-convexity of this constraint. Thus, the problem can be rewritten as

$$\begin{aligned}
\mathrm{P}_4: \quad & \min_{\breve{\zeta},\omega,\boldsymbol{\nu}} \quad \omega\\
\text{s.t.} \quad & P_d\eta_k\Big(\mathrm{Tr}\big(\boldsymbol{U}_{kE}\boldsymbol{V}\big)+|a_{kE}|^2\Big)-\breve{\zeta}\Big(P_d\sum_{k'\neq k}\eta_{k'}\Big(\mathrm{Tr}\big(\boldsymbol{U}_{k'E}\boldsymbol{V}\big)+|a_{k'E}|^2\Big)+\sigma_w^2\Big)\leq\omega,\\
& P_d\eta_k\Big(\mathrm{Tr}\big(\boldsymbol{U}_{kk}\boldsymbol{V}\big)+|a_{kk}|^2\Big)\geq\gamma_{th,k}\Big(P_d\sum_{k'\neq k}\eta_{k'}\Big(\mathrm{Tr}\big(\boldsymbol{U}_{k'k}\boldsymbol{V}\big)+|a_{k'k}|^2\Big)+\sigma_w^2\Big), \ \forall k,\\
& \mathrm{Diag}[V]=1.
\end{aligned} \tag{5.46}$$

It is to be noted that P_4 is a standard semi-definite programming (SDP) problem that can be solved via existing convex optimization software. However, since the P_4 may not yield a rank one solution, we apply the Gaussian randomization to obtain a rank one solution as in [112].

5.3.4.2 Power Allocation

This section discusses the DL power allocation problem for a given set of phase shift coefficients where the problem can be formulated as follows:

$$\begin{aligned} \mathrm{P}_5: \quad & \min_{\boldsymbol{\eta}} \quad \gamma_E \\ & \text{s.t.} \quad \gamma_k \geq \gamma_{th,k}, \quad \forall k, \\ & \qquad 0 \leq \eta_k \leq 1, \quad \forall k, \\ & \qquad \sum_{k=1}^{K} \eta_k \leq 1. \end{aligned} \tag{5.47}$$

To solve P_5, we apply the Dinkelbach's transform to reformulate the problem as follows:

$$\begin{aligned} \mathrm{P}_6: \quad & \min_{\varkappa,\boldsymbol{\eta}} \quad P_d\eta_k\Big(\mathrm{Tr}\big(\boldsymbol{U}_{kE}\boldsymbol{V}\big) + |a_{kE}|^2\Big) - \varkappa\Big(P_d\sum_{k'\neq k}\eta_{k'}\Big(\mathrm{Tr}\big(\boldsymbol{U}_{k'E}\boldsymbol{V}\big) + |a_{k'E}|^2\Big) + \sigma_w^2\Big), \\ & \text{s.t.} \quad P_d\eta_k\Big(\mathrm{Tr}\big(\boldsymbol{U}_{kk}\boldsymbol{V}\big) + |a_{kk}|^2\Big) \geq \gamma_{th,k}\Big(P_d\sum_{k'\neq k}\eta_{k'}\Big(\mathrm{Tr}\big(\boldsymbol{U}_{k'k}\boldsymbol{V}\big) + |a_{k'k}|^2\Big) + \sigma_w^2\Big), \quad \forall k, \\ & \qquad 0 \leq \eta_k \leq 1, \quad \forall k, \\ & \qquad \sum_{k=1}^{K} \eta_k \leq 1, \end{aligned} \tag{5.48}$$

where the auxiliary variable $\varkappa$ is iteratively updated until convergence is reached. The optimal value of $\varkappa$ at the $\breve{j}^{\text{th}}$ iteration is given by

$$\varkappa^* = \frac{P_d\eta_k^{\breve{j}-1}\Big(\mathrm{Tr}\big(\boldsymbol{U}_{kE}\boldsymbol{V}\big) + |a_{kE}|^2\Big)}{P_d\sum\limits_{k'\neq k}\eta_{k'}^{\breve{j}-1}\Big(\mathrm{Tr}\big(\boldsymbol{U}_{k'E}\boldsymbol{V}\big) + |a_{k'E}|^2\Big) + \sigma_w^2}. \tag{5.49}$$

One can note that the problem P_6 is a standard linear programming in $\boldsymbol{\eta}$. Thus, it can be solved via existing convex optimization software. Based on sub-Problems P_4 and P_6, an iterative algorithm has been introduced by alternately solving both sub-problems at each iteration, which is summarized in Algorithm 5.1.

Algorithm 5.1: Algorithm to solve P_1

1. At the first iteration $\breve{n} = 1$, initialize $\boldsymbol{\eta}^{(0)} = [\eta_1^{(0)}, \eta_2^{(0)}, \cdots, \eta_K^{(0)}]$.
2. Solve P_4 to determine the optimal phase shifts $\boldsymbol{\nu}^{(\breve{n})}$ for a given $\boldsymbol{\eta}^{(\breve{n}-1)}$.
3. Solve P_6 to compute the optimal power allocation $\boldsymbol{\eta}^{(\breve{n})}$ for a given $\boldsymbol{\nu}^{(\breve{n})}$.
4. Stop if $\gamma_E^{\breve{n}} - \gamma_E^{\breve{n}-1} < \epsilon$, where ϵ is a certain threshold to preserve convergence. Otherwise, set $\breve{n} = \breve{n} + 1$ and repeat Steps 2 and 3.

5.3.5 Simulation Results

We consider RIS-aided CF mMIMO network in which APs, users, and RISs are uniformly distributed in a square area of size $0.5 \times 0.5\ km^2$. The carrier frequency $f_c = 2$ GHz. The UL pilot transmission power of legitimate users and Eve $P_p = P_E = 0.1$ Watt and the DL data transmission power $P_d = 0.2$ Watt. The noise variance $\sigma_w^2 = 290 \times \kappa \times B \times NF$ where κ is the Boltzman constant, $B =$ 20 MHz, denoting the system bandwidth, and $NF =$ 9 dB is the noise figure. Unless otherwise specified, we consider that the simulation area includes $M = 30$ APs, $T = 100$ RIS panels, and $K = 10$ users. Each AP is equipped with $N_{ap} = 10$ antennas while each RIS panel contains $\dot{\mathcal{L}} = 50$ passive elements. The target user is selected randomly from the existing legitimate users. Then, the active Eve is located randomly in a circle with radius 10 m around the target user's location. The length of non-orthogonal pilot sequences in the UL training phase is $\tau_{u,p} = 5$. Besides, we set the threshold $\gamma_{th,k}$ for each user k to the achievable SINR when no RIS is activated. In other words, RISs are exploited for security purposes only through preserving the same performance of legitimate users while minimizing the information leakage to the active Eve.

Due to the higher number of deployed RISs compared to the number of APs, we assume that the Eve has LoS channels with activated RISs while it has NLoS channels with APs. Also, the target legitimate user has LoS channels with activated RISs while other legitimate users has NLoS channels with both activated RISs and APs. The large-scale fading coefficient is given by [113]

$$\beta = \begin{cases} -30.18 - 26\log_{10}(d) + \mathcal{F} & \text{if} \quad \text{LoS} \\ -34.53 - 38\log_{10}(d) + \mathcal{F} & \text{if} \quad \text{NLoS}, \end{cases} \tag{5.50}$$

where d is the distance in meters and $\mathcal{F}$ denotes the correlated shadow fading coefficient. Also, the Rician K-factor is calculated by $K = 10^{1.3-0.003d}$ for LoS channels while it is set to zero for NLoS channels where there is a possibility of having a LoS link within a distance $d = 300$m [113].

In what follows, we analyze the average leakage rate, average secrecy rate, and the secrecy outage probability as they represent indicative metrics for the secrecy performance of the proposed system operation. The average leakage rate $\bar{R}_E$ and average secrecy rate $\bar{R}_{sec}$ are the averaging of R_E and R_{sec} over the different generated network realizations, respectively. Finally, the outage probability $P_{out} = \mathbb{P}(R_{sec} <= R_{sec}^{th})$ depicts the probabil-

ity that the achievable secrecy rate is less than a certain non-negative threshold secrecy rate.

Fig. 5.6a reflects the potential of applying the joint power allocation and phase shift optimization in limiting the secrecy outage probability compared to the conventional system operation without RIS. The simulations are obtained under two different number of RIS panels $T = 100$ and $T = 200$. Also, we consider $T_A = 1$ such that only the first nearest RIS panel to the Eve is activated and optimized to limit the information leakage to the Eve. As one can note, applying the joint power allocation and phase optimization significantly limits the secrecy outage probability. In addition, a CF mMIMO network with more deployed RIS panels ($T = 200$) provides lower outage probabilities since the distance between the Eve and the activated RIS panel gets smaller.

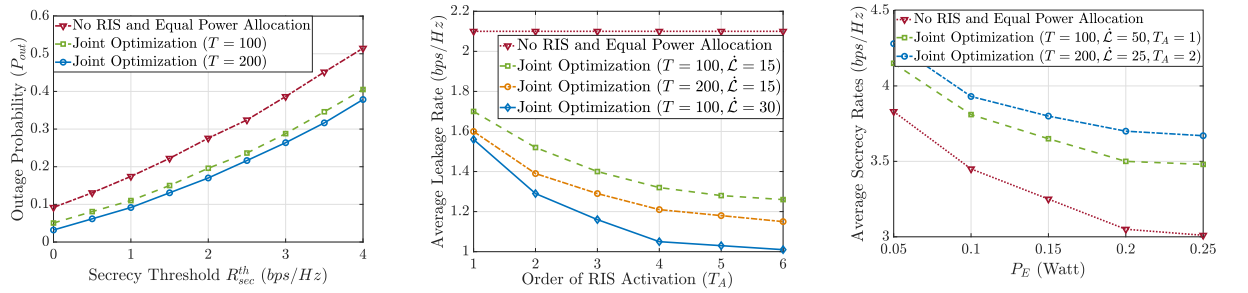

(a) Secrecy outage probability

(b) Average information leakage under different order of activated RISs

(c) Average secrecy rate under different powers of pilot spoofing attacks

Figure 5.6: Secrecy performance of RIS-assisted CF mMIMO systems.

Different from previous results where only the first nearest RIS panel is activated for the system operation, Fig. 5.6b shows the impact of activating higher orders of nearest RIS panels on the system performance. Particularly, Fig. 5.6b depicts the average information leakage to the active Eve for different RIS activation orders (T_A) under different RIS configurations. It is clear that increasing the order of RIS activation order boosts the system robustness against pilot spoofing attack as this reduces the information leakage to the active Eve. This is due to the larger number of activated RIS elements that are exploited to minimize the information leakage to the active Eve. However, there is always a certain order after which the gain of activating more RIS panels becomes negligible. The latter result supports our conjuncture that only a small portion of existing RIS panels suffice to achieve highest secrecy levels. Also, Fig. 5.6b shows that equipping activated RIS panels with further reflecting elements is more beneficial than bringing the activated panels closer to the Eve. This is noted from the lower leakage rate, attained by the RIS

configuration with $T = 100$ and $\dot{\mathcal{L}} = 30$ compared to the one with $T = 200$ and $\dot{\mathcal{L}} = 15$.

Finally, Fig. 5.6c depicts the robustness of CF mMIMO against power of pilot spoofing attacks. Notably, increasing the spoofing pilot power degrades the achievable secrecy rates. This is due to the higher degradation of the channel estimation quality at higher powers of spoofing pilots. However, the RIS-aided system is more robust against higher powers of spoofing pilots compared to the conventional counterpart without RISs. Besides, under the same number of activated RIS elements, deploying larger number of RIS panels with smaller number of RIS elements ($T = 200, \dot{\mathcal{L}} = 25, T_A = 2$) is more beneficial than deploying smaller number of RIS panels with large number of RIS elements ($T = 100, \dot{\mathcal{L}} = 50, T_A = 1$).

5.3.6 Summary

We investigated the DL performance of CF mMIMO systems in the presence of pilot spoofing attacks. Particularly, we proposed two promising approaches to improve the secrecy performance of CF mMIMO systems. In the first approach, we focused on the case where APs do not have statistical information about the Eve that strives to estimate its DL channel coefficients with APs capitalizing on the DL transmission strategy. In that, we introduced a novel DL pilots transmission approach to improve the legitimate users' rates while limiting the information leakage to the active Eve. The performance of the proposed DL transmission technique is compared with different techniques in the literature, namely no DL pilots and DL beamforming training. Results revealed that the proposed DL pilots technique attains superior secrecy rates. Furthermore, the proposed technique is shown to be more robust to high spoofing pilot powers than the DL beamforming training technique.

In the second approach, we investigated the potential of RIS in improving the secrecy capacities offered in CF mMIMO in the presence of active Eve. To this end, we proposed a novel RIS-based system operation in which RIS phase shifts and DL power control coefficients are jointly optimized to minimize the information leakage to the active Eve while maintaining the legitimate users' performance above certain thresholds. Results revealed that RISs have a great potential in improving the secrecy capacities of CF mMIMO systems and boosting the system robustness against higher powers of spoofing pilot attacks. Also, we showed that only few RIS panels need to be activated to limit the information leakage to the active Eve.

Chapter 6
Limited-Fronthaul Capacity Effect on DL Performance of CF mMIMO

6.1 Introduction

A prerequisite to achieve the the reported performance in previous chapters is to have ideal fronthaul links between the CPU and APs. This is due to the pivotal role of the fronthaul network in handling the data exchange between the CPU and APs. In particular, the larger amount of data to be transferred through the fronthaul network, the higher requirements of fronthaul capacities. The CF mMIMO performance under limited-fronthaul capacity has been widely investigated in the literature [90–95, 114–119]. The majority of these works investigated the limited-fronthaul capacity effect on the UL performance of the system [90, 92–95, 114–117], whereas the works in [90, 91] studied such effect on the DL performance.

The UL performance of limited-fronthaul CF mMIMO systems has been investigated in-terms of the spectral efficiency in [92–94, 114–116] and the energy efficiency in [92,95,117]. The UL transmission schemes in these works can be classified into three different approaches, namely, compress-forward-estimate (CFE), estimate-compress-forward (ECF), and estimate-detect-compress-forward (EDCF). In CFE, the received data and pilot signals at APs are compressed and transmitted to the CPU where both channel estimation and users' data detection are carried out. In ECF, all APs firstly estimate the users' channels, then compress the estimated channels as well as the received data signals and transmit both to the CPU where the detection process is performed. On the other hand, in EDCF, both channel estimation and UL data detection are carried out locally at the APs. The APs, then, compress the local detected signals and send them to the CPU.

The work in [92] investigates the UL data rate maximization problem of limited-fronthaul CF mMIMO using MRC detection. In doing so, a low-complexity water-filling

approach is proposed to allocate the available fronthaul capacity among users. Then, a line search technique is applied for capacity allocation between pilot and data transmission. Results revealed that ECF attains superior performance than CFE and EDCF. Also, applying the water-filling fronthaul capacity allocation significantly enhances the achievable data rates of EDCF. In addition, for ECF and CFE, it has been shown that there is an optimal portion of the fronthaul capacity to be assigned for the pilot transmission to maximize the sum UL data rates. Considering the max-min fairness problem for a two-stage UL data detection technique, the authors in [94,114] decoupled this non-convex problem into two sub-problems, namely, receiver filter design and UL power allocation where the optimal solution is obtained by solving these sub-problems iteratively. Results revealed that applying the two-stage UL data detection while optimizing the receiver filter coefficients can significantly improve the achievable UL data rates. It is also pointed out that there is an optimal number of users to be served by each AP to alleviate the limited-fronthaul capacity effect. Considering both ECF and EDCF, and aiming at maximizing the UL sum data rate, a LSF-based deep convolutional neural network is proposed to establish a mapping between the LSF coefficients and the optimal power control coefficients [116]. Furthermore, considering the UL operation under ZF detection, the authors in [93] showed that CFE outperforms ECF in-terms of the achievable UL data rates. The energy efficiency of limited-fronthaul CF mMIMO is maximized under two-stage UL data detection in [95,117]. In doing so, the authors adopted the same approach as in [94,114] where the problem is decoupled into two sub-problems of receiver coefficient optimization and UL power allocation. Results revealed that the proposed approach can achieve almost twice the UL energy efficiency compared to the case of equal power allocation.

Regarding the DL performance, the authors in [91] investigated the limited-fronthaul effect on a distributed system operation. In that, APs performs the channel estimation and the DL precoding processes where local CB precoding is applied for DL transmission. Besides, the authors in [90] discussed the limited-fronthaul effect on both distributed and centralized system operations. In that, the APs and the CPU are responsible for performing the channel estimation and precoding processes in the distributed and centralized operations, respectively. Also, the authors considered normalized CB precoding for both distributed and centralized system operations assuming single antenna APs. Results revealed that the centralized operation provides superior performance under limited-

fronthaul effect.

Different from previous works, we analyze the DL performance of CF mMIMO systems assuming multiple antenna APs and different precoding techniques for the distributed and centralized system operations. More specifically, due to the low processing capabilities of the APs, we apply CB precoding, supported by beamforming training for the distributed system operation. On the other hand, we exploit the high processing capabilities of the CPU to apply ZF precoding for the centralized system operation.

6.2 System Model

6.2.1 Channel Model

We consider a CF mMIMO system with M multi-antenna APs and K single-antenna users. We consider block fading channels. Also, we consider Rayleigh fading channels where the the channel vector between user k and AP m is modeled by

$$\boldsymbol{g}_{mk} = \sqrt{\beta_{mk}}\boldsymbol{h}_{mk}, \tag{6.1}$$

where $\boldsymbol{h}_{mk} \in \mathbb{C}^{N_{ap}\times 1}$ represents the small-scale fading coefficients whose entries are i.i.d. $\mathcal{CN}(0,1)$. Besides, β_{mk} is the large-scale fading coefficient that accounts for path-loss and shadowing effects as defined in (3.2).

6.2.2 System Operations

We consider two different DL transmission operations, namely, distributed and centralized operations. Regarding the distributed system operation, the signal processing functionalities are carried out in APs and the fronthaul network is exploited to transfer the users' data between the CPU and APs. On the other hand, in the centralized system operation, the signal processing functionalities are performed at the CPU. In that, the fronthaul network transfers the received pilot sequences at APs to the CPU to carry out the channel estimation process and calculate the DL precoding vectors. Then, the fronthaul network transfers the precoded data symbols from the CPU to APs which convey them to the users.

6.2.3 Data Compression

We consider that each AP is connected to a CPU via a limited capacity fronthaul link with a capacity C_m bps/Hz. Due to the limited capacity fronthaul links, a finite number of bits are used to transfer the signals between APs and the CPU. Hence, signal compression is required to transfer signals through the fronthaul network links. This in turn leads to a compression distortion noise, accompanying the transmitted signals. To model the distortion noise effect, we adopt the same model in [91, 92] that depends on the rate distortion theory [120]. In that, to compress a signal $X \sim f_X(x)$ with zero mean and variance P, subject to a distortion measure $d(X, \hat{X})$ with $\mathbb{E}\{d(X, \hat{X})\} \leq Q$, the rate distortion function can be defined by

$$R(Q) = \min_{f(\hat{x}|x):\mathbb{E}\{|\hat{X}-X|^2\}\leq Q} I(\hat{X}; X), \tag{6.2}$$

where the compressed signal can be defined as $\hat{X} = X + q$, with $q \sim \mathcal{CN}(0, Q)$, is independent of X and denotes the additive distortion noise [91, 92]. The amount of information to be transmitted in a fronthaul link with capacity C_m can be expressed as a function of the differential entropy by

$$C_m = I(\hat{X}; X) = h(\hat{X}) - h(\hat{X}|X) \leq \log_2(1 + P/Q_m). \tag{6.3}$$

As such, the quantization noise power Q_m will be [92]

$$Q_m = \frac{P}{2^{C_m} - 1}. \tag{6.4}$$

6.3 Performance Analysis

6.3.1 Distributed Operation

Regarding the distributed system operation, we apply local CB precoding at APs due to its low processing requirements that fit with the low processing capabilities of APs. Besides, we apply beamforming training due to its high potential in improving the achievable DL rates [121].

6.3.1.1 Channel Estimation

In the distributed system operation, the channel estimation process is carried out at APs. Thus, the quality of estimated channels is not affected by the capacity of fronthaul links. Also, we assume that users are assigned non-orthogonal training sequences during the UL

channel estimation phase. The received training sequence vector $\boldsymbol{y}_{p,m,l} \in \mathbb{C}^{1\times\tau_{u,p}}$, at the l^{th} antenna element in the m^{th} AP will be

$$\boldsymbol{y}_{p,m,l} = \sqrt{P_p\tau_{u,p}}\sum_{k'=1}^{K} g_{mk',l}\boldsymbol{\psi}_{k'}^T + \boldsymbol{w}_{p,m,l}, \tag{6.5}$$

Then, the MMSE estimated channel for user k with the l^{th} antenna element in the m^{th} AP under non-orthogonal pilot sequences can be determined by

$$\hat{g}_{mk,l} = \mathcal{C}_{m,k,l}\bar{y}_{p,m,l,k}, \tag{6.6}$$

with $\bar{y}_{p,m,l,k} = \boldsymbol{y}_{p,m,l}\boldsymbol{\psi}_k^*$ is the projection of the received pilot sequence on $\boldsymbol{\psi}_k^*$ and

$$\mathcal{C}_{m,k,l} = \frac{\sqrt{P_p\tau_{u,p}}\beta_{mk}}{P_p\tau_{u,p}\sum\limits_{k'=1}^{K}\beta_{mk'}\left|\boldsymbol{\psi}_{k'}^T\boldsymbol{\psi}_k^*\right|^2+\sigma_w^2}. \tag{6.7}$$

Let $\tilde{g}_{mk,l} = g_{mk,l} - \hat{g}_{mk,l}$, be the channel estimation error. The MMSE estimate $\hat{g}_{mk,l}$ and the estimation error $\tilde{g}_{mk,l}$ are independent random variables and distributed as

$$\hat{g}_{mk,l} \sim \mathcal{CN}(0, \zeta_{mk}), \quad \tilde{g}_{mk,l} \sim \mathcal{CN}(0, \beta_{mk} - \zeta_{mk}), \tag{6.8}$$

where $\zeta_{mk} = \sqrt{P_p\tau_{u,p}}\beta_{mk}\mathcal{C}_{m,k,l}$.

6.3.1.2 Downlink Transmission

Similar to Section 5.2.3.2, we apply beamforming training to improve the DL performance due to the lack of channel hardening in CF mMIMO systems [75]. In this chapter, the length of DL pilot sequences for DL training is denoted by $\tau_{d,p}$. Also, $\boldsymbol{\phi}_k \in \mathbb{C}^{1\times\tau_{d,p}}$, represents the DL training sequence, sent from all APs for the channel gain estimation of the k^{th} user, where $\|\boldsymbol{\phi}_k\|^2 = 1$. We consider that orthogonal DL pilots are allocated to users with $\tau_{d,p} \geq K$. As such, the transmitted pilot sequence matrix $\boldsymbol{X}_{p,m} \in \mathbb{C}^{N_{ap}\times\tau_{d,p}}$ from the m^{th} AP will be

$$\boldsymbol{X}_{p,m} = \sqrt{P_d\tau_{d,p}}\sum_{k'=1}^{K}\sqrt{\eta_{mk'}}\hat{\boldsymbol{g}}_{mk'}^*\boldsymbol{\phi}_{k'}^T, \tag{6.9}$$

where the power control coefficient are set according to equal power allocation criterion, discussed in previous chapters. The received pilot sequence vector at user k will be

$$\boldsymbol{r}_{p,k} = \sqrt{P_d\tau_{d,p}}\sum_{k'=1}^{K} a_{kk'}\boldsymbol{\phi}_{k'}^T + \boldsymbol{w}_{p,k}, \tag{6.10}$$

where $a_{kk'} = \sum\limits_{m=1}^{M}\sqrt{\eta_{mk'}}\boldsymbol{g}_{mk}^T\hat{\boldsymbol{g}}_{mk'}^*$. After user k receives the DL training signals, it estimates its channel gain a_{kk}. In doing so, it firstly projects the received training signal on ϕ_k^* as

$$\tilde{y}_{p,k} = \sqrt{P_d\tau_{d,p}}a_{kk} + \boldsymbol{w}_{p,k}\boldsymbol{\phi}_k^*. \tag{6.11}$$

Following the same procedure as in Section 5.2.3.2, the MMSE estimated channel gain can be expressed by [121]

$$\hat{a}_{kk} = \mathbb{E}\{a_{kk}\} + \frac{\sqrt{P_d \tau_{d,p}} Var\{a_{kk}\}}{P_d \tau_{d,p} Var\{a_{kk}\} + \sigma_w^2} \Big(\tilde{y}_{p,k} - \sqrt{P_d \tau_{d,p}} \mathbb{E}\{a_{kk}\} \Big), \tag{6.12}$$

with

$$\begin{aligned} \mathbb{E}\{\hat{a}_{kk}\} &= \mathbb{E}\{a_{kk}\}, \\ Var\{\hat{a}_{kk}\} &= \frac{P_d \tau_{d,p} \big(Var\{a_{kk}\}\big)^2}{P_d \tau_{d,p} Var\{a_{kk}\} + \sigma_w^2}. \end{aligned} \tag{6.13}$$

Also, the estimation error $\tilde{a}_{kk} = a_{kk} - \hat{a}_{kk}$ is uncorrelated but not independent of the channel gain a_{kk} with

$$\mathbb{E}\{|\tilde{a}_{kk}|^2\} = \frac{Var\{a_{kk}\}}{P_{d,p} \tau_{d,p} Var\{a_{kk}\} + \sigma_w^2}. \tag{6.14}$$

After the beamforming training phase, the CPU starts the DL transmission phase. In the distributed system operation, the CPU compresses the users' data symbols and sends the compressed symbols to APs. In that, the compressed transmitted signal for user k in the fronthaul link to the m^{th} AP will be

$$\hat{s}_{m,k} = s_k + q_{d,m,k}, \tag{6.15}$$

where $q_{d,m,k} \sim \mathcal{CN}(0, Q_{d,m,k})$, represents the quantization noise resulted from the compression of the k^{th} user data symbol at the CPU. Let $C_{d,m,k}$ represents the fronthaul capacity, assigned for the k^{th} user's data such as

$$C_{d,m,k} = \frac{\tau_c - \tau_{u,p} - \tau_{d,p}}{\tau_c} \log_2 \Big(1 + \frac{1}{Q_{d,m,k}} \Big). \tag{6.16}$$

Since each user's data can be compressed and transmitted separately, we consider two different capacity allocation techniques. The first capacity allocation is equal capacity allocation as follows:

$$C_{d,m,k} = \frac{C_m}{K}, \qquad \forall k = 1, \cdots, K. \tag{6.17}$$

On the other hand, the second capacity allocation is a simple water-filling capacity allocation scheme in which the allocated capacity for each user is proportional to its channel gain with the AP as follows:

$$C_{d,m,k} = \frac{\beta_{mk}}{\sum_{k'=1}^{K} \beta_{mk'}} C_m, \qquad \forall k = 1, \cdots, K. \tag{6.18}$$

After APs receive the compressed users' data symbols, they perform precoding for DL transmission. In particular, each AP exploits the locally estimated channels of users to perform local CB precoding. Consequently, the combined received signal at user k will be

$$r_k^{Dis} = \sqrt{P_d} \sum_{m=1}^{M} \sum_{k'=1}^{K} \sqrt{\eta_{mk'}} \hat{\boldsymbol{g}}_{mk'}^{*} \hat{s}_{k',m} \boldsymbol{g}_{mk}^{T} \boldsymbol{x}_m + w_k, \tag{6.19}$$

which can be expressed by

$$r_k^{Dis} = \sqrt{P_d} a_{kk} s_k + \sqrt{P_d}\Omega_k + \sqrt{P_d}\sum_{k' \neq K} a_{kk'} s_{k'} + w_k, \tag{6.20}$$

where the first term represents the desired signal. Also, $\Omega_k = \sum_{m=1}^{M} \sqrt{\eta_{mk}} \boldsymbol{g}_{mk}^T \hat{\boldsymbol{g}}_{mk}^* q_{d,m,k}$, reflects the compression distortion noise of the k^{th} user data. In addition, the third and fourth terms denote the interference from other users' data and the noise effect. Considering the fact that uncorrelated Gaussian noise represents the worst-case interference [21], the achievable DL rate for user k can be calculated using

$$R_k^{Dis} = \frac{\tau_c - \tau_{u,p} - \tau_{d,p}}{\tau_c} \times \mathbb{E}\left\{ \log_2 \left(1 + \frac{P_d |\hat{a}_{kk}|^2}{P_d \mathbb{E}\{|\tilde{a}_{kk}|^2\} + P_d \mathbb{E}\{|\Omega_k|^2\} + P_d \sum\limits_{k' \neq k} \mathbb{E}\{|a_{kk'}|^2 \Big| \hat{a}_{kk}\} + \sigma_w^2} \right) \right\}, \tag{6.21}$$

However, (6.21) is not a closed-form, thus, we follow the same procedure as [121] to obtain a closed-from of the achievable DL rate by applying the following approximation

$$\mathbb{E}\left\{ \log_2 \left(1 + \frac{\mathcal{X}_1}{\mathcal{X}_2} \right) \right\} \approx \log_2 \left(1 + \frac{\mathbb{E}\{\mathcal{X}_1\}}{\mathbb{E}\{\mathcal{X}_2\}} \right), \tag{6.22}$$

where $\mathcal{X}_1$ and $\mathcal{X}_2$ are both sums of non-negative random variables. Applying (6.22) in (6.21), a closed-form approximation of the achievable DL is given by (6.23) where different terms in (6.23) can be calculated as follows.

$$\breve{R}_k^{Dis} = \frac{\tau_c - \tau_{u,p} - \tau_{d,p}}{\tau_c} \log_2 \left(1 + \frac{P_d \mathbb{E}\{|\hat{a}_{kk}|^2\}}{P_d \mathbb{E}\{|\tilde{a}_{kk}|^2\} + P_d \mathbb{E}\{|\Omega_k|^2\} + P_d \sum\limits_{k' \neq k} \mathbb{E}\{|a_{kk'}|^2\} + \sigma_w^2} \right), \tag{6.23}$$

Firstly, the desired power can be calculated by

$$\begin{aligned} P_d \mathbb{E}\{|\hat{a}_{kk}|^2\} &= P_d \Big(Var\{\hat{a}_{kk}\} + \big(\mathbb{E}\{\hat{a}_{kk}\}\big)^2 \Big) \\ &= P_d \frac{P_d \tau_{d,p} \Big(\sum\limits_{m=1}^{M} \eta_{mk} N_{ap} \beta_{mk} \zeta_{mk} \Big)^2}{P_d \tau_{d,p} \sum\limits_{m=1}^{M} \eta_{mk} N_{ap} \beta_{mk} \zeta_{mk} + \sigma_w^2} + P_d \Big(\sum_{m=1}^{M} \sqrt{\eta_{mk}} N_{ap} \zeta_{mk} \Big)^2. \end{aligned} \tag{6.24}$$

In addition, the channel gain estimation error will be

$$P_d \mathbb{E}\{|\tilde{a}_{kk}|^2\} = P_d \frac{\sum\limits_{m=1}^{M} \eta_{mk} N_{ap} \beta_{mk} \zeta_{mk}}{P_d \tau_{d,p} \sum\limits_{m=1}^{M} \eta_{mk} N_{ap} \beta_{mk} \zeta_{mk} + \sigma_w^2}. \tag{6.25}$$

Also, the quantization noise distortion power is given by

$$P_d \mathbb{E}\{|\Omega_k|^2\} = P_d \sum_{m=1}^{M} Q_{d,k,m} \eta_{mk} \Big(N_{ap} \beta_{mk} \zeta_{mk} + N_{ap}^2 \zeta_{mk}^2 \Big). \tag{6.26}$$

Finally, the interference due to transmitted data to user k' is given by

$$P_d\mathbb{E}\{|a_{kk'}|^2\} = P_d\sum_{m=1}^{M}\eta_{mk'}N_{ap}\beta_{mk}\zeta_{mk'} + P_d\Big(\sum_{m=1}^{M}\sqrt{\eta_{mk'}}N_{ap}\zeta_{mk'}\frac{\beta_{mk}}{\beta_{mk'}}\Big)^2|\boldsymbol{\psi}_k\boldsymbol{\psi}_{k'}^{\mathsf{H}}|^2. \quad (6.27)$$

6.3.2 Centralized Operation

For the centralized system operation, we exploit the high processing capabilities of the CPU to apply ZF precoding due to its high potential in improving the DL achievable rates.

6.3.2.1 Channel Estimation

In the centralized system operation, the CPU is the responsible entity to carry out the channel estimation task. After APs receive the training sequence vectors, transmitted from users in the channel estimation phase, APs compress the received training sequence vectors and send it through the fronthaul links to the CPU. In that, we assume that the received training vector at each antenna element is compressed separately. Therefore, the compressed vector at the l^{th} antenna element in the m^{th} AP will be

$$\hat{\boldsymbol{y}}_{p,m,l} = \boldsymbol{y}_{p,m,l} + \boldsymbol{q}_{p,m,l}, \quad (6.28)$$

where $\boldsymbol{q}_{p,m,l}$ denotes the quantization noise vector whose entries are i.i.d. $\mathcal{CN}(0, Q_{p,m,l})$. We assume that the training vectors at different antenna elements are assigned equal capacity and different pilot symbols within the same training vector are assigned equal capacity. Let us consider $C_{p,m}$ as the assigned capacity for pilot symbols transmission from the l^{th} antenna element in the m^{th} AP such as

$$C_{p,m} = \frac{C_m}{N_{ap}} = \frac{\tau_{u,p}}{\tau_c}\log_2\left(1 + \frac{P_p\sum\limits_{k'=1}^{K}\beta_{mk'} + \sigma_w^2}{Q_{p,m,l}}\right), \quad (6.29)$$

where the term $P_p\sum\limits_{k'=1}^{K}\beta_{mk'} + \sigma_w^2$ represents the composite received power of each training symbol. Based on this, the received training sequence matrix from the m^{th} AP at the CPU will be

$$\hat{\boldsymbol{Y}}_{p,m} = \sqrt{P_p\tau_{u,p}}\sum_{k'=1}^{K}\boldsymbol{g}_{mk'}\boldsymbol{\psi}_{k'}^T + \boldsymbol{\Omega}_{p,m} + \boldsymbol{W}_{p,m}, \quad (6.30)$$

where $\boldsymbol{\Omega}_{p,m} \in \mathbb{C}^{N_{ap}\times\tau_{u,p}}$ denotes the matrix of pilot compression quantization noise. After the signals are received at the CPU, the CPU estimates the channel coefficients of all users. In that, to estimate the k^{th} user channel with the l^{th} antenna element in the m^{th}

AP, the CPU performs MMSE channel estimation technique as follows

$$\breve{g}_{m,k,l} = \breve{\mathcal{C}}_{m,k,l}\hat{\boldsymbol{y}}_{p,m,l}\boldsymbol{\psi}_k^*, \tag{6.31}$$

with

$$\breve{\mathcal{C}}_{m,k,l} = \frac{\sqrt{P_p\tau_{u,p}}\beta_{mk}}{P_p\tau_{u,p}\sum\limits_{k'=1}^{K}\beta_{mk'}\left|\boldsymbol{\psi}_{k'}^T\boldsymbol{\psi}_k^*\right|^2+Q_{p,m,l}+\sigma_w^2}. \tag{6.32}$$

According to the MMSE estimation, the estimated channel at the CPU $\breve{g}_{m,k,l}$ and the corresponding channel estimation error $\grave{g}_{m,k,l}$ are independent and distributed as

$$\breve{g}_{m,k,l} \sim \mathcal{CN}(0, \breve{\zeta}_{mk}), \quad \grave{g}_{m,k,l} \sim \mathcal{CN}(0, \beta_{mk} - \breve{\zeta}_{mk}), \tag{6.33}$$

with $\breve{\zeta}_{mk} = \sqrt{P_p\tau_{u,p}}\beta_{mk}\breve{\mathcal{C}}_{m,k,l}$.

6.3.2.2 Downlink Transmission

Capitalizing on the estimated users' channel conditions and the high processing capabilities at the CPU, the CPU applies centralized ZF precoding for DL data transmission. The precoding vector, used by the CPU towards the k^{th} user is

$$\bar{\boldsymbol{\varpi}}_k = \frac{\breve{\boldsymbol{G}}^*\left(\breve{\boldsymbol{G}}^T\breve{\boldsymbol{G}}^*\right)^{-1}\boldsymbol{e}_k}{\sqrt{\left\|\breve{\boldsymbol{G}}^*\left(\breve{\boldsymbol{G}}^T\breve{\boldsymbol{G}}^*\right)^{-1}\boldsymbol{e}_k\right\|^2}}, \tag{6.34}$$

where $\breve{\boldsymbol{G}}$ represents the estimated channel matrix at the CPU. Also, $\boldsymbol{e}_k$ is the k^{th} column in the identity matrix $\boldsymbol{I}_k$. Thus, the precoded data vector at the CPU will be

$$\boldsymbol{x} = \sum_{k=1}^{K}\bar{\boldsymbol{\varpi}}_k s_k. \tag{6.35}$$

Due to the limited capacity of fronthaul links, the CPU firstly compresses the precoded data vector where the compressed data vector to be transmitted to APs will be

$$\hat{\boldsymbol{x}} = \boldsymbol{x} + \boldsymbol{q}_d, \tag{6.36}$$

with $\boldsymbol{q}_d$ being the vector of compression noise. Note that, in the centralized system operation, the CPU sends N_{ap} compressed signals to each AP. In that, we assume that these signals are allocated equal capacity $C_{d,m}$. Let $q_{d,m,l} \sim \mathcal{CN}(0, Q_{d,m,l})$ be the quantization noise signal, accompanying the transmitted precoded signal to the l^{th} antenna element in the m^{th} AP where

$$C_{d,m} = \frac{C_m}{N_{ap}} = \frac{\tau_c - \tau_{u,p}}{\tau_c}\log_2\left(1 + \frac{\mathbb{E}\{|x_{m,l}|^2\}}{Q_{d,m,l}}\right). \tag{6.37}$$

After APs receive the precoded DL data vector, they operate as relays to convey the signal to users. Consequently, the received signal at the k^{th} user is given by

$$r_k^{Cen} = \sqrt{P_d}\boldsymbol{g}_k^T\bar{\boldsymbol{\varpi}}_k s_k + \sqrt{P_d}\sum_{k'\neq k}\boldsymbol{g}_k^T\bar{\boldsymbol{\varpi}}_{k'}s_{k'} + \sqrt{P_d}\boldsymbol{g}_k^T\boldsymbol{q}_d + w_k, \tag{6.38}$$

where the first term includes the desired signal while the second term represents the interference due to transmitted data to other users. Also, the third and fourth terms denote the quantization and thermal noise effects, respectively. Note that, we do not consider DL pilots when applying ZF precoding. This is due to its effect in canceling out the dependence of the desired received signal on the small-scale fading coefficients. Thus, the achievable DL rate of user k can be determined by

$$R_k^{Cen} = \frac{\left(\tau_c - \tau_{u,p}\right)}{\tau_c} \times \log_2\left(1 + \frac{P_d\left|\mathbb{E}\left\{\boldsymbol{g}_k^T \bar{\boldsymbol{\varpi}}_k\right\}\right|^2}{P_d \sum\limits_{k'=1}^{K} \mathbb{E}\left\{\left|\boldsymbol{g}_k^T \bar{\boldsymbol{\varpi}}_{k'}\right|^2\right\} - P_d\left|\mathbb{E}\left\{\boldsymbol{g}_k^T \bar{\boldsymbol{\varpi}}_k\right\}\right|^2 + P_d\mathbb{E}\left\{\left|\boldsymbol{g}_k^T \boldsymbol{q}_d\right|^2\right\} + \sigma_w^2}\right), \tag{6.39}$$

6.4 Numerical Results and Simulations

We consider that APs and users are uniformly distributed in a square area of size 0.5×0.5 km^2. The carrier frequency $f_c = 2$ GHz. The UL pilot transmission power $P_p = 0.1$ Watt and the DL data and pilot transmission power $P_d = 0.2$ Watt. The noise variance $\sigma_w^2 = 290 \times \kappa \times B \times NF$ where κ is the Boltzman constant, $B =$ 20 MHz, denoting the system bandwidth, and $NF =$ 9 dB is the noise figure. Also, we consider a coherence time interval $\tau_c = 400$ samples. The coverage area includes 100 APs where each is equipped with $N_{ap} = 4$ antenna elements to serve 40 users. Also, we consider non-orthogonal UL training with $\tau_{u,p} = 20$.

We firstly analyze the impact of limited-fronthaul capacity on the distributed system operation as depicted in Fig. 6.1. Two different capacity allocation are considered, namely, equal capacity allocation and water-filling capacity allocation in (6.17) and (6.18), respectively. We consider ideal fronthaul links with $C_m = Inf$ bps/Hz and limited-fronthaul capacity links with $C_m = 1$ and 5 bps/Hz. Notably, limiting the capacity of fronthaul links significantly degrades the DL achievable rates. Also, applying the water-filling capacity allocation improves the system performance compared to equal capacity allocation. As such, in the sequel, we consider the distributed operation performance under water-filling capacity allocation.

Fig. 6.2 shows the impact of limited-fronthaul links capacity on the performance of the centralized and distributed system operations. It is clear that the centralized system oper-

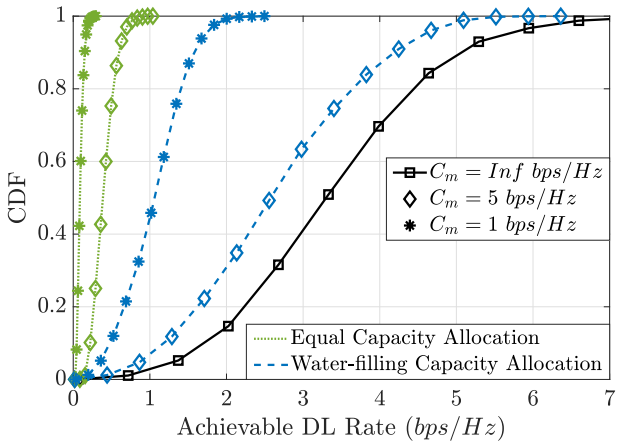

Figure 6.1: CDF of achievable DL rates assuming distributed operation with limited-fronthaul capacity and different capacity allocation techniques.

ation using ZF precoding significantly outperforms the distributed counterpart using CB precoding with beamforming training under ideal fronthaul links with $C_m = Inf$ bps/Hz. However, the impact of limited-fronthaul capacity with $C_m = 10$ and 5 bps/Hz is more prominent in the centralized system operation. Consequently, as the fronthaul capacity decreases, the number of users, attains higher DL rates from the distributed system operation increases.

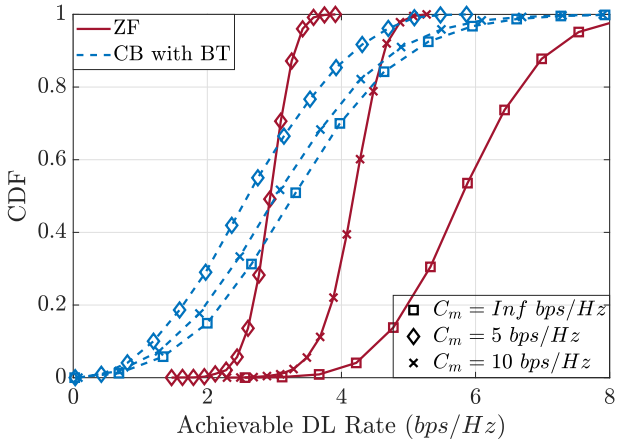

Figure 6.2: CDF of achievable DL rates under different system operations and different capacities of fronthaul links.

Fig. 6.3 depicts the effect of increasing the number of antennas per AP (N_{ap}) on the performance of distributed and centralized system operations. We consider two different number of antennas per AP with $N_{ap} = 4$ and 8 antennas and a limited-fronthaul capacity with $C_m = 5$ bps/Hz. Also, we consider two different user configurations and pilot sequence length with $K = 40, \tau_{u,p} = 20$ and $K = 20, \tau_{u,p} = 5$. It is clear that increasing

the number of antennas per AP improves the achievable DL rates of distributed system operation. On the other hand, unexpectedly, increasing N_{ap} from 4 to 8 degrades the performance of the centralized system operation. This is a consequence that the number of pilot and precoded data signals to be transmitted between each AP and the CPU is increasing linearly with the number of antennas per AP which leads to a corresponding increase in the quantization noise power.

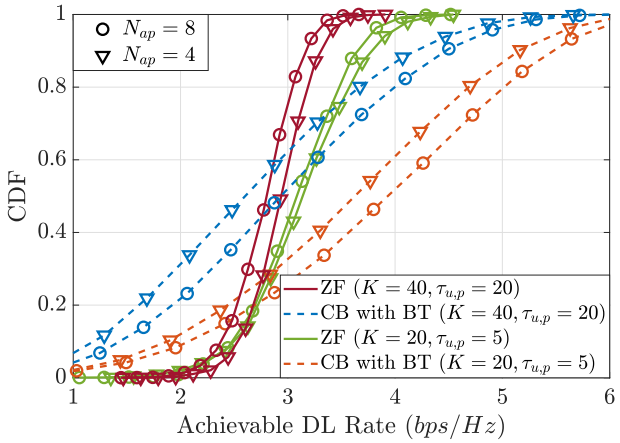

Figure 6.3: CDF of achievable DL rates assuming different number of antennas per APs and limited-fronthaul capacity link with $C_m = 5$ bps/Hz.

Fig. 6.4 compares the average DL rate of distributed and centralized system operations under different capacity of fronthaul links and different number of antennas at APs. Notably, as the capacity of fronthaul links increases, the average DL rates of both system operations improve. Regarding the centralized system operation using ZF precoding, while increasing the number of antennas at APs is not beneficial at small capacities of fronthaul links, this significantly boosts the system performance at high capacities of fronthaul links. This is a consequence of the high quantization noise at low capacities of fronthaul links. It is also noted that increasing the number of antennas at APs is always beneficial to improve the performance of the distributed system operation with no regard to the fronthaul capacity. Finally, it is noted that, applying local CB precoding with bamforming training outperforms the centralized ZF precoding at low capacities of fronthaul links. However, the centralized ZF precoding is more preferable at high capacities of fronthaul links.

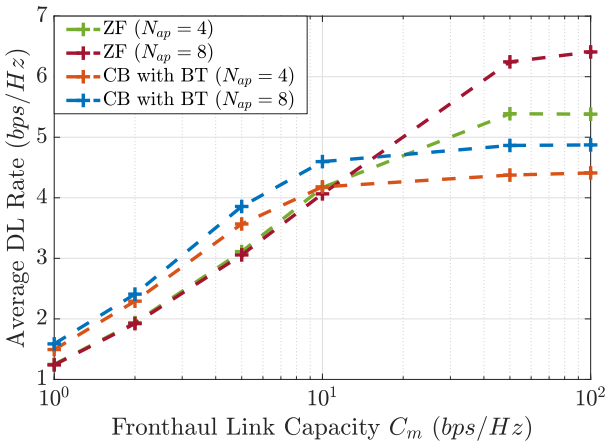

Figure 6.4: Average DL rate under different capacities of fronthaul links and different number of antennas at APs.

6.5 Summary

We studied the DL performance of CF mMIMO systems under limited capacity of wired fronthaul links. We derived the achievable DL rates assuming two different system operations assuming Rayleigh fading channels between users and APs. The first operation is a distributed operation in which APs apply local CB precoding, supported by beamforming training for DL transmission. On the other hand, the second operation is a centralized operation in which the CPU estimates users' channels and applies ZF precoding for DL transmission. Results showed that the limited-fronthaul capacity effect is more prominent on the centralized system operation. In addition, while the centralized operation outperforms the distributed counterpart under high capacities of fronthaul links, the distributed operation is more preferable for systems with low capacities of fronthaul links.

Chapter 7
CF mMIMO Performance Under A Wireless-Based Fronthaul Network

7.1 Introduction

Despite previous works analyzed the impact of limited capacity fronthaul links on the performance of CF mMIMO systems, the reported results therein are limited to CF mMIMO systems with wired fronthaul links as illustrated in chapter 6. In this regard, they considered APs connecting to CPU through wired fronthaul links with fixed capacity. In fact, deploying a wired fronthaul network can provide a lossless transmission over high capacity of fronthaul links, especially using high speed optical fiber cables. Nevertheless, this significantly increases the construction cost due to the massive number of links to be established between APs and CPU. Consequently, a more feasible solution is to support APs with wireless-based fronthaul links.

Here we thoroughly investigate the DL performance of CF mMIMO under a wireless-based fronthaul network. To this end, we assume that the network consists of multiple ECPs that independently carry out the CPU functionalities for their associated APs. The fronthaul communication between ECPs and their associated APs is a mMIMO-based communication that can be carried out under one of three possible fronthaul operations, namely, microwave, mmWave, or hybrid microwave/mmWave. Besides, we consider two different microwave-based access link operations for the communication between users and APs, namely distributed and centralized system operations as discussed in chapter 6.

7.2 System Model

7.3 Network Topology

We consider a user-centric CF mMIMO system with uniformly distributed multi-antenna APs, single-antenna users, ECPs, and blockages, i.e., buildings as shown in Fig. 7.1. Also, we consider a wireless mMIMO-based fronthaul network in which each AP communicates with its nearest ECP over a wireless fronthaul link. In this regard, three different fronthaul operations are considered for the communication between ECPs and their associated APs, namely, microwave-based operation, mmWave-based operation, and hybrid microwave/mmWave operation as shown in Fig. 7.1a, Fig. 7.1b, and Fig. 7.1c, respectively.

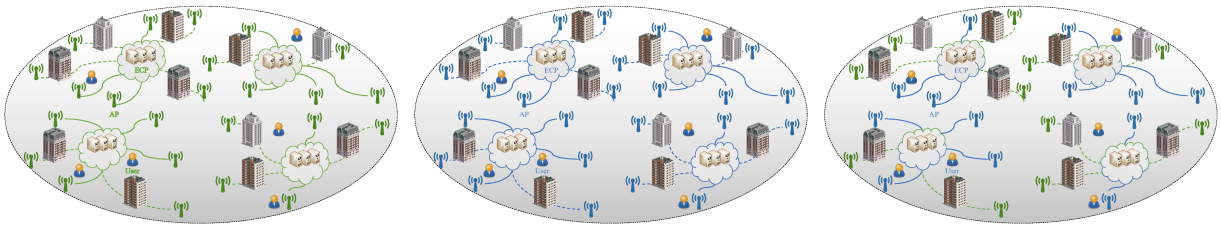

(a) Microwave-based fronthaul operation (b) MmWave-based fronthaul operation (c) hybrid microwave/mmWave fronthaul

Figure 7.1: CF mMIMO system model with wireless fronthaul network. Solid and broken lines represent LoS and NLoS links, respectively.

Co-located mMIMO-based data transmission is considered for the communication between each ECP and its associated APs over the different considered fronthaul operations. In this regard, ZF beamforming/detection technique is applied for data transmission/reception between each ECP and its associated APs [122]. To this end, for the microwave/mmWave-based fronthaul operations (Fig. 7.1a / Fig. 7.1b), each ECP is equipped with $\mathcal{N}^{\jmath}$ microwave/mmWave antennas where $\jmath \in \{\mu, mm\}$ refers to the operating band with μ and mm stand for microwave and mmWave bands, respectively. In addition, each AP is equipped with single microwave/mmWave antenna, dedicated for the communication with its serving ECP in the microwave/mmWave-based fronthaul operation.

For the hybrid microwave/mmWave fronthaul operation (Fig. 7.1c), each ECP includes multiple mmWave and microwave antennas simultaneously. Also, each AP includes one antenna for the microwave-based fronthaul operation and another one for the

mmWave counterpart. However, only one antenna will be exploited for the fronthaul communication, i.e., each AP will have either a mmWave or a microwave fronthaul link. Particularly, if the AP has a LoS link with its serving ECP, the fronthaul communication will be carried out on the mmWave band. However, the fronthaul communication will be performed on the microwave band if the fronthaul link is exposed to blockages. This is due to the harsh effect of blockages on the transmitted signals on the mmWave bands [123]. Note that, for the fronthaul communication, blockages are the only components that may prevent the presence of LoS links between an AP and its serving ECP. Thus, to decide if an AP has a LoS link with its serving ECP, we check if the direct link between the AP and the ECP is exposed to any of the existing blockages or not.

Different from the fronthaul communication, the environment around users is more dynamic and rich with moving obstacles that may completely block the LoS links between users and APs. Due to the harsh impact of blockages on the transmitted signals on the mmWave bands, and aiming at having reliable communication links between users and APs, the access communication between users and APs is carried out over the microwave band only. Due to the dynamic nature of the environment around users, we do not follow the same approach of the fronthaul network to check the presence of LoS links. Instead, we adopt the proposed 3GPP model in [113] to decide if users have LoS links with APs. We consider two microwave-based access links operations. The first one is a distributed operation in which APs apply CB along with DL beamforming training for the DL data transmission, whereas the second one is a centralized operation in which ECPs apply ZF precoding to generate the DL precoded symbols to be transmitted from APs to users.

7.3.1 Channel Model

Both access and fronthaul channels are modeled as Rician fading channels. To differentiate between the access link channels and fronthaul channels, we use the superscripts AL and FH, respectively. In particular, the access link channel vector $\boldsymbol{g}_{mk}^{AL} \in \mathbb{C}^{N_{ap}\times 1}$ between the m^{th} AP and the k^{th} user as well as the fronthaul channel vector $\boldsymbol{g}_{nm}^{FH_\jmath} \in \mathbb{C}^{\mathcal{N}_\jmath\times 1}$ between the m^{th} AP and the n^{th} ECP in the fronthaul operating band $\jmath$ can be expressed by

$$\boldsymbol{g}_{uv}^{\check{\ell}} = \sqrt{\beta_{uv}^{\check{\ell}}}\Big(\sqrt{\frac{\mathcal{K}_{uv}^{\check{\ell}}}{\mathcal{K}_{uv}^{\check{\ell}}+1}}\bar{\boldsymbol{h}}_{uv}^{\check{\ell}} + \sqrt{\frac{1}{\mathcal{K}_{uv}^{\check{\ell}}+1}}\big(\boldsymbol{\Delta}_{uv}^{\check{\ell}}\big)^{0.5}\boldsymbol{h}_{uv}^{\check{\ell}}\Big). \tag{7.1}$$

where $uv \in \{mk, nm\}$ and $\breve{\ell} \in \{AL, FH_j\}$. Also, $\mathcal{K}_{uv}^{\breve{\ell}}$ denotes the Rician $\mathcal{K}$-factor and $\beta_{uv}^{\breve{\ell}}$ represents the large-scale fading coefficient which accounts for the channel path-loss and shadowing effects. The term $\bar{\boldsymbol{h}}_{uv}^{\breve{\ell}}$ accounts for the LoS component while $\boldsymbol{h}_{uv}^{\breve{\ell}}$ is a vector of small-scale fading coefficients whose entries are independent circularly symmetric complex Gaussian random variables with zero mean and unit variance $\mathcal{CN}(0,1)$. In addition, $\boldsymbol{\Delta}_{uv}^{\breve{\ell}}$ represents the channel correlation matrix. As such, $\boldsymbol{g}_{uv}^{\breve{\ell}} \sim \mathcal{CN}(\bar{\boldsymbol{g}}_{uv}^{\breve{\ell}}, \boldsymbol{R}_{uv}^{\breve{\ell}})$ with

$$\bar{\boldsymbol{g}}_{uv}^{\breve{\ell}} = \sqrt{\frac{\beta_{uv}^{\breve{\ell}} \mathcal{K}_{uv}^{\breve{\ell}}}{\mathcal{K}_{uv}^{\breve{\ell}} + 1}} \bar{\boldsymbol{h}}_{uv}^{\breve{\ell}}, \qquad \boldsymbol{R}_{uv}^{\breve{\ell}} = \frac{\beta_{uv}^{\breve{\ell}}}{\mathcal{K}_{uv}^{\breve{\ell}} + 1} \boldsymbol{\Delta}_{\boldsymbol{uv}}^{\breve{\boldsymbol{\ell}}}, \tag{7.2}$$

where $\boldsymbol{R}_{uv}^{\breve{\ell}}$ is a positive semi-definite covariance matrix that reflects the channel correlation characteristics of the NLoS component. Also, the LoS components $\bar{\boldsymbol{h}}_{mk}^{AL}$ and $\bar{\boldsymbol{h}}_{nm}^{FH_j}$ are given by

$$\begin{aligned} \bar{\boldsymbol{h}}_{mk}^{AL} &= [1, e^{-j2\pi\chi^{AL} sin(\theta_{mk}^{AL})}, \cdots, e^{-j2\pi\chi^{AL}(N_{ap}-1) sin(\theta_{mk}^{AL})}], \\ \bar{\boldsymbol{h}}_{nm}^{FH_j} &= [1, e^{-j2\pi\chi^{FH_j} sin(\theta_{nm}^{FH_j})}, \cdots, e^{-j2\pi\chi^{FH_j}(\mathcal{N}^j-1) sin(\theta_{nm}^{FH})}], \end{aligned} \tag{7.3}$$

where $\chi^{\breve{\ell}}$ represents the antenna spacing divided by the carrier wavelength and $\theta_{uv}^{\breve{\ell}} \sim U[-\pi, \pi]$ is the signal arrival angle. The channel correlation matrix $\boldsymbol{\Delta}_{uv}^{\breve{\ell}}$ can be modeled by

$$[\boldsymbol{\Delta}_{uv}^{\breve{\ell}}]_{n_1,n_2} = (r_{uv}^{\breve{\ell}})^{|n_1-n_2|}, \tag{7.4}$$

where $0 < r_{uv}^{\breve{\ell}} \leq 1$ denotes the channel correlation coefficient.

7.4 Distributed System Operation

7.4.1 Fronthaul Communication

In the distributed system operation, both channel estimation and DL precoding are carried out at APs. Therefore, the payload data of different users is the only information to be sent from ECPs to their associated APs. We consider that the available bandwidth for fronthaul communication in both microwave/mmWave bands is divided equally among the deployed ECPs in the coverage area. Then, the available microwave/mmWave bandwidth at each ECP is divided equally among its served users. In fact, APs will have different fronthaul capacities based on their channel conditions with their serving ECPs. Accordingly, for any user k, each ECP needs to send different compressed versions of the user's payload data to its associated APs. This can be considered as a beamforming problem in which each ECP is required to send different compressed data symbols to different APs on the same time-frequency resources. We assume that each ECP has perfect CSI

for its associated APs. This can be justified as both APs and ECPs are deployed at fixed locations with high-altitude antenna elements. This leads to wireless fronthaul links with long channel coherence time in which a perfect channel estimation of the deployed APs can be readily obtained. Moreover, to perfectly mitigate the mutual interference from the transmitted signals to different APs, we apply ZF precoding for data transmission between ECP and its associated APs. Note that, ZF precoding can be performed in the microwave band operation using digital beamforming while it can be carried out in the mmWave band using hybrid beamforming with the aid of the Block Coordinate Descent algorithm [118, 124].

Let us consider $\hat{s}^{\jmath}_{m,k}$ as the compressed signal of user k to be transmitted to the m^{th} AP over the fronthaul band $\jmath$. Thus, the received signal at the m^{th} AP for user k from its serving ECP n_m is given by

$$r^{Dis,\jmath}_{m,k} = \sqrt{P^{\jmath}_{d}} \sum_{m' \in \mathcal{M}^{\jmath}_{n_m}} \sqrt{\gamma^{\jmath}_{m'}} (\boldsymbol{g}^{FH_{\jmath}}_{n_m m})^T \boldsymbol{\mathcal{Q}}^{\jmath}_{m'} \hat{s}^{\jmath}_{m',k} + w^{\jmath}_{m,k}, \tag{7.5}$$

where $P^{\jmath}_{d,f}$ denotes the DL transmission power of ECP antennas and $\mathcal{M}^{\jmath}_{n_m}$ being the set of associated APs to the ECP n_m. In addition, $w^{\jmath}_{m,k}$ reflects the additive thermal noise at the m^{th} AP. The precoding vector $\boldsymbol{\mathcal{Q}}^{\jmath}_{m'}$ for the data to be transmitted to AP $m' \in \mathcal{M}^{\jmath}_{n_m}$ on band $\jmath$ is given by

$$\boldsymbol{\mathcal{Q}}^{\jmath}_{m'} = \big(\boldsymbol{G}^{FH_{\jmath}}_{n_m}\big)^* \Big(\big(\boldsymbol{G}^{FH_{\jmath}}_{n_m}\big)^T \big(\boldsymbol{G}^{FH_{\jmath}}_{n_m}\big)^* \Big)^{-1} \boldsymbol{e}_{m'}, \tag{7.6}$$

where $\boldsymbol{G}^{FH_{\jmath}}_{n_m}$ represents the fronthaul channel matrix between the ECP n_m and its associated APs on band $\jmath$. Also, $\boldsymbol{e}_{m'}$ denotes the m'^{th} column in the identity matrix $\boldsymbol{I}_{M^{\jmath}_{n_m}}$ where $M^{\jmath}_{n_m}$ represents the number of associated APs to the ECP n_m on band $\jmath$. The term $\gamma^{\jmath}_{m'}$ denotes the power normalization factor for the precoding vector of AP $m' \in \mathcal{M}^{\jmath}_{n_m}$ that can be calculated as follows:

$$\gamma^{\jmath}_{m'} = \frac{1}{M_{n_m} \mathbb{E}\Big\{ \Big[\Big(\big(\boldsymbol{G}^{FH_{\jmath}}_{n_m}\big)^T \big(\boldsymbol{G}^{FH_{\jmath}}_{n_m}\big)^* \Big)^{-1} \Big]_{(m',m')} \Big\}}. \tag{7.7}$$

Thus, the received signal at the m^{th} AP can be rewritten as follows:

$$r^{Dis,\jmath}_{m,k} = \sqrt{P^{\jmath}_{d} \gamma^{\jmath}_{m}} \hat{s}^{\jmath}_{m,k} + w^{\jmath}_{m,k}. \tag{7.8}$$

Let us denote $\mathcal{B}^{\jmath}_{F}$ as the bandwidth of the fronthaul band $\jmath$ and N as the number of deployed ECPs at a specific realization. Consequently, the fronthaul capacity in bps/Hz according to which the transmitted signals towards the m^{th} generic AP are compressed is given by

$$C^{Dis,\jmath}_{m} = \frac{\mathcal{B}^{\jmath}_{F}}{N K_{n_m} \mathcal{B}_{A}} \log_2 \Big(1 + \frac{P^{\jmath}_{d} \gamma^{\jmath}_{m}}{(\sigma^{\jmath}_{w})^2} \Big), \tag{7.9}$$

where K_{n_m} denotes the number of served users by APs $\mathcal{M}^{J}_{n_m}$. Note that $C^{Dis,J}_{m}$ is a normalized fronthaul capacity that reflects the assigned fronthaul capacity for each $1Hz$ in the access communication link since the calculated capacity is divided by the access link bandwidth $\mathcal{B}_A$.

7.4.2 Access Communication

This section discusses the communication phases between users and deployed APs under a TDD-based system operation, namely, the channel estimation phase and DL data transmission phase. As previously stated, both channel estimation and DL precoding are performed at the APs for the distributed system operation. Due to the limited processing capabilities of APs, we adopt CB precoding for DL transmission thanks to its low processing requirements. Along with that, we apply beamforming training due to its high potential in improving the achievable DL data rates as discussed in chapter 6.

7.4.2.1 Channel Estimation

The received training sequence matrix $\boldsymbol{Y}_{p,m} \in \mathbb{C}^{N_{ap}\times\tau_{u,p}}$ at AP m is given by

$$\boldsymbol{Y}_{p,m} = \sqrt{P_p\tau_{u,p}}\sum_{k'=1}^{K}\boldsymbol{g}^{AL}_{mk'}\boldsymbol{\psi}^{T}_{k'} + \boldsymbol{W}_{p,m}. \tag{7.10}$$

Since the LoS component $\bar{\boldsymbol{g}}^{AL}_{mk}$ and $\boldsymbol{R}^{AL}_{mk}$ are changing slowly with respect to the channel coherence time, they are assumed to be available at APs. As such, one can apply MMSE-based channel estimation where the estimated channel vector of user k at the m^{th} AP will be

$$\hat{\boldsymbol{g}}^{AL}_{mk} = \bar{\boldsymbol{g}}^{AL}_{mk} + \sqrt{P_p\tau_{u,p}}\boldsymbol{R}^{AL}_{mk}\boldsymbol{\Phi}^{AL}_{mk}\Big(\boldsymbol{Y}_{p,m}\boldsymbol{\psi}^{*}_{k} - \sqrt{P_p\tau_{u,p}}\sum_{k'=1}^{K}\bar{\boldsymbol{g}}^{AL}_{mk'}\boldsymbol{\psi}^{T}_{k'}\boldsymbol{\psi}^{*}_{k}\Big), \tag{7.11}$$

with

$$\boldsymbol{\Phi}^{AL}_{mk} = \left(\sum_{k'=1}^{K}P_p\tau_{u,p}\boldsymbol{R}^{AL}_{mk'}\boldsymbol{\psi}^{T}_{k'}\boldsymbol{\psi}^{*}_{k} + \sigma^2\boldsymbol{I}_{N_{ap}}\right)^{-1}. \tag{7.12}$$

Let $\tilde{\boldsymbol{g}}^{AL}_{mk} = \boldsymbol{g}^{AL}_{mk} - \hat{\boldsymbol{g}}^{AL}_{mk}$ be the channel estimation error vector. The MMSE estimate $\hat{\boldsymbol{g}}^{AL}_{mk}$ and the estimation error $\tilde{\boldsymbol{g}}^{AL}_{mk}$ are independent random variables where

$$\hat{\boldsymbol{g}}^{AL}_{mk} \sim \mathcal{CN}(\bar{\boldsymbol{g}}^{AL}_{mk}, \boldsymbol{\Gamma}^{AL}_{mk}), \qquad \tilde{\boldsymbol{g}}^{AL}_{mk} \sim \mathcal{CN}(\boldsymbol{0}, \boldsymbol{R}^{AL}_{mk} - \boldsymbol{\Gamma}^{AL}_{mk}), \tag{7.13}$$

with $\boldsymbol{\Gamma}^{AL}_{mk} = P_p\tau_{u,p}\boldsymbol{R}^{AL}_{mk}\boldsymbol{\Phi}^{AL}_{mk}\boldsymbol{R}^{AL}_{mk}$ represents the estimation covariance matrix.

7.4.2.2 Downlink Transmission

The compressed signal of user k to be transmitted to the m^{th} AP $\hat{s}^{\jmath}_{m,k}$ is represented by

$$\hat{s}^{\jmath}_{m,k} = s_k + q^{\jmath}_{m,k}, \tag{7.14}$$

where $q^{\jmath}_{m,k} \sim \mathcal{CN}(0, Q^{\jmath}_{m,k})$ represents the compression quantization noise with $Q^{\jmath}_{m,k}$ denoting the compression quantization power such that:

$$C^{Dis,\jmath}_{m} = \frac{\tau_c - \tau_{u,p} - \tau_{d,p}}{\tau_c} \log_2\Big(1 + \frac{1}{Q^{\jmath}_{m,k}}\Big), \tag{7.15}$$

with $\tau_{d,p}$ denotes the length of the DL pilot sequence for the beamforming training operation as will be discussed later. Thus, the received signal at the m^{th} AP from its serving ECP given in (7.8) can be rewritten as follows:

$$r^{Dis,\jmath}_{m,k} = \sqrt{P^{\jmath}_d \gamma^{\jmath}_m}(s_k + q^{\jmath}_{m,k}) + \delta w^{\jmath}_{m,k} = \mathcal{E}^{\jmath}_m(s_k + q^{\jmath}_{m,k}) + \delta w^{\jmath}_{m,k}, \tag{7.16}$$

where $P^{\jmath}_d$ denotes the DL transmit power in the fronthaul network on band $\jmath$. Also, $\delta \in \{0, 1\}$ reflects two different approaches that APs can follow before carrying out the precoding process. The first approach with $\delta = 1$ considers precoding the received signal including the added thermal noise at the AP $w^{\jmath}_{m,k}$. Differently, the second one with $\delta = 0$ considers decoding the signal from the added thermal noise before carrying out the precoding process. Also,

$$\mathcal{E}^{\jmath}_m = \sqrt{P^{\jmath}_d \gamma^{\jmath}_m}, \tag{7.17}$$

denotes the fronthaul impact on the directed data towards the m^{th} AP. Since the fronthaul impact parameter towards the m^{th} AP changes slowly over time, it can be available at the AP. Thus, each AP can cancel the fronthaul effect on the k^{th} user signal s_k as follows:

$$\dot{r}^{Dis,\jmath}_{m,k} = s_k + q^{\jmath}_{m,k} + \delta\big(\mathcal{E}^{\jmath}_m\big)^{-1} w^{\jmath}_{m,k}. \tag{7.18}$$

Next, let us define $\mathcal{K}(m)$ as the set of served users by the m^{th} AP. Accordingly, the transmitted CB precoded signal from the m^{th} AP will be

$$\boldsymbol{x}^{Dis,\jmath}_{m} = \sqrt{P_d} \sum_{k' \in \mathcal{K}(m)} \sqrt{\eta_{mk'}} \big(\hat{\boldsymbol{g}}^{AL}_{mk'}\big)^{*} \dot{r}^{Dis,\jmath}_{m,k'}. \tag{7.19}$$

Also, we assume equal power allocation for the DL power control coefficients. Then, let $\mathcal{M}(k)$ denotes the set of serving APs for user k. Also, let M and K represent the total number of APs and users, respectively, at a certain network realization. Thus, the received signal at user k is given by

$$r^{Dis}_{k} = \sum_{m=1}^{M} \big(\boldsymbol{g}^{AL}_{mk}\big)^{T} \boldsymbol{x}^{Dis,\jmath}_{m} + w_k, \tag{7.20}$$

which can be rewritten as

$$r_k^{Dis} = \sqrt{P_d} a_{kk} s_k + \sqrt{P_d}\big(\Omega_k + \mathcal{V}_k\big) + \sqrt{P_d} \sum_{k' \neq K} \big(a_{kk'} s_{k'} + \Omega_{k'} + \mathcal{V}_{k'}\big) + w_k, \tag{7.21}$$

with

$$a_{kk'} = \sum_{m \in \mathcal{M}(k')} \sqrt{\eta_{mk'}} \big(\boldsymbol{g}_{mk}^{AL}\big)^T \big(\hat{\boldsymbol{g}}_{mk'}^{AL}\big)^*, \qquad \Omega_{k'} = \sum_{m \in \mathcal{M}(k')} \sqrt{\eta_{mk'}} \big(\boldsymbol{g}_{mk}^{AL}\big)^T \big(\hat{\boldsymbol{g}}_{mk'}^{AL}\big)^* q_{m,k'}^{\jmath},$$

$$\mathcal{V}_{k'} = \delta \sum_{m \in \mathcal{M}(k')} \sqrt{\eta_{mk'}} \big(\mathcal{E}_m^{\jmath}\big)^{-1} \big(\boldsymbol{g}_{mk}^{AL}\big)^T \big(\hat{\boldsymbol{g}}_{mk'}^{AL}\big)^* w_{m,k'}^{\jmath},$$

where a_{kk} and $a_{kk'}$ denote the desired channel gain for user k and the interference channel gain due to the transmitted signals of user k'. Also, $\Omega_{k'}$ reflects the compression effect of user k' data symbol. In addition, $\mathcal{V}_{k'}$ represents the effect of the amplified thermal noise at APs towards the user side.

We consider that beamforming training is applied for DL transmission to enhance the DL system performance as in chapter 6. In that, orthogonal DL pilots with $\tau_{d,p} \geq K$ are applied for DL channel estimation. Hence, the transmitted pilot sequence matrix $\boldsymbol{\mathcal{Y}}_{p,m} \in \mathbb{C}^{N_{ap} \times \tau_{d,p}}$ from the m^{th} AP is given by

$$\boldsymbol{\mathcal{Y}}_{p,m} = \sqrt{P_d \tau_{d,p}} \sum_{k' \in \mathcal{K}(m)} \sqrt{\eta_{mk'}} \hat{\boldsymbol{g}}_{mk'}^* \boldsymbol{\phi}_{k'}^T. \tag{7.22}$$

Consequently, the received pilot sequence vector at user k will be

$$\boldsymbol{y}_{p,k} = \sqrt{P_d \tau_{d,p}} \sum_{k' \in \mathcal{K}(m)} a_{kk'} \boldsymbol{\phi}_{k'}^T + \boldsymbol{w}_{p,k}. \tag{7.23}$$

After user k receives the DL training signals, it estimates its channel gain a_{kk} with its serving APs. In doing so, it firstly projects the received training signal on ϕ_k as follows:

$$\tilde{y}_{p,k} = \sqrt{P_d \tau_{d,p}} a_{kk} + \boldsymbol{w}_{p,k} \boldsymbol{\phi}_k^*. \tag{7.24}$$

Applying MMSE, the estimated channel gain can be expressed by

$$\hat{a}_{kk} = \mathbb{E}\{a_{kk}\} + \frac{\sqrt{P_d \tau_{d,p}} Var\{a_{kk}\}}{P_d \tau_{d,p} Var\{a_{kk}\} + \sigma_w^2} \Big(\tilde{y}_{p,k} - \sqrt{P_d \tau_{d,p}} \mathbb{E}\{a_{kk}\}\Big). \tag{7.25}$$

with

$$\mathbb{E}\{\hat{a}_{kk}\} = \mathbb{E}\{a_{kk}\}, \qquad Var\{\hat{a}_{kk}\} = \frac{P_d \tau_{d,p} \big(Var\{a_{kk}\}\big)^2}{P_d \tau_{d,p} Var\{a_{kk}\} + \sigma_w^2}, \tag{7.26}$$

where the statistics of the channel gain a_{kk} are given in Lemma 7.1. Let $\tilde{a}_{kk}$ denotes the estimation error of the channel gain a_{kk} where $\tilde{a}_{kk} = a_{kk} - \hat{a}_{kk}$. In that, $\tilde{a}_{kk}$ has a zero mean while the error variance is given by

$$Var\{\tilde{a}_{kk}\} = \mathbb{E}\{|\tilde{a}_{kk}|^2\} = \frac{Var\{a_{kk}\}}{P_{d,p} \tau_{d,p} Var\{a_{kk}\} + \sigma_w^2}. \tag{7.27}$$

Lemma 7.1. *The expectation and variance of the channel gain a_{kk} of the k^{th} user are*

given by

$$\begin{aligned}\mathbb{E}\{a_{kk}\} &= \sum_{m\in\mathcal{M}(k)} \sqrt{\eta_{mk}}\big(tr(\mathbf{\Gamma}_{mk}^{AL}) + \big\|\bar{\boldsymbol{g}}_{mk}^{AL}\big\|^2\big),\\ Var\{a_{kk}\} &= \sum_{m\in\mathcal{M}(k)} \eta_{mk}\Big(tr(\mathbf{\Gamma}_{mk}^{AL}\boldsymbol{R}_{mk}^{AL}) + \big(\bar{\boldsymbol{g}}_{mk}^{AL}\big)^H \boldsymbol{R}_{mk}^{AL}\bar{\boldsymbol{g}}_{mk}^{AL} + \big(\bar{\boldsymbol{g}}_{mk}^{AL}\big)^H \mathbf{\Gamma}_{mk}^{AL}\bar{\boldsymbol{g}}_{mk}^{AL}\Big).\end{aligned} \tag{7.28}$$

Proof. $\mathbb{E}\{a_{kk}\}$ can be calculated as follows:

$$\begin{aligned}\mathbb{E}\{a_{kk}\} &= \mathbb{E}\Big\{\sum_{m\in\mathcal{M}(k)} \sqrt{\eta_{mk}}(\tilde{\boldsymbol{g}}_{mk}^{AL})^T(\hat{\boldsymbol{g}}_{mk}^{AL})^*\Big\}\\ &= \sum_{m\in\mathcal{M}(k)} \sqrt{\eta_{mk}}\mathbb{E}\big\{(\hat{\boldsymbol{g}}_{mk}^{AL})^T(\hat{\boldsymbol{g}}_{mk}^{AL})^* + (\tilde{\boldsymbol{g}}_{mk}^{AL})^T(\hat{\boldsymbol{g}}_{mk}^{AL})^*\big\}.\end{aligned} \tag{7.29}$$

Based on the MMSE estimation properties,$\hat{\boldsymbol{g}}_{mk}^{AL}$ and $\tilde{\boldsymbol{g}}_{mk}^{AL}$ are independent. Also, $\tilde{\boldsymbol{g}}_{mk}^{AL}$ has zero mean, thus, $\mathbb{E}\{a_{kk}\}$ can be calculated by

$$\begin{aligned}\mathbb{E}\{a_{kk}\} &= \sum_{m\in\mathcal{M}(k)} \sqrt{\eta_{mk}}\mathbb{E}\big\{\big\|\hat{\boldsymbol{g}}_{mk}^{AL}\big\|^2\big\}\\ &= \sum_{m\in\mathcal{M}(k)} \sqrt{\eta_{mk}}\big(tr(\mathbf{\Gamma}_{mk}^{AL}) + \big\|\bar{\boldsymbol{g}}_{mk}^{AL}\big\|^2\big).\end{aligned} \tag{7.30}$$

Regarding the variance of the channel gain $Var\{a_{kk}\}$, it can be determined as follows:

$$Var\{a_{kk}\} = \mathbb{E}\big\{\big|a_{kk}\big|^2\big\} - \big(\mathbb{E}\{a_{kk}\}\big)^2, \tag{7.31}$$

where

$$\begin{aligned}\mathbb{E}\big\{\big|a_{kk}\big|^2\big\} &= \mathbb{E}\Big\{\Big|\sum_{m\in\mathcal{M}(k)} \sqrt{\eta_{mk}}(\boldsymbol{g}_{mk}^{AL})^T(\hat{\boldsymbol{g}}_{mk}^{AL})^*\Big|^2\Big\},\\ &= \underbrace{\sum_{m\in\mathcal{M}(k)} \eta_{mk}\mathbb{E}\big\{\big|(\boldsymbol{g}_{mk}^{AL})^T(\hat{\boldsymbol{g}}_{mk}^{AL})^*\big|^2\big\}}_{T_1}\\ &+ \underbrace{\sum_{m\in\mathcal{M}(k)} \sqrt{\eta_{mk}} \sum_{t\in\mathcal{M}(k)} \sqrt{\eta_{tk}}\mathbb{E}\big\{(\boldsymbol{g}_{mk}^{AL})^T(\hat{\boldsymbol{g}}_{mk}^{AL})^*\big\}\mathbb{E}\big\{(\boldsymbol{g}_{tk}^{AL})^T(\hat{\boldsymbol{g}}_{tk}^{AL})^*\big\}}_{T_2}.\end{aligned} \tag{7.32}$$

The first term in (7.32) can be calculated as

$$T_1 = \sum_{m\in\mathcal{M}(k)} \eta_{mk}\Big(\mathbb{E}\big\{\big\|\hat{\boldsymbol{g}}_{mk}^{AL}\big\|^4\big\} + \mathbb{E}\big\{\big|(\tilde{\boldsymbol{g}}_{mk}^{AL})^T(\hat{\boldsymbol{g}}_{mk}^{AL})^*\big|^2\big\}\Big), \tag{7.33}$$

in which $\mathbb{E}\big\{\big\|\hat{\boldsymbol{g}}_{mk}^{AL}\big\|^4\big\}$ can be determined as follows:

$$\begin{aligned}\mathbb{E}\big\{\big\|\hat{\boldsymbol{g}}_{mk}^{AL}\big\|^4\big\} &= \big(tr(\mathbf{\Gamma}_{mk}^{AL})\big)^2 + tr(\mathbf{\Gamma}_{mk}^{AL}\mathbf{\Gamma}_{mk}^{AL}) + \big\|\bar{\boldsymbol{g}}_{mk}^{AL}\big\|^4 + 2tr(\mathbf{\Gamma}_{mk}^{AL})\big\|\bar{\boldsymbol{g}}_{mk}^{AL}\big\|^2\\ &\quad + 2(\bar{\boldsymbol{g}}_{mk}^{AL})^H\mathbf{\Gamma}_{mk}^{AL}\bar{\boldsymbol{g}}_{mk}^{AL},\\ &= tr(\mathbf{\Gamma}_{mk}^{AL}\mathbf{\Gamma}_{mk}^{AL}) + 2(\bar{\boldsymbol{g}}_{mk}^{AL})^H\mathbf{\Gamma}_{mk}^{AL}\bar{\boldsymbol{g}}_{mk}^{AL} + \big(tr(\mathbf{\Gamma}_{mk}^{AL}) + \big\|\bar{\boldsymbol{g}}_{mk}^{AL}\big\|^2\big)^2,\end{aligned} \tag{7.34}$$

and $\mathbb{E}\big\{\big|(\tilde{\boldsymbol{g}}_{mk}^{AL})^T(\hat{\boldsymbol{g}}_{mk}^{AL})^T\big|^2\big\}$ can be calculated by

$$\mathbb{E}\big\{\big|(\tilde{\boldsymbol{g}}_{mk}^{AL})^T(\hat{\boldsymbol{g}}_{mk}^{AL})^*\big|^2\big\} = tr\big(\mathbf{\Gamma}_{mk}^{AL}(\boldsymbol{R}_{mk}^{AL} - \mathbf{\Gamma}_{mk}^{AL})\big) + (\bar{\boldsymbol{g}}_{mk}^{AL})^H(\boldsymbol{R}_{mk}^{AL} - \mathbf{\Gamma}_{mk}^{AL})\bar{\boldsymbol{g}}_{mk}^{AL}. \tag{7.35}$$

The second term in (7.32) can be represented as

$$T_2 = \sum_{m\in\mathcal{M}(k)} \sqrt{\eta_{mk}} \sum_{t\in\mathcal{M}(k)} \sqrt{\eta_{tk}}\big(\big\|\bar{\boldsymbol{g}}_{mk}^{AL}\big\|^2 + tr(\mathbf{\Gamma}_{mk}^{AL})\big)\big(\big\|\bar{\boldsymbol{g}}_{tk}^{AL}\big\|^2 + tr(\mathbf{\Gamma}_{tk}^{AL})\big), \tag{7.36}$$

From (7.32)-(7.36), one can obtain

$$\begin{aligned}\mathbb{E}\{|a_{kk}|^2\} &= \sum_{m\in\mathcal{M}(k)} \eta_{mk}\Big(tr(\boldsymbol{\Gamma}_{mk}^{AL}\boldsymbol{R}_{mk}^{AL}) + (\bar{\boldsymbol{g}}_{mk}^{AL})^H\boldsymbol{\Gamma}_{mk}^{AL}\bar{\boldsymbol{g}}_{mk}^{AL} + (\bar{\boldsymbol{g}}_{mk}^{AL})^H\boldsymbol{R}_{mk}^{AL}\bar{\boldsymbol{g}}_{mk}^{AL} \\ &\quad + \big(tr(\boldsymbol{\Gamma}_{mk}^{AL}) + \|\bar{\boldsymbol{g}}_{mk}^{AL}\|^2\big)^2\Big) + \sum_{m\in\mathcal{M}(k)}\sqrt{\eta_{mk}}\sum_{t\in\mathcal{M}(k)}\sqrt{\eta_{tk}} \\ &\quad \times \big(\|\bar{\boldsymbol{g}}_{mk}^{AL}\|^2 + tr(\boldsymbol{\Gamma}_{mk}^{AL})\big)\big(\|\bar{\boldsymbol{g}}_{tk}^{AL}\|^2 + tr(\boldsymbol{\Gamma}_{tk}^{AL})\big), \qquad (7.37) \\ &= \sum_{m\in\mathcal{M}(k)} \eta_{mk}\Big(tr(\boldsymbol{\Gamma}_{mk}^{AL}\boldsymbol{R}_{mk}^{AL}) + (\bar{\boldsymbol{g}}_{mk}^{AL})^H\boldsymbol{\Gamma}_{mk}^{AL}\bar{\boldsymbol{g}}_{mk}^{AL} + (\bar{\boldsymbol{g}}_{mk}^{AL})^H\boldsymbol{R}_{mk}^{AL}\bar{\boldsymbol{g}}_{mk}^{AL}\Big) \\ &\quad + \Big(\sum_{m\in\mathcal{M}(k)}\sqrt{\eta_{mk}}\big(\|\bar{\boldsymbol{g}}_{mk}^{AL}\|^2 + tr(\boldsymbol{\Gamma}_{mk}^{AL})\big)\Big)^2.\end{aligned}$$

Finally, substituting (7.30) and (7.37) in (7.31), $Var\{a_{kk}\}$ can be calculated as

$$Var\{a_{kk}\} = \sum_{m\in\mathcal{M}(k)} \eta_{mk}\Big(tr(\boldsymbol{\Gamma}_{mk}^{AL}\boldsymbol{R}_{mk}^{AL}) + (\bar{\boldsymbol{g}}_{mk}^{AL})^H\boldsymbol{R}_{mk}^{AL}\bar{\boldsymbol{g}}_{mk}^{AL} + (\bar{\boldsymbol{g}}_{mk}^{AL})^H\boldsymbol{\Gamma}_{mk}^{AL}\bar{\boldsymbol{g}}_{mk}^{AL}\Big). \qquad (7.38)$$

■

Applying the same approximation as in (6.22), a closed-form approximation for the DL achievable data rates is given by

$$R_k^{Dis} = \frac{\tau_c - \tau_{u,p}}{\tau_c}\times \log_2\left(1 + \frac{P_d\mathbb{E}\{|\hat{a}_{kk}|^2\}}{P_d\Big(\mathbb{E}\{|\tilde{a}_{kk}|^2\} + \mathbb{E}\{|\Omega_k + \mathcal{V}_k|^2\} + \sum\limits_{k'\neq k}\mathbb{E}\{|a_{kk'}s_{k'} + \Omega_{k'} + \mathcal{V}_{k'}|^2\}\Big) + \sigma_w^2}\right). \qquad (7.39)$$

Then, by introducing the following variables

$$\begin{aligned}&A_{m,k,k'} \triangleq \eta_{mk'}\Big(tr(\boldsymbol{\Gamma}_{mk'}^{AL}\boldsymbol{R}_{mk}^{AL}) + (\bar{\boldsymbol{g}}_{mk'}^{AL})^H\boldsymbol{R}_{mk}\bar{\boldsymbol{g}}_{mk'}^{AL} + (\bar{\boldsymbol{g}}_{mk}^{AL})^H\boldsymbol{\Gamma}_{mk'}^{AL}\bar{\boldsymbol{g}}_{mk}^{AL}\Big), \\ &B_{m,k,k} \triangleq \sqrt{\eta_{mk}}\big(\|\bar{\boldsymbol{g}}_{mk}^{AL}\|^2 + tr(\boldsymbol{\Gamma}_{mk}^{AL})\big), \quad C_{m,k,k'} \triangleq (\bar{\boldsymbol{g}}_{mk}^{AL})^H\bar{\boldsymbol{g}}_{mk'}^{AL}, \qquad (7.40) \\ &D_{m,k,k'} \triangleq tr(\boldsymbol{R}_{mk}^{AL}\boldsymbol{\Phi}_{mk}^{AL}\boldsymbol{R}_{mk'}^{AL}),\end{aligned}$$

the different terms in (7.39) can be determined as follows. Firstly, the desired signal power can be derived as follows:

$$\begin{aligned}P_d\mathbb{E}\{|\hat{a}_{kk}|^2\} &= P_d\big(\big(\mathbb{E}\{\hat{a}_{kk}\}\big)^2 + Var\{\hat{a}_{kk}\}\big), \\ &= P_d\Big(\sum_{m\in\mathcal{M}(k)} B_{m,k,k}\Big)^2 + P_d\frac{P_d\tau_{d,p}\Big(\sum\limits_{m\in\mathcal{M}(k)} A_{m,k,k}\Big)^2}{P_d\tau_{d,p}\sum\limits_{m\in\mathcal{M}(k)} A_{m,k,k} + \sigma_w^2}. \qquad (7.41)\end{aligned}$$

Using (7.27), (7.38), and the definition of $A_{m,k,k}$ in (7.40), the channel estimation error power can be determined as

$$P_d\mathbb{E}\{|\tilde{a}_{kk}|^2\} = P_d\frac{\sum\limits_{m\in\mathcal{M}(k)} A_{m,k,k}}{P_d\tau_{d,p}\sum\limits_{m\in\mathcal{M}(k)} A_{m,k,k} + \sigma_w^2}. \qquad (7.42)$$

The composite interference power of the received quantization noise Ω_k and the received

additive thermal noise $\mathcal{V}_k$, defined in (7.21), can be determined as follows:

$$\begin{aligned}
P_d\mathbb{E}\{|\Omega_k+\mathcal{V}_k|^2\} &= P_d\mathbb{E}\Big\{\Big|\sum_{m\in\mathcal{M}(k)}\sqrt{\eta_{mk}}(\boldsymbol{g}_{mk}^{AL})^T(\hat{\boldsymbol{g}}_{mk}^{AL})^*\big(q_{m,k}^{\jmath}+\delta(\mathcal{E}_m^{\jmath})^{-1}w_{m,k}^{\jmath}\big)\Big|^2\Big\},\\
&\overset{(a)}{=} P_d\sum_{m\in\mathcal{M}(k)}\eta_{mk}\mathbb{E}\big\{\big|(\boldsymbol{g}_{mk}^{AL})^T(\hat{\boldsymbol{g}}_{mk}^{AL})^*\big|^2\big\}\Big(\mathbb{E}\{|q_{m,k}^{\jmath}|^2\}+\delta(\mathcal{E}_m^{\jmath})^{-2}\mathbb{E}\{|w_{m,k}^{\jmath}|^2\}\Big),\\
&= P_d\sum_{m\in\mathcal{M}(k)}\eta_{mk}\Big(\mathbb{E}\big\{\big\|\hat{\boldsymbol{g}}_{mk}^{AL}\big\|^4\big\}+\mathbb{E}\big\{\big|(\tilde{\boldsymbol{g}}_{mk}^{AL})^T(\hat{\boldsymbol{g}}_{mk}^{AL})^*\big|^2\big\}\Big)\Big(Q_{m,k}^{\jmath}+\delta(\mathcal{E}_m^{\jmath})^{-2}(\sigma_w^{\jmath})^2\Big),
\end{aligned}\tag{7.43}$$

where $\overset{(a)}{=}$ stems from the independence between the quantization noise $q_{m,k}^{\jmath}$ and the thermal noise $w_{m,k}^{\jmath}$ as well as their independence of the user k channel vector g_{mk}^{AL}. Then, using the expressions in (7.34) and (7.35) for $\mathbb{E}\big\{\big\|\hat{\boldsymbol{g}}_{mk}^{AL}\big\|^4\big\}$ and $\mathbb{E}\big\{\big|(\tilde{\boldsymbol{g}}_{mk}^{AL})^T(\hat{\boldsymbol{g}}_{mk}^{AL})^*\big|^2\big\}$, we obtain

$$\begin{aligned}
P_d\mathbb{E}\{|\Omega_k+\mathcal{V}_k|^2\} &= P_d\sum_{m\in\mathcal{M}(k)}\eta_{mk}\Big(tr(\boldsymbol{\Gamma}_{mk}^{AL}\boldsymbol{R}_{mk}^{AL})+(\bar{\boldsymbol{g}}_{mk}^{AL})^H\boldsymbol{R}_{mk}^{AL}\bar{\boldsymbol{g}}_{mk}^{AL}+(\bar{\boldsymbol{g}}_{mk}^{AL})^H\boldsymbol{\Gamma}_{mk}^{AL}\bar{\boldsymbol{g}}_{mk}^{AL}\\
&\qquad+\big(tr(\boldsymbol{\Gamma}_{mk}^{AL})+\big\|\bar{\boldsymbol{g}}_{mk}^{AL}\big\|^2\big)^2\Big)\Big(Q_{m,k}^{\jmath}+\delta(\mathcal{E}_m^{\jmath})^{-2}(\sigma_w^{\jmath})^2\Big),\\
&= P_d\sum_{m\in\mathcal{M}(k)}\Big(A_{m,k,k}+B_{m,k,k}^2\Big)\Big(Q_{m,k}^{\jmath}+\delta(\mathcal{E}_m^{\jmath})^{-2}(\sigma_w^{\jmath})^2\Big).
\end{aligned}\tag{7.44}$$

Finally, the composite interference power due to user k' data symbol including the compression quantization noise and the amplified thermal noise is given by

$$\begin{aligned}
P_d\mathbb{E}\{|a_{kk'}s_{k'}+\Omega_{k'}+\mathcal{V}_{k'}|^2\} &= P_d\mathbb{E}\Big\{\Big|\sum_{m\in\mathcal{M}(k')}\sqrt{\eta_{mk'}}(\boldsymbol{g}_{mk}^{AL})^T(\hat{\boldsymbol{g}}_{mk'}^{AL})^*(s_{k'}+q_{m,k'}^{\jmath}\\
&\qquad+\delta(\mathcal{E}_m^{\jmath})^{-1}w_{m,k'}^{\jmath}\Big)\Big|^2\Big\},\\
&= P_d\mathbb{E}\Big\{\Big|\sum_{m\in\mathcal{M}(k')}\sqrt{\eta_{mk'}}\big((\tilde{\boldsymbol{g}}_{mk}^{AL})^T+(\hat{\boldsymbol{g}}_{mk}^{AL})^T\big)(\hat{\boldsymbol{g}}_{mk'}^{AL})^*(s_{k'}+q_{m,k'}^{\jmath}+\delta(\mathcal{E}_m^{\jmath})^{-1}w_{m,k'}^{\jmath})\Big|^2\Big\},\\
&= P_d\Big(\underbrace{\mathbb{E}\Big\{\Big|\sum_{m\in\mathcal{M}(k')}\sqrt{\eta_{mk'}}(\tilde{\boldsymbol{g}}_{mk}^{AL})^T(\hat{\boldsymbol{g}}_{mk'}^{AL})^*(s_{k'}+q_{m,k'}^{\jmath}+\delta(\mathcal{E}_m^{\jmath})^{-1}w_{m,k'}^{\jmath})\Big|^2\Big\}}_{T_3}\\
&\qquad+\underbrace{\mathbb{E}\Big\{\Big|\sum_{m\in\mathcal{M}(k')}\sqrt{\eta_{mk'}}(\hat{\boldsymbol{g}}_{mk}^{AL})^T(\hat{\boldsymbol{g}}_{mk'}^{AL})^*(s_{k'}+q_{m,k'}^{\jmath}+\delta(\mathcal{E}_m^{\jmath})^{-1}w_{m,k'}^{\jmath})\Big|^2\Big\}}_{T_4}\Big),
\end{aligned}\tag{7.45}$$

where T_3 can be calculated as follows:

$$\begin{aligned}
T_3 &\overset{(a)}{=} \sum_{m\in\mathcal{M}(k')}\eta_{mk'}\mathbb{E}\big\{\big|(\tilde{\boldsymbol{g}}_{mk}^{AL})^T(\hat{\boldsymbol{g}}_{mk'}^{AL})^*\big|^2\big\}\big(\mathbb{E}\{|s_{k'}|^2\}+\mathbb{E}\{|q_{m,k'}^{\jmath}|^2\}+\delta(\mathcal{E}_m^{\jmath})^{-2}\mathbb{E}\{|w_{m,k'}^{\jmath}|^2\}\big),\\
&= \sum_{m\in\mathcal{M}(k')}\eta_{mk'}\Big(tr\big(\boldsymbol{\Gamma}_{mk'}^{AL}(\boldsymbol{R}_{mk}^{AL}-\boldsymbol{\Gamma}_{mk}^{AL})\big)+(\bar{\boldsymbol{g}}_{mk'}^{AL})^H(\boldsymbol{R}_{mk}^{AL}-\boldsymbol{\Gamma}_{mk}^{AL})\bar{\boldsymbol{g}}_{mk'}^{AL}\Big)\\
&\qquad\times\Big((1+Q_{m,k}^{\jmath})+\delta(\mathcal{E}_m^{\jmath})^{-2}(\sigma_w^{\jmath})^2\Big),
\end{aligned}\tag{7.46}$$

with $\overset{(a)}{=}$ stems from the fact that the k'^{th} user signal $s_{k'}$, the quantization noise $q^{\jmath}_{m,k'}$, and the thermal noise $w^{\jmath}_{m,k'}$ are independent and all are independent of users' estimated channels as well as the estimation error. Furthermore, T_4 can be calculated as follows:

$$\begin{aligned}
T_4 = &\sum_{m\in\mathcal{M}(k')} \eta_{mk'}\mathbb{E}\Big\{\Big|(\hat{\boldsymbol{g}}^{AL}_{mk})^T(\hat{\boldsymbol{g}}^{AL}_{mk'})^*(s_{k'}+q^{\jmath}_{m,k'}+\delta(\mathcal{E}^{\jmath}_m)^{-1}w^{\jmath}_{m,k'})\Big|^2\Big\}\\
&+\sum_{m\in\mathcal{M}(k')}\sqrt{\eta_{mk'}}\sum_{t\neq m}\sqrt{\eta_{tk'}}\mathbb{E}\Big\{\Big|(\hat{\boldsymbol{g}}^{AL}_{mk})^T(\hat{\boldsymbol{g}}^{AL}_{mk'})^*(s_{k'}+q^{\jmath}_{m,k'}+\delta(\mathcal{E}^{\jmath}_m)^{-1}w^{\jmath}_{m,k'})\Big|\\
&\qquad\times\Big|(\hat{\boldsymbol{g}}^{AL}_{tk})^T(\hat{\boldsymbol{g}}^{AL}_{tk'})^*(s_{k'}+q^{\jmath}_{t,k'}+\delta(\mathcal{E}^{\jmath}_t)^{-1}w^{\jmath}_{t,k'})\Big|\Big\},\\
=&\sum_{m\mathcal{M}(k')}\eta_{mk'}\mathbb{E}\Big\{\Big|(\hat{\boldsymbol{g}}^{AL}_{mk})^T(\hat{\boldsymbol{g}}^{AL}_{mk'})^*\Big|^2\Big\}\big(\mathbb{E}\{|s_{k'}|^2\}+\mathbb{E}\{|q^{\jmath}_{m,k'}|^2\}+\delta(\mathcal{E}^{\jmath}_m)^{-1}\mathbb{E}\{|w^{\jmath}_{m,k'}|^2\}\big),\\
&+\sum_{m\in\mathcal{M}(k')}\sqrt{\eta_{mk'}}\sum_{t\neq m}\sqrt{\eta_{tk'}}\mathbb{E}\Big\{\Big|(\hat{\boldsymbol{g}}^{AL}_{mk})^T(\hat{\boldsymbol{g}}^{AL}_{mk'})^*\Big|\Big\}\mathbb{E}\Big\{\Big|(\hat{\boldsymbol{g}}^{AL}_{tk})^T(\hat{\boldsymbol{g}}^{AL}_{tk'})^*\Big|\Big\}\mathbb{E}\{|s_{k'}|^2\},\\
=&\sum_{m\in\mathcal{M}(k')}\eta_{mk'}\mathbb{E}\Big\{\Big|(\hat{\boldsymbol{g}}^{AL}_{mk})^T(\hat{\boldsymbol{g}}^{AL}_{mk'})^*\Big|^2\Big\}\big(1+Q^{\jmath}_{m,k}+\delta(\mathcal{E}^{\jmath}_m)^{-2}(\sigma^{\jmath}_w)^2\big),\\
&+\sum_{m\in\mathcal{M}(k')}\sqrt{\eta_{mk'}}\sum_{t\neq m}\sqrt{\eta_{tk'}}\mathbb{E}\Big\{\Big|(\hat{\boldsymbol{g}}^{AL}_{mk})^T(\hat{\boldsymbol{g}}^{AL}_{mk'})^*\Big|\Big\}\mathbb{E}\Big\{\Big|(\hat{\boldsymbol{g}}^{AL}_{tk})^T(\hat{\boldsymbol{g}}^{AL}_{tk'})^*\Big|\Big\},
\end{aligned}\tag{7.47}$$

where

$$\begin{aligned}
\mathbb{E}\Big\{\Big|(\hat{\boldsymbol{g}}^{AL}_{mk})^T(\hat{\boldsymbol{g}}^{AL}_{mk'})^*\Big|^2\Big\} =&tr(\boldsymbol{\Gamma}^{AL}_{mk}\boldsymbol{\Gamma}^{AL}_{mk'})+(\bar{\boldsymbol{g}}^{AL}_{mk'})^H\boldsymbol{R}^{AL}_{mk}\bar{\boldsymbol{g}}^{AL}_{mk'}+(\bar{\boldsymbol{g}}^{AL}_{mk})^H\boldsymbol{\Gamma}^{AL}_{mk'}\bar{\boldsymbol{g}}^{AL}_{mk}\\
&+|(\bar{\boldsymbol{g}}^{AL}_{mk})^H\bar{\boldsymbol{g}}^{AL}_{mk'}|^2+\big|\boldsymbol{\psi}^{\mathsf{H}}_k\boldsymbol{\psi}_{k'}\big|^2\Big(P^2_{p,a}\tau^2_{u,p}\Big|tr(\boldsymbol{R}^{AL}_{mk'}\boldsymbol{\Phi}^{AL}_{mk}\boldsymbol{R}^{AL}_{mk})\Big|^2\\
&+2P_p\tau_{u,p}Re\Big\{tr(\boldsymbol{R}_{mk}\boldsymbol{\Phi}_{mk}\boldsymbol{R}_{mk'})(\bar{\boldsymbol{g}}^{AL}_{mk})^H\bar{\boldsymbol{g}}^{AL}_{mk'}\Big\}\Big)
\end{aligned}\tag{7.48}$$

and

$$\begin{aligned}
\mathbb{E}\Big\{\Big|(\hat{\boldsymbol{g}}^{AL}_{mk})^T(\hat{\boldsymbol{g}}^{AL}_{mk'})^*\Big|\Big\}\mathbb{E}\Big\{\Big|(\hat{\boldsymbol{g}}^{AL}_{tk})^T(\hat{\boldsymbol{g}}^{AL}_{tk'})^*\Big|\Big\} =&\Big|(\bar{\boldsymbol{g}}^{AL}_{mk})^H\bar{\boldsymbol{g}}^{AL}_{mk'}\Big|\Big|(\bar{\boldsymbol{g}}^{AL}_{tk})^H\bar{\boldsymbol{g}}^{AL}_{tk'}\Big|+\big|\boldsymbol{\psi}^{\mathsf{H}}_k\boldsymbol{\psi}_{k'}\big|^2\\
&\times\Big(P_p\tau_{u,p}tr(\boldsymbol{R}^{AL}_{tk}\boldsymbol{\Phi}^{AL}_{tk}\boldsymbol{R}^{AL}_{tk'})\Big|(\bar{\boldsymbol{g}}^{AL}_{mk})^H\bar{\boldsymbol{g}}^{AL}_{mk'}\Big|\\
&+tr(\boldsymbol{R}^{AL}_{mk}\boldsymbol{\Phi}^{AL}_{mk}\boldsymbol{R}^{AL}_{mk'})\Big|(\bar{\boldsymbol{g}}^{AL}_{tk})^H\bar{\boldsymbol{g}}^{AL}_{tk'}\Big|\\
&+P^2_{p,a}\tau^2_{u,p}tr(\boldsymbol{R}^{AL}_{mk}\boldsymbol{\Phi}^{AL}_{mk}\boldsymbol{R}^{AL}_{mk'})tr(\boldsymbol{R}^{AL}_{tk}\boldsymbol{\Phi}^{AL}_{tk}\boldsymbol{R}^{AL}_{tk'})\Big).
\end{aligned}\tag{7.49}$$

Then, substituting (7.48) and (7.49) in (7.4.2.2), the composite interference power due to

user k' can be calculated by applying (7.46) and (7.4.2.2) in (7.45) as follows:

$$P_d\mathbb{E}\{|a_{kk'}s_{k'}+\Omega_{k'}+\mathcal{V}_{k'}|^2\}=\sum_{m\in\mathcal{M}(k')}P_d\Big(1+Q^{\jmath}_{m,k}+\delta(\mathcal{E}^{\jmath}_m)^{-2}(\sigma^{\jmath}_w)^2\Big)\Bigg(A_{m,k,k'}$$
$$+\eta_{mk'}|C_{m,k,k'}|^2+\Big|\boldsymbol{\psi}_k^{\mathsf{H}}\boldsymbol{\psi}_{k'}\Big|^2\eta_{mk'}\Big(P_p^2\tau_p^2D^2_{m,k,k'}+2P_p\tau_{u,p}Re\big\{C_{m,k,k'}D_{m,k,k'}\big\}\Big)$$
$$+P_d\eta_{mk'}\sum_{t\neq m}\sqrt{\frac{\eta_{tk'}}{\eta_{mk'}}}\Bigg(|C_{m,k,k'}||C_{t,k,k'}|+\Big|\boldsymbol{\psi}_k^{\mathsf{H}}\boldsymbol{\psi}_{k'}|^2\Big(|C_{m,k,k'}|D_{j,k,k'}$$
$$+|C_{j,k,k'}|D_{m,k,k'}+P^2_{p,a}\tau^2_{u,p}D_{m,k,k'}D_{j,k,k'}\Big)\Bigg). \tag{7.50}$$

7.5 Centralized System Operation

7.5.1 Fronthaul Communication

In the centralized system operation, both estimation of users' channels and DL precoding of users' data symbols are carried out at ECPs. Particularly, APs forward the received pilot signals from users during the channel estimation phase to their associated ECPs where the channel estimation process is carried out. Based on the estimated users-APs channels, each ECP computes the precoding vectors for served users by its associated APs, precodes the users signals, and sends the precoded signals to its associated APs. Then, APs act as relays to forward the received precoded signals to users. Accordingly, the fronthaul communication in the centralized system operation will be a two way communication, namely fronthaul UL transmission (pilot transmission from APs to ECPs) and fronthaul DL transmission (precoded data transmission from ECPs to APs). Similar to the distributed system operation, each ECP and its associated APs are assigned equal microwave/mmWave bandwidth for the fronthaul communication.

Note that, for the fronthaul UL transmission, the dedicated antenna at the AP for the fronthaul communication needs to transmit different N_{ap} pilot signals (i.e., corresponding to the deployed N_{ap} antennas for access communication) to its serving ECP. In doing so, each AP divides the available bandwidth for fronthaul communication equally among the N_{ap} pilot signals. Also, the corresponding pilot signal for the l^{th} antenna element in all APs $\in \mathcal{M}^{\jmath}_{n_m}$ are transmitted over the same time-frequency resources by means of the ZF detection technique, applied for fronthaul communication. Let $\vartheta^{ul,\jmath}_{m',l}$ denotes the compressed pilot signal to be transmitted from the l^{th} antenna element in AP $m' \in \mathcal{M}^{\jmath}_{n_m}$

to its associated ECP. Thus, the composite received pilot signal at the ECP n_m can be expressed as

$$\boldsymbol{r}_{n_m}^{Cen,ul,\jmath} = \sqrt{P_{u,f}^{\jmath}} \sum_{m' \in \mathcal{M}_{n_m}^{\jmath}} \boldsymbol{g}_{n_m m'}^{FH_\jmath} \vartheta_{m',l}^{ul,\jmath} + \boldsymbol{w}_{n_m}^{\jmath}. \tag{7.51}$$

where $P_{u,f}^{\jmath}$ denotes the UL transmission power of AP antennas in the fronthaul communication. Then, the ECP applies ZF detection to detect the transmitted signal from the l^{th} antenna element at AP $m \in \mathcal{M}_{n_m}^{\jmath}$ as follows:

$$\boldsymbol{z}_{p,m,l}^{Cen,ul,\jmath} = \sqrt{P_{u,f}^{\jmath}} \sum_{m' \in \mathcal{M}_{n_m}^{\jmath}} \mathcal{P}_m^{\jmath} \boldsymbol{g}_{n_m m'}^{FH_\jmath} \vartheta_{m',l}^{ul,\jmath} + \mathcal{P}_m^{\jmath} \boldsymbol{w}_{n_m}^{\jmath}, \tag{7.52}$$

where $\mathcal{P}_m^{\jmath}$ denotes the applied detection vector which can be determined by

$$\mathcal{P}_m^{\jmath} = \left[\left(\left(\boldsymbol{G}_{n_m}^{FH_\jmath} \right)^H \boldsymbol{G}_{n_m}^{FH_\jmath} \right)^{-1} \right]_{(m,:)} \left(\boldsymbol{G}_{n_m}^{FH_\jmath} \right)^H. \tag{7.53}$$

Thus, the received signal at the ECP can be rewritten as follows:

$$\boldsymbol{z}_{p,m,l}^{Cen,ul,\jmath} = \sqrt{P_{u,f}^{\jmath}} \vartheta_{m,l}^{ul,\jmath} + \mathcal{P}_m^{\jmath} \boldsymbol{w}_{n_m}^{\jmath}. \tag{7.54}$$

Accordingly, the UL fronthaul capacity in bps/Hz, according to which the transmitted signals from the m^{th} generic AP are compressed, is given by

$$C_m^{Cen,ul,\jmath} = \frac{\mathcal{B}_F^{\jmath}}{N N_{ap} \mathcal{B}_A} \log_2 \left(1 + \frac{P_{u,f}^{\jmath} \dot{\gamma}_m^{\jmath}}{(\sigma_w^{\jmath})^2} \right), \tag{7.55}$$

with

$$\dot{\gamma}_m^{\jmath} = \frac{1}{\mathbb{E}\left\{ \left[\left(\left(\boldsymbol{G}_{n_m}^{FH_\jmath} \right)^T \left(\boldsymbol{G}_{n_m}^{FH_\jmath} \right)^* \right)^{-1} \right]_{(m,m)} \right\}}. \tag{7.56}$$

Similar to the fronthaul UL transmission, in the fronthaul DL transmission, each ECP divides the available bandwidth to N_{ap} different bands. In the l^{th} band, each ECP sends the intended precoded data signals to the l^{th} antenna elements of its associated APs. let us consider $\vartheta_{m',l}^{dl,\jmath}$ as the DL precoded signal to be transmitted from the ECP n_m for the l^{th} antenna element in AP $m' \in \mathcal{M}_{n_m}^{\jmath}$. Applying ZF precoding, the received signal at AP $m \in \mathcal{M}_{n_m}^{\jmath}$ will be

$$r_{m,l}^{Cen,dl,\jmath} = \sqrt{P_d^{\jmath}} \sum_{m' \in \mathcal{M}_{n_m}^{\jmath}} \sqrt{\gamma_{m'}^{\jmath}} (\boldsymbol{g}_{n_m m}^{FH_\jmath})^T \boldsymbol{\mathcal{Q}}_{m'}^{\jmath} \vartheta_{m',l}^{dl,\jmath} + w_{m,l}^{\jmath} = \mathcal{E}_m^{\jmath} \vartheta_{m,l}^{dl,\jmath} + w_{m,l}^{\jmath}. \tag{7.57}$$

Therefore, the DL fronthaul capacity in bps/Hz according to which the precoded signals for the m^{th} generic AP are compressed is given by

$$C_m^{Cen,dl,\jmath} = \frac{\mathcal{B}_F^{\jmath}}{N N_{ap} \mathcal{B}_A} \log_2 \left(1 + \frac{P_d^{\jmath} \gamma_m^{\jmath}}{(\sigma_w^{\jmath})^2} \right). \tag{7.58}$$

7.5.2 Access Communication

This section analyzes the channel estimation and DL data transmission phases of the centralized system operation while taking into account the proposed fronthaul network.

In that, both channel estimation and DL precoding processes are carried out in the ECPs. Also, ZF precoding is applied for the access link data transmission.

7.5.2.1 Channel Estimation

Different from the distributed system operation, the channel estimation process is performed at ECPs. As such, after APs receive the transmitted pilot sequences from users during the channel estimation phase, they send the received pilot vectors to their serving ECPs. In fact, the received pilot signals at APs consist of fast varying and slow varying components. The fast varying components represent the received pilot signals over the NLoS channels. These components vary from one frame to another. On the other hand, the slow varying components represent the received pilot signals over the LoS channels. Hence, these components can be considered constant over multiple channel frames, hence, assumed available at ECPs. Consequently, APs need only to compress only the fast varying components and send them to their associated ECPs. The fast varying components of the received pilot signal at the l^{th} antenna element of the m^{th} AP are given by

$$\ddot{\boldsymbol{y}}_{p,m,l} = \boldsymbol{y}_{p,m,l} - \sqrt{P_p \tau_{u,p}} \sum_{k'=1}^{K} \bar{\boldsymbol{g}}_{mk'}^{AL} \boldsymbol{\psi}_{k'}^{T}, \tag{7.59}$$

where $\boldsymbol{y}_{p,m,l}$ being the l^{th} row of the matrix $\boldsymbol{Y}_{p,m}$, defined in (7.10) and can be expressed by

$$\boldsymbol{y}_{p,m,l} = \sqrt{P_p \tau_{u,p}} \sum_{k'=1}^{K} g_{mk',l}^{AL} \boldsymbol{\psi}_{k'}^{T} + \boldsymbol{w}_{p,m,l}, \tag{7.60}$$

where $\boldsymbol{w}_{p,m,l}$ denoting the l^{th} row of the matrix $\boldsymbol{W}_{p,m}$. The fast varying component of the pilot signal is then compressed and sent to the serving ECP where the compressed signal is given by

$$\hat{\ddot{\boldsymbol{y}}}_{p,m,l}^{\jmath} = \ddot{\boldsymbol{y}}_{p,m,l} + \boldsymbol{q}_{p,m,l}^{\jmath}, \tag{7.61}$$

with $\boldsymbol{q}_{p,m,l}^{\jmath}$ denotes the quantization noise vector. The entries of $\boldsymbol{q}_{p,m,l}^{\jmath}$ are i.i.d. $\mathcal{CN}(0, Q_{p,m}^{\jmath})$ with $Q_{p,m}^{\jmath}$ being the compression quantization noise power such that:

$$C_m^{Cen,ul,\jmath} = \frac{\tau_{u,p}}{\tau_c} \log_2 \left(1 + \frac{P_p \sum\limits_{k'=1}^{K} \left[R_{mk'}^{AL} \right]_{l,l} + \sigma_w^2}{Q_{p,m}^{\jmath}} \right), \tag{7.62}$$

where $P_p \sum\limits_{k'=1}^{K} \left[R_{mk'}^{AL} \right]_{l,l} + \sigma_w^2$ represents the power of each transmitted pilot symbol from the l^{th} antenna element at the m^{th} AP to its serving ECP. After compressing the received pilot signals, APs forward these signals through the fronthaul network to their associated ECPs. Note that, the detected UL pilot signals for the l^{th} antenna element in AP $m \in \mathcal{M}_{n_m}^{\jmath}$ at

ECP n_m can be expressed using (7.54) through replacing $\vartheta_{m,l}^{ul,\jmath}$ by $\hat{\ddot{\boldsymbol{y}}}_{p,m,l}^{\jmath}$. Consequently, the received signal at the ECP is given by

$$\begin{aligned}\boldsymbol{z}_{p,m,l}^{Cen,ul,\jmath} &= \sqrt{P_{u,f}}\hat{\ddot{\boldsymbol{y}}}_{p,m,l}^{\jmath} + \mathcal{P}_{m,l}^{\jmath}\boldsymbol{w}_{n_m}^{\jmath} \\ &= \sqrt{P_{u,f}}\Big(\sqrt{P_p\tau_{u,p}}\sum_{k'=1}^{K} g_{mk',l}^{AL}\boldsymbol{\psi}_{k'}^{T} + \boldsymbol{q}_{p,m,l}^{\jmath} + \boldsymbol{w}_{p,m,l}\Big) + \mathcal{P}_{m,l}^{\jmath}\boldsymbol{w}_{n_m}^{\jmath}.\end{aligned} \tag{7.63}$$

Since the user's channels at different antenna elements in the same AP are correlated, we jointly estimate these channels at the ECP. To this end, we firstly constitute a matrix of all received pilot sequences as follows:

$$\boldsymbol{Z}_{p,m}^{Cen,ul,\jmath} = \sqrt{P_{u,f}}\Big(\sqrt{P_p\tau_{u,p}}\sum_{k'=1}^{K}\boldsymbol{g}_{mk'}^{AL}\boldsymbol{\psi}_{k'}^{T} + \mathbf{Q}_{p,m}^{\jmath} + \boldsymbol{W}_{p,m}\Big) + \boldsymbol{P}_{m}^{\jmath}\boldsymbol{W}_{n_m}^{\jmath}, \tag{7.64}$$

where $\mathbf{Q}_{p,m}^{\jmath} \in \mathbb{C}^{N_{ap}\times\tau_{u,p}}$ denotes the matrix of quantization noise due to the pilot symbols compression. Also, $\boldsymbol{P}_{m}^{\jmath} \in \mathbb{C}^{N_{ap}\times\mathcal{N}^{\jmath}}$ is a matrix of detection vectors which includes in its l^{th} row the vector $\mathcal{P}_{m,l}^{\jmath}$. Also, $\boldsymbol{W}_{n_m}^{\jmath}$ denotes the noise matrix at the ECP side. As previously mentioned, slow varying LoS components as well as the channel covariance matrices of all users are assumed to be available at APs and ECPs. As such, after each ECP receives the compressed pilot signals from its associated APs, it estimates the small-scale fading channel coefficients using MMSE channel estimation technique. The estimated fast varying channel vector for the k^{th} user with the m^{th} AP is given by

$$\breve{\ddot{\boldsymbol{g}}}_{mk}^{AL} = \sqrt{P_{u,f}P_p\tau_{u,p}}\boldsymbol{R}_{mk}^{AL}\breve{\boldsymbol{\Phi}}_{mk}^{AL}\boldsymbol{Z}_{p,m,l}^{ul,\jmath}\boldsymbol{\psi}_{k}^{*}, \tag{7.65}$$

with

$$\breve{\boldsymbol{\Phi}}_{mk}^{AL} = \Bigg(\sum_{k'=1}^{K} P_{u,f}P_p\tau_{u,p}\boldsymbol{R}_{mk'}^{AL}\boldsymbol{\psi}_{k'}^{T}\boldsymbol{\psi}_{k}^{*} + \big(P_{u,f}(Q_{p,m}^{\jmath}+\sigma_w^2) + (\gamma_m^{\jmath})^{-1}(\sigma_w^{\jmath})^2\big)\boldsymbol{I}_{N_{ap}}\Bigg)^{-1}. \tag{7.66}$$

Thus, the composite estimated channel vector for user k with AP $m \in \mathcal{M}_{n_m}^{\jmath}$ is given by

$$\breve{\boldsymbol{g}}_{mk}^{AL} = \bar{\boldsymbol{g}}_{mk}^{AL} + \breve{\ddot{\boldsymbol{g}}}_{mk}^{AL}. \tag{7.67}$$

Let $\acute{\boldsymbol{g}}_{mk}^{AL} = \boldsymbol{g}_{mk}^{AL} - \breve{\boldsymbol{g}}_{mk}^{AL}$, be the channel estimation error. The MMSE estimate $\breve{\boldsymbol{g}}_{mk}^{AL}$ and the estimation error $\acute{\boldsymbol{g}}_{mk}^{AL}$ are independent random variables that can be modeled as follows:

$$\breve{\boldsymbol{g}}_{mk}^{AL} \sim \mathcal{CN}(\bar{\boldsymbol{g}}_{mk}^{AL}, \breve{\boldsymbol{\Gamma}}_{mk}^{AL}), \qquad \acute{\boldsymbol{g}}_{mk}^{AL} \sim \mathcal{CN}(\mathbf{0}, \boldsymbol{R}_{mk}^{AL} - \breve{\boldsymbol{\Gamma}}_{mk}^{AL}), \tag{7.68}$$

and $\breve{\boldsymbol{\Gamma}}_{mk}^{AL} = P_{u,f}P_p\tau_{u,p}\boldsymbol{R}_{mk}^{AL}\breve{\boldsymbol{\Phi}}_{mk}^{AL}\boldsymbol{R}_{mk}^{AL}$ is the estimation covariance matrix.

7.5.2.2 Downlink Transmission

For the DL data transmission, we consider that each ECP independently determines the precoded data symbols for the served users by its associated APs. A prerequisite for any ECP n to determine the precoding vector for user k is to know the set of served users by its associated APs $\big(\dot{\mathcal{K}}(n)\big)$ as well as the set of APs belonging to this ECP and serving

user k $\big(\dot{\mathcal{M}}_n(k)\big)$. Let $\boldsymbol{\mathcal{G}}_{k,n}^{AL}$ represents the channel matrix between the set of APs $\in \dot{\mathcal{M}}_n(k)$ and the set of users $\in \dot{\mathcal{K}}(n)$. Each ECP applies ZF precoding to generate the precoded symbols for the served users by its associated APs. The ZF precoding vector for user $k \in \dot{\mathcal{K}}(n)$ at the set of APs $\in \dot{\mathcal{M}}_n(k)$ is given by

$$\boldsymbol{\varpi}_{k,n} = \big(\hat{\boldsymbol{\mathcal{G}}}_{k,n}^{AL}\big)^* \Big(\big(\hat{\boldsymbol{\mathcal{G}}}_{k,n}^{AL}\big)^T \big(\hat{\boldsymbol{\mathcal{G}}}_{k,n}^{AL}\big)^* \Big)^{-1} \boldsymbol{e}_k, \tag{7.69}$$

where $\hat{\boldsymbol{\mathcal{G}}}_{k,n}^{AL}$ represents the estimated channel matrix of $\boldsymbol{\mathcal{G}}_{k,n}^{AL}$. Also, $\boldsymbol{e}_k$ is the k^{th} column in the identity matrix $\boldsymbol{I}_{K_n}$. It is important to note that the corresponding entries of the precoding vectors for user k at APs $\in \mathcal{M}_n$ and $\notin \dot{\mathcal{M}}_n(k)$ are set to zero. Thus, the precoded data vector will be

$$\boldsymbol{x}_n = \sqrt{\varsigma_n} \sum_{k \in \dot{\mathcal{K}}(n)} \boldsymbol{\varpi}_{k,n} s_k, \tag{7.70}$$

where ς_n denotes the power normalization factor at the n^{th} ECP that can be calculated by

$$\varsigma_n = \frac{1}{\mathbb{E}\Big\{ tr\Big(\Big(\big(\hat{\boldsymbol{\mathcal{G}}}_{k,n}^{AL}\big)^T \big(\hat{\boldsymbol{\mathcal{G}}}_{k,n}^{AL}\big)^* \Big)^{-1} \Big) \Big\}}. \tag{7.71}$$

After obtaining the precoded data vector, each ECP compresses the precoded data as $\hat{\boldsymbol{x}}_n^{\jmath} = \boldsymbol{x}_n + \boldsymbol{q}_n^{\jmath}$, where $\boldsymbol{q}_n^{\jmath}$ denotes the vector of compression quantization noise at the n^{th} ECP. In that, the precoded data symbol $x_{n,m,l}$ for the l^{th} antenna element in AP $m \in \mathcal{M}_n$ will be accompanied with a compression quantization noise $q_{n,m,l}^{\jmath} \sim \mathcal{CN}(0, Q_{n,m,l}^{\jmath})$ with $Q_{n,m,l}^{\jmath}$ being the compression quantization noise that can be determined according to

$$C_{n,m}^{Cen,dl,\jmath} = \frac{\tau_c - \tau_{u,p}}{\tau_c} \log_2 \Big(1 + \frac{\mathbb{E}\big\{ |x_{n,m,l}|^2 \big\}}{Q_{n,m,l}^{\jmath}} \Big). \tag{7.72}$$

Each ECP then sends the compressed signals to its associated APs which relay these signals to users. Similar to the distributed system operation, we consider two approaches for relaying the signal to users. The first one with $\delta = 1$ corresponds to the case of amplifying the received signal including the noise and sending it to users, whereas in the second approach with $\delta = 0$, APs decode the received signal before conveying the signals to users. In the centralized operation, the first and second approaches reflect the amplify-and-forward (AF) and decode-and-forward (DF) transmissions in relaying systems, respectively. The received precoded signal vector at the m^{th} generic AP from its serving ECP n_m can be expressed by

$$\boldsymbol{r}_m^{Cen,dl,\jmath} = \mathcal{E}_m^{\jmath} \big(\boldsymbol{x}_{n_m,m} + \boldsymbol{q}_{n_m,m}^{\jmath} \big) + \delta \boldsymbol{w}_m^{\jmath}, \tag{7.73}$$

where $\boldsymbol{x}_{n_m,m}$ and $\boldsymbol{q}_{n_m,m}^{\jmath}$ represent the elements of the m^{th} AP in $\boldsymbol{x}_{n_m,m}$ and $\boldsymbol{q}_{n_m,m}^{\jmath}$, respectively. Then, similar to the distributed system operation, the AP m cancels out the

fronthaul effect on the received precoded data signal as follows:

$$\dot{\boldsymbol{r}}_m^{Cen,dl,\jmath} = \boldsymbol{x}_{n_m,m} + \boldsymbol{q}_{n_m,m}^{\jmath} + \delta\big(\mathcal{E}_m^{\jmath}\big)^{-1}\boldsymbol{w}_m^{\jmath}. \tag{7.74}$$

Consequently, the received signal at the k^{th} user is given by

$$\begin{aligned} r_k^{Cen} = \sqrt{P_d}\sum_{m\in\mathcal{M}(k)}\sqrt{\varsigma_{n_m}}\big(\boldsymbol{g}_{mk}^{AL}\big)^T\boldsymbol{\varpi}_{k,n_m,m}s_k + \sqrt{P_d}\sum_{k'\neq k}\sum_{m\in\mathcal{M}(k')}\sqrt{\varsigma_{n_m}}\big(\boldsymbol{g}_{mk}^{AL}\big)^T\check{\boldsymbol{\varpi}}_{k',n_m,m}s_{k'} \\ + \sqrt{P_d}\sum_{m=1}^{M}\big(\boldsymbol{g}_{mk}^{AL}\big)^T\boldsymbol{q}_{n_m,m}^{\jmath} + \sqrt{P_d}\delta\sum_{m=1}^{M}\big(\mathcal{E}_m^{\jmath}\big)^{-1}\big(\boldsymbol{g}_{mk}^{AL}\big)^T\boldsymbol{w}_m^{\jmath} + w_k. \end{aligned} \tag{7.75}$$

Let us define

$$\check{\boldsymbol{\varpi}}_{k',n_m,m} \triangleq \sqrt{\varsigma_{n_m}}\boldsymbol{\varpi}_{k',n_m,m}, \qquad \check{\boldsymbol{w}}_m^{\jmath} \triangleq \big(\mathcal{E}_m^{\jmath}\big)^{-1}\boldsymbol{w}_m^{\jmath}. \tag{7.76}$$

Also,

$$\check{\boldsymbol{\varpi}}_{k'} \triangleq \begin{bmatrix} \check{\boldsymbol{\varpi}}_{k',n_1,1} \\ \cdots \\ \check{\boldsymbol{\varpi}}_{k',n_m,m} \\ \cdots \\ \check{\boldsymbol{\varpi}}_{k',n_M,M} \end{bmatrix}, \quad \check{\boldsymbol{q}}^{\jmath} \triangleq \begin{bmatrix} \boldsymbol{q}_{n_1,1}^{\jmath} \\ \cdots \\ \boldsymbol{q}_{n_m,m}^{\jmath} \\ \cdots \\ \boldsymbol{q}_{n_M,M}^{\jmath} \end{bmatrix}, \quad \check{\boldsymbol{w}}^{\jmath} \triangleq \begin{bmatrix} \check{\boldsymbol{w}}_1^{\jmath} \\ \cdots \\ \check{\boldsymbol{w}}_m^{\jmath} \\ \cdots \\ \check{\boldsymbol{w}}_M^{\jmath} \end{bmatrix}, \quad \check{\boldsymbol{g}}_k \triangleq \begin{bmatrix} \boldsymbol{g}_{1k}^{AL} \\ \cdots \\ \boldsymbol{g}_{mk}^{AL} \\ \cdots \\ \boldsymbol{g}_{Mk}^{AL} \end{bmatrix}. \tag{7.77}$$

Note that, if $m \notin \mathcal{M}(k')$, $\check{\boldsymbol{\varpi}}_{k',n_m,m} = \mathbf{0}^{N_{ap},1}$. Thus, (7.75) can be rewritten as follows:

$$r_k = \sqrt{P_d}\check{\boldsymbol{g}}_k^T\check{\boldsymbol{\varpi}}_k s_k + \sqrt{P_d}\sum_{k'\neq k}\check{\boldsymbol{g}}_k^T\check{\boldsymbol{\varpi}}_{k'}s_{k'} + \sqrt{P_d}\check{\boldsymbol{g}}_k^T\check{\boldsymbol{q}}^{\jmath} + \sqrt{P_d}\delta\check{\boldsymbol{g}}_k^T\check{\boldsymbol{w}}^{\jmath} + w_k, \tag{7.78}$$

where the first term includes the desired signal while the second term represents the interference signals due to transmitted data to other users. The third term denotes the quantization noise effect. Also, the fourth term represents the impact of amplified thermal noise at APs while the fifth term reflects the thermal noise effect at the user side. Consequently, the achievable DL data rate of user k can be determined by

$$\begin{aligned} R_k^{Cen} = \frac{\tau_c - \tau_{u,p}}{\tau_c}\times \\ \log_2\left(1 + \frac{P_d\big|\mathbb{E}\big\{\check{\boldsymbol{g}}_k^T\check{\boldsymbol{\varpi}}_k\big\}\big|^2}{P_d\Big(\sum\limits_{k'=1}^{K}\mathbb{E}\big\{\big|\check{\boldsymbol{g}}_k^T\check{\boldsymbol{\varpi}}_{k'}\big|^2\big\} - \big|\mathbb{E}\big\{\check{\boldsymbol{g}}_k^T\check{\boldsymbol{\varpi}}_k\big\}\big|^2 + \mathbb{E}\big\{\big|\check{\boldsymbol{g}}_k^T\check{\boldsymbol{q}}^{\jmath}\big|^2\big\} + \mathbb{E}\big\{\big|\check{\boldsymbol{g}}_k^T\check{\boldsymbol{w}}^{\jmath}\big|^2\big\}\Big) + \sigma_w^2}\right). \end{aligned} \tag{7.79}$$

7.6 Simulation Results

7.6.1 Simulation Setup

We consider a CF mMIMO system that includes uniformly distributed multi-antenna APs, users, and ECPs in a square area of size 0.5×0.5 km^2 with densities of λ_A, λ_U, and λ_C, respectively. The heights of deployed antennas at APs, UEs, and ECPs are $h_{ap} = 12.5$, $h_{ue} = 1.5$, and $h_{ecp} = 25$ m, respectively. We consider fronthaul blockages that are uniformly distributed within the coverage area with density λ_B. The length and width parameters of blockages have a uniform distribution with $[10, 20]$ and $[5, 15]$, respectively. The APs, users, ECPs, and blockage densities are set to $\lambda_a = 200/km^2$, $\lambda_u = 40/km^2$, $\lambda_c = 8/km^2$, and $\lambda_B = 50/km^2$, respectively. Also, each AP is equipped with $N_{ap} = 10$ antenna elements and each user is served by its five nearest APs. The aforementioned simulation parameters hold for all reported results, unless otherwise specified.

- Access Link (AP-User): We consider the communication between users and APs is carried out on the microwave band over a carrier frequency $f_{c,a} = 1.9$ GHz. The UL pilot transmission power $P_p = 0.1$ Watt while the DL data and pilot transmission power $P_d = 0.2$ Watt. The thermal noise variance at the user side $\sigma_w^2 = 290 \times \kappa \times \mathcal{B}_A \times NF$ where κ is the Boltzman constant, access link bandwidth $\mathcal{B}_A =$ 20 MHz, and $NF =$ 9 dB is the noise figure. We consider a coherence time interval of $\tau_c = 200$ samples. Besides, non-orthogonal pilot sequences are assigned to users for the sake of channel estimation with $\tau_{u,p} = 5$ symbols. The possibility of having a LoS access link is defined as follows [113]:

$$\mathbb{P}(LoS) = \begin{cases} 1 - \frac{d_{mk}^{AL}}{300} & \text{if} \quad 0 < d_{mk}^{AL} < 300 \\ 0 & \text{if} \quad d_{mk}^{AL} \geq 300, \end{cases} \tag{7.80}$$

where d_{mk}^{AL} denotes the distance between AP m and user k in meters. The Rician K-factor is calculated by [113]

$$\mathcal{K}_{mk}^{AL} = \begin{cases} 10^{1.3-0.003 d_{mk}^{AL}} & \text{if} \quad LoS \\ 0 & \text{if} \quad NLoS, \end{cases} \tag{7.81}$$

Also, the large-scale fading coefficient between the m^{th} AP and the k^{th} user is given by [113]

$$\beta_{mk}^{AL} = \begin{cases} -30.18 - 26 \log_{10}(d_{mk}^{AL}) + \mathcal{F}_{mk}^{AL} & \text{if} \quad LoS \\ -34.53 - 38 \log_{10}(d_{mk}^{AL}) + \mathcal{F}_{mk}^{AL} & \text{if} \quad NLoS, \end{cases} \tag{7.82}$$

where $\mathcal{F}_{mk}^{AL} = \sqrt{\epsilon} a_m + \sqrt{1-\epsilon} b_k$, with $\epsilon = 0.5$ represents the correlated shadow fading

coefficient with $a_m \sim \mathcal{N}(0, \sigma_{sh})$ and $b_k \sim \mathcal{N}(0, \sigma_{sh})$. The shadowing standard deviation is set to $\sigma_{sh} = 4\ dB$ and $8\ dB$ in case of LoS and NLoS, respectively.

- Microwave-Based Fronthaul Communication: For the microwave fronthaul communication, the fronthaul links are carried over a center frequency $f_{c,f}^{\mu} = 6.5\ GHz$ with a bandwidth $\mathcal{B}_f^{\mu} =$ 200 MHz. This band has been proposed in [125] for the backhaul/fronthaul communication due to the high available bandwidth that can handle the immense amount of data transfer in the fronthaul network. Also, operating the microwave fronthaul links on such band avoids the interference between these links and access links since they operate in different microwave bands. Also, each ECP is equipped with $\mathcal{M}^{\mu} = 50$ antennas. The DL and UL transmission powers for the fronthaul communication are set to $P_{d,f}^{\mu} = 0.2$ Watt and $P_{u,f} = 0.2$ Watt. The large-scale fading coefficient between the n^{th} ECP and the m^{th} AP over the adopted microwave fronthaul band is given by [126]

$$\beta_{nm}^{FH_{\mu}} = \begin{cases} -32.4 - 20\log_{10}(f_{c,f}^{\mu}(GHz)) - 20\log_{10}(d_{nm}^{FH}) + \xi_{nm}^{\mu} & \text{if} \quad LoS \\ -32.4 - 20\log_{10}(f_{c,f}^{\mu}(GHz)) - 30\log_{10}(d_{nm}^{FH}) + \xi_{nm}^{\mu} & \text{if} \quad NLoS, \end{cases} \tag{7.83}$$

with $\xi_{nm}^{\mu} \sim \mathcal{N}(0, \sigma_{sh}^{\mu})$ denoting the shadowing coefficient where the shadowing standard deviation is set to $\sigma_{sh}^{\mu} = 4\ dB$ and $7.8\ dB$ in case of LoS and NLoS, respectively.

- MmWave-Based Fronthaul Communication: The mmWave band with a center frequency $f_{c,f}^{mm} = 28\ GHz$ is adopted for the fronthaul communication. This is thanks to the low rain attenuation, atmospheric absorption, and path loss in this band compared to other mmWave bands as well as the immense amount of available bandwidth. The mmWave bandwidth is considered as a multiple of the microwave counterpart as $\mathcal{B}_f^{mm} = \alpha_f \mathcal{B}_f^{\mu}$. Also, the number of deployed mmWave antennas at the ECPs for the fronthaul communication is considered as multiple of the microwave counterpart as $\mathcal{N}^{mm} = \rho_f \mathcal{N}^{\mu}$. For a fair comparison between the microwave and mmWave fronthaul operations, the DL transmit power in the mmWave-based operation is set to $P_{d,f}^{mm} = \rho_f^{-1} P_{d,f}^{\mu}$. The values of α_f and ρ_f are set to 5 and 10, respectively, unless otherwise specified. The large-scale fading coefficient between the n^{th} ECP and the m^{th} AP over the adopted mmWave fronthaul band is given by [123]

$$\beta_{nm}^{FH_{mm}} = \begin{cases} -61.4 - 20\log_{10}(d_{nm}^{FH}) + \xi_{nm}^{mm} & \text{if} \quad LoS \\ -72 - 29.2\log_{10}(d_{nm}^{FH}) + \xi_{nm}^{mm} & \text{if} \quad NLoS, \end{cases} \tag{7.84}$$

with $\xi_{nm}^{mm} \sim \mathcal{N}(0, \sigma_{sh}^{mm})$ denoting the shadowing coefficient where the shadowing standard

deviation is set to $\sigma_{sh}^{mm} = 5.8\ dB$ and $8.7\ dB$ in case of LoS and NLoS, respectively.

- Hybrid-Based Fronthaul Communication: For the hybrid-based fronthaul operation, since each ECP is equipped with microwave and mmWave antennas, the DL transmission powers of microwave and mmWave antennas at the n^{th} ECP are set to $P_{d,f,hy}^{\mu} = \frac{M_n^{\mu}}{M_n^{\mu}+M_n^{mm}} P_{d,f}^{\mu}$ and $P_{d,f,hy}^{mm} = \frac{M_n^{mm}}{M_n^{\mu}+M_n^{mm}} P_{d,f}^{mm}$, respectively, to keep the total power budget at ECPs constant under the different applied wireless fronthaul operations.

7.6.2 Performance of Fronthaul Network

This section discusses the provided DL fronthaul capacities by the aforementioned wireless-based fronthaul operations, namely, microwave, mmWave, and hybrid microwave/mmWave fronthaul operations under different fronthaul network configurations. In this section, we focus on the DL fronthaul capacities since we noted that their impact is more prominent than the UL fronthaul capacities on the achievable users' rates. Also, one can note from (7.55) and (7.58) that the UL fronthaul capacity will follow a similar behavior to that of the DL fronthaul capacity under different network configurations. More specifically, we discuss the impacts of blockage densities, ECP configurations, and APs configurations on the provided fronthaul capacities to deployed APs. In this regard, according to (7.9) and (7.58), one can note that under different density of blockages λ_B, density of ECPs λ_C, and number of antennas at ECPs $\mathcal{N}^j$, the achievable DL fronthaul capacities of the centralized system operation follows the same behavior as the distributed counterpart. Consequently, for the impact of blockages and ECP configurations, we only consider the achievable fronthaul capacities under the distributed system operation. On the other hand, the achievable fronthaul capacities under the distributed and centralized system operations are affected differently by the APs density λ_A and the number of deployed antennas per AP N_{ap}. Thus, we investigate the impact of different APs configurations on the achievable fronthaul capacities for both system operations.

- Blockage Effect: Fig. 7.2 depicts the CDF of the achievable DL fronthaul capacities for the distributed system operation under different density of blockages. One can note that the mmWave-based fronthaul operation significantly outperforms the microwave counterpart for the vast majority of the deployed APs. However, the microwave-based fronthaul operation provides higher capacities than the mmWave counterpart for APs with poor channel conditions, i.e., APs with low fronthaul capacities. Besides, as the blockage

density increases, the achievable fronthaul capacities decrease, and the microwave-based operation becomes more preferable than the mmWave one for a larger portion of APs. This is a consequence of the more harsh impact of blockages on mmWave channels. Aside from that, the hybrid microwave/mmWave fronthaul operation outperforms both the microwave and mmWave counterparts by providing APs with different channel conditions with higher fronthaul capacities.

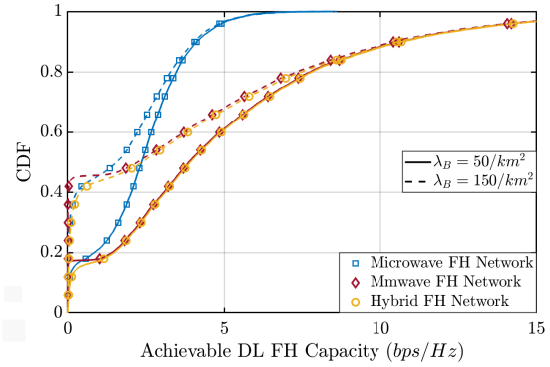

Figure 7.2: CDF of the achievable DL fronthaul capacities under different blockage density

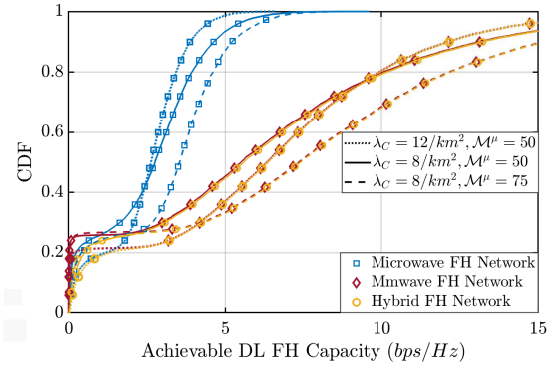

Figure 7.3: CDF of the achievable DL fronthaul capacities under different ECPs configurations

- Different ECPs Configurations: Fig. 7.3 depicts the CDF of the achievable DL fronthaul capacities for the distributed system operation under different ECP configurations. Particularly, we show the impact of increasing the density of deployed ECPs or the number of deployed antennas per ECP on the achievable DL fronthaul capacity. Let us consider the performance of the ECP configuration with $\lambda_C = 8/km^2$, $\mathcal{M}^\mu = 50$ as a reference for the other considered ECP configurations. Firstly, one can note that increasing the number of deployed antennas per ECP ($\lambda_C = 8/km^2$, $\mathcal{M}^\mu = 75$) significantly improves the achievable fronthaul capacities thanks to the higher beamforming gain accompanying such increase in number of antennas. On the other hand, despite increasing the density of ECPs ($\lambda_C = 12/km^2$, $\mathcal{M}^\mu = 50$) is advantageous for some APs, it may affect the achievable fronthaul capacity of other APs badly. This can be interpreted as follows. On one hand, increasing the density of deployed ECPs improves the provided beamforming gain to APs due to the reduced number of connected APs to each ECP and the reduced path-loss of APs with their serving ECPs. On the other hand, increasing the density of deployed ECPs reduces the assigned fronthaul bandwidth to each ECP and its associated APs accordingly. Thus, increasing the ECPs density degrades the delivered fronthaul capacities to APs under favorable channel conditions, i.e., APs with high fron-

thaul capacities, since improving the beamforming gain for such APs cannot compensate for the bandwidth reduction at higher density of ECPs. In contrary, increasing the ECPs density enhances the provided fronthaul capacities to APs under poor channel conditions since improving the beamforming gain to such APs overcomes the capacity loss due to bandwidth reduction. The latter discussion also illustrates the cross-over between the achievable capacities for the two considered configurations with $\lambda_C = 12/km^2,\ \mathcal{M}^{\mu} = 50$ and $\lambda_C = 8/km^2,\ \mathcal{M}^{\mu} = 75$.

- Different APs Configurations: Fig. 7.4a and 7.4b depict the CDF of the achievable DL fronthaul capacities under different APs configurations for distributed and centralized system operations, respectively. In that, the average number of deployed antennas in all configurations is equal. According to the achievable DL fronthaul capacities under the distributed system operation in (7.9), the achievable DL fronthaul capacity is not affected by the number of antennas per APs (N_{ap}). Nevertheless, it is affected by the density of APs (λ_A). The reason is that increasing λ_A increases the number of associated APs to each ECP which in turn reduces the provided beamforming gains in the fronthaul network. Consequently, increasing λ_A degrades the achievable DL fronthaul capacities. In contrary to the distributed operation, the achievable DL fronthaul capacities under the centralized counterpart decrease with increasing N_{ap} as illustrated in (7.58). However, decreasing λ_A improves the provided beamforming gains to deployed APs. Accordingly, for the centralized system operation, deploying a small number of APs with large number of antennas ($\lambda_A = 100/km^2,\ N_{ap} = 20$) provides higher fronthaul capacities to APs under poor channel conditions. On the other hand, deploying a large number of APs with small number of antennas ($\lambda_A = 400/km^2,\ N_{ap} = 5$) provides higher fronthaul capacities to APs under favorable channel conditions.

7.6.3 End-User DL Data Rates

Fig. 7.5 depicts the achievable users' DL data rates of the two considered approaches of APs operation ($\delta = 0$ and $\delta = 1$ which mimicking APs with and without decoding capabilities, respectively) for the distributed and centralized system operations under different density of blockages. It is clear that empowering APs with decoding capabilities ($\delta = 0$) remarkably improves the achievable users' data rates under all considered fronthaul network operations. Let us consider firstly the system performance under $\delta = 0$ for both

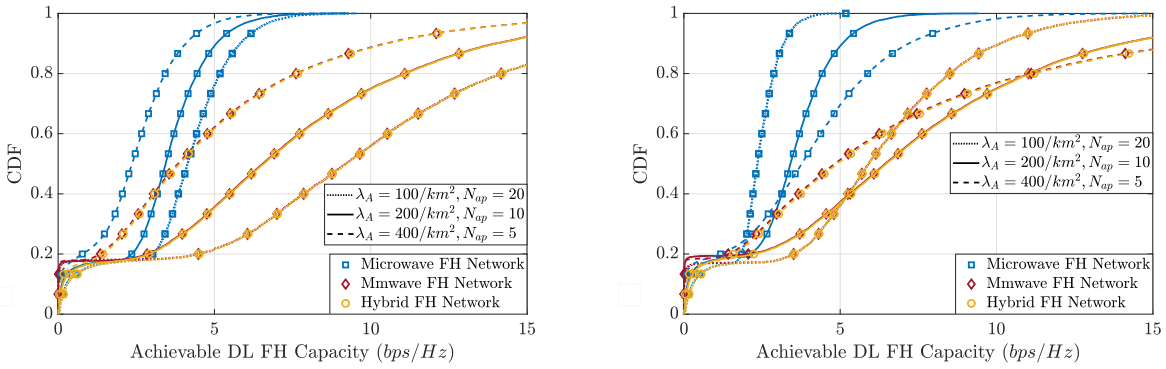

(a) Distributed Operation

(b) Centralized Operation

Figure 7.4: CDF of the achievable DL fronthaul capacities under different APs configurations.

distributed and centralized system operations. In such case, the main controlling factor of both system performances will be the compression quantization noise accompanying the data transmission over the limited-capacity wireless fronthaul links. For low blockage scenarios with $\lambda_B = 25/km^2$, operating the fronthaul network on the mmWave band provides higher DL data rates to a larger portion of users than operating the fronthaul network on the microwave counterpart as shown in Fig. 7.5a and 7.5c. On the other hand, as depicted in Fig. 7.2, at high blockage density with $\lambda_B = 150/km^2$, the mmWave band provides higher fronthaul capacities for $\sim 55\%$ of the deployed APs than the microwave counterpart. Nevertheless, operating the fronthaul network on the mmWave band significantly worsen the achievable DL data rates. This reflects that the APs with low fronthaul capacities have the dominant effect on the achievable DL data rates. Interestingly, the hybrid-based fronthaul operation leads to higher DL data rates under low and high density of blockages.

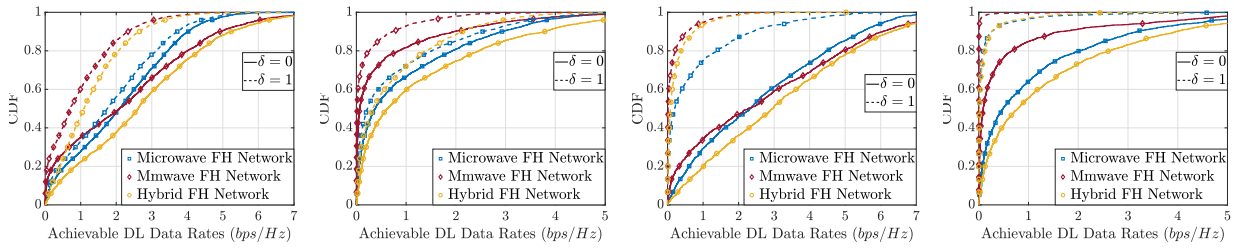

(a) Distributed Operation ($\lambda_B = 25/km^2$)

(b) Distributed Operation ($\lambda_B = 150/km^2$)

(c) Centralized Operation ($\lambda_B = 25/km^2$)

(d) Centralized Operation ($\lambda_B = 150/km^2$)

Figure 7.5: CDF of the achievable DL rates for distributed and centralized operations under different blockage densities and fronthaul operations.

Let us focus now on the second approach of APs operation with $\delta = 1$. Different from

the first approach with $\delta = 0$, one can note that the microwave-based fronthaul operation provides superior DL data rates to the other fronthaul operations. This is a consequence of the smaller path-loss of the microwave bands that leads to higher values of the fronthaul channel gain $\mathcal{E}_m^{\jmath}$ defined in (7.17) such that $\mathcal{E}_m^{\mu} > \mathcal{E}_m^{mm}$. This in turn reduces the power of the term representing the amplified thermal noise effect and improves the achievable DL data rates. The performance of the hybrid-based fronthaul operation approaches that of the microwave counterpart at high density of blockages ($\lambda_B = 150/km^2$). This is due to the higher percentage of APs that will have NLoS links with their serving ECPs under $\lambda_B = 150/km^2$, and thus, will be served by microwave fronthaul links. An interesting remark on the system performance under the second APs operation approach with $\delta = 1$ is that the channel gains of the fronthaul links have higher impact on the achievable DL data rates than the available bandwidth for the fronthaul communication.

Fig. 7.6 depicts the average DL data rates of the centralized and distributed system operations under different values of fronthaul bandwidth ratio α_f, i.e., bandwidth of the mmWave fronthaul band. Similar to the reported findings in Fig. 7.5, Fig. 7.6 reveals that the hybrid-based and microwave-based fronthaul operations attains higher average DL rates for the first approach ($\delta = 0$) and second approach ($\delta = 1$) of APs operation, respectively. In addition, increasing the bandwidth of the mmWave fronthaul band remarkably improves the performance of both hybrid-based and mmWave-based fronthaul operations when $\delta = 0$. This is due to the improved fronthaul capacities which in turn reduces the compression quantization noise power. However, such increase in the mmWave fronthaul bandwidth is not beneficial for the hybrid-based and mmWave-based fronthaul operations when $\delta = 1$. This is a consequence of the dominated impact of the fronthaul channel gains over the fronthaul bandwidth under such mode of APs operation.

Fig. 7.7 compares the average achievable DL data rates of the centralized and distributed system operations at different densities of blockages under the two considered approaches for APs operation ($\delta = 0$ and $\delta = 1$). As one can note, increasing the blockage density remarkably degrades the average achievable DL data rates under both approaches of APs operation. Besides, as depicted in Fig. 7.7a, the centralized system operation provides higher average DL data rates than the distributed counterpart when $\delta = 0$, thanks to the higher capabilities of ZF in mitigating the inter-user interference. On the other hand, the amplified thermal noise impact is more prominent on the centralized sys-

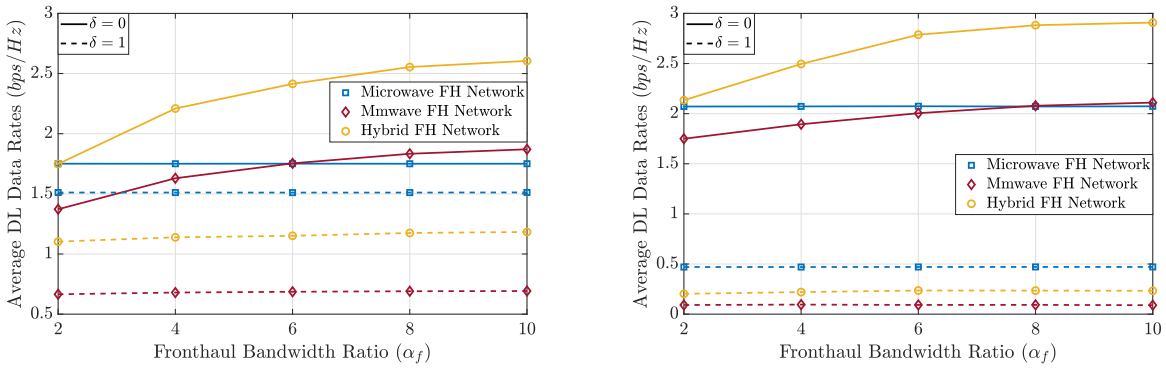

(a) Distributed Operation

(b) Centralized Operation

Figure 7.6: Average achievable DL data rates under different fronthaul bandwidth ratios.

tem operation which in turn renders the distributed system performance superior to the centralized counterpart when $\delta = 1$. This is due to the generated thermal noise at APs being directly amplified and transmitted to users in the centralized operation. However, in the distributed counterpart, the generated thermal noise vectors at a certain AP are firstly multiplied by the precoding vectors for users before being amplified which in turn decreases the power of such amplified noise terms.

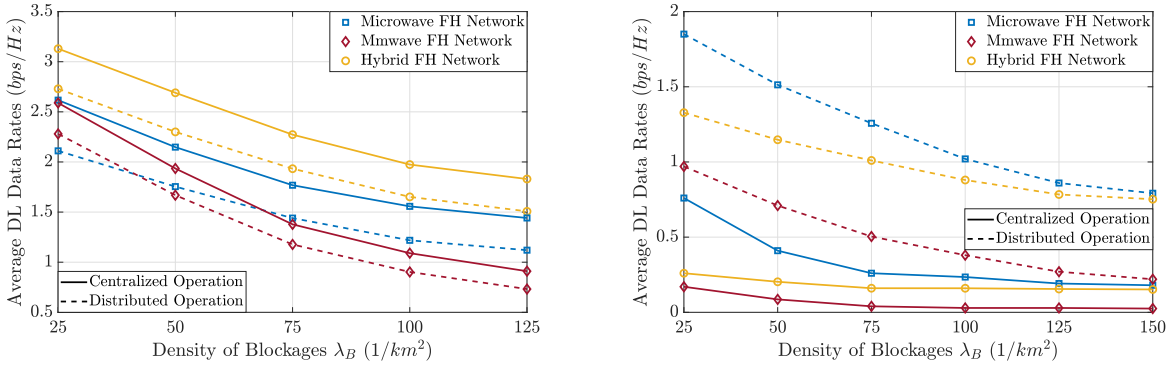

(a) $\delta = 0$

(b) $\delta = 1$

Figure 7.7: Average achievable DL data rates under different blockage densities.

7.6.4 Comparison Between Different Deployment Approaches

This section analyzes the access link performance under different network deployment approaches for APs and ECPs. This has been conducted while considering APs with/without decoding capabilities. In this regard, we consider the hybrid-based and microwave-based fronthaul operations for the first approach ($\delta = 0$) and the second approach ($\delta = 1$) of APs operation since they offer maximum performance for both approaches, respectively.

- Different ECPs Configurations: Fig. 7.8 investigates the preferred ECPs deployment criterion for the distributed and centralized system operations under both APs operation with $\delta = 0$ and $\delta = 1$. More specifically, the reported results reveal whether is more advantageous, deploying more microwave/mmWave antennas per ECP or deploying more ECPs within the coverage area. For fair comparison, we consider two different configurations that have the same average number of microwave/mmWave antennas for the fronthaul communication. As one can note, the obtained results show a similar behavior to the one reported in Fig. 7.7 where the centralized and distributed operations attain higher data rates under $\delta = 0$ and $\delta = 1$, respectively. Besides, deploying more ECPs with small number of antennas ($\lambda_C = 12/km^2,\ \mathcal{M}^{\mu} = 50$) is more beneficial than increasing the number of deployed antennas per ECP ($\lambda_C = 8/km^2,\ \mathcal{M}^{\mu} = 75$) under $\delta = 0$ and $\delta = 1$. This is due to the provided improvement by $\lambda_C = 12/km^2,\ \mathcal{M}^{\mu} = 50$ to the fronthaul capacity of APs with low-fronthaul capacities as depicted in Fig. 7.3 which in turn leads to higher DL data rates. Also, deploying more ECPs improves the channel gains of fronthaul links, and hence, increases the value of $\mathcal{E}_m^j$ which in turn decreases the power of the term representing the amplified thermal noise effect and introduces further improvement to the achievable DL data rates under $\delta = 1$.

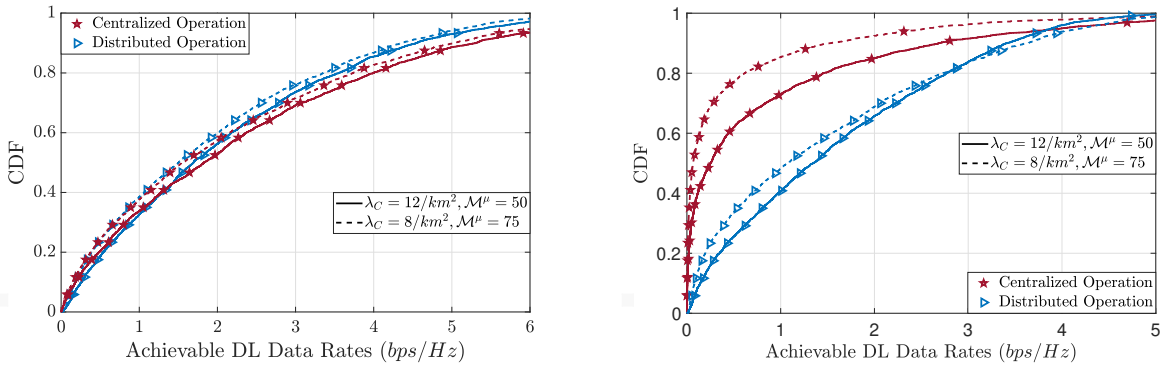

(a) $\delta = 0$ (b) $\delta = 1$

Figure 7.8: CDF of the achievable DL data rates under different ECPs configurations.

- Different APs Configurations: Fig. 7.9 depicts the preferred APs deployment criterion for the distributed and centralized system operations under both APs operations with $\delta = 0$ and $\delta = 1$. As noted, deploying small number of APs with large number of antennas ($\lambda_A = 100/km^2,\ N_{ap} = 20$) attains higher DL data rates than other deployment criteria for both distributed and centralized system operations and under both approaches of APs operation. The better performance under $\delta = 0$ is due to the higher achievable

fronthaul capacities, provided by such APs configuration for all APs in the distributed system operation and for APs with low fronthaul capacities in the centralized system operations as shown in Fig. 7.4. In addition, decreasing the number of deployed APs increases the provided fronthaul beamforming gains to deployed APs as a consequence of reducing the number of associated APs to each ECP. This in turn increases the fronthaul channel gain $\mathcal{E}_m^j$, and hence boosts the achievable DL data rates under $\delta = 1$.

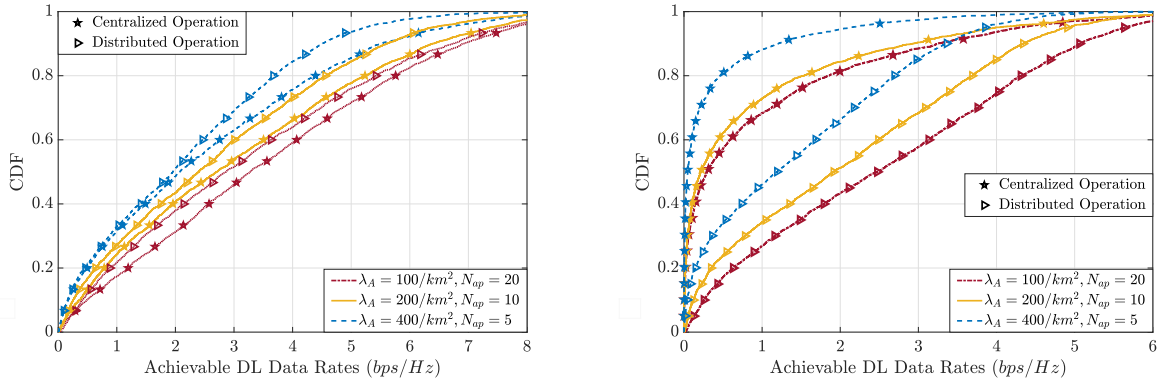

(a) $\delta = 0$ (b) $\delta = 1$

Figure 7.9: CDF of the achievable DL data rates under different APs configurations.

7.7 Summary

We thoroughly investigated the DL performance of CF mMIMO under a wireless mMIMO-based fronthaul network operation. Particularly, we consider multiple ECPs to which APs are associated in a distance-based criterion. In addition, three different wireless operations are considered for the fronthaul communication between APs and their serving ECPs, namely, microwave, mmWave, and hybrid microwave/mmWave. Besides, two different access link operations are considered for the communication between users and APs, namely, distributed and centralized system operations. The achievable DL data rates for both system operations are analyzed under the proposed wireless fronthaul network assuming correlated Rician fading channels and considering APs with/without decoding capabilities. Results revealed that the channel gains of the fronthaul links have higher impact on the achievable DL data rates than the available bandwidth for the fronthaul communication. Consequently, suppressing the fronthaul channel gains effect through empowering APs with decoding capabilities results in a significant improvement in the achievable DL data rates. Besides, we revealed that the hybrid-based fronthaul operation

is the best candidate for the fronthaul communication if APs are supported with decoding capabilities. However, the microwave fronthaul operation provides ultimate performance to systems include APs without decoding capabilities. Furthermore, the centralized operation outperforms the distributed counterpart when APs have decoding capabilities whereas the distributed one provides better performance when APs are not provided with decoding capabilities.

Chapter 8
Conclusions and Future Works

8.1 Conclusions

CF mMIMO is a promising system that can efficiently meet the unprecedented requirements of 5G and beyond networks. Despite the significant theoretical gains of CF mMIMO systems, the system performance may be prone to severe degradation due to several practical limitations. In this thesis, we have managed to analyze the CF mMIMO performance under various practical system considerations. Also, we have developed promising solutions to circumvent the negative impact of such practical system considerations on its performance. Particularly, we have addressed the following critical questions to facilitate the realization of a scalable and practical CF mMIMO system:

1. Is it possible to equip APs and UEs with non-ideal hardware components without affecting the system performance badly?

2. Does the system have the ability to provide high-mobility scenarios with a comparable performance to the low-mobility counterparts?

3. Is the system able to provide a secure data transmission to served users?

4. How to operate the system under limited-capacity of fronthaul links?

5. Can we operate the system in a scalable manner?

We have successfully answered these questions and come up with profound insights to bring out the full potential of CF mMIMO in practice. We briefly summarize these insights in the following.

1. We revealed that CF mMIMO outperforms other candidates (i.e., SC systems) that share the same architecture under non-ideal hardware components of APs. Also, we can mitigate the inevitable impact of non-ideal hardware components by increasing

the number of deployed APs or the number of antennas per APs. Differently, the system cannot tolerate the negative impact of non-ideal UEs. Thus, it is preferred to equip UEs with ideal hardware components.

2. We showed that CF mMIMO is more robust than SC systems under high-mobility scenarios. Besides, we proposed a hybrid CF mMIMO/SC system with low-complexity distributed operation under to support different mobility conditions with high data rates simultaneously. Furthermore, we proposed a novel framework to limit the performance loss of CF mMIMO under high-mobility scenarios.

3. We proposed two different promising approaches to boost the provided security levels of CF mMIMO systems. In the first approach, we developed a simple distributed DL transmission techniques that limits the Eve's capability in decoding the transmitted signals to legitimate users. Differently, the second approach is a centralized one that exploits the distinctive features of RISs to limit the performance leakage to the Eve. Both approaches showed substantial gains in the provided secrecy capacities of the system.

4. We analyzed the negative impact of limited capacity of wired-based fronthaul links on the DL performance of CF mMIMO. Besides, we revealed that it is preferred to operate the system in a distributed manner under low-capacity of fronthaul links. Differently, the centralized system operation is the preferred system operation under high-capacity fronthaul links.

5. We proposed a wireless-based fronthaul network that enables operating CF mMIMO in a scalable manner. In this regard, we revealed that APs should be provided with signal decoding capabilities to take advantage of the proposed wireless-based fronthaul operation. Furthermore, we have proposed a hybrid mmWave/microwave fronthaul operation that can significantly boost the achievable DL rates of the system compared to operating the fronthaul on the mmWave band or the microwave band.

8.2 Future Works

In what follows, we propose further research directions that empowers CF mMIMO system with substantial gains to support the diverse applications of 5G and beyond networks. Particularly, we firstly propose two more directions to attain further improvements in the achievable data rates, namely mmWave-Based Access Communication and Rate-Splitting Multiple Access (RSMA). Then, we propose vital directions that enables CF mMIMO to embrace internet of things (IoT)-based applications.

mmWave-Based Access Communication: The possible marriage mmWave and CF mMIMO should be thoroughly investigated for further improvements in the provided data rates. In fact, operating the communication links between APs and users in mmWave bands is still a premature subject that needs further investigations. For instance, wide-band channel estimation techniques are required to enable the data transmissions over the large amount of available bandwidth in mmWave bands. Moreover, as one of the main impediments of wireless communications in high frequency bands is the lack of LoS communication links, the ability of the CF mmWave massive mMIMO systems in supporting realistic scenarios with moving objects where the probability of having LoS links decreases should be thoroughly investigated. In this regard, relays/RISs may play an important role to create LoS paths between APs and users.

Rate Splitting Multiple-Access: Compared to orthogonal multiple-access (OMA), non-orthogonal multiple-access (NOMA), and SDMA, a more general, robust, and powerful DL transmission framework for multiple-antenna systems is the RSMA which embraces both NOMA and SDMA [127,128]. In particular, RSMA relies on the rate splitting strategy at the transmitter and successive interference cancellation (SIC) at the receiver to flexibly manage the interference by allowing the interference to be partially decoded and partially treated as noise. In doing so, the message intended for one user is split into a private part and a common part that is drawn from a public codebook. The private messages for different users are transmitted by means of ZF precoding using a fraction of the total power while the common message is superimposed on top of the ZF-precoded private messages using the residual power. At the receiver side, the common message is decoded by treating all the private messages as noise. After removing the decoded common message from the received signal by SIC, each user decodes their own private messages. Several

works in the literature have adopted the RSMA transmission for co-located mMIMO systems to tackle the detrimental effects of the multiuser interference. Results revealed that high potential of RSMA in achieving superior performance than other conventional transmission techniques, especially at high signal-to-noise ratio regime [129]. Nevertheless, no previous works have considered RSMA for DL transmission in the context of CF mMIMO systems which in turn makes it an interesting direction for future works.

Supporting Massive Machine-Type Communication: One of the open issues that still needs to be tackled is the presence of mMTC, i.e., IoT devices. Indeed, IoT has recently become the key enabler for a wide range of emerging applications including e-health and autonomous vehicles, to name a few [12]. The potential of CF mMIMO in supporting massive IoT devices is still in its early stages where few studies only have analyzed the IoT-based CF mMIMO system performance ([130–132] and references therein). However, various impractical assumptions are considered in these studies. Particularly, previous works considered small numbers of IoT devices which does not reflect the reality of future networks where massive number of devices will exist. This in turn lessens the potential of the proposed solutions in these works.

Co-existence of Human and Machine-Type Communications: In accordance with the presence of massive IoT devices in 5G and beyond networks, one of the crucial problems that needs further attention is the coexistence of MTC along with the conventional human-type communication (HTC) [2]. However, previous works have not analyzed the potential of CF mMIMO in supporting both communication types with their diverse QoS requirements simultaneously. As such, we plan to provide a novel framework that boosts the CF mMIMO capabilities in meeting the distinct needs of MTC and HTC simultaneously. More specifically, a framework that enables CF mMIMO systems to provide HTC users with high data rates while supporting massive IoT devices with low-latency reliable communication links. In this regard, we believe that power-domain NOMA will play an important role to support both types of communications simultaneously. This is thanks to the efficient use of resources by NOMA which in turn gives it the potential to support a larger number of communication links with good QoS compared to the conventional orthogonal multiple access techniques.

Appendix:

List of Publications

Journal Articles

1. S. Elhoushy, M. Ibrahim and W. Hamouda, "Exploiting RIS for Limiting Information Leakage to Active Eavesdropper in Cell-Free Massive MIMO," in *IEEE Wireless Communications Letters*, vol. 11, no. 3, pp. 443-447, March 2022.

2. S. Elhoushy, M. Ibrahim and W. Hamouda, "Cell-Free Massive MIMO: A Survey,". in *IEEE Communications Surveys & Tutorials*, vol. 24, no. 1, pp. 492-523, Firstquarter 2022.

3. S. Elhoushy and W. Hamouda, "Limiting Doppler Shift Effect on Cell-Free Massive MIMO Systems: A Stochastic Geometry Approach," in *IEEE Transactions on Wireless Communications*, vol. 20, no. 9, pp. 5656-5671, Sept. 2021.

4. S. Elhoushy and W. Hamouda, "Towards High Data Rates in Dynamic Environments Using Hybrid Cell-Free Massive MIMO/Small-Cell System," in *IEEE Wireless Communications Letters*, vol. 10, no. 2, pp. 201-205, Feb. 2021.

5. S. Elhoushy and W. Hamouda, "Performance of Distributed Massive MIMO and Small-Cell Systems Under Hardware and Channel Impairments," in *IEEE Transactions on Vehicular Technology*, vol. 69, no. 8, pp. 8627-8642, Aug. 2020.

6. S. Elhoushy, M. Ibrahim and W. Hamouda, "Downlink Performance of CF Massive MIMO Under Wireless-Based Fronthaul Network," in *IEEE Transactions on Communications*, (Submitted).

Conference Proceedings

1. S. Elhoushy and W. Hamouda, "Downlink Performance of Limited-Fronthaul Cell-Free Massive MIMO,". in *ICC 2021 - IEEE International Conference on Commu-*

nications, 2021, pp. 1-6.

2. S. Elhoushy and W. Hamouda, "Nearest APs-Based Downlink Pilot Transmission for High Secrecy Rates in Cell-Free Massive MIMO,". in *GLOBECOM 2020 - 2020 IEEE Global Communications Conference*, 2020, pp. 1-6.

Bibliography

[1] Samsung, "White paper: The vision of 6G bring the next hyper-connected experience to every corner of life." *Samsung*, 2020. [Online]. Available: https://research.samsung.com/next-generation-communications

[2] M. Elbayoumi, M. Kamel, W. Hamouda, and A. Youssef, "NOMA-assisted machine-type communications in UDN: State-of-the-art and challenges," *IEEE Communications Surveys & Tutorials*, vol. 22, no. 2, pp. 1276–1304, 2020.

[3] W. Saad, M. Bennis, and M. Chen, "A vision of 6G wireless systems: Applications, trends, technologies, and open research problems," *IEEE Network*, vol. 34, no. 3, pp. 134–142, 2020.

[4] Y. Wu, S. Singh, T. Taleb, A. Roy, H. S. Dhillon, M. R. Kanagarathinam, and A. De, *6G mobile wireless networks*. Springer, 2021.

[5] H. Chen, R. Abbas, P. Cheng, M. Shirvanimoghaddam, W. Hardjawana, W. Bao, Y. Li, and B. Vucetic, "Ultra-reliable low latency cellular networks: Use cases, challenges and approaches," *IEEE Communications Magazine*, vol. 56, no. 12, pp. 119–125, 2018.

[6] H. Ji, S. Park, J. Yeo, Y. Kim, J. Lee, and B. Shim, "Ultra-reliable and low-latency communications in 5G downlink: Physical layer aspects," *IEEE Wireless Communications*, vol. 25, no. 3, pp. 124–130, 2018.

[7] P. Schulz, M. Matthe, H. Klessig, M. Simsek, G. Fettweis, J. Ansari, S. A. Ashraf, B. Almeroth, J. Voigt, I. Riedel *et al.*, "Latency critical IoT applications in 5G: Perspective on the design of radio interface and network architecture," *IEEE Communications Magazine*, vol. 55, no. 2, pp. 70–78, 2017.

[8] A. Willig, K. Matheus, and A. Wolisz, "Wireless technology in industrial networks," *Proceedings of the IEEE*, vol. 93, no. 6, pp. 1130–1151, 2005.

[9] M. Luvisotto, Z. Pang, and D. Dzung, "Ultra high performance wireless control for critical applications: Challenges and directions," *IEEE Transactions on Industrial Informatics*, vol. 13, no. 3, pp. 1448–1459, 2016.

[10] C. Bockelmann, N. Pratas, H. Nikopour, K. Au, T. Svensson, C. Stefanovic, P. Popovski, and A. Dekorsy, "Massive machine-type communications in 5G: Physical and mac-layer solutions," *IEEE Communications Magazine*, vol. 54, no. 9, pp. 59–65, 2016.

[11] C. Bockelmann, N. K. Pratas, G. Wunder, S. Saur, M. Navarro, D. Gregoratti, G. Vivier, E. De Carvalho, Y. Ji, Č. Stefanović *et al.*, "Towards massive connectivity support for scalable mMTC communications in 5G networks," *IEEE access*, vol. 6, pp. 28 969–28 992, 2018.

[12] Ericsson, "Ericsson mobility report june 2020." *Ericsson*, 2020. [Online]. Available: https://www.ericsson.com/en/reports-and-papers/mobility-report

[13] G. Interdonato, *Cell-Free Massive MIMO: Scalability, Signal Processing and Power Control*. Linköping University Electronic Press, 2020, vol. 2090.

[14] I. A. Hemadeh, K. Satyanarayana, M. El-Hajjar, and L. Hanzo, "Millimeter-wave communications: Physical channel models, design considerations, antenna constructions, and link-budget," *IEEE Communications Surveys & Tutorials*, vol. 20, no. 2, pp. 870–913, 2018.

[15] A. N. Uwaechia and N. M. Mahyuddin, "A comprehensive survey on millimeter wave communications for fifth-generation wireless networks: Feasibility and challenges," *IEEE Access*, vol. 8, pp. 62 367–62 414, 2020.

[16] M. Kamel, W. Hamouda, and A. Youssef, "Ultra-dense networks: A survey," *IEEE Communications Surveys & Tutorials*, vol. 18, no. 4, pp. 2522–2545, 2016.

[17] E. G. Larsson, O. Edfors, F. Tufvesson, and T. L. Marzetta, "Massive MIMO for next generation wireless systems," *IEEE Communications Magazine*, vol. 52, no. 2, pp. 186–195, February 2014.

[18] T. L. Marzetta and H. Yang, *Fundamentals of massive MIMO*. Cambridge University Press, 2016.

[19] T. L. Marzetta, "Noncooperative cellular wireless with unlimited numbers of base station antennas," *IEEE Transactions on Wireless Communications*, vol. 9, no. 11, pp. 3590–3600, November 2010.

[20] H. Q. Ngo, E. G. Larsson, and T. L. Marzetta, "Aspects of favorable propagation in massive MIMO," in *2014 22nd European Signal Processing Conference (EUSIPCO)*, 2014, pp. 76–80.

[21] H. Q. Ngo, A. Ashikhmin, H. Yang, E. G. Larsson, and T. L. Marzetta, "Cell-free massive MIMO versus small cells," *IEEE Transactions on Wireless Communications*, vol. 16, no. 3, pp. 1834–1850, March 2017.

[22] A. Papazafeiropoulos, P. Kourtessis, M. Di Renzo, S. Chatzinotas, and J. M. Senior, "Performance analysis of cell-free massive MIMO systems: A stochastic geometry approach," *IEEE Transactions on Vehicular Technology*, pp. 1–1, 2020.

[23] J. Hoydis, S. ten Brink, and M. Debbah, "Massive MIMO in the UL/DL of cellular networks: How many antennas do we need?" *IEEE Journal on Selected Areas in Communications*, vol. 31, no. 2, pp. 160–171, February 2013.

[24] K. T. Truong and R. W. Heath, "Effects of channel aging in massive MIMO systems," *Journal of Communications and Networks*, vol. 15, no. 4, pp. 338–351, Aug 2013.

[25] Y. Wu, A. Khisti, C. Xiao, G. Caire, K. Wong, and X. Gao, "A survey of physical layer security techniques for 5G wireless networks and challenges ahead," *IEEE Journal on Selected Areas in Communications*, vol. 36, no. 4, pp. 679–695, 2018.

[26] D. G. Brennan, "Linear diversity combining techniques," *Proceedings of the IRE*, vol. 47, no. 6, pp. 1075–1102, 1959.

[27] E. Telatar, "Capacity of multi-antenna Gaussian channels," *European transactions on telecommunications*, vol. 10, no. 6, pp. 585–595, 1999.

[28] G. J. Foschini, "Layered space-time architecture for wireless communication in a fading environment when using multi-element antennas," *Bell labs technical journal*, vol. 1, no. 2, pp. 41–59, 1996.

[29] G. J. Foschini and M. J. Gans, "On limits of wireless communications in a fading environment when using multiple antennas," *Wireless personal communications*, vol. 6, no. 3, pp. 311–335, 1998.

[30] G. G. Raleigh and J. M. Cioffi, "Spatio-temporal coding for wireless communication," *IEEE Transactions on communications*, vol. 46, no. 3, pp. 357–366, 1998.

[31] E. Alexanderson, "Transatlantic radio communication," *Proceedings of the American Institute of Electrical Engineers*, vol. 38, no. 10, pp. 1077–1093, 1919.

[32] S. Swales, M. Beach, D. Edwards, and J. McGeehan, "The performance enhancement of multibeam adaptive base-station antennas for cellular land mobile radio systems," *IEEE Transactions on Vehicular Technology*, vol. 39, no. 1, pp. 56–67, 1990.

[33] D. Gesbert, M. Kountouris, R. Heath, C. Chae, and T. Salzer, "From single user to multiuser communications: shifiting the MIMO paradigm," *IEEE Signal Processing Magazine*, 2008.

[34] P. Viswanath and D. Tse, "Sum capacity of the vector Gaussian broadcast channel and uplink–downlink duality," *IEEE Transactions on Information Theory*, vol. 49, no. 8, pp. 1912–1921, 2003.

[35] S. Vishwanath, N. Jindal, and A. Goldsmith, "Duality, achievable rates, and sum-rate capacity of Gaussian MIMO broadcast channels," *IEEE Transactions on Information Theory*, vol. 49, no. 10, pp. 2658–2668, 2003.

[36] G. Caire and S. Shamai, "On the achievable throughput of a multiantenna Gaussian broadcast channel," *IEEE Transactions on Information Theory*, vol. 49, no. 7, pp. 1691–1706, 2003.

[37] T. L. Marzetta, "How much training is required for multiuser MIMO?" in *2006 Fortieth Asilomar Conference on Signals, Systems and Computers*, 2006, pp. 359–363.

[38] F. Rusek, D. Persson, B. K. Lau, E. G. Larsson, T. L. Marzetta, O. Edfors, and F. Tufvesson, "Scaling up MIMO: Opportunities and challenges with very large arrays," *IEEE Signal Processing Magazine*, vol. 30, no. 1, pp. 40–60, 2013.

[39] T. L. Marzetta, "Massive MIMO: An introduction," *Bell Labs Technical Journal*, vol. 20, pp. 11–22, 2015.

[40] Martínez *et al.*, "Massive MIMO properties based on measured channels: Channel hardening, user decorrelation and channel sparsity," in *2016 50th Asilomar Conference on Signals, Systems and Computers*, 2016, pp. 1804–1808.

[41] S. Gunnarsson, J. Flordelis, L. Van Der Perre, and F. Tufvesson, "Channel hardening in massive MIMO: Model parameters and experimental assessment," *IEEE Open Journal of the Communications Society*, vol. 1, pp. 501–512, 2020.

[42] H. Q. Ngo, E. G. Larsson, and T. L. Marzetta, "Energy and spectral efficiency of very large multiuser MIMO systems," *IEEE Transactions on Communications*, vol. 61, no. 4, pp. 1436–1449, April 2013.

[43] E. Björnson, J. Hoydis, and L. Sanguinetti, *Massive MIMO Networks: Spectral, Energy, and Hardware Efficiency.* Now Foundations and Trends, 2017.

[44] E. Björnson, E. G. Larsson, and M. Debbah, "Massive MIMO for maximal spectral efficiency: How many users and pilots should be allocated?" *IEEE Transactions on Wireless Communications*, vol. 15, no. 2, pp. 1293–1308, 2016.

[45] A. Zappone, L. Sanguinetti, G. Bacci, E. Jorswieck, and M. Debbah, "Energy-efficient power control: A look at 5G wireless technologies," *IEEE Transactions on Signal Processing*, vol. 64, no. 7, pp. 1668–1683, 2016.

[46] H. V. Cheng, E. Björnson, and E. G. Larsson, "Optimal pilot and payload power control in single-cell massive MIMO systems," *IEEE Transactions on Signal Processing*, vol. 65, no. 9, pp. 2363–2378, 2017.

[47] H. Yang and T. L. Marzetta, "Massive MIMO with max-min power control in line-of-sight propagation environment," *IEEE Transactions on Communications*, vol. 65, no. 11, pp. 4685–4693, 2017.

[48] T. Van Chien, E. Björnson, and E. G. Larsson, "Joint pilot design and uplink power allocation in multi-cell massive MIMO systems," *IEEE Transactions on Wireless Communications*, vol. 17, no. 3, pp. 2000–2015, 2018.

[49] A. Ghazanfari, H. V. Cheng, E. Björnson, and E. G. Larsson, "Enhanced fairness and scalability of power control schemes in multi-cell massive MIMO," *IEEE Transactions on Communications*, vol. 68, no. 5, pp. 2878–2890, 2020.

[50] W. Choi and J. G. Andrews, "Downlink performance and capacity of distributed antenna systems in a multicell environment," *IEEE Transactions on Wireless Communications*, vol. 6, no. 1, pp. 69–73, Jan 2007.

[51] R. Irmer, H. Droste, P. Marsch, M. Grieger, G. Fettweis, S. Brueck, H. Mayer, L. Thiele, and V. Jungnickel, "Coordinated multipoint: Concepts, performance, and field trial results," *IEEE Communications Magazine*, vol. 49, no. 2, pp. 102–111, 2011.

[52] Z. Liu and L. Dai, "A comparative study of downlink MIMO cellular networks with co-located and distributed base-station antennas," *IEEE Transactions on Wireless Communications*, vol. 13, no. 11, pp. 6259–6274, 2014.

[53] Q. Ye, O. Y. Bursalioglu, and H. C. Papadopoulos, "Harmonized cellular and distributed massive MIMO: Load balancing and scheduling," in *2015 IEEE Global Communications Conference (GLOBECOM)*, Dec 2015, pp. 1–6.

[54] J. Wang and L. Dai, "Asymptotic rate analysis of downlink multi-user systems with co-located and distributed antennas," *IEEE Transactions on Wireless Communications*, vol. 14, no. 6, pp. 3046–3058, 2015.

[55] K. T. Truong and R. W. Heath, "The viability of distributed antennas for massive MIMO systems," in *2013 Asilomar Conference on Signals, Systems and Computers*, Nov 2013, pp. 1318–1323.

[56] E. Nayebi, A. Ashikhmin, T. L. Marzetta, and H. Yang, "Cell-free massive MIMO systems," in *2015 49th Asilomar Conference on Signals, Systems and Computers*, Nov 2015, pp. 695–699.

[57] E. Nayebi, A. Ashikhmin, T. L. Marzetta, H. Yang, and B. D. Rao, "Precoding and power optimization in cell-free massive MIMO systems," *IEEE Transactions on Wireless Communications*, vol. 16, pp. 4445–4459, 2017.

[58] A. Abdallah and M. M. Mansour, "Efficient angle-domain processing for FDD-based cell-free massive MIMO systems," *IEEE Transactions on Communications*, vol. 68, no. 4, pp. 2188–2203, 2020.

[59] ——, "Angle-based multipath estimation and beamforming for FDD cell-free massive MIMO," in *2019 IEEE 20th International Workshop on Signal Processing Advances in Wireless Communications (SPAWC)*, 2019, pp. 1–5.

[60] S. Kim and B. Shim, "AoD-based statistical beamforming for cell-free massive MIMO systems," in *2018 IEEE 88th Vehicular Technology Conference (VTC-Fall)*, 2018, pp. 1–5.

[61] ——, "FDD-based cell-free massive MIMO systems," in *2018 IEEE 19th International Workshop on Signal Processing Advances in Wireless Communications (SPAWC)*, 2018, pp. 1–5.

[62] M. Alrabeiah and A. Alkhateeb, "Deep learning for TDD and FDD massive MIMO: Mapping channels in space and frequency," in *2019 53rd Asilomar Conference on Signals, Systems, and Computers*, 2019, pp. 1465–1470.

[63] E. Bjornson and B. Ottersten, "A framework for training-based estimation in arbitrarily correlated rician MIMO channels with rician disturbance," *IEEE Transactions on Signal Processing*, vol. 58, no. 3, pp. 1807–1820, 2010.

[64] T. Marzetta and B. Hochwald, "Fast transfer of channel state information in wireless systems," *IEEE Transactions on Signal Processing*, vol. 54, no. 4, pp. 1268–1278, 2006.

[65] T. L. Marzetta, G. Caire, M. Debbah, I. Chih-Lin, and S. K. Mohammed, "Special issue on massive MIMO," *Journal of Communications and Networks*, vol. 15, no. 4, pp. 333–337, 2013.

[66] E. Björnson, E. G. Larsson, and T. L. Marzetta, "Massive MIMO: ten myths and one critical question," *IEEE Communications Magazine*, vol. 54, no. 2, pp. 114–123, February 2016.

[67] O. Elijah, C. Y. Leow, T. A. Rahman, S. Nunoo, and S. Z. Iliya, "A comprehensive survey of pilot contamination in massive MIMO-5G system," *IEEE Communications Surveys Tutorials*, vol. 18, no. 2, pp. 905–923, Secondquarter 2016.

[68] S. M. Kay, *Fundamentals of statistical signal processing*. Prentice Hall PTR, 1993.

[69] S. Buzzi and C. D'Andrea, "User-centric communications versus cell-free massive MIMO for 5G cellular networks," in *WSA 2017; 21th International ITG Workshop on Smart Antennas*, 2017, pp. 1–6.

[70] S. Buzzi and A. Zappone, "Downlink power control in user-centric and cell-free massive MIMO wireless networks," in *2017 IEEE 28th Annual International Symposium on Personal, Indoor, and Mobile Radio Communications (PIMRC)*, Oct 2017, pp. 1–6.

[71] S. Buzzi, C. D'Andrea, A. Zappone, and C. D'Elia, "User-centric 5G cellular networks: Resource allocation and comparison with the cell-free massive MIMO approach," *IEEE Transactions on Wireless Communications*, pp. 1–1, 2019.

[72] S. Buzzi, C. D'Andrea, and C. D'Elia, "User-centric cell-free massive MIMO with interference cancellation and local ZF downlink precoding," in *2018 15th International Symposium on Wireless Communication Systems (ISWCS)*, 2018, pp. 1–5.

[73] E. Nayebi, A. Ashikhmin, T. L. Marzetta, H. Yang, and B. D. Rao, "Precoding and power optimization in cell-free massive MIMO systems," *IEEE Transactions on Wireless Communications*, vol. 16, no. 7, pp. 4445–4459, 2017.

[74] E. Björnson and L. Sanguinetti, "Scalable cell-free massive MIMO systems," *IEEE Transactions on Communications*, pp. 1–1, 2020.

[75] Z. Chen and E. Björnson, "Channel hardening and favorable propagation in cell-free massive MIMO with stochastic geometry," *IEEE Transactions on Communications*, vol. 66, no. 11, pp. 5205–5219, Nov 2018.

[76] E. Björnson and L. Sanguinetti, "Cell-free versus cellular massive MIMO: What processing is needed for cell-free to win?" in *2019 IEEE 20th International Workshop on Signal Processing Advances in Wireless Communications (SPAWC)*, 2019, pp. 1–5.

[77] ——, "Making cell-free massive MIMO competitive with MMSE processing and centralized implementation," *IEEE Transactions on Wireless Communications*, vol. 19, no. 1, pp. 77–90, 2020.

[78] E. Björnson, M. Matthaiou, and M. Debbah, "Massive MIMO with non-ideal arbitrary arrays: Hardware scaling laws and circuit-aware design," *IEEE Transactions on Wireless Communications*, vol. 14, no. 8, pp. 4353–4368, Aug 2015.

[79] E. Björnson, J. Hoydis, M. Kountouris, and M. Debbah, "Massive MIMO systems with non-ideal hardware: Energy efficiency, estimation, and capacity limits," *IEEE Transactions on Information Theory*, vol. 60, no. 11, pp. 7112–7139, Nov 2014.

[80] J. Zhang, Y. Wei, E. Björnson, Y. Han, and S. Jin, "Performance analysis and power control of cell-free massive MIMO systems with hardware impairments," *IEEE Access*, vol. 6, pp. 55 302–55 314, 2018.

[81] A. K. Papazafeiropoulos and T. Ratnarajah, "Uplink performance of massive MIMO subject to delayed CSIT and anticipated channel prediction," in *2014 IEEE International Conference on Acoustics, Speech and Signal Processing (ICASSP)*, May 2014, pp. 3162–3165.

[82] A. Papazafeiropoulos and T. Ratnarajah, "Linear precoding for downlink massive MIMO with delayed CSIT and channel prediction," in *2014 IEEE Wireless Communications and Networking Conference (WCNC)*, April 2014, pp. 809–914.

[83] A. K. Papazafeiropoulos, "Impact of general channel aging conditions on the downlink performance of massive MIMO," *IEEE Transactions on Vehicular Technology*, vol. 66, no. 2, pp. 1428–1442, Feb 2017.

[84] K. E. Baddour and N. C. Beaulieu, "Autoregressive modeling for fading channel simulation," *IEEE Transactions on Wireless Communications*, vol. 4, no. 4, pp. 1650–1662, July 2005.

[85] R. Chopra, C. R. Murthy, H. A. Suraweera, and E. G. Larsson, "Performance analysis of FDD massive MIMO systems under channel aging," *IEEE Transactions on Wireless Communications*, vol. 17, no. 2, pp. 1094–1108, Feb 2018.

[86] J. Li, D. Wang, P. Zhu, and X. You, "Uplink spectral efficiency analysis of distributed massive MIMO with channel impairments," *IEEE Access*, vol. 5, pp. 5020–5030, 2017.

[87] X. Zhou, B. Maham, and A. Hjorungnes, "Pilot contamination for active eavesdropping," *IEEE Transactions on Wireless Communications*, vol. 11, no. 3, pp. 903–907, 2012.

[88] D. Kapetanovic, G. Zheng, and F. Rusek, "Physical layer security for massive MIMO: An overview on passive eavesdropping and active attacks," *IEEE Communications Magazine*, vol. 53, no. 6, pp. 21–27, 2015.

[89] R. G. Stephen and R. Zhang, "Joint millimeter-wave fronthaul and OFDMA resource allocation in ultra-dense CRAN," *IEEE Transactions on Communications*, vol. 65, no. 3, pp. 1411–1423, 2017.

[90] G. Femenias and F. Riera-Palou, "Fronthaul-constrained cell-free massive MIMO with low resolution ADCs," *IEEE Access*, pp. 1–1, 2020.

[91] P. Parida, H. S. Dhillon, and A. F. Molisch, "Downlink performance analysis of cell-free massive MIMO with finite fronthaul capacity," in *2018 IEEE 88th Vehicular Technology Conference (VTC-Fall)*, Aug 2018, pp. 1–6.

[92] H. Masoumi and M. J. Emadi, "Performance analysis of cell-free massive MIMO system with limited fronthaul capacity and hardware impairments," *IEEE Transactions on Wireless Communications*, pp. 1–1, 2019.

[93] D. Maryopi, M. Bashar, and A. Burr, "On the uplink throughput of zero forcing in cell-free massive MIMO with coarse quantization," *IEEE Transactions on Vehicular Technology*, vol. 68, no. 7, pp. 7220–7224, 2019.

[94] M. Bashar *et al.*, "Max–Min rate of cell-free massive MIMO uplink with optimal uniform quantization," *IEEE Transactions on Communications*, vol. 67, no. 10, pp. 6796–6815, 2019.

[95] ——, "Energy efficiency of the cell-free massive MIMO uplink with optimal uniform quantization," *IEEE Transactions on Green Communications and Networking*, vol. 3, no. 4, pp. 971–987, 2019.

[96] S. Buzzi and C. D'Andrea, "Cell-free massive MIMO: User-centric approach," *IEEE Wireless Communications Letters*, vol. 6, no. 6, pp. 706–709, Dec 2017.

[97] S. Boyd and L. Vandenberghe, *Convex optimization*. Cambridge university press, 2004.

[98] J. Zhang, S. Chen, Y. Lin, J. Zheng, B. Ai, and L. Hanzo, "Cell-free massive MIMO: A new next-generation paradigm," *IEEE Access*, vol. 7, pp. 99 878–99 888, 2019.

[99] J. Nocedal and S. Wright, *Numerical optimization*. Springer Science & Business Media, 2006.

[100] S. Kashyap, C. Mollén, E. Björnson, and E. G. Larsson, "Performance analysis of TDD massive MIMO with Kalman channel prediction," in *2017 IEEE International Conference on Acoustics, Speech and Signal Processing (ICASSP)*, March 2017, pp. 3554–3558.

[101] S. M. Azimi-Abarghouyi, B. Makki, M. Nasiri-Kenari, and T. Svensson, "Stochastic geometry modeling and analysis of finite millimeter wave wireless networks," *IEEE Transactions on Vehicular Technology*, vol. 68, no. 2, pp. 1378–1393, 2019.

[102] S. M. Azimi-Abarghouyi, B. Makki, M. Haenggi, M. Nasiri-Kenari, and T. Svensson, "Stochastic geometry modeling and analysis of single- and multi-cluster wireless networks," *IEEE Transactions on Communications*, vol. 66, no. 10, pp. 4981–4996, 2018.

[103] D. Moltchanov, "Distance distributions in random networks," *Ad Hoc Networks*, vol. 10, no. 6, pp. 1146–1166, 2012.

[104] X. Zhang, D. Guo, K. An, Z. Ding, and B. Zhang, "Secrecy analysis and active pilot spoofing attack detection for multigroup multicasting cell-free massive MIMO systems," *IEEE Access*, vol. 7, pp. 57 332–57 340, 2019.

[105] T. M. Hoang, H. Q. Ngo, T. Q. Duong, H. D. Tuan, and A. Marshall, "Cell-free massive MIMO networks: Optimal power control against active eavesdropping," *IEEE Transactions on Communications*, vol. 66, no. 10, pp. 4724–4737, 2018.

[106] M. Di Renzo *et al.*, "Smart Radio Environments Empowered by Reconfigurable Intelligent Surfaces: How It Works, State of Research, and The Road Ahead," *IEEE Journal on Selected Areas in Communications*, vol. 38, no. 11, pp. 2450–2525, 2020.

[107] Y. Zhang, B. Di, H. Zhang, J. Lin, Y. Li, and L. Song, "Reconfigurable Intelligent Surface Aided Cell-free MIMO Communications," *IEEE Wireless Communications Letters*, pp. 1–1, 2020.

[108] M. Bashar, K. Cumanan, A. G. Burr, P. Xiao, and M. Di Renzo, "On the performance of reconfigurable intelligent surface-aided cell-free massive MIMO uplink," in *GLOBECOM 2020 - 2020 IEEE Global Communications Conference*, 2020, pp. 1–6.

[109] Z. Tang, T. Hou, Y. Liu, J. Zhang, and C. Zhong, "A novel design of RIS for enhancing the physical layer security for RIS-aided NOMA networks," *IEEE Wireless Communications Letters*, pp. 1–1, 2021.

[110] X. Zhou, S. Yan, Q. Wu, F. Shu, and D. W. K. Ng, "Intelligent reflecting surface (IRS)-aided covert wireless communications with delay constraint," *IEEE Transactions on Wireless Communications*, pp. 1–1, 2021.

[111] G. Interdonato, H. Q. Ngo, E. G. Larsson, and P. Frenger, "How much do downlink pilots improve cell-free massive MIMO?" in *2016 IEEE Global Communications Conference (GLOBECOM)*, 2016, pp. 1–7.

[112] Q. Wu and R. Zhang, "Intelligent reflecting surface enhanced wireless network via joint active and passive beamforming," *IEEE Transactions on Wireless Communications*, vol. 18, no. 11, pp. 5394–5409, 2019.

[113] 3GPP, "Technical Specification Group Radio Access Network; Spatial Channel Model for Multiple Input Multiple Output (MIMO) Simulations," *3GPP TR 25.996 version 16.0.0 Release 16,*, July 2020.

[114] M. Bashar, K. Cumanan, A. G. Burr, H. Q. Ngo, and M. Debbah, "Cell-free massive MIMO with limited backhaul," in *2018 IEEE International Conference on Communications (ICC)*, May 2018, pp. 1–7.

[115] D. Maryopi and A. Burr, "Few-bit CSI acquisition for centralized cell-free massive MIMO with spatial correlation," in *2019 IEEE Wireless Communications and Networking Conference (WCNC)*, 2019, pp. 1–6.

[116] M. Bashar *et al.*, "Exploiting deep learning in limited-fronthaul cell-free massive MIMO uplink," *IEEE J. Sel. Areas Commun.*, 2020.

[117] M. Bashar, K. Cumanan, A. G. Burr, H. Q. Ngo, E. G. Larsson, and P. Xiao, "On the energy efficiency of limited-backhaul cell-free massive MIMO," in *ICC 2019 - 2019 IEEE International Conference on Communications (ICC)*, 2019, pp. 1–7.

[118] G. Femenias *et al.*, "Cell-free millimeter-wave massive MIMO systems with limited fronthaul capacity," *IEEE Access*, vol. 7, pp. 44 596–44 612, 2019.

[119] ——, "Reduced-complexity downlink cell-free mmWave massive MIMO systems with fronthaul constraints," in *2019 27th European Signal Processing Conference (EUSIPCO)*, 2019, pp. 1–5.

[120] T. Cover and A. Joy, *Elements of Information Theory*. John Wiley & Sons, New York, USA, 2012.

[121] G. Interdonato *et al.*, "Downlink training in cell-free massive MIMO: A blessing in disguise," *IEEE Transactions on Wireless Communications*, vol. 18, no. 11, pp. 5153–5169, 2019.

[122] M. A. Albreem, M. Juntti, and S. Shahabuddin, "Massive MIMO detection techniques: A survey," *IEEE Communications Surveys & Tutorials*, vol. 21, no. 4, pp. 3109–3132, 2019.

[123] Akdeniz *et al.*, "Millimeter Wave Channel Modeling and Cellular Capacity Evaluation," *IEEE J. Sel. Areas Commun.*, vol. 32, no. 6, pp. 1164–1179, 2014.

[124] M. Alonzo and S. Buzzi, "Cell-free and user-centric massive MIMO at millimeter wave frequencies," in *2017 IEEE 28th Annual International Symposium on Personal, Indoor, and Mobile Radio Communications (PIMRC)*, 2017, pp. 1–5.

[125] Ericsson, "Enhancing 5G with microwave," *Ericsson*, 2020. [Online]. Available: https://www.ericsson.com/4a811d/assets/local/reports-papers/microwave-outlook/2020/2020-ericsson-microwave-outlook-report-digital.pdf

[126] 3GPP, "Study on channel model for frequency spectrum above 6 GHz," *3GPP TR 38.900 version 14.3.1 Release 14*, june 2017.

[127] B. Clerckx, H. Joudeh, C. Hao, M. Dai, and B. Rassouli, "Rate splitting for MIMO wireless networks: a promising PHY-layer strategy for LTE evolution," *IEEE Communications Magazine*, vol. 54, no. 5, pp. 98–105, 2016.

[128] S. Naser, P. C. Sofotasios, L. Bariah, W. Jaafar, S. Muhaidat, M. Al-Qutayri, and O. A. Dobre, "Rate-Splitting Multiple Access: Unifying NOMA and SDMA in MISO VLC Channels," *IEEE Open Journal of Vehicular Technology*, vol. 1, pp. 393–413, 2020.

[129] M. Dai, B. Clerckx, D. Gesbert, and G. Caire, "A Rate Splitting Strategy for Massive MIMO With Imperfect CSIT," *IEEE Transactions on Wireless Communications*, vol. 15, no. 7, pp. 4611–4624, 2016.

[130] U. K. Ganesan, E. Björnson, and E. G. Larsson, "An algorithm for grant-free random access in cell-free massive MIMO," in *2020 IEEE 21st International Workshop on Signal Processing Advances in Wireless Communications (SPAWC)*, 2020, pp. 1–5.

[131] X. Zhang, H. Qi, X. Zhang, and L. Han, "Energy-efficient resource allocation and data transmission of cell-free internet of things," *IEEE Internet of Things Journal*, vol. 8, no. 20, pp. 15 107–15 116, 2021.

[132] H. Yan, A. Ashikhmin, and H. Yang, "A scalable and energy-efficient IoT system supported by cell-free massive MIMO," *IEEE Internet of Things Journal*, vol. 8, no. 19, pp. 14 705–14 718, 2021.